

A mineralogical and fluid inclusion study of modified, contact-style Ni-Cu-PGE ores in the #1 and #4 shear zones, Garson Mine, Sudbury, Ontario, Canada

By
Darren Thomas LeFort

A Thesis Submitted to Saint Mary's University, Halifax, Nova Scotia in Partial
Fulfillment of the Requirements for the Degree of Master of Science in Applied Science

April 16, 2012, Halifax, Nova Scotia

© Darren Thomas LeFort

Approved: Dr. Jacob Hanley
Supervisor
Department of Geology

Approved: Dr. James Mungall
External Examiner
Department of Geology
University of Toronto

Approved: Dr. Victor Owen
Supervisory Committee
Department of Geology

Approved: Dr. Marcos Zentilli
Supervisory Committee
Department of Geology
Dalhousie University

Approved: Dr. Kevin Vessey
Dean of Graduate Studies &
Research

Date: April 16, 2012



Library and Archives
Canada

Published Heritage
Branch

395 Wellington Street
Ottawa ON K1A 0N4
Canada

Bibliothèque et
Archives Canada

Direction du
Patrimoine de l'édition

395, rue Wellington
Ottawa ON K1A 0N4
Canada

Your file Votre référence

ISBN: 978-0-494-87943-6

Our file Notre référence

ISBN: 978-0-494-87943-6

NOTICE:

The author has granted a non-exclusive license allowing Library and Archives Canada to reproduce, publish, archive, preserve, conserve, communicate to the public by telecommunication or on the Internet, loan, distribute and sell theses worldwide, for commercial or non-commercial purposes, in microform, paper, electronic and/or any other formats.

The author retains copyright ownership and moral rights in this thesis. Neither the thesis nor substantial extracts from it may be printed or otherwise reproduced without the author's permission.

AVIS:

L'auteur a accordé une licence non exclusive permettant à la Bibliothèque et Archives Canada de reproduire, publier, archiver, sauvegarder, conserver, transmettre au public par télécommunication ou par l'Internet, prêter, distribuer et vendre des thèses partout dans le monde, à des fins commerciales ou autres, sur support microforme, papier, électronique et/ou autres formats.

L'auteur conserve la propriété du droit d'auteur et des droits moraux qui protège cette thèse. Ni la thèse ni des extraits substantiels de celle-ci ne doivent être imprimés ou autrement reproduits sans son autorisation.

In compliance with the Canadian Privacy Act some supporting forms may have been removed from this thesis.

While these forms may be included in the document page count, their removal does not represent any loss of content from the thesis.

Conformément à la loi canadienne sur la protection de la vie privée, quelques formulaires secondaires ont été enlevés de cette thèse.

Bien que ces formulaires aient inclus dans la pagination, il n'y aura aucun contenu manquant.

Canada

Abstract

A mineralogical and fluid inclusion study of modified, contact-style Ni-Cu-PGE ores in the #1 and #4 shear zones, Garson Mine, Sudbury, Ontario, Canada

By Darren Thomas LeFort

The Garson deposit is a structurally and hydrothermally modified contact-style nickel-copper-platinum-group element ('PGE') magmatic sulphide deposit, located in the South Range of the Sudbury Igneous Complex, Ontario, Canada. The ores are hosted mainly in shear zones and are exceptionally enriched in arsenic, platinum, and palladium. Bulk rock arsenic is controlled by the abundance of cobaltite-gersdorffite solid solution (CGSS) and nickeline in the ore assemblages. Laser ablation-ICPMS analyses show that exceptionally high concentrations of PGE are found in these sulfarsenides and arsenides with high PPGE/IPGE ratios (avg. >30). In contrast, the base metal sulphides are consistently depleted in PGE and arsenic (rarely >1 ppm). The arsenic-rich phases are also rich in PGE mineral inclusions. The arsenic-rich phases (i) may represent the accumulation of phenocrysts from arsenic-saturated sulphide melt, or (ii) may have formed during metamorphic reheating, recrystallization or partial melting of originally arsenic-rich sulphide ore bodies.

April 16, 2012

Acknowledgments

I would like to thank Dr. Jacob Hanley for his guidance and support throughout this project as primary supervisor. I would also like to thank Dr. Victor Owen (Saint Mary's University) and Dr. Marcos Zentilli (Dalhousie University) for their support as my committee members and Dr. James Mungall (University of Toronto) as my external supervisor. I would also like to acknowledge Vale Canada Limited for their support and access to ore and drill core as well as Christopher Davis, Chris Gauld, John Townend, Linda Desjardins, Michelle Chalifoux, Stan Kedziersky, Darrell Butt, Kalevi Hannila and Brian Gauveau for all of their help. I would like to thank Dr. Simon Jackson and Dr. Jung Hun Seo for assisting with LA ICP-MS analyses and Xiang Yang for assisting with SEM-EDS.

Table of Contents

| | |
|---|-----------|
| Abstract | 2 |
| Acknowledgements | 3 |
| Table of Contents | 4 |
| List of Figures | 6 |
| List of Tables | 7 |
| Chapter 1: Introduction | 8 |
| 1.0 Structure of the thesis | 8 |
| 1.1 Primary objective of thesis | 8 |
| 1.2 Secondary objective of thesis | 10 |
| 1.3 List of acronyms | 10 |
| Chapter 2: Mineralogy and distribution of arsenic and the platinum-group elements in shear-hosted magmatic sulphide ores, Garson Mine, Sudbury, Canada | 11 |
| Abstract | 11 |
| 2.0 Introduction | 15 |
| 2.1 Regional Geology | 19 |
| 2.1.1 The Sudbury Structure and its ores | 19 |
| 2.1.2 Geology of the Garson Deposit | 23 |
| 2.2 Sampling and Analytical Methods | 29 |
| 2.2.1 Bulk rock analyses of the ores | 29 |
| 2.2.2 Trace/accessory mineral identification and analysis | 30 |
| 2.2.3 Microprobe analysis of arsenic carriers | 31 |
| 2.2.4 Trace element analyses of As-carriers and base metal sulphides by LA-ICPMS | 31 |
| 2.2.5 Mass Balances | 33 |
| 2.3 Results | 35 |
| 2.3.1 Mineralogy of major base metal sulphide phases | 35 |
| 2.3.2 Trace elements within major sulphide phases | 37 |
| 2.3.2.1 Pyrrhotite | 37 |
| 2.3.2.2 Pentlandite | 38 |
| 2.3.2.3 Chalcopyrite | 39 |
| 2.3.3 Mineralogy of the sulfarsenides and arsenides | 39 |
| 2.3.3.1 General characteristics | 39 |
| 2.3.3.2 Nickeline-chalcopyrite intergrowths | 47 |
| 2.3.3.3 Glaucodot-gersdorffite solid solution | 47 |
| 2.3.4 Trace elements in arsenides and sulfarsenides | 48 |
| 2.3.4.1 Cobaltite-gersdorffite solid solution | 48 |
| 2.3.4.2 Nickeline | 51 |
| 2.3.5 Characteristics of the PGE minerals | 51 |
| 2.3.6 Other accessory minerals | 55 |
| 2.4 Discussion | 57 |
| 2.4.1 The association between PGE and As in magmatic sulphide deposits | 57 |
| 2.4.2 Review of As-free and As-bearing sulphide systems | 58 |

| | |
|--|----|
| 2.4.3 Formation of arsenides/sulfarsenides by magmatic accumulation | 61 |
| 2.4.4 Formation of arsenides/sulfarsenides by partial melting or solid state diffusion during metamorphism | 69 |
| 2.4.5 Limitations/problems with a magmatic or metamorphic origin of sulfarsenides/arsenides | 71 |
| 2.4.6 Source and process of arsenic contamination | 74 |
| 2.4.7 Reliability of bulk As, Pd, Pt estimation based on modal analysis of minerals in thin section | 78 |
| 2.4.8 Major controls on arsenic distribution and abundance | 80 |
| 2.4.9 Major controls on PGE distribution and abundance | 85 |
| 2.4.10 The effects of PGE and accessory mineral micrograins | 93 |
| 2.5 Conclusions | 94 |
| 2.6 References | 97 |

Chapter 3: A fluid inclusion study of quartz-sulphide breccias veins in shear-hosted magmatic sulphide ores, Garson Mine, Sudbury, Canada

| | |
|--|------------|
| Abstract | 128 |
| 3.0 Introduction | 131 |
| 3.1 Regional geology | 132 |
| 3.1.1 The Sudbury Structure and its ores | 132 |
| 3.1.2 Geology of the Garson Deposit | 135 |
| 3.2 Sampling and analytical methods | 136 |
| 3.2.1 Microthermometric analyses | 139 |
| 3.2.2 Mineral identification and analysis by SEM | 140 |
| 3.2.3 LA-ICPMS analyses | 140 |
| 3.3 Results | 143 |
| 3.3.1 Vein petrography, classification and timing | 143 |
| 3.3.2 Fluid inclusion petrography and microthermometry | 145 |
| 3.3.3 Metastable phases | 152 |
| 3.4 Laser ablation ICP-MS analysis of fluid inclusions | 155 |
| 3.4.1 Aqueous inclusions | 155 |
| 3.4.2 Type IV CO ₂ inclusions | 156 |
| 3.5 Discussion | 156 |
| 3.5.1 Comparison to other studies | 156 |
| 3.5.2 Post-entrapment modifications | 160 |
| 3.5.3 Evolution of the fluids along the South Range of the SIC | 166 |
| 3.6 Conclusions | 173 |
| 3.7 References | 175 |

| | |
|-------------------------------|------------|
| Chapter 4: Application | 184 |
| 4.0 Mineral processing | 184 |
| 4.1 Sampling | 185 |
| 4.2 Exploration | 186 |

List of Figures

In Chapter 2

| | |
|---|----|
| 2.1 Geological map of the Sudbury Igneous Complex | 20 |
| 2.2 Cross section of the Garson ore bodies facing east (2640 E section) | 25 |
| 2.3 Plan view of shear zones with arsenic and PGE grades | 26 |
| 2.4 Major and minor ore types in hand sample | 28 |
| 2.5 Distribution of major phases, As-minerals (CGSS-GGSS-nickeline), and silicate gangue by ore type | 34 |
| 2.6 SEM backscattered electron images showing textural characteristics of tellurides and other accessory phases | 41 |
| 2.7 CoAsS-NiAsS-FeAsS ternary diagram (section at 650°C) showing range of composition of CGSS-GGSS grains | 43 |
| 2.8 Reflected light photomicrographs and SEM back-scattered electron images of arsenide and sulfarsenides | 44 |
| 2.9 Summary of LA-ICPMS analyses of Pd in gersdorffite by level | 49 |
| 2.10 Back-scattered electron images showing textural characteristics of IPGE minerals and Pd-tellurides | 52 |
| 2.11 Schematic depicting a proposed genetic model for the Garson deposit involving preservation of magmatic accumulation of sulfarsenides/arsenides | 64 |
| 2.12 Logarithmic plot of bulk rock assay As concentrations versus predicted As concentrations | 79 |
| 2.13 Logarithmic plot of bulk rock assay Pd concentrations versus predicted Pd concentrations | 81 |
| 2.14 Pie graphs showing mineralogical controls on As in observed minerals within low and high bulk rock As samples in different ore types | 83 |
| 2.15 Pie graphs showing mineralogical controls on As on different levels and shears at Garson | 86 |
| 2.16 Pie graphs showing mineralogical controls on Pd in observed minerals within low and high bulk rock Pd samples in different ore types at Garson | 87 |
| 2.17 Pie graphs showing mineralogical controls on Pt in observed minerals within low and high bulk rock Pt samples in different ore types at Garson | 89 |
| 2.18 Graph showing the distribution of Pt and Pd with respect to As concentration | 91 |

In Chapter 3

| | |
|--|-----|
| 3.1 Geological map of the Sudbury Igneous Complex | 133 |
| 3.2 Plan view and cross section of Garson deposit | 137 |
| 3.3 Representative signals of elements from an ablated inclusion hosted in quartz by LA-ICPMS | 142 |
| 3.4 Petrographic characteristics of a sulphide-quartz breccias vein handsample, containing a fragment of wall rock | 144 |
| 3.5 Photomicrograph and hot cathodoluminescence (CL) image of a single quartz grain | 146 |
| 3.6 Types of fluid inclusions observed in sulphide, quartz breccias veins in the Garson deposit | 148 |

| | |
|---|-----|
| 3.7 Fluid inclusion map and microphotographs of fluid inclusion assemblages of the dominant type IIA | 149 |
| 3.8 Salinity versus temperature of vapor homogenization relationships for microthermometric data | 153 |
| 3.9 Plot showing typical ranges in salinity and vapor homogenization temperature in individual assemblages | 154 |
| 3.10 Plot of relationship between salinity and trace element concentrations, determined by LA-ICPMS | 157 |
| 3.11 Comparison of element concentrations in quartz hosted fluids from type IIA and IIC, occurring along the South Range (this study) to fluid inclusion compositions in other magmatic-hydrothermal systems and formational waters | 161 |
| 3.12 Box and whisker plots of microthermometric characteristics of individual inclusion assemblages | 164 |
| 3.13 Schematic representation showing the relationship between temperature of vapor disappearance and temperature of halite dissolution | 170 |
| 3.14 Constraints on pressure-temperature (P-T) evolution of dominant fluid types observed at the Garson Mine | 171 |

List of Tables – Appendices A and B

In Appendix A

| | |
|---|-----|
| 2.1 Pyrrhotite LA-ICPMS results | 108 |
| 2.2 Pentlandite LA-ICPMS results | 110 |
| 2.3 Chalcopyrite LA-ICPMS results | 112 |
| 2.4 Gersdorffite LA-ICPMS results | 114 |
| 2.5 Nickeline LA-ICPMS results | 115 |
| 2.6 Sphalerite LA-ICPMS results | 116 |
| 2.7 Summary of distribution of arsenic-bearing minerals | 117 |
| 2.8 Electron microprobe analyses of arsenic-bearing minerals | 118 |
| 2.9 Summary of distribution of platinum group minerals | 119 |
| 2.10 SEM analyses of trace phases and platinum group minerals | 120 |
| 2.11 Assay results | 121 |
| 2.12 Ramp assay results | 126 |

In Appendix B

| | |
|---|-----|
| 3.1 Microthermometric data | 181 |
| 3.2 Fluid inclusion LA-ICPMS results | 184 |
| 3.3 CO ₂ inclusion LA-ICPMS count rate | 185 |

Chapter 1: Introduction

1.0 Structure of the thesis

This study has two main parts. Chapter 2 describes the mineralogy of the Garson deposit with a focus on As and PGE distribution, while Chapter 3 is a fluid inclusion study of pre-sulphide, regional fluids circulating along the South Range of the Sudbury Igneous Complex. The two chapters are independent from each other and, therefore, are repetitive to some degree (e.g., use of similar maps and descriptions of regional and deposit geology). Chapters 2 and 3 are prepared as separate, stand alone manuscripts for submission to Economic Geology. Chapter 1 summarizes briefly the main objectives of the study. Chapter 4 briefly reviews potential applications of the findings of Chapters 2 and 3 to mining, mineral processing and exploration, and suggests possible future work.

1.1 Primary objectives of thesis

The primary objective of this study was to characterize the mineralogical controls (mineral species, abundances, textural associations, and composition) and spatial distribution of the trace metals As and PGE (platinum group elements) as well as Au, Sb, Co, Ag, Cd, Pb, Zn, Se, Re Te, Bi, Sb and Sn in sulphide ores that are to be mined in the next 5 years (from 2011) at the Garson Mine (Vale Canada Ltd.), Sudbury, Ontario, Canada. The focus of the study was on As and the PGE. The determination of the mineralogy and spatial distributions of these metals will enable Vale Canada Limited to (i) avoid areas of the deposit that contain unusually high concentrations of As at the mining stage thereby avoiding associated smelter penalties; and (ii) to improve PGE recovery. High concentrations of As are particularly problematic in the smelting process

and will modify Bessemer matte morphology. The presence of As in high abundance will decrease the size of Cu particulates and thus cause metal phases to be dispersed in the matte which inhibits sinter generation (Christopher Davis, personal communication; Toguri et al., 1995). The ores at Garson mine are typically richer in As than other Sudbury ores. Typical Sudbury ores contain an average of ~3 ppm As, whereas Garson ores contain on average ~1000 ppm As. Currently, ores mined by Vale Canada Limited. From the Sudbury deposits are blended with Garson ore that contributes ~7-10% of the mill feed. At these levels the As concentrations are usually diluted to level where they do not cause a problem. However, in the near future, the amount of Garson ore sent to the mill feed will increase, so areas with high As will have a greater effect on the overall bulk As of the feed.

The ultimate intention of this project was to identify mineralogical criteria that mine and exploration geologists can use to recognize, in hand sample and thin section or by evaluation of assay data, potential problem areas of the ore body that are rich in As, encountered during routine drilling, mapping and grade control. The research also focuses on understanding how the ores became so concentrated in these metals during their formation, and what geological processes led to the diverse metal associations present at the Garson Mine. Generally, this study revises the existing genetic model (Christopher Davis, personal communication) for As-rich mineralization at the Garson deposit.

1.2 Secondary objective of thesis

A secondary objective of this thesis was to conduct a preliminary evaluation of fluid inclusions within early (pre-sulphide), magmatic-hydrothermal veins that are pervasive throughout the Garson ores. These quartz veins were studied by fluid inclusion, petrographic and geochemical techniques in order to (i) characterize the physical and chemical conditions at the time of fluid entrapment of vein formation, and to elucidate the relationship of these fluids to the Garson ores; (ii) determine the chemical composition of fluids and compare to other magmatic-hydrothermal fluids and (iii) evaluate the effects of post-entrapment modification on the South Range to assess validity of fluid inclusion studies.

1.3 List of acronyms

The following is a list of commonly used terms throughout the thesis:

CGSS – cobaltite-gersdorffite solid solution
CSIS – contorted schist inclusion sulphide
DISS – disseminated sulphide
EMP – electron microprobe
GGSS – glaucodot-gersdorffite solid solution
INMS – inclusion-rich massive sulphide
IPGE – iridium group platinum group elements (Ru, Ir, Os)
ISS – intermediate solid solution
LA-ICPMS – laser ablation inductively coupled mass spectroscopy
MASU – massive sulphide
MSS – monosulphide solid solution
PGE – platinum group elements
PPGE – platinum group platinum group elements (Pt, Pd, Rh)
SEM – scanning electron microscope
SEM-BSE – scanning electron microscope back-scattered electrons
SEM-EDS – scanning electron microscope energy dispersive spectroscopy
SIC – Sudbury Igneous Complex
Wr – wall rock

Chapter 2: Mineralogy and distribution of arsenic and the platinum-group elements in shear-hosted magmatic sulphide ores, Garson Mine, Sudbury, Canada

Darren LeFort*, Jacob Hanley

Dept. of Geology, Saint Mary's University, Halifax, Nova Scotia, Canada

Christopher Davis

Ontario Operations, Vale Ltd., Sudbury, Ontario, Canada

Simon Jackson

Natural Resources Canada, Ottawa, Ontario, Canada

*corresponding author email address: darrenlefort@gmail.com

Number of pages of text: 61

Number of figures: 18

Number of tables: 12 + 1 supplementary data table

For submission to Economic Geology

Abstract

The Garson deposit is a structurally and hydrothermally modified contact-style Ni-Cu-platinum-group element ('PGE') magmatic sulphide deposit, located in the Sudbury mining camp, Ontario, Canada. The ores are hosted mainly in shear zones related to syn- to post-sulphide deformation (Penokean and Mazatzal-Labradorian orogenic events) and are exceptionally enriched in As (avg. ~1030 ppm, range bdl-36 wt%; n=13727), PPGE ("platinum-group" platinum-group elements) and to a lesser extent IPGE ("iridium-group" platinum group elements). The major sulphide phases present are pyrrhotite, pentlandite, and chalcopyrite with minor pyrite, and very locally, minor sphalerite and galena. The main ore types observed are classified as inclusion-rich massive sulphide (INMS), disseminated massive sulphide (DISS), massive sulphide (MASU) and minor "contorted schist" massive sulphide (CSIS). The major control on bulk rock As abundance in the ore is the abundance of cobaltite-gersdorffite solid solution (CGSS) and nickeline in the ore assemblages. Both minerals show similar compositional ranges

($\text{Fe}_{0.11-0.41}\text{Co}_{0.01-0.73}\text{Ni}_{0.15-0.77}\text{As}_{0.71-1.23}\text{S}_{0.60-1.06}$) and are distinguished only by their differing crystal forms (GGSS grains are orthorhombic dipyramidal; CGSS grains are isometric tetartoidal) and relative grain sizes [GGSS grains are smaller (1-120 μm ; avg. $\sim 20 \mu\text{m}$), while CGSS grains are larger ($\sim 20 \mu\text{m}$ to mm scale; avg. $\sim 500 \mu\text{m}$)]. To a lesser extent, nickeline (NiAs) and sperrylite (PtAs_2) contribute to bulk rock As in samples where these minerals are present in significant abundance. Grains of CGSS and GGSS most commonly occur as inclusions hosted in major base metal sulphide phases, while nickeline is complexly intergrown with CGSS and chalcopyrite. Laser ablation-ICPMS analyses show that exceptionally high concentrations of PGE are found in these sulfarsenides (avg. 199 ppm Pd, up to ~ 1500 ppm Pd; avg. 88 ppm Pt, up to ~ 940 ppm Pt) and arsenides (avg. 44 ppm Pd, up to 130 ppm Pd) with high PPGE/IPGE ratios (avg. >30). In contrast, the base metal sulphides are consistently depleted in PGE and As (rarely >1 ppm), with the exception of Pd in pentlandite in rare samples that tend to have high abundances of chalcopyrite and nickeline. Bulk rock assays yielding high As typically coincide with highest Pd values observed and increasing Pd/Pt ratios coincide with higher abundances of CGSS and nickeline.

In general, Pd and Pt bulk grades are predominantly controlled by significant amounts of these metals dissolved in the sulfarsenides and arsenides, and by the abundance of discrete grains of telluropalladinite ($\text{PdTe} \pm \text{Cd, Sn, Sb}$), Pd-rich michenerite (PdBiTe), and sperrylite (PtAs_2) that are commonly spatially and texturally associated with the sulfarsenides and arsenides. PGE minerals ('PGM') are commonly hosted in CGSS and nickeline, along grain boundaries but dominantly as vuggy infillings (open space filling) and may have exsolved from the host sulfarsenides/arsenides as minerals or semimetal-

rich melt, or may have a secondary hydrothermal origin. They commonly occur as composite (polymineralic) grains attached to other discrete phases within the vugs including sphalerite, and Ag-, Ni-, Pb-, Bi-tellurides. Irarsite-hollingworthite [(Ir,Ru,Rh,Pt)AsS-(Rh,Pt,Pd)AsS], paolovite (Pd₂Sn), and Sn-Ni-Pd-selenide play only a minor role in PGE distribution. Irarsite-hollingworthite grains are commonly present as inclusions hosted in, or associated with, crystals of GGSS, possibly forming by exsolution from the host GGSS.

A likely source of the high As content of the sulphide ores at Garson is contamination by the metasedimentary rocks (e.g., greywackes, quartzites) of the Stobie and McKim formations which comprise the southern contact of the deposit, and can contain anomalously high As (up to 140 ppm bulk rock) up to several tens of metres from ores in barren areas. The Sudbury Igneous Complex (SIC) magma may have initially scavenged/assimilated As from these host rocks, leading to early enrichment of the melt sheet in As. Upon separation of an As-enriched sulphide liquid from this SIC magma, an early stage of sulfarsenide/arsenide saturation occurred, forming in CGSS-GGSS and nickeline phenocrysts that scavenged PGE and other trace/accessory metals from the sulphide liquid, prior to MSS crystallization. Sulfarsenides and arsenides began to accumulate at contact of the SIC (norite) and its metasedimentary and metabasaltic host rocks which made up the original footwall contact (floor) of the deposit. Arsenides (nickeline) rather than sulfarsenides may have formed locally as a result of lower fO_2 in areas where more graphitic metasediments were present, or where excess water from dehydrating (contact metamorphosed) country rocks reacted with existing sulfarsenides. After crystallization of sublayer norite and deformation, the sulphide accumulation

containing sulfarsenide/arsenide phenocrysts at its base, was thrust-faulted and emplaced into shear zones within, or along contacts between, sublayer norite and metabasalt/metasedimentary rocks. Exsolution of some PGM from sulfarsenides occurred upon cooling. As the sulphide liquid crystallized MSS, a late-stage semimetal-rich melt or fluid began to precipitate Pd-bearing and other trace minerals in open vugs in the partially crystallized MSS. Subsequent overturning of the deposit *after* partial MSS crystallization preserved sulfarsenide/arsenide cumulates along the former base (original footwall) of the sulphide-sulfarsenide-arsenide accumulation, which now comprises the hanging wall in each shear-hosted ore body.

As an alternative to the magmatic model, As-rich areas of the shear-hosted ore zones may represent zones of accumulation of an As-rich partial melt that formed during regional metamorphism of the sulfide ore bodies during or after emplacement while in a solid state (rather than partially liquid mush). There are major limitations to both magmatic and metamorphic models for the development of As-rich ores at the Garson Mine.

The high concentrations of PGE and other elements (i.e., Sb, Au, Te, Bi) occurring as dissolved metals and/or discrete mineral inclusions in arsenide and sulfarsenide phases highlights the role of As-bearing cumulate phases in scavenging of the majority of precious metals in contaminated magmatic sulphide systems to potentially produce highly PGE-enriched regions in sulphide ore bodies, but stresses the ultimate importance of discrete PGM (rather than dissolved PGE in sulfarsenides/arsenides) as the dominant mineralogical host phases for the PGE in As-rich and As-poor ores.

2.0 Introduction

Arsenic plays an important role in ore deposition and metal accumulation, but also negatively impacts mining and smelting techniques. High concentrations of As during smelting will modify Bessemer matte morphology by decreasing Cu_2S grain size, and causes metal phases to be dispersed in the matte which inhibits sinter generation (Christopher Davis, personal communication; Toguri et al., 1995). Arsenic may be released into the atmosphere and also cause fusing of the roasting bed during the roasting process (Christopher Davis, personal communication; Toguri et al., 1995). Arsenic is also a toxic metal with carcinogenic effects and a long residence time in the environment. Therefore, understanding its geochemical behavior and the factors controlling its distribution in ore-forming environments, and its paragenetic relationship to other sought-after ore metals in magmatic Ni-Cu-PGE systems is worthwhile. Experimental studies show that arsenide and sulfarsenide minerals, and As-rich sulphide or semimetal ($\text{As} \pm \text{Bi}$, Te , Sb) melt phases sequester high concentrations of platinum-group elements ('PGE') in magmatic systems (Gervilla et al., 1996; Gervilla et al., 1998; Gervilla et al., 2004). Ore metals show genetic and spatial associations with As, especially in Ni-Cu-PGE deposits associated with mafic-ultramafic rocks (e.g., Skinner et al., 1976; Makovicky et al., 1990, 1992; Arehart et al., 1993; Fleet et al., 1993; Gervilla et al., 1996; Wood, 2003; Hem and Makovicky, 2004a, b; Hanley, 2007; Dare et al., 2010a), epithermal Cu-Au deposits (e.g., Sillitoe, 1983; Panteleyev, 1986; Taylor, 2007; Lefort et al., 2011), five-metal (As, Co, Ni, Ag, Fe) association silver veins e.g., McDonald, 1987; Lang et al., 2003), disseminated and replacement gold (e.g., Pan and Fleet, 1990; Tomkins et al., 2004), cassiterite-arsenopyrite-dominant base metal deposits (Heinrich and Eadington, 1986) and Archean

greenstone-hosted quartz-carbonate Au-bearing veins (e.g., Dubé and Gosselin, 2007; and authors therein). However, in magmatic Ni-Cu-PGE systems, As is not a prerequisite for PGE enrichment. Base metal sulphides (BMS), which are volumetrically dominant compared to As phases, also show a strong affinity for PGE, leading to the formation of world-class Ni-Cu-PGE deposits, such as those hosted in the Bushveld Complex, where PGE are intimately associated with pyrrhotite and pentlandite devoid of As enrichment (Ballhaus and Sylvester, 2000; Barnes et al., 2006; Holwell and McDonald, 2007; Godel et al., 2007; Barnes et al., 2008; Godel and Barnes, 2008; González-Jiménez et al., 2010).

Other elements such as Bi, Sb and Te may also serve an important role in precious metal concentration in some magmatic sulphide deposits; Hutchinson and McDonald (2008) proposed that the chalcophile semimetals such as As, Sb, Bi, and Te act to lower the solubility of PGE in the base metal sulphides by inducing or promoting saturation of discrete PGE minerals ('PGM'), such as sperrylite (PtAs_2) and geversite (PtSb_2). Provided that the assimilation of sufficient As, Sb, Bi and Te into a silicate or sulphide melt occurs from surrounding host rocks, the saturation of PGM containing these metals may be an important process for PGE enrichment in otherwise low grade sulphides that do not undergo more conventional or better understood processes that typically concentrate the PGE to economically mineable levels (e.g., sulphide liquid fractionation at Sudbury; Ebel and Naldrett, 1996; Li and Naldrett, 1993).

Arsenic concentrations in basaltic melts are far too low for arsenide/sulfarsenide saturation to occur, therefore, contamination from an external source is critical (Wood, 2003). Contamination occurs when As is extracted from spatially associated sedimentary host rocks via diffusion or assimilation. The superheated SIC is thought to have

assimilated several hundred metres of footwall rocks (Prevec and Cawthorn, 2002). The contamination of sulphide melts by adjacent sedimentary rocks has been observed in the Turfspruit area of the Bushveld Complex, where As and Sb-rich footwall rocks are assimilated into the sulphide melt (Hutchinson and McDonald, 2008). Although the genesis of the Bushveld Complex and its PGE ores differs from that of the SIC, the local effects of As contamination are likely similar (i.e., the formation of As-minerals and concentration of PGE within As-minerals; Hutchinson and McDonald, 2008).

The Sudbury Igneous Complex (SIC), located along the boundary between the Superior and Southern Provinces in Ontario, Canada, hosts large reserves of magmatic Ni-Cu-PGE. The production of PGE from this system of deposits was recently ranked third in the world next to the Bushveld Complex, South Africa and Noril'sk, Russia (Farrow and Lightfoot, 2002; Ames and Farrow, 2007). Arsenic-bearing accessory minerals and mineral assemblages have been recognized in magmatic Ni-Cu-PGE sulphide ores at Sudbury in previous studies and occur almost exclusively in deposits of the South Range (Barlow, 1904; Lausen, 1930; Davidson, 1946; Hawley and Hewitt, 1948; Hawley et al., 1968; Aniol and Brown, 1979; Magyarosi et al., 2002; Dare et al., 2010a). Limited work on the spatial distribution shows that the As phases tend to be found along the margins of the sulphide ore bodies and commonly comprise intergrowths of Co-Ni-Fe sulfarsenides and arsenides (e.g., Hawley et al., 1968; Dare et al., 2010a). However, these textural associations have not been investigated in detail. The PGE tend to be hosted by PGM, namely PGE-bearing tellurides, bismuth-tellurides, arsenides and sulfarsenides, and not within BMS (Cabri and Laflamme, 1976, 1984; Cabri, 1988; Li et al., 1993; Farrow and Lightfoot, 2002; Huminicki et al., 2005; Dare et al., 2010a).

The PGM at Sudbury are generally considered to be late magmatic and/or may have hydrothermal origins (Cabri and Laflamme, 1976; Li and Naldrett, 1993; Li et al., 1993; Farrow, 1994; Farrow and Watkinson, 1997; Carter et al., 2001, 2009; Molnár et al., 2001; Farrow and Lightfoot, 2002; Magyarosi et al., 2002; Szentpéteri et al., 2002; Hanley et al., 2005; Péntek et al., 2008), although other studies have proposed or suggested an early magmatic origin for certain PGM (e.g., irarsite, hollingworthite; Szentpéteri et al., 2002; Dare et al., 2010a).

At the Garson mine, shear-hosted sulphide ores are commonly PGE-rich and host some of the highest concentrations of As in the Sudbury camp (avg. ~1030 ppm, range bdl – 36%; n=13727; Christopher Davis, personal communication). Compared to other deposits along the South Range in which As phases have been described (e.g., Creighton deposit; Dare et al., 2010a), As-bearing minerals at Garson are far more abundant and in some cases occur as minor phases (up to several vol%) within the sulphides. However, the ores at Garson show great variability in metal tenor and significant variations in PGE:As ratios from one section of the deposit to another which suggests a complex history. This study represents the first mineralogical and mineral chemical characterization of the PGE-As associations at the Garson Mine, performed with the intention of elucidating (i) the impact that As phases have on grade and metal ratio variation; (ii) the relative importance of magmatic, contact and regional metamorphic, and hydrothermal processes on As and PGE distribution; and (iii) the metallurgical/mineral processing implications of the PGE-As mineralogical associations.

2.1 Regional Geology

2.1.1 The Sudbury Structure and its ores

The Sudbury Structure is the result of a bolide impact that occurred at 1850 Ma and is the second largest known impact structure on Earth (Dietz, 1964; Naldrett and Hewins, 1984; Figure 2.1). The impact caused massive amounts of brecciation and shock- and heat-induced melting of the country rocks and lower crust (Naldrett and Hewins, 1984; Mungall et al., 2004; Lightfoot and Zotov, 2005). The elliptical (~60x27 km) Sudbury Structure lies in the Canadian Shield at the intersection of three large structural provinces: the Superior, Southern and Grenville (Dressler, 1984; Therriault et al., 2002). Regional-scale deformation associated with the Mazatzal-Labradorian and Penokean orogenic events modified the original circular impact crater and crystallizing/crystallized melt sheet to become a northeast-southwest trending oval shaped structure (Rousell, 1984; Figure 2.1).

These periods of deformation were also responsible for several phases of localized structural modification of the units of the SIC and its contact with its host rocks, hydrothermal activity and low-intermediate-grade metamorphism, most notably along the South Range (Rousell, 1984; Magyarosi et al., 2002). Important constituents of the Sudbury Structure include (i) the Whitewater Group (crater fill), comprised of the Onaping, Onwatin and Chelmsford Formations, (ii) the Sudbury Igneous Complex ('SIC'), and (iii) brecciated, contact metamorphosed, and partially melted Archean and Paleoproterozoic country rocks located in the footwall of the SIC (Therriault et al., 2002). Due to the crustal component incorporated into the melt sheet, the SIC is much more intermediate in composition (i.e., richer in SiO₂) than conventional layered mafic-

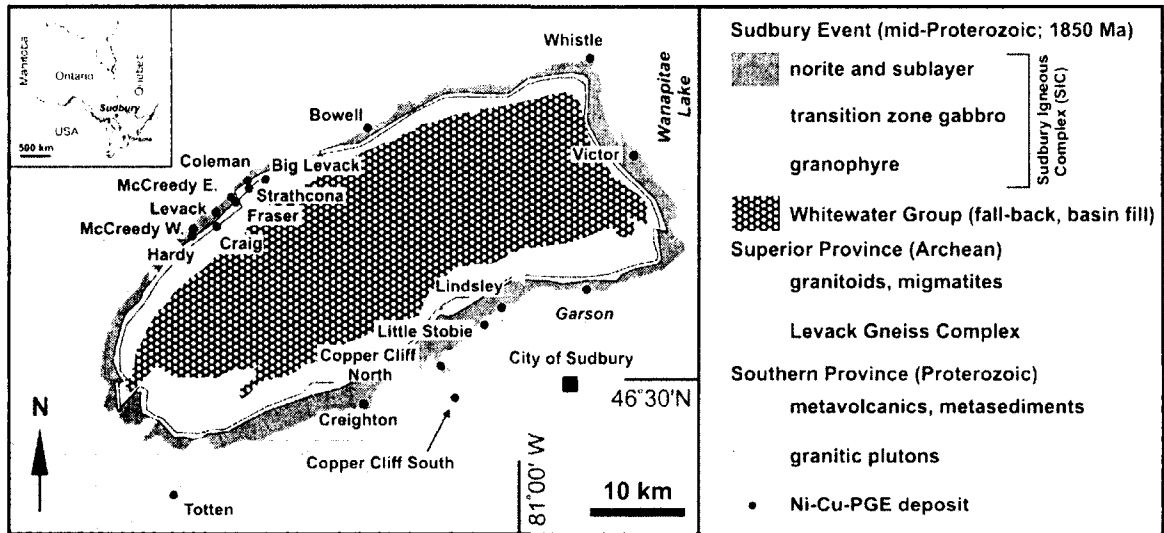


Figure 2.1: Geological map of the Sudbury Igneous Complex. The distribution of the offset dikes, sublayer, norite, transition zone gabbro, and granophyre, the location of Ni-Cu-PGE deposits (including the Garson Mine, the area of study), and associated country rocks are shown. Inset shows the location of Sudbury in central Ontario.

ultramafic intrusions (Naldrett and Hewins, 1984; Therriault et al., 2002; Mungall et al., 2004). The SIC is also different from melt sheets associated with other terrestrial impacts because of its great thickness, distinct layering, and exceptional degree of preservation (Therriault et al., 2002). Authors have described the SIC as a differentiated impact melt sheet (e.g., Naldrett, 1999; Therriault et al., 2002). The impact melt differentiated into the observable lithological units and became saturated in sulphide liquid (Naldrett, 1999). Rock types observed within the SIC include noritic and gabbroic mesocumulates topped with granophyric residue, and early diorite emplaced and crystallized into radial and concentric offset dykes in the country rocks. The South Range country rocks are comprised of Huronian-age metavolcanics (basalts and rhyolites), associated granitic plutons, and metasedimentary rocks (e.g., mainly greywackes and quartzites; Figure 2.1) of the Southern Province. The North Range country rocks are comprised of Archean-age granitoids and (dominantly) tonalitic gneisses of the Levack gneiss complex and Cartier granite of the Superior Province (Figure 2.1).

Several different types of Ni-Cu-PGE mineralization are observed at Sudbury (Naldrett et al., 1984; Farrow and Lightfoot, 2002; Farrow et al., 2005; Ames and Farrow, 2007). These mineralization types include (i) Cu-Ni-PGE-rich ores occurring in concentric or radially extensive dioritic offset dykes from the main complex where the ore is hosted in inclusion-rich quartz diorite (e.g., Kelly Lake and Totten deposits), (ii) contact style, PGE-poor, Ni-rich ores that are hosted within the basal units of the SIC (norite, sublayer) or in partially melted country rocks associated with heterolithic footwall breccia-rich depressions (“embayments”) at the base of the SIC (e.g., Whistle and Craig deposits, and Garson is a structurally modified version of this deposit type), and (iii)

footwall-style Cu-PGE-rich ores which comprise massive sulphide veins (“high-sulphide”) or blebby-disseminated sulphide ores (“low sulphide”) within shock-induced breccia (e.g., McCreedy PM zone, Podolsky).

While Naldrett (1984a, b) stated that the varying concentration of PGE, Ni and Cu in the deposits depends on the mass of silicate that a sulphide liquid interacts with (i.e., the R-factor); it has been shown that the variations in deposit types, Ni:Cu, and PGE ratios were due to fractional and/or equilibrium crystallization of monosulphide solid solution (MSS) with formation of an immiscible sulphide melt, leading to the formation of the relatively PGE-poor, Ni-rich contact ores and the Cu-PGE-rich variety footwall of ores (e.g., Li et al, 1992, Naldrett et al, 1999; Mungall, 2007). These characteristic magmatic processes produced MSS cumulate phases enriched in Fe, Ni, Co, Rh, Ru, Ir, and Os, and fractionated residual sulphide liquids enriched in Cu, Pt, Pd and Au. Footwall-style ores are thought to be a result of a separated, fractionated Cu-rich liquid crystallizing ISS, while contact-style deposits are the result of the accumulation of sulphides in embayments where MSS and ISS remain in contact with each other during crystallization (e.g., Li et al., 1992; Naldrett et al, 1999; Mungall, 2007). Continued fractionation and gravitational settling are thought to be responsible for the zoning observed in several Sudbury ores (e.g., Creighton and Frood deposits; Cheney and Lange, 1967; Naldrett, 1984a, b).

Studies of the South Range deposits and the SIC, in general have been numerous, while specific studies of the unique Garson deposit are lacking. Previous studies are limited to Hawley et al. (1968) and Aniol and Brown (1979). A current Ph. D. project on

the structural aspects of the Garson deposit is in progress (Mukwakwami et al., 2011a, 2011b).

2.1.2 Geology of the Garson deposit

The Garson deposit is a structurally modified contact style deposit located along the South Range and is hosted along the contact between norite of the SIC sublayer and the metasedimentary-metabasaltic rocks of the Huronian-age Stobie and McKim formations. The development and current morphology of the Garson deposit was strongly influenced by shear zones, and local enrichment in As is a key compositional characteristic of the ores. The Garson Fault is the main structure in the deposit and has a similar orientation as the main ore bodies (Cochrane, 1991), which are each hosted in one of four, east-west trending shear zones (named the #1, #2, #3, and #4 shears). The host rocks have experienced several phases of deformation which led to the fragmentation, separation and overturning of the ore zones and current orientation dipping steeply to the south (Figure 2.2; Figure 2.3; Mukwakwami et al, 2011a). The thickness of the current sulphide ore zones within each shear ranges widely from a few centimetres to ~60 metres, averaging 3 to 15 metres in width (Figure 2.2, Figure 2.3). The main lithologies observed at the Garson Mine are: (i) metavolcanics (basalts) and metasediments (e.g., greywackes, quartzites) of the Stobie and McKim formations, serving as the main host rocks to the ores, (ii) the SIC sublayer: a noritic, inclusion-rich unit, located at the base of the SIC and encloses ore in some areas, (iii) Sudbury breccia, comprised of impact (shock) brecciated/melted footwall material dispersed through the host rocks; and (iv) an olivine diabase dyke which intersects the shear zones and ore bodies. Of the four main shear

zones, #1 shear is the most economically important mineralized shear zone at Garson due to its Ni high grade and tonnage. At depths less than 4000 ft, the #1 shear lies at the contact of the footwall sublayer norite and the metasedimentary/metavolcanic rocks of the hanging wall (Figure 2.2). From the 4000 level and below, the #1 shear is hosted entirely within metavolcanic rocks and dips steeply to the south (Figure 2.2). The #2 and #3 shears converge with #1 shear below the 1000 level and below the 2800 level, respectively (Figure 2.2). The #2 shear is hosted along the contact between the sublayer norite and metasediments, while the #3 shear is hosted entirely within the sublayer norite (Figure 2.2). The #2 and #3 shear ore bodies are minor contributions to the overall Garson deposit tonnage and are not currently being mined. The #4 shear, a volumetrically significant ore body, strikes east-west and dips steeply to the south. It is bound by metavolcanics in its hanging wall and norite along its footwall, a reversal of the #1 shear hanging wall and footwall units.

Several ore types are observed at the Garson deposit (Figure 2.4; Figure 2.5). The main ore types observed in this study are inclusion-rich massive sulphide (INMS), disseminated sulphide ore (DISS) and massive sulphide (MASU; Figure 2.4, Figure 2.5). Other minor ore types include contorted schist inclusion sulphide (CSIS), breccia sulphide (BXSU), gabbro-peridotite inclusion sulphide (GPIS), disseminated (DISS), and ragged disseminated sulphide (RDSU). The ore types vary greatly at the metre scale with MASU occurring in the center of the ore bodies and INMS, DISS and other ore types occurring along the margins of the ore bodies (Figure 2.4). The ore types can grade into one another gradually or sharply. Volumetrically minor, chalcopyrite-rich ore is characteristic of an area known as the Ramp and is located adjacent to the main shears

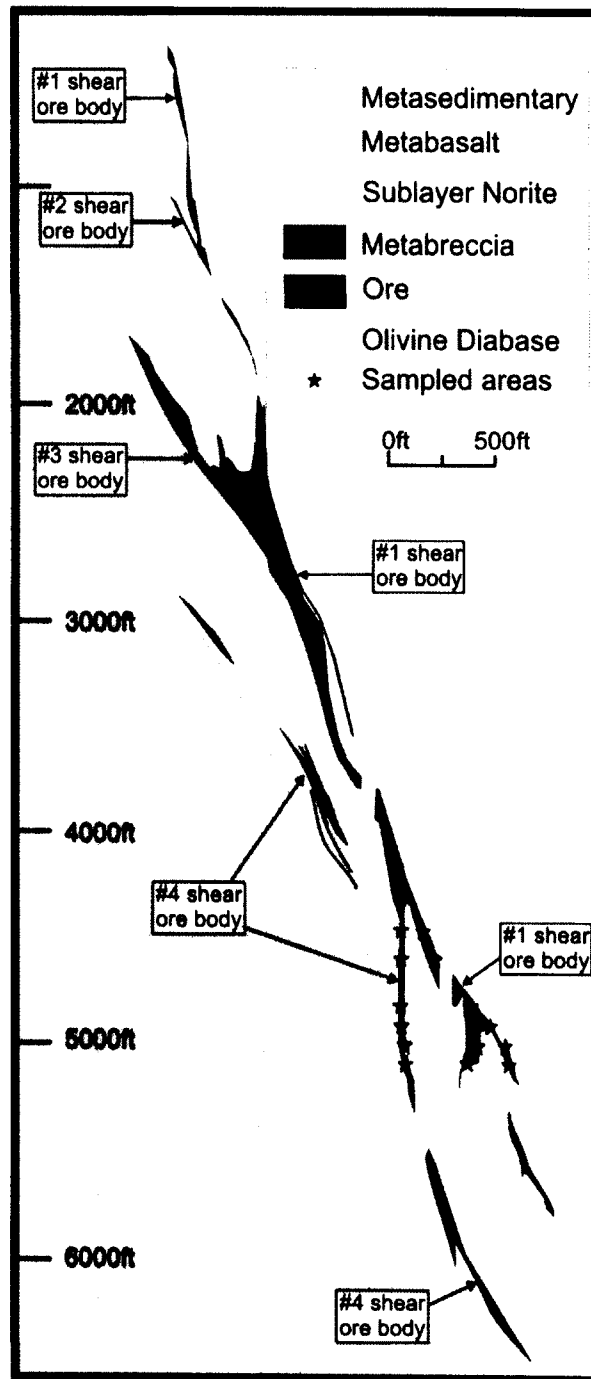


Figure 2.2: Cross section of the Garson ore bodies facing east (2640 E section). The current orientation is the result of overturning of the ore bodies, which was originally shallowly north-dipping. The #1 and #4 shear zones are hosted at the contact of sublayer norite and metabasalts/metasediments. Below the 4370 level, the #4 shear is hosted entirely in metabasalt. Modified from Aniol and Brown (1979). Stars indicate sampled levels within #1 and #4 shear.

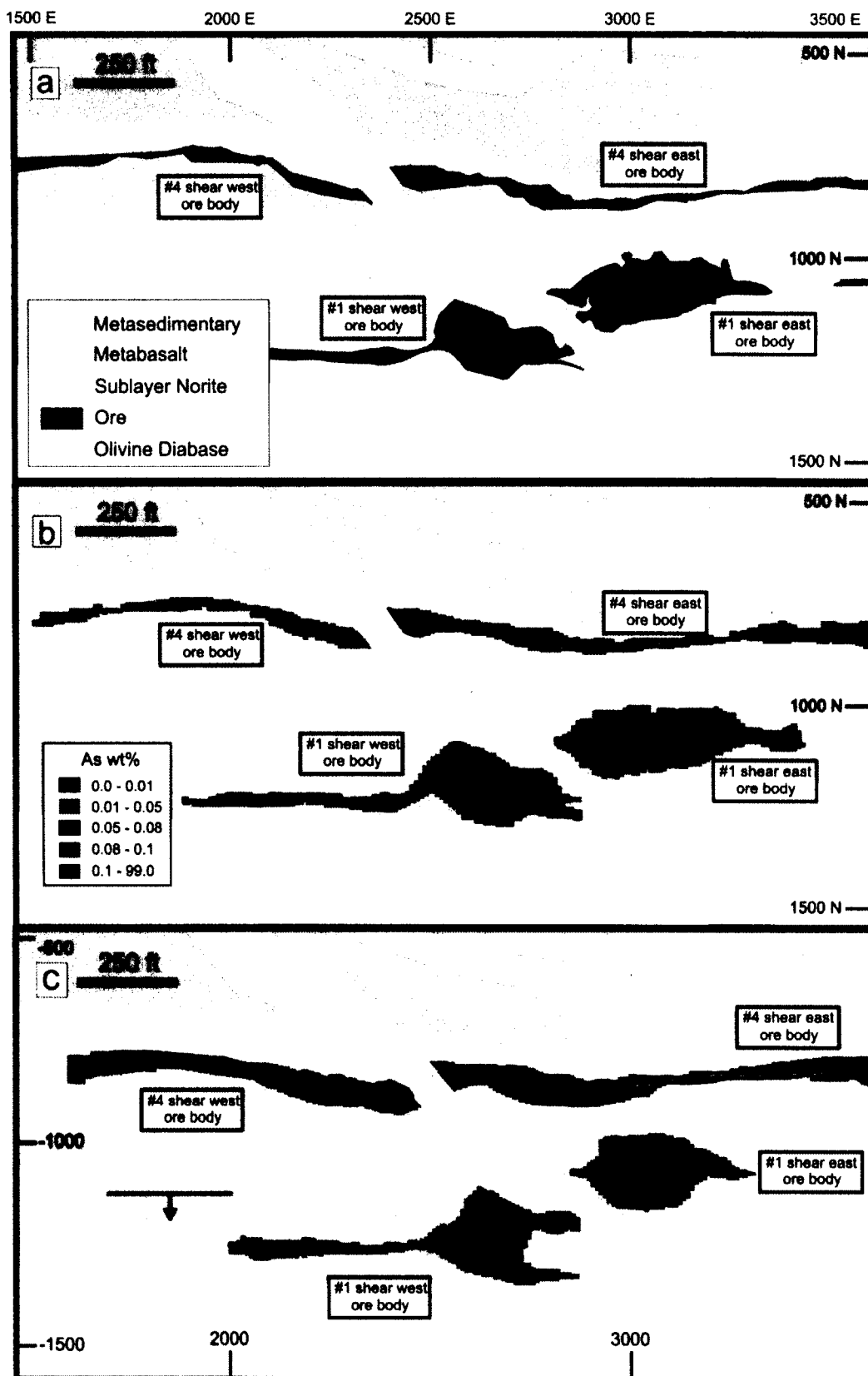


Figure 2.3 (previous page): Plan view of shear zones with arsenic and PGE grades. a) Plan view of the #1 and #4 shear-hosted ore bodies on the 5000 level; b) Plan view of the #1 and #4 shear-hosted ore bodies showing As grades on the 5000 level; c) Plan view of the #1 and #4 shear-hosted ore bodies showing As grades on the 5100 level. Discontinuous high As regions in the ore are present mainly along the current hanging wall (former footwall) and generally not on both sides of the ore zones. Note that on these levels sulphide ore bodies are exclusively hosted in metabasalt and not in metasediment (see text for explanation). Line and arrow indicate current dip direction.

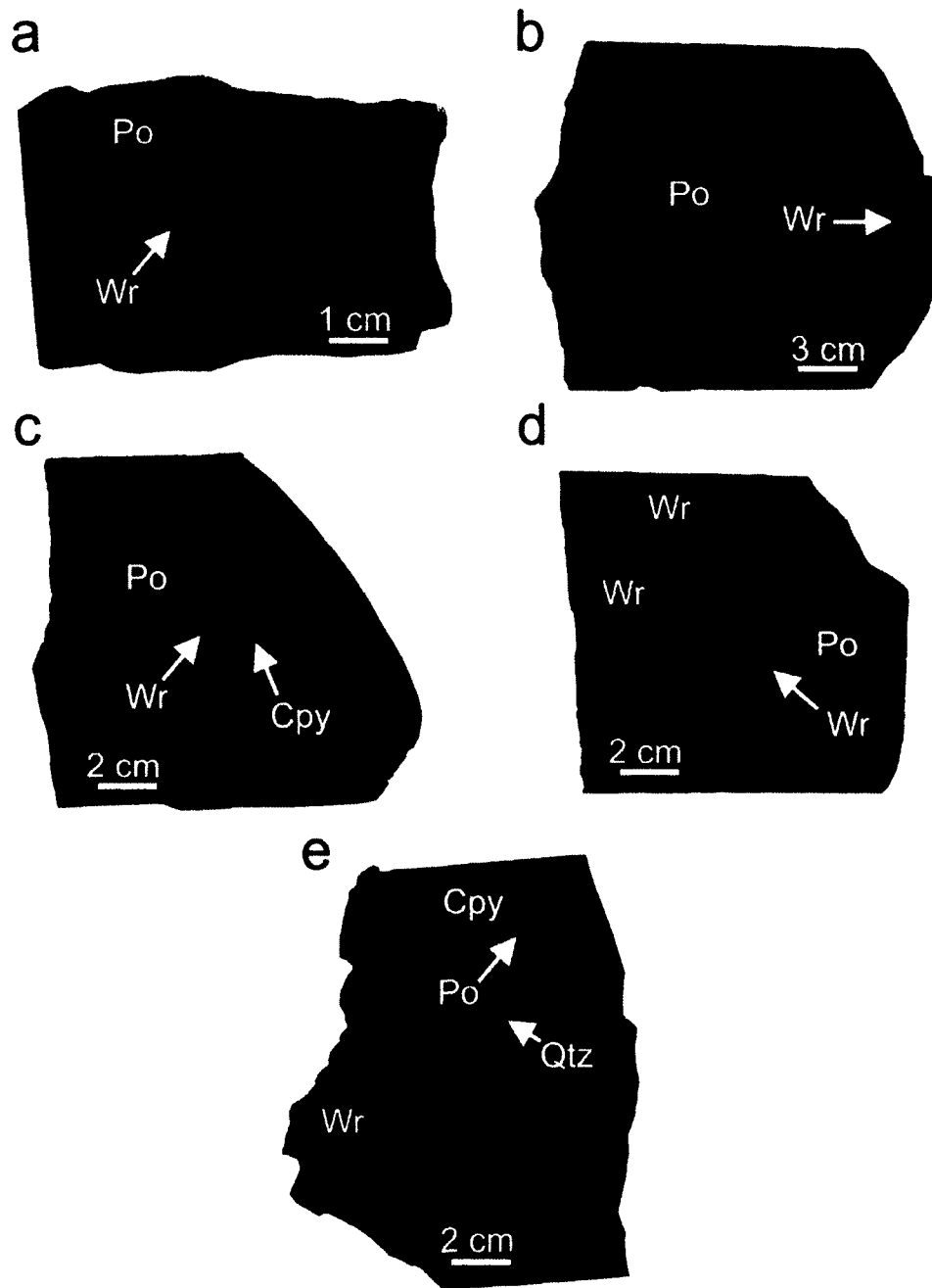


Figure 2.4: Major and minor ore types in hand sample. a) Volumetrically minor "contorted schist" ore containing foliated fragments of wall rock and sulphides; b) Massive sulphide ore containing massive Po, less than 10% wall rock inclusions by volume; c) Inclusion-rich massive sulphide containing Po and Cpy, with more than 10% inclusions; d) Inclusion-rich massive sulphide with abundant wall rock inclusions (20%); e) Volumetrically minor chalcopyrite-rich ore from the Garson ramp; Abbreviations: Cpy= chalcopyrite; Qtz= quartz; Po= pyrrhotite; Wr= wall rock.

(Figure 2.4e). The Ramp ore is hosted mainly along the contacts between the Frood-Stobie Breccia belt, metavolcanics, olivine diabase and norite. Although some assay data was acquired and is discussed below, the area was not a major focus of this study.

2.2 Sampling and analytical methods

The proportions of samples obtained for this study tend to be biased toward the INMS type. This is because most samples were gathered in mined-out areas from the margins of the ore bodies. Where possible, fresh rock faces containing MASU ore were also sampled. Approximately 150 thin sections were made from 110 chip samples gathered on the 4470, 4600, 4800, 4900, 5000 and 5100 levels at the Garson Mine (Figure 2.2). Special attention was made to sample stopes with varying As and PGE grades as indicated in company assay databases (i.e., areas with high As-high PGE, high As-low PGE, low As-high PGE, low As-low-PGE). Additionally, several large chip samples (30-45 cm width) were sectioned into thin sections and chip samples in order to determine the hand sample-scale variations in As and PGE grade and mineralogy at the sub-metre scale. Several chip samples were taken from an active mining face to determine variation in the same characteristics on the stope scale.

2.2.1 Bulk rock analyses of the ores

The chip samples were prepared for bulk rock assay to be performed at ALS Minerals, Sudbury, Ontario. The bulk rock samples all had corresponding thin sections made to determine the possible mineralogical controls for various metals. Samples for assay were prepared by cutting larger chip samples into multiple smaller ($\sim 8\text{cm}^3$) blocks. The

samples were then packaged and delivered to be assayed. Each sample was crushed to a size of 10 mesh (2mm) using Boyd crusher-rotary sample divider combo unit and then ring pulverized to 85% -200 mesh (74 μ m).

All samples were analyzed for Cu, Ni, Co, Fe, S, As, Pb, Zn, Sb, and Bi using the ME-ICP81 procedure, an ICP-MS based method. Sample masses of 0.2g were fused with a sodium peroxide flux (2.6g) at 670°C in a furnace and then cooled and dissolved in 30% HCl solution. Nickel, Cu, Co, Fe, S, As, Pb, Zn, Sb, and Bi and in solution were determined using a Varian Vista (ICP-OES). Gold, Pt and Pd were determined by a Pb-fire assay/ICP-MS technique on 30g of sample. Silver was determined by aqua regia dissolution/atomic absorption spectroscopy on 2g samples.

2.2.2 Trace/accessory mineral identification and analysis

Scanning electron microscopy (SEM) was used extensively to image and map out the distribution of, and, with electron dispersion spectroscopy (EDS) to analyze the chemical composition of, As-bearing and other trace/accessory phases observed in the Garson ores. Samples were characterized with a Leo 1450 VL SEM (Saint Mary's University, Nova Scotia) at an accelerating voltage of 20kV and a beam current ranging from 5-20 nA. The SEM was also used to estimate modal abundance through point counting and grain size determinations from BSE images. Thirty-three samples were chosen for detailed grain and trace phase modal analysis within the ores (Supplementary Table 1, Appendix A).

2.2.3 Microprobe analysis of As carriers

Arsenides and sulfarsenides were analyzed by electron microprobe (EMP; Dalhousie University, Nova Scotia). Samples containing phases analyzed by microprobe include M19, 20 (# 4 east 4900L), M32, 46 (#1 west 5000L) M66 (#4 west 5000L), M81-86, 88, 89 (#1 west 5100L) 91 (#4 west 5100L), M105-107, 110 (#4 west 4470L; Figure 2.2, Figure 2.3; Tables 2.1-2.5, 2.11, Appendix A). The instrument used was a JEOL 8200 electron microprobe operated at an accelerating voltage of 15 kV, a beam current of 20 nA and an on-peak count time for each element of 10s. Standards used for calibration of analyte sensitivities and peak position determinations were in-house, stoichiometric pyrrhotite (Fe), pentlandite (Ni), chalcopyrite (Cu), arsenopyrite (As), and cobaltite (Co).

2.2.4 Trace element analyses of As-carriers and base metal sulphides

Laser ablation inductively-coupled plasma mass spectroscopy (LA-ICPMS) was performed at the Geological Survey of Canada, Ottawa, Canada (Tables 2.1-2.5, Appendix A). Samples were chosen based on their bulk As and PGE concentrations, the presence of arsenic-bearing minerals identified during preliminary SEM and optical petrographic analysis, and priority of company mine plans.

Sulphides, sulfarsenides and arsenides were analyzed for the following isotopes: S³⁴, Fe⁵⁷, Co⁵⁹, Ni⁶⁰, Ni⁶¹, Zn⁶⁶, As⁷⁵, Se⁷⁷, Ru⁹⁹, Ru¹⁰¹, Ru¹⁰², Rh¹⁰³, Pd¹⁰⁵, Pd¹⁰⁶, Pd¹⁰⁸, Ag¹⁰⁷, Ag¹⁰⁹, Cd¹¹¹, Sn¹¹⁸, Sb¹²¹, Te¹²⁵, Ta¹⁸¹ Re¹⁸⁵, Os¹⁸⁹, Ir¹⁹³, Pt¹⁹⁵, Au¹⁹⁷, Hg²⁰², Pb²⁰⁶, Pb²⁰⁸ and Bi²⁰⁹. Other isotopes were also measured during LA-ICPMS analyses to monitor possible contamination by host silicate minerals (Si²⁹, Sr⁸⁸, Y⁸⁹ and Zr⁹⁰). Generally, the central portions of large grains were chosen [typically larger than ~35 µm and visibly free

of platinum-group mineral (PGM) inclusions] to ensure that signals obtained were from uncontaminated, pure phases. A laser spot size of up to 52 μm was used whenever possible to obtain higher count rates. Each measurement was performed at a fluence of 4 mJ/cm^2 (attenuated to 4%), and at a pulse rate of 10 Hz. Owing to the unreasonably long washout times and contamination problems associated with measuring As, analyses of As-rich phases were obtained at the end of the session to avoid elevated backgrounds due to transient contamination (and therefore, higher limits of detection for subsequent analyses) when analyzing the BMS. Synthetic standards used for calibration of analyte sensitivities were a basaltic glass (GSE-1; produced by the USGS), a chemically precipitated sulphide (MASS-1; produced by the USGS), and pyrrhotite and a quenched NiS fire assay fusion mixture (Po726 and Po689, produced at Memorial University, St. John's, Newfoundland). Data reduction was performed using Glitter™ data reduction software for the laser ablation microprobe. Intervals that showed prolonged and consistent count rate intensities (i.e., excluding any short-lived, high intensity peaks representing PGE mineral inclusions) were integrated during data reduction. Incorporation of high intensity spikes during data reduction resulted in highly variable trace element concentrations (e.g., PGE, Te, Bi, Ag) from one spot to another within a single mineral grain. In comparison, exclusion of these spikes during data reduction yielded consistent and very narrow concentration ranges within single grains (see below). Internal standardization utilized the Fe content of BMS based on stoichiometry and the Fe or Ni of arsenides/sulfarsenides based on EMP analyses. Manual corrections for argide interferences were performed. High purity (99.999% Cu) copper metal was analyzed to determine, and manually correct for, the interference of $\text{Cu}^{63}\text{Ar}^{40}$ on Rh^{103} and $\text{Cu}^{65}\text{Ar}^{40}$.

on Pd^{105} , where necessary. Other interferences (Cd^{106} on Pd^{106} ; $\text{Zr}^{90}\text{O}^{16}$ on Pd^{106} ; $\text{Y}^{89}\text{O}^{16}$ on Pd^{105} ; and $\text{Zn}^{66}\text{Ar}^{40}$ on Pd^{106}) were determined to be negligible by monitoring and comparing count rates and calculated concentrations of potentially affected isotopes to those isotopes of the same element with no known interferences.

2.2.5 Mass balances

Petrographic analysis of 74 thin sections (Supplementary Table 1, Appendix A) was performed in order to determine major base metal sulphide, sulfarsenide and arsenide abundances to predict the bulk rock As, Pt and Pd in each corresponding sample. Major phase abundances (pyrrhotite, chalcopyrite, pentlandite, As-minerals and silicate gangue) were reported from each ore type sample (74 samples) in Figure 2.5 as modal (area) per cent based on visual identification by petrographic microscope. Modal per cent values were then converted to weight per cent using standard mineral specific gravities as well as an average specific gravity for wallrock fragments of 3.25. Combining LA-ICPMS and EMP data for As, Pt and Pd from major sulphide and sulfarsenide/arsenide phases with the determined weight per cent abundances of these minerals, the proportion of each metal (As, Pt, and Pd) hosted in each mineral phase was calculated as well as a predicted assay value for each metal. Predicted values were then compared to the corresponding bulk rock analyses for As and the PGE in order to determine the effectiveness of using thin section and hand sample petrography for mass balance determinations and grade control (Supplementary Table 1, Appendix A). For those samples in which PGE mass balances were performed (33 samples), modal analysis of PGE was done by SEM-BSE,

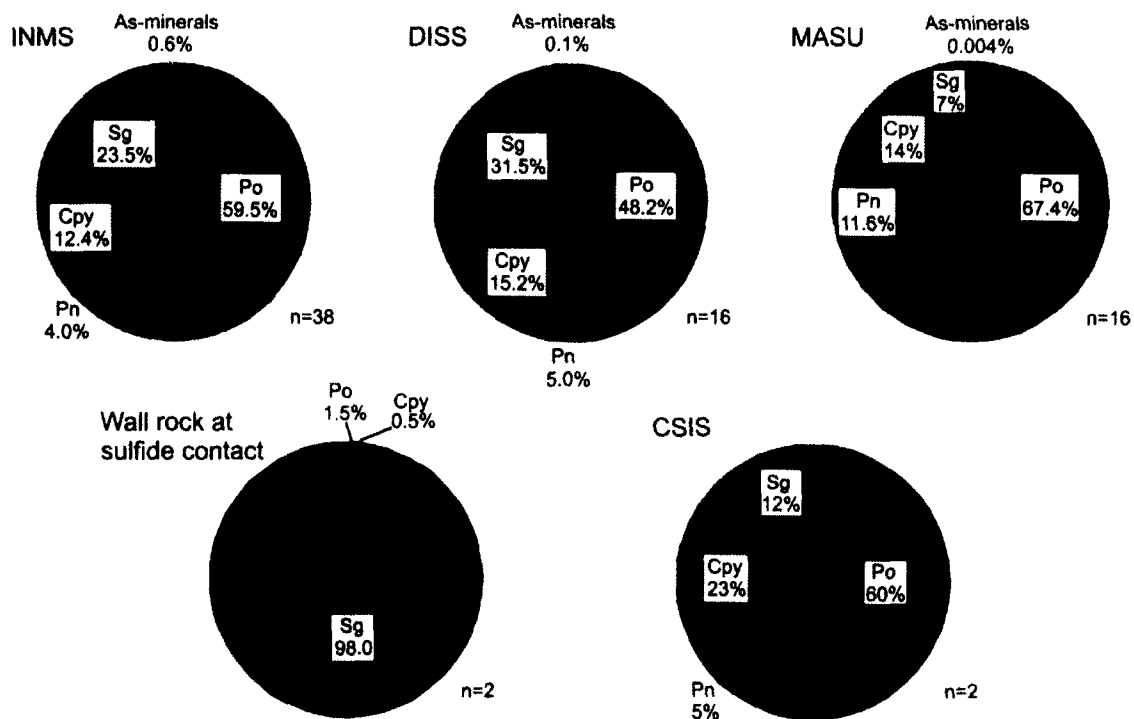


Figure 2.5: Distribution of major phases, As-minerals (CGSS-GGSS-nickeline), and silicate gangue by ore type. On average, there is a higher abundance of As-minerals in DISS and INMS than in MASU. Ore type abbreviation: CSIS=contorted schist sulphide; DISS= disseminated sulphide; INMS= inclusion-rich massive sulphide; MASS= massive sulphide. Mineral abbreviation: CGSS= cobaltite-gersdorffite solid solution; Mineral abbreviations: Cpy= chalcopyrite; GGSS= glaucodot-gersdorffite solid solution; Pn= pentlandite; Po= pyrrhotite; Sg= silicate gangue; n=number of samples studied/analyzed.

whereby within representative areas (with specific μm^2 measured) PGM grain dimensions were measured and modal % combined with published mineral compositions or quantitative analyses obtained by SEM were used to predict their contributions to total Pt or Pd grade. To account for Pt and Pd occurring in BMS, sulfarsenides and arsenides, LA-ICPMS values were averaged for each PGE. If the mass balances were being performed on samples with corresponding LA-ICPMS data, then values specific to those samples were used. If mass balances were performed on samples without corresponding LA-ICPMS data, then an average from the corresponding shear or level.

2.3 Results

2.3.1 Mineralogy of major base metal sulphide phases

Major ore styles (INMS, MASU, and DISS; Figure 2.5) were observed in both #1 and #4 shears. Of the samples sent out for bulk rock analysis, the proportion of each ore type represented is as follows: INMS (43%), DISS (34%), MASU (11%), and CSIS (2%) as well as host rocks sampled at varying distances from sulphide contacts (10%).

The ores are primarily composed of pyrrhotite with varying amounts of pentlandite and chalcopyrite (Figure 2.5). Based on samples gathered for this study, MASU is comprised of mainly pyrrhotite (avg. ~67 vol%), pentlandite (~12%) and chalcopyrite (14%), and contain abundant host rock fragments and silicate mineral grain inclusions as well (<10%; avg. ~7%; Figure 2.4, Figure 2.5). INMS comprises of similar proportions of major sulphides with significantly more inclusions of silicates and rock fragments (>10%, avg. ~23.5%; Figure 2.4, Figure 2.5). Disseminated sulphide ores are characterized by still higher proportions of silicates and rock fragments (avg. ~32%; Figure 2.4, Figure 2.5).

Pyrrhotite occurs as massive polycrystalline aggregates, but can also occur as disseminated grains hosted in chalcopyrite and in host rocks/silicates. Pyrrhotite aggregates comprise the matrix in most of the samples and have poorly defined grain boundaries. The massive pyrrhotite contains inclusions of pentlandite, chalcopyrite, and magnetite with lesser sphalerite, galena, arsenides, sulfarsenides, and other trace/accessory phases as well as abundant inclusions of host lithology fragments, silicate crystals (small inclusions or recrystallized silicate remnants) and quartz vein fragments. In samples where pyrrhotite is disseminated, it forms ragged, anhedral grains and often shows open space-filling textures within silicates in the host rocks or occurs as inclusions within other sulphides. Pyrrhotite grain size ranges greatly from sample to sample and within single samples from μm to cm-sized grains. Pentlandite most commonly occurs as μm to mm wide stringers that occur along pyrrhotite grain boundaries. Like pyrrhotite, pentlandite grains commonly contain host rock fragments, silicate grains and quartz. In many cases, pentlandite stringers commonly rim pyrrhotite grains. Pentlandite also occurs as anhedral, equant to sub-equant porphyroblasts (“eyes”) in pyrrhotite and chalcopyrite that range from $\sim 100\ \mu\text{m}$ to $\sim 1\ \text{cm}$ in size. Pentlandite exsolution lamellae in pyrrhotite are present but uncommon.

Chalcopyrite occurs high abundances in some samples. It occurs as large grains showing mutual (equilibrium) boundaries with, or as disseminated inclusions in, pyrrhotite. Chalcopyrite also exhibits secondary textures (e.g., space filling and net texture, post-dating pyrrhotite and pentlandite crystallization) in pyrrhotite and host rocks. Chalcopyrite is often abundant in wall rocks adjacent to massive sulphide.

Inclusions of metabasalt, metasedimentary host rocks, and quartz fragments (from brecciated, pre-sulphide metamorphic quartz veins) are ubiquitous within ore types found at the Garson deposit (Figure 2.5). The host rock fragments are rich in amphibole such as hornblende, ferrotschermakite (Mukwakwami et al., 2011a; 2011b) and minor riebeckite, which commonly occur as tabular crystals. In the metasedimentary rocks, a strong foliation is observed. Metabasalts are characterized by abundant prismatic black amphibole porphyroblasts (up to 3 mm) in a medium-dark green matrix of amphibole-quartz-biotite-plagioclase-ilmenite±garnet (Mukwakwami et al., 2011b). Metasedimentary rocks observed at Garson are typically metamorphosed greywackes that are massive, fine-grained and dark grey in hand sample (Mukwakwami et al., 2011b). The metagreywackes are composed of 60-70% quartz, 10-20% plagioclase, 15-25% ferrotschermakite intergrown with biotite.

2.3.2 Trace elements within major sulphide phases

The LA-ICPMS results show that the major sulphides contain consistently very low concentrations of As and other deleterious trace metals (e.g., Cd, Sb, and Pb), and are generally poor in PGE (Tables 2.1-2.6, Appendix A), demonstrating that they do not contribute significantly to bulk rock abundances of these elements.

2.3.2.1 Pyrrhotite

Pyrrhotite has As concentrations consistently below detection limit (bdl), with rare values above detection limits reaching up to ~12 ppm (see section 2.4.8 *The effects of PGE and accessory mineral micrograins*). Pyrrhotite shows a wide range in dissolved Ni

and Co contents, from 0.2 to 1.1 wt% and 3 to 240 ppm, respectively (Table 2.1, Appendix A). Cobalt-poor pyrrhotite and pentlandite are consistently found in nickeline-rich samples (samples A86-91 #1 west shear 5000L; A59-61; #1 west shear 5100L; Table 2.1, 2.2, Appendix A). Concentrations of Se in pyrrhotite are consistent (up to 181 ppm, avg. 108 ppm, n=117).

2.3.2.2 Pentlandite

Pentlandite shows a wider range of As than reported in pyrrhotite. Whereas many pentlandite analyses report As below detection limits, average As concentration in pentlandite with detectable amounts is ~1.5 ppm, with a range from bdl to 28 ppm; anomalously high values are due to the presence of micrograins of sulfarsenides or arsenides (Table 2.2, Appendix A). Arsenic concentrations in pentlandite are highest in stope 2424 (#4 west 4470L) and stopes 1291 (#1 west 5000L) and 1321 (#1 west 5100L). Cobalt values for pentlandite range from 500 ppm up to wt%, with the lowest Co values occurring in arsenide-rich samples (#1 west shear 5000L). Pentlandite in nickeline-rich samples from two stopes (1291 of 5000L #1 west shear and 1321 of 5100L #1 west shear; Table 2.7, 2.11, Appendix A) have consistently higher Pd than other samples, ranging from 8-22 ppm. Pentlandite from nickeline-absent samples has much lower concentrations of Pd, similar to the concentrations found in all other samples (Table 2.2, Appendix A). Pentlandite has relatively consistent values of Pd, ranging from 0.1 - 2.3 ppm (avg. ~1 ppm). The highest values of Ru in pentlandite were observed in the nickeline-free sample from stope 1291 (#1 west shear 5000L), while pentlandite from all other samples have values for Ru above detection limit, ranging 0.03 - 2.12 ppm.

Tellurium concentrations tend to increase with depth, while Rh concentrations decrease with depth (Table 2.2, Appendix A). Antimony concentrations are low in pentlandite (bdl – 1.2 ppm; Table 2.2, Appendix A). Concentrations of Se in pentlandite are consistent (up to 193 ppm, avg. 105, n=76).

2.3.2.3 Chalcopyrite

Chalcopyrite shows As values consistently below detection limit, with highest values reaching only 7 ppm (#1 west shear 5000L; higher values are affected by micrograins; Table 2.3, Appendix A). Chalcopyrite contains varying amounts of Ag, with an average of 4 ppm and a range from bdl - 25 ppm. Chalcopyrite has low Sb concentrations, ranging from bdl - 1.3 ppm, but shows slightly higher concentrations (3-7 ppm) in stope 2774 (4900L #4 east; Table 2.3, Appendix A). Gold, Pt, Cd and Se concentrations in chalcopyrite show an overall increase with depth (Table 2.3, Appendix A). Palladium and Zn tend to be consistent with depth, while Ru shows an overall decrease with depth (Table 2.3, Appendix A). Other elements such as Ag, Ir and Os show no trends and values are variable (Table 2.3, Appendix A). Concentrations of Se in chalcopyrite (up to 200 ppm, avg. 106 ppm, n=108) are consistent and similar to other base metal sulphides in the Garson ores.

2.3.3 Mineralogy of the sulfarsenides and arsenides

2.3.3.1 General characteristics

The major As-bearing phase in the Garson ore bodies is cobaltite-gersdorffite solid solution (CGSS) with glaucodot-gersdorffite solid solution (GGSS) as a minor phase.

Macroscopic CGSS grains can be observed in thin section at low magnification or in hand sample, and display a wide range in grain size from ~20 μm to several mm (avg. ~500 μm). The grains are dull grey, anhedral to euhedral and commonly show resorbed/corroded cores described originally as “spongy” by Hawley et al. (1968; Figure 2.6a, c). Modal abundance of CGSS can reach up to 2 vol% (Table 7, Appendix A). Figure 2.7 and Table 2.8 (Appendix A) show a wide range of CGSS-GGSS compositions in Ni-rich, Co-poor compositions near the gersdorffite end-member to values close to the cobaltite/glaucodot end-member. Concentrations of Co and Ni in CGSS vary significantly vertically through individual ore bodies (0.3 to 25% Co, and 5 to 30% Ni) but also within single samples and single grains (0.3% to 22% Co, and 9 to 23% Ni; Figure 6a, Box 2; Table 2.8, Appendix A). The compositions of CGSS-GGSS have a range of $\text{Fe}_{0.11-0.41}\text{Co}_{0.01-0.73}\text{Ni}_{0.15-0.77}\text{As}_{0.71-1.23}\text{S}_{0.60-1.06}$. The compositional range of CGSS and GGSS show significant overlap, and they are only distinguished from one another by their crystal morphology as observed in thin section or by SEM-BSE, and by grain size (see below). The grains are often compositionally zoned from denser (brighter in BSE) Ni-rich areas to Co-rich (Figure 2.8a, Box 2). The grains also contain inclusions of nickeline and a variety of trace/accessory phase (Figure 2.8; Box 2). CGSS is hosted as inclusions in pyrrhotite (35%), chalcopyrite (11%), pentlandite (3%), silicate gangue (3%), as well as commonly occurring along boundaries between pyrrhotite and chalcopyrite (5%), pentlandite (15%), or silicate gangue (22%). The remaining 6% of CGSS grains are hosted along grain boundaries between combinations of these minerals. It should be noted that even in chalcopyrite or silicate gangue-rich samples, minor amounts of pyrrhotite are always spatially associated with CGSS. Of the 57 samples that were studied in detail by

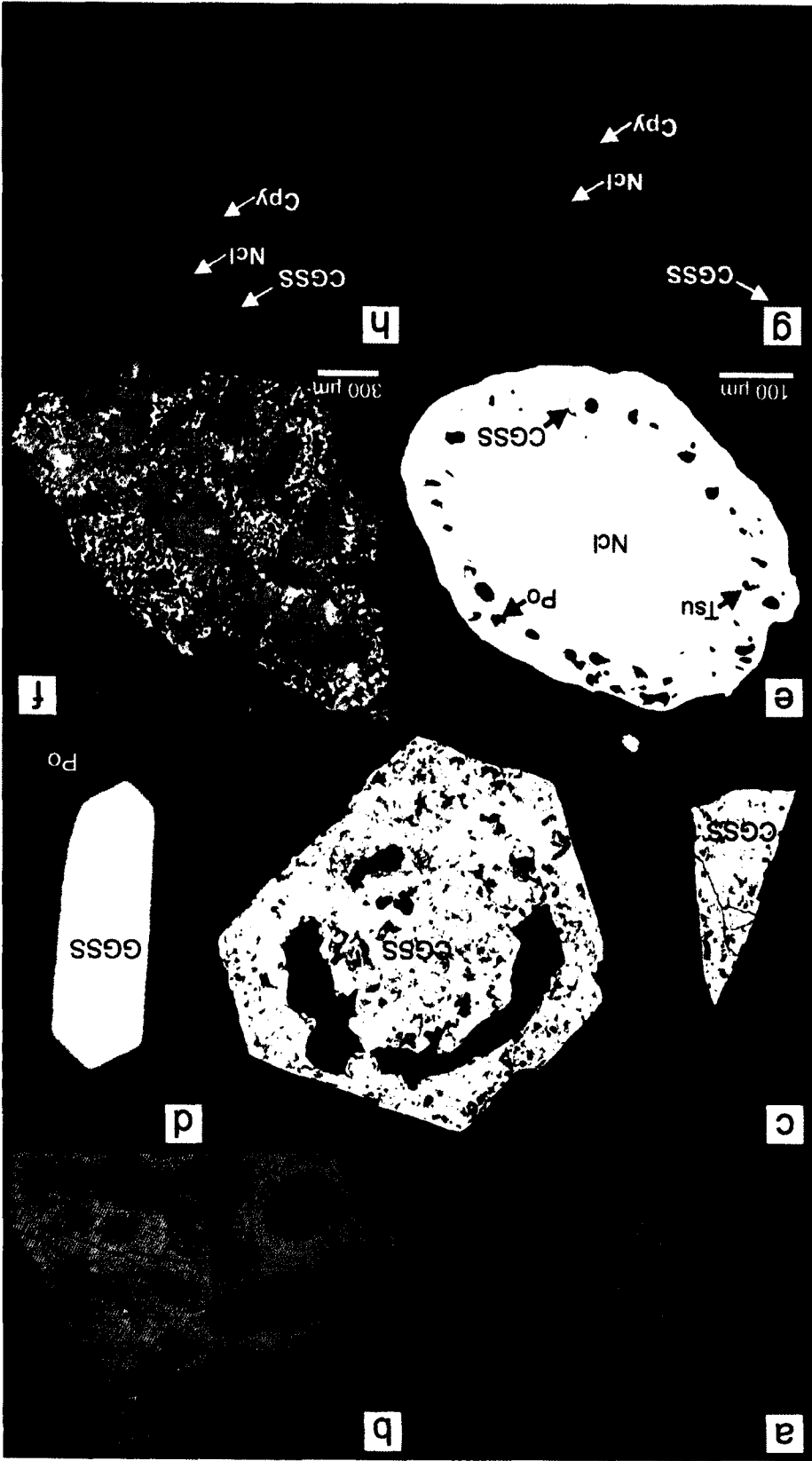


Figure 2.6 (previous page): Reflected light photomicrographs and SEM back-scattered electron images of arsenide and sulfarsenides. a) Reflected light photomicrograph of a large CGSS grain containing abundant nickeline inclusions; b) Reflected light photomicrograph showing an enlargement of frame a); c) Back-scattered image of a large, euhedral CGSS grain with a resorbed or “spongy” core; d) Back-scattered image of a GGSS grain showing characteristic habit in comparison to CGSS (see frame c); CGSS and GGSS have overlapping compositional ranges and are only distinguished from one another by their crystal system and grain size; e) Back-scattered image of a rounded grain of Ncl with abundant inclusions of CGSS, Po and Tsu occurring in the rim, CGSS formed before or synchronously with Ncl; f) Back-scattered image of a composite grain of GGSS and Ncl showing complex their intergrowth; g) and h) Back-scattered images of Cpy-Ncl intergrowths with minor CGSS. Mineral abbreviations: CGSS= cobaltite-gersdorffite solid solution; Cpy= chalcopyrite; GGSS=glaucodot-gersdorffite solid solution; Ncl= nickeline; Pn= pentlandite; Po= pyrrhotite; Tsu= tsumoite.

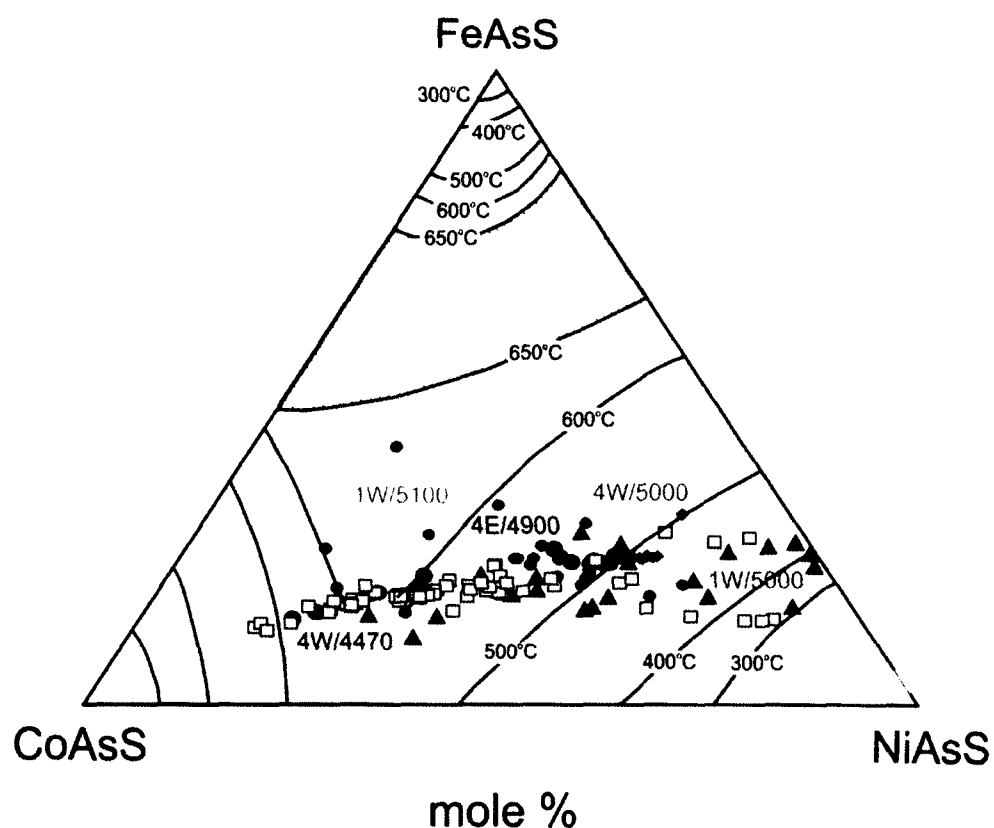


Figure 2.7: CoAsS-NiAsS-FeAsS ternary diagram (section at 650°C) showing range of composition of CGSS-GGSS grains. CGSS-GGSS compositions analyzed from the Garson ores range significantly from Co- to Ni-end members but there is considerable compositional overlap between encountered compositional ranges at different levels and in different shears. Numbers correspond to shear and level in feet, in either east or west areas of the shears. The hatched field shows the intersection of the immiscibility gap at the 650°C section, and isotherms lying on the solvus surface. Modified after Klemm (1965) and Hanley (2007).

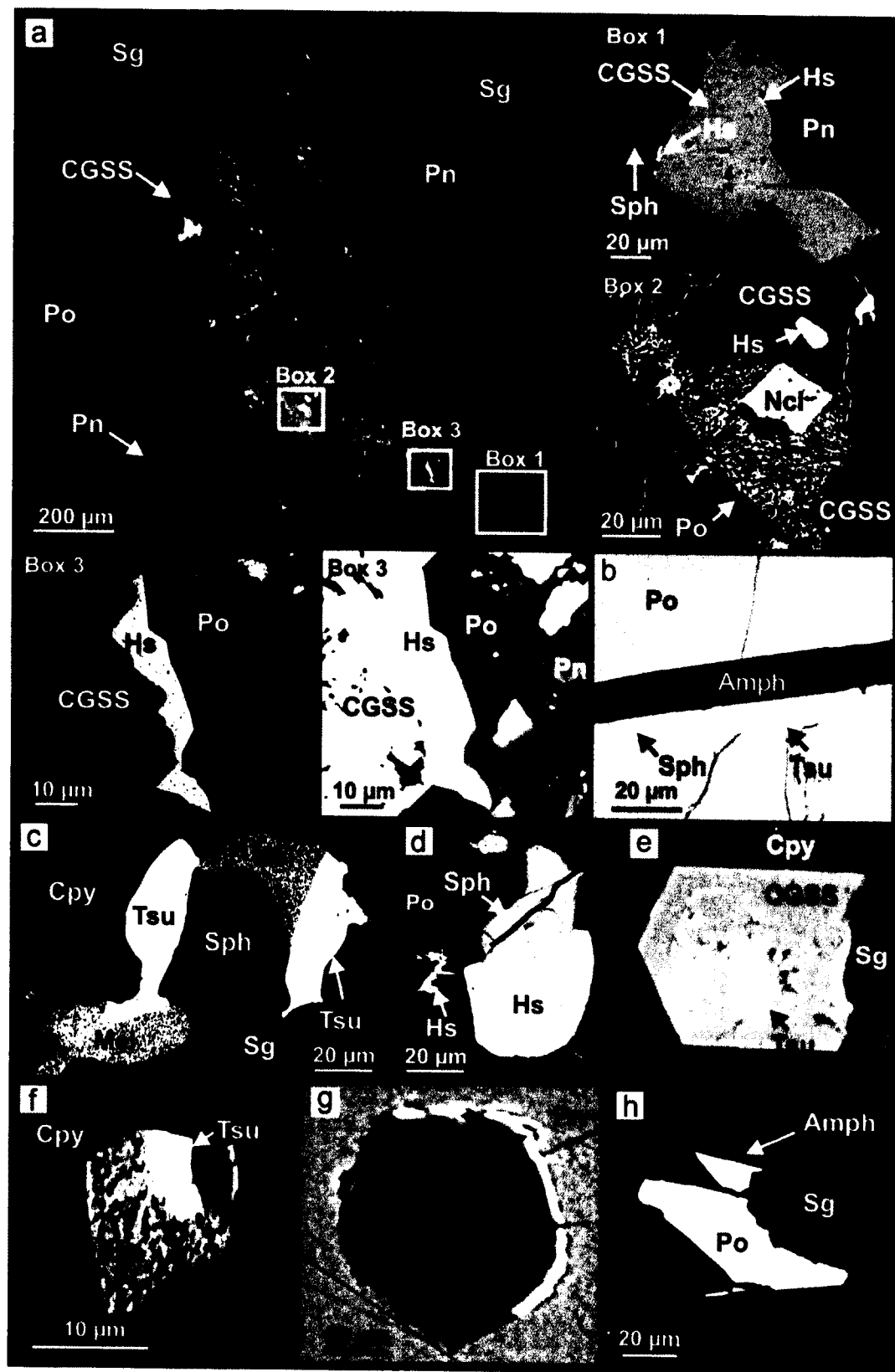


Figure 2.8 (previous page): SEM backscattered electron images showing textural characteristics of tellurides and other accessory phases. Note open space filling, grain boundary hosted textures, composite grain nature of inclusion, and some textural associations between CGSS and accessory phases. a) Large anhedral CGSS grain hosted between Po and Pn, with abundant Ncl, Hs and Po grains. Box 1 shows a composite grain of CGSS, Hs, and Sph, hosted within Pn. Box 2 shows a Ncl grain and intergrowths with the host CGSS. The lighter areas in the CGSS are zoned portions of the mineral with higher Co-Ni ratios. Box 3 shows a large Hs grain as a vug infilling along a boundary between Po and CGSS; b) Composite grain of Tsu and Sph hosted along Pn and silicate gangue boundary; c) Composite grain of Tsu, Mel and Sph filling a cavity near a Cpy and Sg boundary; d) Composite grain of Hs and Sph showing vuggy infilling texture in Po; e) Euhedral CGSS grain with Tsu filling in its resorbed core, hosted along a Cpy and silicate boundary; f) Composite grain of BiTe and Hs hosted in Cpy; g) Narrow Gal stringer rimming spherical grain of Po, hosted in Pn; h) Pyrrhotite hosted in silicate gangue located ~70 m into the host rock. Mineral abbreviations: Amph= amphibole; Cpy= chalcopyrite; gal= galena; CGSS= cobaltite-gersdorffite solid solution; Hs= hessite; Mel= melonite; Ncl= nickeline; Pn= pentlandite; Po= pyrrhotite; Sph= Sphalerite; Sg= silicate gangue; Tsu= tsumoite.

petrographic analysis, 26 were found to contain an abundance of CGSS grains. Of the samples which contain CGSS grains, 62% were INMS type ore, while DISS (23%), MASU (13%), and wall rock (2%) ore types account for the remaining 38%. CGSS forms symplectic intergrowths with nickeline in several As-rich samples from stope 1291 of the #1 west shear on 5000L (M46, A86, 87, 89-91; Supplementary Table 1, Appendix A). The intergrowths are usually large ($\sim 1 \text{ mm}^2$ areas) and can contain abundant sulphide and trace/accessory phase inclusions (Figure 2.6f). The intergrowths commonly show the crystal form of CGSS (Figure 2.6f). Significant quantities of nickeline can be hosted in CGSS (Figure 2.6a, b) and CGSS can occur as rims on nickeline grains in rare cases (Figure 2.6e). Anhedral blebs of CGSS are observed that contain sub-spherical nickeline inclusions in As-rich samples (Figure 2.6b, e). Nickeline forms rounded, subhedral blebs which range in size from $>5 \text{ }\mu\text{m}$ to $\sim 2 \text{ mm}$ (Figure 2.6b, e). The nickeline is hosted as inclusions in pyrrhotite (32%), chalcopyrite (27%), silicate gangue (3%), CGSS (2%), and often occurs along the boundaries between pyrrhotite and chalcopyrite (21%), silicate gangue (4%) and chalcopyrite and silicate gangue (11%). Nickeline can also occur as small ($\sim 5\text{-}50 \text{ }\mu\text{m}$) inclusions and intergrowths in CGSS (Figure 2.8a, Box 2; Figure 2.6a, b, f-h). Inclusions of base metal sulphides, CGSS-GGSS and trace phases occur in the rims of nickeline grains (Figure 2.6a). Nickeline grains were observed in 10 of the 57 samples studied in detail by petrographic analysis. Of the samples that contain nickeline, 70% were INMS, while DISS and MASU comprised the remaining 20 and 10% of ore type samples, respectively.

Nickeline contains trace abundances of inclusions of hessite, tsumoite, tellurobismuthite, michenerite, and electrum in the rims of the grain, or along grain

boundaries between other minerals (Figure 2.6e). Nickeline is the dominant As carrier in 8 As-rich samples whereas CGSS is dominant in 11 (Table 2.7, Appendix A) and occurs as a trace phase in many others (Supplementary Table 1, Appendix A).

Several samples taken from stope 1291 (#1 west shear 5000L; Figure 2) and stope 1321 (#1 west shear 5100L; Figure 2) show high abundances of nickeline and/or nickeline-CGSS intergrowth, ranging from 0.5 to 5.5 modal % (Supplementary Table 1, Appendix A). These samples are described in the following section.

2.3.3.2 Nickeline-chalcopyrite intergrowths

Nickeline displays a very complex texture with chalcopyrite in one MASU sample [A62/DTL 11B (2); stope 1321, #1 west shear 5100L; Figure 2.6]. The sample consists of massive chalcopyrite with abundant nickeline inclusions (Figure 2.6g, h). The abundance of nickeline inclusions is much higher than in other samples, based on visual estimates; ~40 vol% of the sample consists of blebs of nickeline grains hosted primarily in massive chalcopyrite. Approximately 15 vol% of the sample is, with grains ranging from <5 to 70 μm , (avg. of ~40 μm ; Figure 2.6 g, h). The remaining nickeline grains are larger, averaging ~200-300 μm . Within this sample are symplectic intergrowths of chalcopyrite and nickeline (Figure 2.6g, h).

2.3.3.3 Glaucodot-gersdorffite solid solution

Glaucodot-gersdorffite solid solution (GGSS) is a minor As-bearing phase in Garson ores. The major and trace element concentrations in GGSS are very similar to CGSS. Other than average grain size, the crystal class of GGSS is the only characteristic

distinguishing it from CGSS. GGSS commonly occur as small (1-120 μm ; avg. $\sim 20 \mu\text{m}$), thin lath-like crystals (orthorhombic dipyramidal), whereas CGSS tends to be larger tabular grains or amorphous grains (orthorhombic dipyramidal to isometric tetartoidal system; Figure 2.6c, d; 8b, d). The majority of GGSS grains are hosted within pyrrhotite (51%), but many grains have been commonly observed in chalcopyrite (3%) and pentlandite (5%), or along boundaries between pyrrhotite and silicate gangue (26%), and pentlandite (4%). The remaining 11% of CGSS grains are hosted along grain boundaries between combinations of these minerals. GGSS grains are found in 20 of the 57 samples studied by petrographic analysis and occur in INMS (60%), DISS (25%), MASU (10%), and CSIS (5%) ore types. GGSS tends to be present in many ore types but contributes little to bulk As in samples, owing to its small grain size and relatively low abundance compared to CGSS (Supplementary Table 1, Appendix A). Only when GGSS is present in samples with very low bulk rock As content, does the GGSS control a significant % of As (Table 2.7, Appendix A).

2.3.4 Trace elements in arsenides and sulfarsenides

2.3.4.1 Cobaltite-gersdorffite solid solution

CGSS contains elevated Ag (up to 540 ppm, avg. 38 ppm, n=53) and contains significant PGE; Ru (up to 260 ppm, avg. 23 ppm, n=56), Rh (up to 90.1 ppm; avg. 7.5 ppm, n=39; up to 4240 ppm, avg. 568 ppm on 5100L, n=14), Pd (1100-1500 ppm in stope 2221 of 4600L #4 west shear, n=3; up to 350 ppm, avg. 160 ppm, n=54, in all other shears and levels), Pt (up to 940 ppm, avg. 88 ppm, n=51; 1844-3650 ppm, avg. 2750

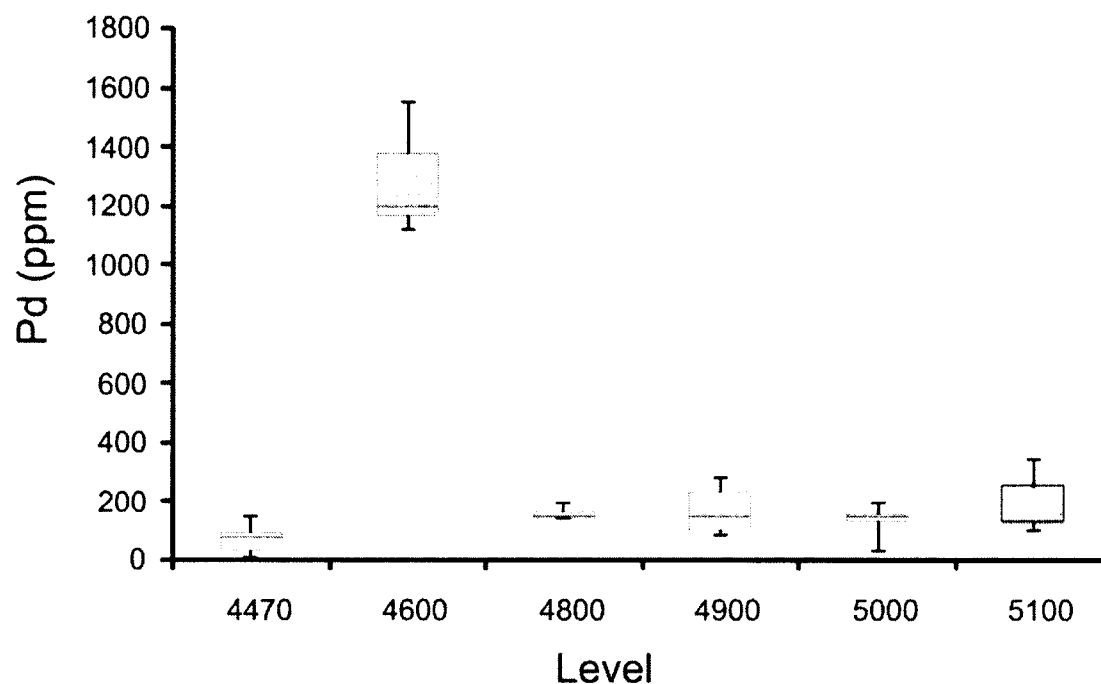


Figure 2.9: Summary of LA-ICPMS analyses of Pd in gersdorffite by level. Box and whisker plots showing concentrations of Pd in gersdorffite grains. Note consistent concentrations from level to level (with exception to one level) and narrow ranges in concentration within all grains analyzed from single levels.

ppm, n=2, in rare cases #1 west shear on 5000 and 5100L), Os (up to 85 ppm, avg. 3.6 ppm, n=37), and Re (up to 2.1 ppm, avg. 0.46 ppm, n=21). Palladium is fairly homogeneously distributed in the CGSS structure. The highest Pd concentrations in CGSS are an order of magnitude higher than the average and are found on #4 west shear of the 4600 level. Palladium in gersdorffite shows similar concentrations from level to level, except the 4600 level where Pd values are an order of magnitude higher (Figure 2.9). Ranges in Pd concentration in gersdorffite are narrow for all shears, highlighting the validity of approach to data reduction for signals showing the presence of accidental PGE mineral inclusions in such host phases (Figure 2.9). The highest concentrations of Pt in CGSS are in #4 shear west 4800 level and #1 shear west 5000 level (Table 2.4, Appendix A). The LA-ICPMS data for Pt show a wide range of concentrations within single samples and single grains, suggesting that Pt is partially distributed in CGSS as micro-inclusions of PGM. This observation is supported by SEM observations of small grains of sperrylite in the CGSS.

CGSS contains significant concentration of Sb (113-1065 ppm; avg. 305 ppm) and can contain Ag, Te, Pb and Bi (Table 2.4, Appendix A). Apparent concentrations of these elements in CGSS can be artificially increased by the presence of micrograins of hessite, altaite, tellurobismuthite and tsumoite which are common trace phases found hosted in sulfarsenides (Table 2.4, Appendix A). CGSS host the highest concentrations of Se (up to 1643 ppm, avg. 310 ppm, n=59). GGSS grains are too small to analyze using LA-ICPMS.

2.3.4.2 Nickeline

Nickeline contains consistent but relatively low Co (from sample to sample) when compared to CGSS (144-540 ppm, avg. 285 ppm, n=26). Nickeline contains the highest concentrations of Sb than any other mineral (1230-3360 ppm, avg. 2260 ppm, n=26), with average values reaching an order of magnitude greater than those observed in CGSS. Concentrations of Te range from 615 to 1680 ppm, with an average of 998 ppm (n=26). Concentrations of Au in nickeline range from 3 to 16 ppm (avg. 6.8 ppm, n=26). Nickeline hosts the lowest concentrations of Se (up to 134, avg. 69, n=26).

2.3.5 Characteristics of the PGE minerals

Thirty-three representative ore samples were studied in detail by SEM-EDS and SEM-BSE (back scattered electron) in order to determine PGM and trace phase composition and distribution (Table 2.9, Appendix A). Present in several samples are Ir and Rh-bearing sulfarsenides, which are most likely non-ideal irarsite-hollingworthite (Figure 2.10a-d; Table 2.9, Appendix A). These mineral grains are very small (<1-2 μm) and are primarily hosted as inclusions in CGSS/GGSS or along mineral grain boundaries with CGSS/GGSS (Figure 2.10a-d). Analyses of non-ideal irarsite-hollingworthite were attempted by electron microprobe but the grains were too small to obtain reliable results. A single grain of Re-sulphide (rheniite) was observed hosted in chalcopyrite (Table 2.9, 2.10, Appendix A). A variety of Pd-bearing tellurides have been observed in samples with low bulk As (Figure 2.10e, f), as well as high As samples, and are texturally associated with the arsenides and sulfarsenides (Figure 2.10g, h). The Pd-bearing minerals are predominantly telluropalladinite and michenerite, with minor paolovite

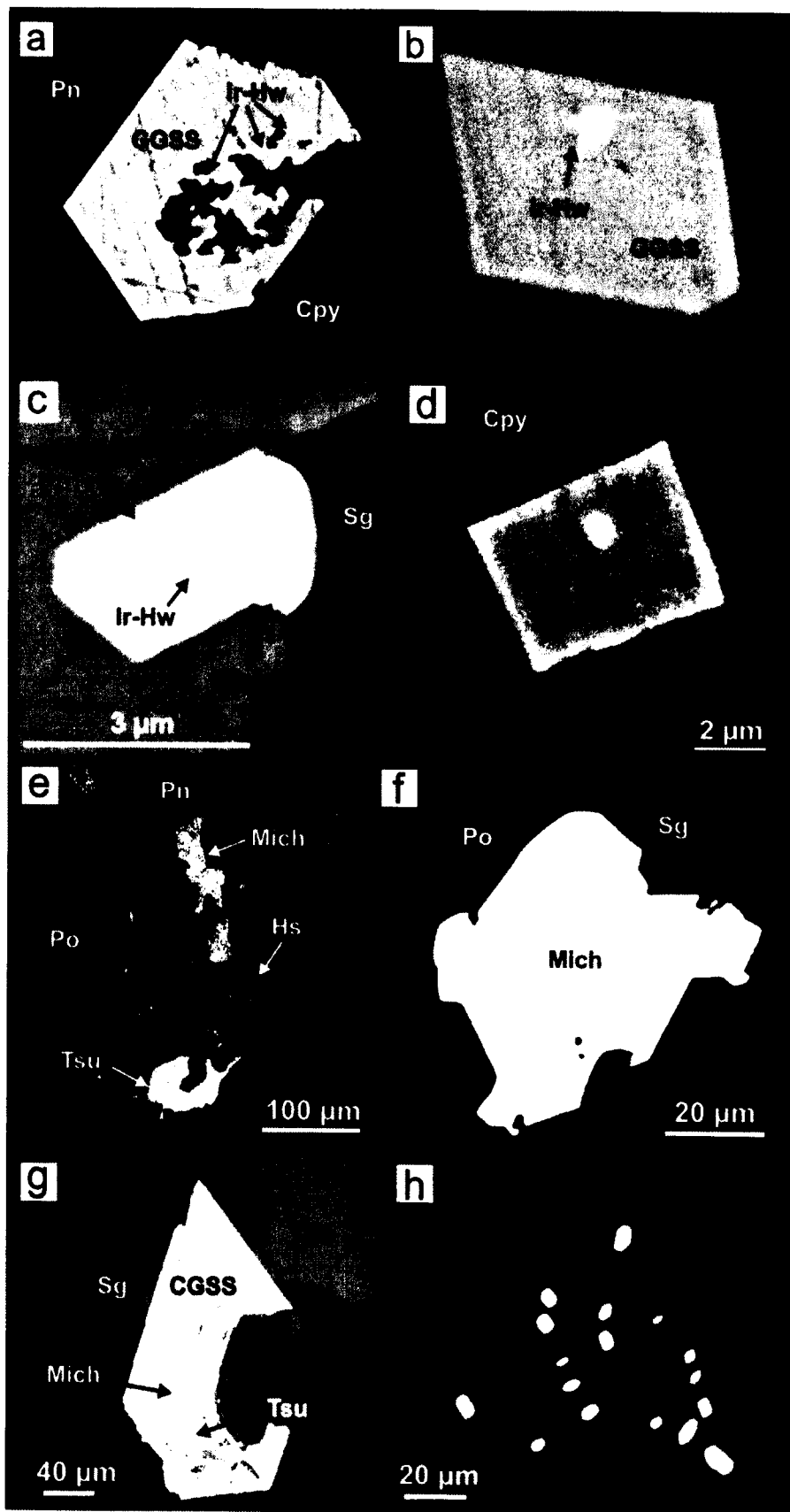


Figure 2.10 (previous page): Back-scattered electron images showing textural characteristics of IPGE minerals and Pd-tellurides. Note the resorption textures in GGSS, the exsolved nature of IPGE minerals and open-space filling textures displayed by the Pd-tellurides. a) Euhedral GGSS grain with resorbed core hosting Ir-Hw along Cpy and Pn boundary; b) Small anhedral Ir-Hw grain hosted in euhedral GGSS in Po; c) Composite grain of euhedral GGSS, Ir-Hw and Tsu grains hosted along contact of Po and silicate gangue grains; d) Small anhedral Ir-Hw grain hosted in euhedral GGSS in Cpy e) Composite grain of Mich, Hs, and Tsu within an open cavity cutting across a Po and Pn grain boundary; f) Large Mich grain hosted in a vuggy cavity along Po and silicate gangue (Sg) grain boundaries g) Small grains of Mich and Tsu grains hosted in CGSS occurring along Po and Sg grain boundary; h) A cluster of Mich, Hs and Tsu grains hosted within a single Ncl grain. Mineral abbreviations: CGSS= cobaltite-gersdorffite solid solution; GGSS= glaucodot-gersdorffite solid solution; Hs= hessite; Ir-Hw= irarsite-hollingworthite; Mich= michenerite; Ncl= Nickeline; Po= pyrrhotite; Sg= silicate gangue; Tsu= tsumoite

(Sb₂Pd) and in rare examples, an unnamed (Sn, Ni)PdSe was observed (Table 2.9, 2.10, Appendix A). Average telluropalladinite grain sizes are ~12.3 µm (~1-100 µm). Telluropalladinite contains some Cd, Ni, and Sb, while paolovite can contain Sb (Supplementary Table 2.1; Table 2.10, Appendix A). Telluropalladinite grains are mainly hosted as inclusions in CGSS (25%), with the remainder as inclusions in silicate gangue (15%) and chalcopyrite (10%), and hosted along grain boundaries between pyrrhotite and nickeline (15%), or pyrrhotite and silicate gangue (10%; Table 2.9, Appendix A). Michenerite is commonly hosted along grain boundaries, often between pyrrhotite and nickeline (25%), but can also occur along grain boundaries between silicate gangue, CGSS, chalcopyrite and sphalerite (Table 2.9, Appendix A). Michenerite grain sizes are similar to telluropalladinite (~12.5 µm avg., 4-90 µm). Only a small number of michenerite grains (25%) are not hosted along such boundaries (Table 2.9, Appendix A). Those not hosted along grain boundaries are hosted as inclusions in nickeline (55%), CGSS (35%), pyrrhotite (10%) and chalcopyrite (10%; Table 2.9, Appendix A). Telluropalladinite and michenerite are texturally associated with sulfarsenides and arsenides, with ~50% of telluropalladinite grains and ~80% of michenerite grains occurring as either inclusions in As-minerals or as inclusions hosted along boundaries between sulfarsenides-arsenides and base metal sulphides or silicate gangue (Figure 2.10e-h; Table 2.9, Appendix A). Michenerite commonly forms composite (polymineralic) inclusions joined to hessite (AgTe), tsumoite (BiTe), tellurobismuthite (Bi₂Te₃) as well as sphalerite (Figure 2.10e; Table 2.9, Appendix A). The composite inclusions are anhedral, show open space-filling textures, and range from 3 - 90 µm in size, but are usually <20 µm (Figure 2.10e-h). Inclusions of telluropalladinite and

michenerite are most common in nickeline and CGSS, where they appear to be infilling small vuggy cavities (Figure 2.10g, h). The grains often fill vugs that cross boundaries between two adjacent minerals (Figure 2.10e). Quantitative analyses of these minerals by electron microprobe were not obtained due to their very small grain size, although they have been reported by SEM-EDS (Table 2.10, Appendix A).

Sperrylite (PtAs_2) is the main Pt-bearing mineral observed the samples studied (Christopher Davis, personal communication; Supplementary Table 2.1, Table 2.9, Appendix A). Sperrylite is subhedral and 50% of all grains are hosted along grain boundaries between adjacent chalcopyrite and nickeline (Table 2.9, Appendix A). The grains are small with an average size of $\sim 12 \mu\text{m}$ ($\sim 5\text{-}25\mu\text{m}$). Iridium-Rh-bearing minerals contain minor amounts of Pt, but the scarcity of these grains suggests that they contribute very little to overall Pt concentrations in the ores. Presumably, they must significantly contribute to the IPGE concentrations in the ores (Supplementary Table 2.1, Appendix A). Irarsite-hollingworthite grains are hosted predominantly in GGSS (55%), pyrrhotite (40%) and chalcopyrite (5%), as well as commonly occurring along boundaries between pyrrhotite and chalcopyrite (5%). All grains are spatially related to CGSS (Table 2.9, Appendix A).

2.3.6 Other accessory minerals

Sphalerite and magnetite occur in many of the Garson ore samples as a minor phase. The sphalerite is predominantly hosted in pyrrhotite and range in grain size from 20 to $120 \mu\text{m}$. Sphalerite contains significant amounts of Cd ($\sim 1.5\text{-}2.5 \text{ wt}\%$), Se ($\sim 150\text{-}200 \text{ ppm}$), and contains up to $\sim 16 \text{ ppm}$ Ag (Table 2.6, Appendix A). Sphalerite is found in all major

base metal sulphide phases and can occur in composite grains attached to CGSS, hessite and tsumoite (Figure 2.8a, b).

Magnetite is present in many samples as rounded, 20 to 150 μm grains containing microfractures infilled with pyrrhotite and chalcopyrite.

Tellurobismuthite and tsumoite grains usually occur as anhedral grains are found in pyrrhotite (25%), chalcopyrite (21%), CGSS (25%) and pentlandite (4%), with the remaining 25% occurring along the grain boundaries between base metal sulphides and wall rock fragments or sulfarsenides and arsenides (Figure 2.8b, c, e, f; Table 2.9, 2.10, Appendix A). They also occur as composite grains attached to tellurides, sphalerite and PGM, as well as inclusions in CGSS-GGSS (Figure 2.8b, c, e, f; Table 2.9, Appendix A). Nickel-Pb-tellurides and hessite are also present and have similar textural occurrences as tellurobismuthite, commonly occurring as composite grains with sphalerite and other trace phases (Figure 2.8b-d, f; Table 2.9, Appendix A). The inclusions are typically very small (avg. 15 μm) but are larger than texturally associated micrograins of PGM. Their presence can be inferred from the LA-ICPMS signals based on overlapping high intensity count rate, short lived peaks for Pb, Te, Ag and Bi. The most common of these tellurides is hessite which is hosted in nickeline (35%), pyrrhotite (10%), chalcopyrite (10%), and pentlandite (5%) as well as along grain boundaries between pyrrhotite and pentlandite (10%), with the remaining 30% occurring along the grain boundaries between base metal sulphides and wall rock fragments or sulfarsenides and arsenides (Table 2.9, Appendix A). Other trace phases include galena, occurring as small ($\sim 10 \mu\text{m}$) laths or grains hosted primarily in wall rocks, but also occurring in sulphides, and very rare scheelite, and Pb-

selenide (Figure 2.8g). Stringers of galena, sphalerite, quartz and calcite are found within the Garson ores and contribute to bulk rock Pb (galena) and Zn (sphalerite).

2.4 Discussion

2.4.1 The association between PGE and As in magmatic sulphide deposits

Recent detailed mineralogical studies of magmatic Ni-Cu-PGE deposits have shown that PGE are hosted within BMS or within trace abundances of PGM (Ballhaus and Sylvester, 2000; Barnes et al., 2006; Holwell and McDonald, 2007; Godel et al., 2007; Barnes et al., 2008; Godel and Barnes, 2008).

Studies performed at Sudbury show that PGM such as froodite (PdBi_2), insizwaite $[\text{Pt}(\text{Bi},\text{Sb})]$, irarsite-hollingworthite, kotulskite $[\text{Pd}(\text{Te},\text{Bi})]$, merenskyite $[(\text{Pd},\text{Pt})(\text{Te},\text{Bi})_2]$, mertieite II $[\text{Pd}_8(\text{Sb},\text{As})_3]$, michenerite $[(\text{Pd},\text{Pt})\text{BiTe}]$, moncheite $[(\text{Pt},\text{Pd})(\text{Te},\text{Bi})_2]$, niggliite (PtSn), sperrylite, and sudburyite $[(\text{Pd},\text{Ni})\text{Sb}]$, and to a lesser extent PGE-bearing sulfarsenides (cobaltite-gersdorffite) and arsenides [nickeline, maucherite ($\text{Ni}_{11}\text{As}_8$)] dominate PGE mineralization, with <10% of the bulk Pt, Pd, Ir, Rh, and <30% of the bulk Ru being hosted in solid-solution (dissolved) within BMS (Cabri, 1981, 1988; Cabri and Laflamme, 1984; Li et al, 1993; Huminicki et al., 2005; Dare et al., 2010a). The PGM and sulfarsenides listed above are found in trace abundances in many typical, unmodified deposit styles along the South Range (Hawley and Stanton, 1962; Cabri and Laflamme, 1976; Cabri, 1981; Farrow and Watkinson, 1999; Stewart et al, 1999; Carter, 2001; Magyarosi et al., 2002; Szentpéteri et al., 2002; Ames et al., 2003, Ames and Farrow, 2007). These phases are interpreted to be either hydrothermal in origin (Carter, 2001; Magyarosi et al., 2002; Szentpéteri et al., 2002;

Ames et al, 2003, Ames and Farrow, 2007) or early magmatic in origin (Szentpéteri et al., 2002; Dare et al., 2010a). Dare et al. (2010a) first proposed an early magmatic origin for PGE sulfarsenides (irarsite-hollingworthite, and PGE-bearing cobaltite) that crystallized at high temperatures (1000-1200°C) as phenocrysts from a sulphide liquid and were later enclosed in MSS cumulates (Dare et al., 2010a).

In other magmatic ore deposit styles, As-phases have also played an important role in controlling the distribution of the PGE. For example, very thin, lens-like accumulations of gersdorffite and nickeline have been found at the base of magmatic sulphide horizons in komatiite flows at Dundonald Beach, Ontario (Hanley, 2007). These sulfarsenide-arsenide layers are considerably more enriched in PGE than the associated base metal sulphide horizons (Hanley, 2007). The PGE-rich lenses are thought to be the result of accumulation of now-crystallized immiscible sulfarsenide melt droplets or sulfarsenide phenocrysts that became saturated in the silicate or sulphide liquid (Hanley, 2007). Some layered intrusions or areas within layered intrusions (e.g., chromitite horizons at Marikana, western Bushveld Complex; the Vammala Ni-Cu-PGE deposit, Finland; Merkle, 1992; Gervilla et al., 1996, 1998) also show bulk arsenic concentrations that correlate closely with precious metal concentrations.

2.4.2 Review of As-free and As-bearing sulphide systems

In As-free magmatic sulphide systems, the metal content and composition of the sulphide melt in a magmatic system will be determined partly by the composition of the silicate magma from which it separated (Naldrett et al., 1999). Natural sulphide liquids generally coexist with silicate melts at very high temperatures, ranging from ~850 to

~1600°C and typically at an oxygen fugacity close to the fayalite-magnetite-quartz buffer (Mungall, 2007). The crystallization of monosulphide solid solution (MSS) from a sulphide melt initiates control on the variation in composition and mineralogy of magmatic sulphide deposits (Hawley, 1965; Craig and Kullerud, 1969; Naldrett, 1969; Li et al, 1992; Naldrett et al, 1994a; Zientek et al., 1994; Mungall et al., 2004). At a temperature of ~1200°C, a sulphide liquid will separate from a silicate melt, and will then start to crystallize MSS at ~1000°C with Ni partitioning into the MSS at lower temperatures (~900°C; Mungall et al., 2005). This process leaves a Cu-rich residual sulphide liquid which starts to crystallize intermediate solid solution (ISS) at slightly lower temperatures (900°C; Holwell and McDonald, 2010). Upon further cooling, the MSS recrystallizes to pyrrhotite and exsolves pentlandite, whereas the ISS recrystallizes to chalcopyrite and cubanite (Holwell and McDonald, 2010). Mungall (2007) proposed that the contact-style Sudbury sulphide ores represent accumulations of ISS and MSS cumulates that formed via equilibrium crystallization rather than MSS-only fractional crystallization, as is commonly accepted for the genesis for Sudbury footwall style ores.

Experimental studies have shown that Ir, Ru and Rh are compatible in MSS at high values of fS_2 , while Cu, Pt, Pd and Au are incompatible in MSS at all conditions (Naldrett et al., 1999; Mungall et al., 2005). The crystallization of MSS typically leads to the formation of Fe-Ni-rich, Pt-Pd-poor pyrrhotite-dominant assemblage and a Cu-Pt-Pd-Au-(Ni)-rich residual liquid, which can migrate distances through solidified cumulate rocks and country rocks to form chalcopyrite-rich stockworks (Mungall, 2002; Mungall et al., 2005). Ebel and Naldrett (1996), Li and Naldrett (1993), Li et al. (1992) and Naldrett et al. (1994b) showed that footwall style deposits at Sudbury formed by separation of Cu-

rich liquid from MSS, followed by fractional crystallization of the ISS into the footwall, leading to extreme Cu, PGE and Au enrichments. Although the Garson ores most commonly contain an assemblage of pyrrhotite, chalcopyrite, and pentlandite suggesting that ISS and MSS crystallized together, the Cu-rich Ramp zone at Garson could be a possible footwall-style equivalent of those deposits on the North Range (i.e., the main ores at the Garson deposit formed by equilibrium crystallized and the Ramp formed due to the fractionation of a Cu-rich liquid). Based on bulk rock assays alone, As appears to have not partitioned preferentially between ISS and MSS along the South Range since the As concentrations Cu-rich Ramp ores and Ni-rich pyrrhotite-dominated are comparable (Table 2.11, 2.12, Appendix A).

In As-bearing magmatic sulphide systems, the timing of sulfarsenide-arsenide formation is important as this will impact PGE distribution. It has been shown, based on experimental work and in field studies other than at Sudbury, that As or other semimetal-rich melts behave immiscibly with sulphide liquid, and scavenge the PGE to eventually crystallize PGE-rich sulfarsenides or arsenides (Skinner et al., 1976; Makovicky et al., 1990, 1992; Fleet et al., 1993; Gervilla et al., 1996; Wood, 2003; Hanley, 2007). Palladium and Pt are preferentially incorporated into As-rich (sulfarsenide) melts relative to sulphide liquids with a partition coefficient of approximately 30 (Wood, 2003; Hanley, 2007). Natural sulfarsenides and arsenides containing Fe, Co and Ni commonly contain concentrations of Pd and Pt dissolved in their structure, and PGM are also commonly spatially and texturally associated with sulfarsenides and arsenides (Chen et al., 1993; Gervilla et al., 2004; Hem and Makovicky, 2004a, b; Hanley, 2007; Dare et al., 2010a).

Two additional observations from experimental studies provide insight into the composition and formation of the Garson ores. First, Makovicky et al. (1990) showed that in the Pt-Fe-As-S system at high temperatures (850°C), platarsite (PtAsS) will be the dominant PGM at high fS_2 rather than sperrylite (PtAs₂). Second, at low temperatures (470°C), an As-S melt can still exist and is the only remaining liquid in the system. The temperature at which As-S melts are stable could also be lowered by the presence of additional low-melting-point chalcophile elements (e.g., Sb, Bi, Te, Sn, Cd, Au, Ag; Tomkins et al., 2006). Other authors have argued that rather than Pd and Pt being preferentially incorporated into the ISS or Cu-rich residual liquid, they could be concentrated in this very late-stage semimetal-rich melt (Holwell and McDonald, 2010).

2.4.3 Formation of arsenides/sulfarsenides by magmatic accumulation

We propose that the SIC magma became contaminated with As from the surrounding country rocks along the South Range during melt sheet formation. The reasoning for this process rather than local contamination during shearing is described below. Sulphide saturation occurred and the resulting sulphide melt, rich in As, became saturated in sulfarsenides (CGSS-GGSS) and arsenide (nickeline) at high temperatures (>1000°C), similar to the proposed genesis of these phases at the Creighton deposit (Dare et al., 2010a; Figure 2.11). Experimental data shows that cobaltite-gersdorffite solid solution is a stable phase at temperatures between 700°C and 1000°C (Yund, 1962; Maurel and Picot, 1974). The CGSS-GGSS and nickeline phenocrysts scavenged the PGE, Sb, Au, Ag, Te, Se and Bi from the sulphide melt, with Pd being more compatible in CGSS-GGSS and nickeline than Pt, and Pd and Pt being more compatible in CGSS-GGSS than

in nickeline. Some PGM (irarsite-hollingworthite, telluropalladinite, michenerite) occur as inclusions near the cores of small grains of CGSS, GGSS or nickeline (Figure 2.10a-d, g, h). These PGM may have exsolved upon cooling or were saturated phases in the sulphide melt even before the sulfarsenides and arsenides formed, consistent with the observed timing of growth of these phases in synthetic basalt-FeS-FeAs experimental systems (Wood, 2003). Possible evidence for the sulfarsenides and arsenides being primary magmatic phenocrysts includes: (i) CGSS-GGSS grains that have well-defined euhedral shapes and exsolved PGM at their cores (Figure 2.8a, Box 2; Figure 2.7; Figure 2.6c; Figure 2.10a-d, g); (ii) nickeline grains that show primary growth zones rich in silicate, pyrrhotite and CGSS inclusions (Figure 2.6e); (iii) very similar compositional ranges for unmixed CGSS-GGSS, implicating a common parental liquid from which they crystallized (Figure 2.7); (iv) the dominant occurrence of these sulfarsenides and arsenides along one wall rock contact in each shear zone implying gravitational settling onto the former footwall at the base of the original sulphide accumulation at Garson before shearing and overturning; and (v) strong and widespread depletion of the BMS in As and PGE reflecting extraction of these elements by the crystallization of CGSS-GGSS and nickeline from the original sulphide melt (Table 2.1-2.3, Appendix A).

As the sulphide melt passed into constricted regions of the shear zones, sulfarsenide and arsenide phenocrysts would remain suspended in a partially crystallized sulphide melt. In less restricted portions of the shear zones, phenocrysts would begin to settle in response to decreased sulphide velocity. This would explain why the much smaller GGSS phenocrysts are found dispersed throughout the ore bodies, as they would take a longer time to settle at the base of a sulphide melt. The presence of abundant wall rock

fragments in the shear zones may have also promoted the removal of the sulfarsenide and arsenide phenocrysts from suspension by impeding flow of the sulphide melt. The introduction of relatively cooler wall rock fragments (~450°C) would also enhance cooling of the sulphide melt, which would cause the melt to crystallize more rapidly and would not allow phenocrysts to completely accumulate along the base of the shears. This would explain cases where some high As samples occur away from the metabasalt and metasedimentary contacts (Figure 2.3b). The sulphide ore bodies would have to have crystallized completely before overturning of the system for the phenocrysts to remain mainly along the original footwall contact. These mechanisms are analogous to the early stage accumulation of sulphide droplets during the flow/emplacement of mafic-ultramafic silicate melt (Mungall and Naldrett, 2008). Euhedral grains of CGSS-GGSS with resorbed or “spongy” cores hosted in major base metal sulphides were first described by Hawley et al. (1968). The resorbed cores are suggestive of magmatic phenocrysts that experienced a later disequilibrium event associated with the formation of major base metal sulphides. Upon recrystallization of pyrrhotite and pentlandite from the MSS, Ni may have been scavenged from pyrrhotite surrounding the CGSS-GGSS grains, leading to this resorption or corrosion (Figure 2.6c; Figure 2.10a). Within the corroded cores of some of these grains are remnants of primary PGM (Figure 2.10a).

Compositional zoning within CGSS observed by SEM-BSE, EMP and in reflected light microscopy is due to varying Ni/Co ratios. The range in composition of CGSS-GGSS shown in Figure 2.7 could be the result of down-temperature unmixing of the original grains of CGSS-GGSS and/or reequilibration of CGSS-GGSS during the

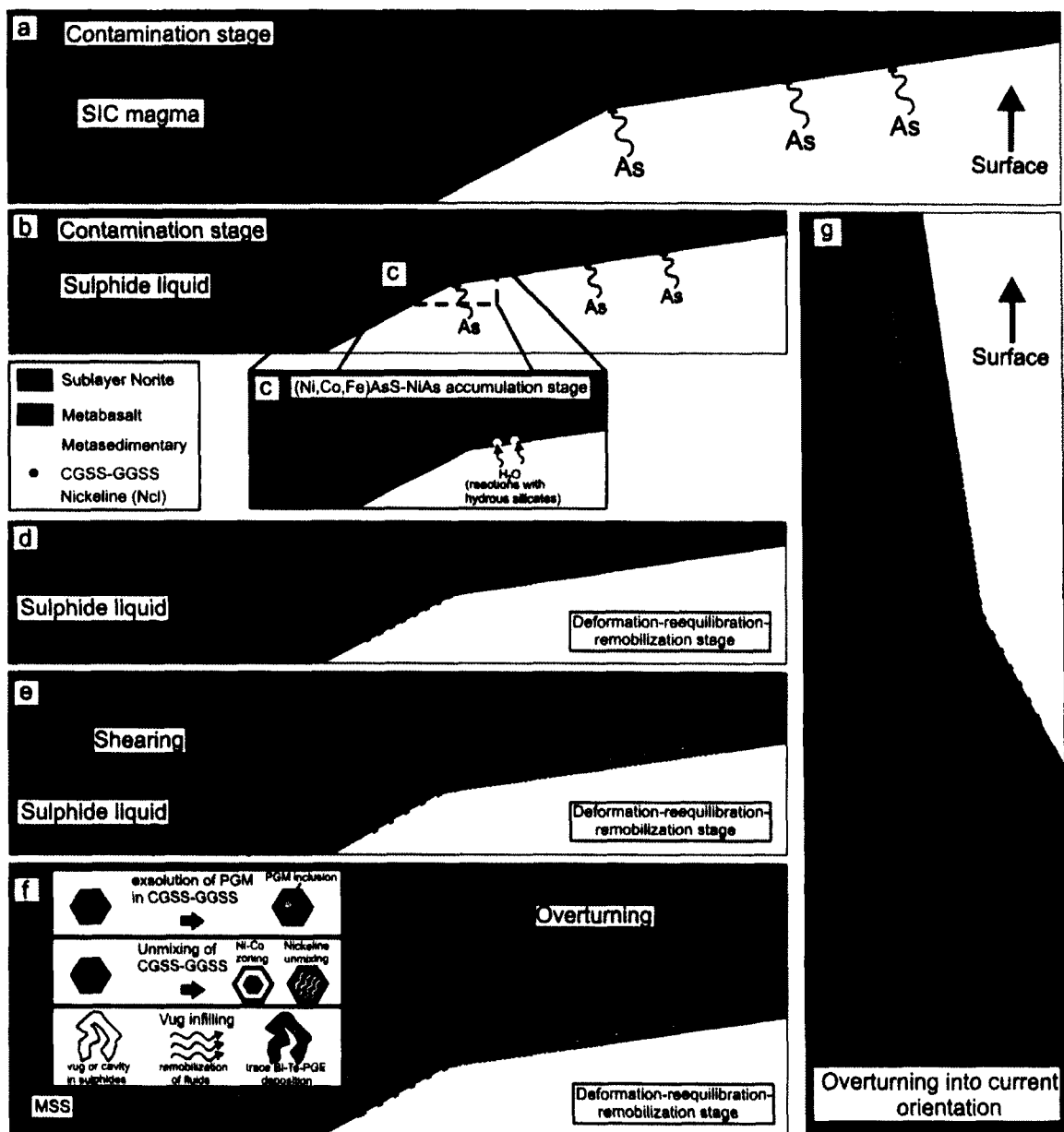
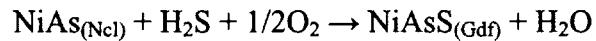


Figure 2.11 (previous page): Schematic depicting a proposed genetic model for the Garson deposit involving preservation of magmatic accumulation of sulfarsenides/arsenides. See text for detailed explanation. a) Contamination of SIC magma by As-rich footwall rocks leading to As saturation; b) Sulphide liquid accumulating along host rock contact with sublayer norite; c) As temperature decreases and As saturation is reached, CGSS-GGSS grains start accumulating along the footwall contact of the deposit, settling as cumulate grains through the sulphide liquid. Nickeline starts to form in areas where water is introduced via reactions with hydrous silicates in the wall rocks or where conditions were locally more reducing; d and e) Intense shearing of the host rocks occurs while the sulphides are still in partly liquid state allowing for mobilization of the sulphides along shear planes and the separation and redistribution of CGSS-GGSS grain accumulations and sulphide mush into individual shear zones; f) As temperature continues to decrease, the exsolution of the earliest PGM (irarsite-hollingworthite) from GGSS occurs. Unmixing of CGSS-GGSS grains produces the Co/Ni rich zoning. Unmixing of CGSS produces some CGSS-nickeline intergrowths locally. Exsolution (from CGSS) or remobilization of PGE and accessory metals leads to the formation of PGE-Bi-Ni-Ag tellurides that fill vugs in partially solidified MSS. g) Current orientation of the Garson deposit. Overturning of the ore bodies occurred after base metal sulphides had crystallized sufficiently to prevent movement of the sulfarsenide/arsenide accumulations away from former footwall contacts.

recrystallization of surrounding MSS to pyrrhotite and pentlandite. As pentlandite exsolves from pyrrhotite Ni could be scavenged from the CGSS-GGSS grains leading to ranges in compositions (as well as resorbed textures as stated earlier). However, unmixing is most likely the cause of the zoning due to the compositional span across limbs of a two phase field being similar for all zones/shears. This indicates that regardless of location, the earliest CGSS-GGSS compositions that crystallized from the original sulphide melt all had the same initial composition and cooled to the same conditions. CGSS also contains substantial amounts of Sb and Bi, which substitute for As (Yund, 1962; Hem and Makovicky, 2004a, b; Hanley, 2007).

The formation of nickeline as a primary phenocryst rather than CGSS-GGSS is likely due to localized variations in f_{H_2S} , f_{O_2} and f_{H_2O} (Fanlo et al., 2006). According to Fanlo et al. (2006), the reaction governing the formation of nickeline over gersdorffite is as follows:



At Sudbury, the formation of nickeline may have been promoted when water, which may be derived from the local host rocks during contact metamorphism, reacted with some sulphides along the contact horizons pushing the reaction above to the left. Nickeline may have also formed in more reducing areas along this contact (i.e., where sediments of the Stobie and McKim formations are locally graphitic). Nickeline and CGSS also show evidence of coeval formation. Small, euhedral inclusions of CGSS are found in growth zones in nickeline indicating a period of synchronous existence/growth (Figure 2.6e).

Similar to other deposits along the South Range (Creighton; Dare et al, 2010a), the Garson deposit experienced metamorphic overprinting and deformation, both synchronous to and post-dating the cooling of the SIC and sulphide ore formation (e.g., Klimczak et al., 2007; Mukwakwami et al, 2011a; 2011b). The ore is currently overturned and hosted in shear zones that developed during lower amphibolite grade metamorphism, during the Penokean and Mazatzal-Labradorian orogeny (*c.f.* Cowan and Schwerdtner, 1994; Klimczak et al., 2007; Mukwakwami et al, 2011a; 2011b). The main shearing event that separated the contact sulphides into “sheets” (single shear-hosted ore zones) must have occurred after the norite was completely solidified, as suggested by the presence of angular fragments of norite hosted in sulphides. Overturning of the ore zones must have occurred after the sulphides had partly or completely crystallized. We infer this from the observation that arsenides and sulfarsenides originally gravitationally accumulated along the metabasalt and metasedimentary footwall contact (currently the hanging wall contact; Figure 2.2; Figure 2.3a, b). If overturning occurred while the sulphides were liquid or if pre-existing shears (in their current orientation) were infilled by a sulphide liquid rather than a partly crystallized sulphide mush, the denser CGSS-GGSS grains would have resettled along the contact with the norite (currently the footwall; Figure 2; Figure 2.3a-b, Figure 2.11f, g).

Amphibolite grade metamorphism is characterized by temperatures in the range of ~500 to 700°C, which is approximately the temperature range of the final equilibration of BMS ores based on the compositions of CGSS-GGSS determined by EMP (Figure 2.7). The lack of pentlandite flames, the presence of pentlandite ‘eyes’ overprinting metamorphic amphiboles (Mukwakwami et al, 2011a; 2011b), the recrystallization of

pentlandite along pyrrhotite grain boundaries, and the resorbed cores of CGSS infilled by BMS are consistent with the sulphide ores having partly recrystallized after reverting back to MSS at metamorphic conditions. However, in almost all samples, the sulphides do not show extensive metamorphic fabrics or textures, except for rare contorted schist ores where the sulphides are disseminated in sheared and foliated host rocks and locally at some contacts, sulphides also show a foliation (Figure 2.4a). The shearing events were also responsible for the introduction of quartz fragments (from brecciation of early quartz veins) and host rock fragments (from wall rocks) that characterize the INMS, DISS and to a lesser extent MASU ores (Figure 2.4; Figure 2.11d-f). Rounded wall rock and quartz vein fragments are observed in greatest abundance in INMS samples, formed by the brecciation and milling of pre-existing quartz veins *prior* to sulphide introduction into the shears (Figure 2.4d).

It is possible that a late-stage semimetal melt (rich in Ag, PGE, Bi and Te) could have deposited some Pd that now occurs in composite inclusions (Figure 2.8a-f; Figure 2.10e-g). Semimetal-rich liquids are known to persist to very low temperatures (Tomkins et al., 2004). These grains do not appear to have exsolved from, or were trapped in, CGSS-GGSS and nickeline or BMS during their crystallization. Rather, they have the appearance of crystallized former segregations of liquid that filled cavities in sulfarsenides, arsenides and sulphides near the end of their crystallization history (Figure 2.8b-d, f, g; Figure 2.10e, f). They cannot represent exclusively exsolved phases since the vugs cut across grain boundaries in adjacent host phases (Figure 2.8c; Figure 2.10e). This could explain the observation that, while a significant % of Pd is often hosted in CGSS-

GGSS (as PGM inclusions or in solid solution), Pd and As bulk rock values do not always correlate with one another.

An ISS-forming liquid that may have formed the Garson ramp zone ore body must have remained in contact with As-rich MSS. The chalcopyrite-rich ore in the ramp is also enriched in As indicating that As does not preferentially partition between MSS crystals and the ISS-forming liquid. The chalcopyrite-rich ore from the ramp suggests that fractionation of a Cu-rich liquid resulted from the crystallization of MSS and separated from the ore body. Within the main shear zones, however, ISS seems to have remained in contact with the MSS as the ores are still rich in chalcopyrite. The intergrowth textures between chalcopyrite and nickeline (Figure 2.6g, h) had been reported in Sudbury ores previously as a hydrothermal replacement of gersdorffite (Lausen, 1930; Hawley et al., 1968). However, the symplectic texture, reminiscent of two phases that co-crystallize at a minimum, and the absence of any residual CGSS in this intergrowth indicate that this texture is not a replacement of CGSS but rather a late magmatic feature (Figure 2.6g, h).

2.4.4 Formation of arsenides/sulfarsenides by partial melting or solid state diffusion during metamorphism

It is uncertain what effects the Penokean Orogeny had on sulphide ores during crystallization and cooling of the SIC and whether this deformational event was responsible for the deformation and modification of the ore zones seen at Garson. Microstructural and paleomagnetic constraints place the timing of the Penokean Orogeny at ~1.89 to 1.83 Ga (Shanks and Schwerdtner, 1991a, b; Milkereit et al., 1992; Cowan and Schwerdtner, 1994; Boerner and Milkereit, 1999; Cowan et al., 1999; Szabó and

Halls, 2006; Klimczak et al., 2007; Riller et al., 2010) and attribute major deformation of the structure's southern limb to this process, synchronous to the cooling of the hot but already crystallized SIC. Other authors point out that the SIC and its ores would have cooled completely within ~70-100 Ka of the Sudbury event (Prevec and Cawthorn, 2002), and therefore, any deformation resulting from the early stages of the Penokean Orogeny within that short time span would not have generated the amount of deformation observed in the ore zones at Garson. Rather, it has been suggested that post-SIC orogenic events, such as the Mazatzal-Labradorian (~1.7-1.6 Ga) and Chieflakian orogenic events (~1.5-1.45 Ga) may have been responsible for major deformation along the South Range (Mukwakwami et al., 2011b). Alternately, if the Penokean had been responsible for the deformation, it must have occurred long after the SIC had cooled and its ores had crystallized when peak metamorphic conditions associated with the Penokean had been reached.

If shearing and overturning of the deposit occurred after the SIC and its ores had cooled completely (late Penokean) or during these other orogenic periods, the sulphides ores at Garson would have been emplaced in the solid state into the shear zones and arguments put forward here concerning a partially molten state for the sulphides would be invalid. The presence of deformed wall rock fragments included in the sulphide ore bodies at Garson suggests deformation and emplacement of the sulphides in a solid rather than liquid or semi-liquid state. In such a case, emplacement of solid sulphide ore into shear zones would have been facilitated by the ductile manner in which massive sulphides behave during metamorphism (e.g., Cook et al., 1993 and others therein). During emplacement, anatexis of the sulphides along wall-rock contacts could have produced a

small amount of partial melt from either pre-existing As-rich sulphides (with either As contained within primary magmatic phenocrysts or dissolved in base metal sulphides) or assimilation of As through interactions with As-rich country rocks. Experiments have shown that As-rich melts may exist at a temperature as low as ~470°C (e.g., Yund, 1962), which falls within the range of temperatures characteristic of upper greenschist to lower amphibole grade regional metamorphism (Yardley, 1969; Makovicky et al., 1992). Small aliquots of a partial melt could scavenge and transport some PGE and other metals from the base metal sulphides and, upon migration into discrete, structurally-controlled zones, could recrystallize to form the As-rich (and PGE, Bi, Te-rich) assemblages along wall rock-sulphide contacts.

2.4.5 Limitations/problems with a magmatic or metamorphic origin of sulfarsenides/arsenides

The origin and timing of sulfarsenide/arsenide mineralization in magmatic sulphide systems has been discussed by a number of authors (e.g., Gervilla et al., 1996; Hanley et al., 2007; Dare et al., 2010) and sulfarsenide and PGM phenocrysts of magmatic origin have been suggested at other deposits along the South Range of the SIC (the Creighton deposit; Dare et al., 2010). However, there are several problems with a magmatic origin for these mineral phases as phenocrysts.

First, although experimental studies show that CGSS is stable at magmatic temperatures (Maurel and Picot, 1974; Yund, 1964), an Fe-S melt would have to contain several wt% As to saturate an Fe-As phase based on limited experimental studies (Wood, 2003). It is unlikely that these concentrations of As were reached given the average As

content of the Garson ores (both high As and low As; based on ~13,500 assays; Christopher Davis, personal communication) is only on the order of ~1000 ppm. Sufficiently elevated concentrations of As to saturate the system in sulfarsenide/arsenide crystals could have been reached in sulphides occurring near the footwall contact where local contamination by As from country rocks was enhanced, or during the latest stages of sulphide crystallization if As behaves incompatibly (Tomkins, 2010). However, the lack of any enrichment in As in the “Ramp” ore zone at Garson (interpreted to represent a fractionated sulphide liquid) compared to the pyrrhotite-pentlandite rich ores of the #1 and #4 shear zones suggests that removal of MSS did not result in enrichment in As in residual sulphide liquid.

Second, complete massive sulphide recrystallization during slow cooling of primary sulphide ores and/or metamorphic reheating occurs rapidly and pervasively at very low temperatures (i.e., within weeks at ~230°C; Jim Mungall, personal communication). The occurrence of silicate inclusions within pentlandite and large (mm-size) pentlandite eyes (rather than primary exsolution lamellae) confirm that sulphides at Garson have undergone extensive recrystallization. Therefore, it is difficult to interpret any textures/crystals as primary at Garson given that primary magmatic textures should have been obliterated, unless sulfarsenides and arsenides recrystallize much more slowly than sulphide minerals. Likewise, owing to extensive deformation associated with structural modification of the Garson ores, the apparent spatial preservation of primary accumulations of sulfarsenide/arsenide phenocrysts along the former base of a sulphide pile would be very unlikely.

There are also several problems with a metamorphic origin for the sulfarsenides and arsenides at Garson. Semimetal melts (*c.f.* metamorphic sulfosalt melts; Tomkins, 2010) formed at even peak metamorphic conditions expected for the South Range should be restricted in composition to As-S liquids (not As-sulphide, and not Ni-Fe bearing) in equilibrium with Ni-Fe-sulphide minerals, based on the observed compositions of such liquids in experimental systems (Yund, 1962; Barton, 1969). Within increasing temperature and pressure (above metamorphic conditions for the South Range of the SIC), or with the appropriate parental assemblages present (e.g., stibnite, arsenopyrite; Tomkins et al., 2004; Tomkins et al., 2007), partial melting may generate more complex liquids containing many metals (e.g., Pt, Pd, Bi, Te, Au, As, Sb) and upon recrystallization, these liquids should crystallize polymetallic mineral assemblages (Tomkins et al., 2004; Hanley, 2007; Tomkins, 2010). These findings are in complete disagreement with the observed As phases at Garson. First, the As mineral assemblages are not polymineralic, being comprised of only CGSS or nickeline with trace amounts of Pt-Pd-Bi-Te-As phases as inclusions. Crystallization of a partial melt would not form stoichiometric sulfarsenide or arsenide phases.

Second, at upper greenschist to lower amphibolite conditions, the partial melt would not contain base metals (Co, Ni, Fe) but should contain As and S. The only polymineralic grains that could be interpreted as partial melt products could be the Te-rich inclusions in base metal sulphides but these are completely devoid of As and S so this seems very unlikely. They could, on the other hand, be late crystallization products in the original magmatic, having solidified at much higher temperatures (Tomkins, 2010).

Third, in magmatic sulphide systems, partial melting is severely limited by the absence of pyrite required to buffer sulphur fugacity to the levels required to destabilize pre-existing sulfarsenides (Tomkins et al., 2007). Pyrrhotite destabilization can occur to promote melting but an appropriate precursor assemblage is still required to generate any reasonable amount of partial melt (Tomkins et al., 2007). Without pre-existing magmatic sulfarsenides, partial melting of As-rich base metal sulphides would likely not have been able to generate the significant amount of As-rich melt required to later accumulate As mineral phases along wall-rock contacts.

Fourth, arsenic bulk rock assay grades and field observations show that the majority of sulfarsenides and arsenides occur only along the current hanging walls of the shear-hosted ore zones. Partial melting would not explain this phenomenon since both the upper and lower contacts of the ore zones represent lithotectonic contacts that underwent shearing. The sulphide ores should have experienced anatexis along the contacts with metabasalts and metasediments as well as along the contact with the adjacent sublayer norite.

Finally, the pervasive depletion of As and PGE within base metal sulphides is also inconsistent with a partial melting or diffusion-reconcentration model for As. Not all areas of the sulphide ore bodies would have experienced partial melting, especially those away from lithotectonic contacts.

2.4.6 Source and process of arsenic contamination

The amount of As in typical magmatic systems is lower than that required to saturate the system in As-bearing phases, especially systems with natural basaltic and komatiitic compositions (Wood, 2003). Even when systems have crystallized 95% of their mass (as

silicates), the amount of arsenic is still far below saturation (Wood, 2003). Silicate melts will be saturated in As at 1200°C and 1 GPa at a dissolved As concentration of ~3300 ppm (Wood, 2003). When As is introduced and becomes saturated in a sulphide melt, PGE, for example, will be potentially scavenged by any As phase that separates or crystallizes, leading to the formation of PGE-rich sulfarsenides as discussed above. Scavenging of some semimetals (As and Sb) from assimilated sedimentary country rocks and xenoliths by a silicate melt is suggested in cases where PGE mineralization tends to be dominated by As- or Sb-bearing PGM, and not associated with large quantities of BMS (e.g., in the Platreef at Turfspruit, Bushveld Complex; Hutchinson and McDonald, 2008; Holwell and McDonald, 2010). The As concentrations in sulphide-silicate magmas have been clearly increased by the magmatic assimilation of As-bearing metasedimentary and sedimentary rocks in other magmatic ore styles as well (Hanley, 2007), but contamination can also occur by the melting of pre-existing As-bearing minerals (e.g., arsenopyrite, tennantite, orpiment, realgar) during metamorphism (Tomkins et al., 2006). Sulphide melts are highly mobile during metamorphism and may be integral to remobilizing and concentrating precious metals by this remelting process (Tomkins et al., 2004; Tomkins et al, 2006).

The probable source of the As in the Garson shear-hosted ore zones is the metasedimentary rocks of the Stobie and McKim formation. These rocks (e.g., graywackes and quartzites) comprise part of southern contact of the Garson deposit, along with metabasaltic rocks of the same formations. Bulk rock assays from the study area indicate significant concentrations of As in the adjacent metasedimentary rocks at considerable distances from the shear-hosted ore zones (up to 140 ppm). These host rocks

contain sulphide minerals that are likely As-bearing although the timing of their formation relative to the shear-hosted ores at Garson is unclear (Figure 2.8h; Table 2.11, Appendix A). However, there are several observations that suggest that the primary contamination did not occur locally when a partially crystallized sulphide melt was introduced into the shear zones, or by late interaction of the sulphides with metasedimentary wall rocks.

First, As and lithophile elements (e.g., Sr) show no correlation in bulk rock assays (Table 2.11, Appendix A) and the proportion of wall rock clasts within the sulphides does not show any relationship to As content in the samples. Moreover, the physical introduction of wall rock fragments into the sulphide melt was not synchronous to As contamination. Samples of massive sulphide from shear-hosted ore zones that are poor in wall-rock fragments can be As-rich (>700 ppm), and although very high As contents are associated with INMS and DISS ores from the hanging wall contact, it is clear that similarly wall-rock rich ore styles from the current footwall contact are not as rich in As (Figure 2.3). Several stopes, especially along the footwall contact, have average As grades > 0.1 wt% (> 1000 ppm; Figure 2.3b, c), whereas average As grades observed in metasediments are only ~40 ppm (up to 140 ppm; Table 2.11, Appendix A), approximately 25 times lower than As in the high As stopes. Enrichment of the sulphide in As by an order of magnitude or more compared to the wall rocks seems unlikely unless the wall rocks had melted, which there is little evidence for. Contact between metasedimentary wall rock fragments and sulphide liquid would not likely have been efficient enough to extract the large amounts of As to account for As contents in the ores at Garson (Figure 2.3b, c; Table 2.11, Appendix A).

Second, the compositional ranges of CGSS-GGSS and nickeline are very similar in each shear, whereas localized contamination would have produced highly variable compositional ranges due to the range in wall rock composition (norite, gabbro, metasediment; variable As content) and temperature with proximity to the SIC, suggesting CGSS-GGSS originated from a parental sulphide liquid or primary phenocrysts and became physically separated into different shears after their accumulation (Figure 2.7; Figure 2.11; Table 2.8, Appendix A).

Third, as stated previously, CGSS-GGSS and nickeline are concentrated mainly along one side of each shear zone and, in most cases, the shears are hosted entirely within norite or volcanics and not in metasediments (Figure 2, 3b, c). This is consistent with other deposits along the South Range (Totten, Creighton) that contain locally high As regions but are not hosted in metasedimentary rocks at all. Rather, they are hosted by inclusion-rich quartz diorite and granite, respectively, suggesting that the As was not locally derived during sulphide emplacement.

Based on the points raised above, the main shearing event did not contribute significantly to the overall bulk As content of the ores; rather, shearing segregated pre-existing accumulations of CGSS-GGSS-nickeline crystals in a sulphide mush into individual ore zones. The As enrichment at Garson was part of a South Range-wide process of As-contamination of the original SIC magma. Melt inclusion studies of magmatic systems from a number of environments (intrusion-related gold systems, Hanley, 2007; barren granites, Audetat and Pettke, 2003; alkali basalts and alkalic porphyry systems; Hanley et al., 2012, submitted) show that sulphide melts are expected

to be enriched by 1-2 orders of magnitude in As compared to the coexisting silicate magma.

2.4.7 Reliability of bulk As, Pd, Pt estimation based on modal analysis of minerals in thin section

In many cases, predicted As bulk rock concentrations determined from modal point counting, image analysis, EMP analysis and LA-ICPMS analysis of minerals in 74 thin sections correspond to actual bulk rock As values (Figure 2.12; Supplementary Table 2.1; Table 2.7, Appendix A). This is especially true in samples with high As concentrations. When As is high, As-bearing phases are abundant and the probability of observing them in thin section is likely. Therefore, estimation of bulk assays based on thin sections alone will be robust. Such samples will be problematic for production. For samples with lower As (< 500 ppm; Figure 2.12), predicted As concentrations are commonly lower than bulk assays. This is likely due to fact that the As carriers hav a smaller grain size, are rare and are distributed more heterogeneously.

While the “spotty-grade” phenomenon is clearly observed on the scale of a single level and shear zone, variation can also occur on a much smaller scale (cm). Therefore, the representativeness of routine chip sampling from high-grade ore and underground drill core sampling is questionable. A small volume of ore with high CGSS-GGSS abundance can contaminate an entire stope, or conversely a stope that is relatively As-poor may be stored on surface or avoided altogether due to a single, misrepresentative assay yielding high As. It may be beneficial to avoid ore that is close to wall rock-sulphide contacts due to the spatial association of As minerals with the former footwall (current hanging wall)

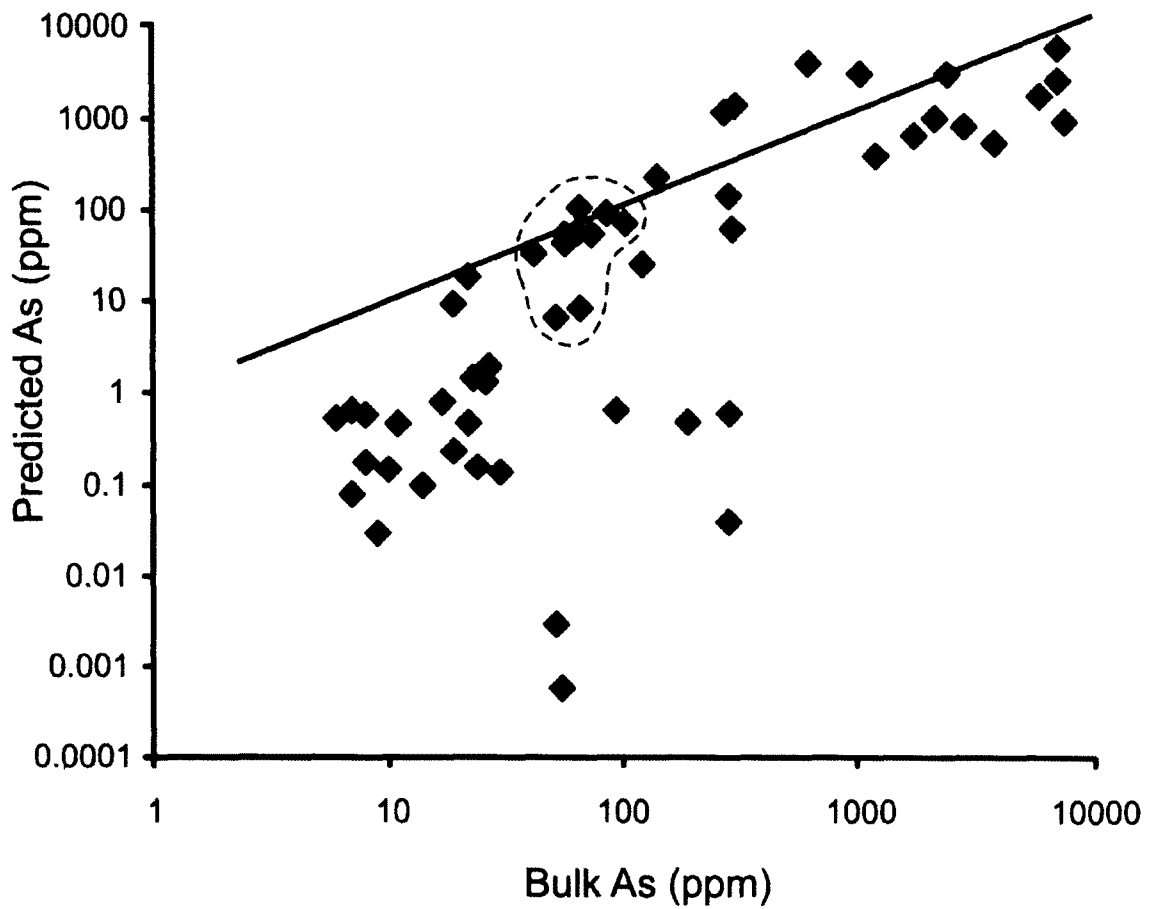


Figure 2.12: Logarithmic plot of bulk rock assay As concentrations versus predicted As concentrations. Figure shows that predicted values for high As samples are representative of bulk assays, while low As predicted samples are underestimate bulk rock values. Line indicates a one-to-one relationship (perfect correlation). Circled data points are for several assays from a single chip sample.

contact where CGSS-GGSS and nickeline grains are concentrated (Figure 2.3). The same effect is responsible for the “spotty” variation of Pd and Pt values also observed in the ores. The predicted Pd and Pt values determined from modal point counting, image analysis, EMP analysis and LA-ICPMS analysis of minerals in thin section show that predicted values based on mineralogy tend to underestimate actual bulk concentrations (Figure 2.13). This may be due to failure in accurately quantifying Pd or Pt-bearing minerals in the samples for which thin sections are, again, misrepresentative. The method of characterizing several slides from a single hand sample (~30 cm) seems to yield sufficient information to be texturally and compositionally representative of the slab (Figure 2.12; Figure 2.13). But the textural characteristics and abundances of major base metal sulphides, CGSS-GGSS, and nickeline grains based on slab analysis sample scale cannot be extrapolated to the stope scale. In general, predicting As concentrations by modal analysis through examination of core samples, chip samples and thin sections may prove difficult. While many predicted As values correspond to actual assayed values of As this is not always the case (Supplementary Table 2.1, Appendix A). Thin sections or hand samples are not necessarily representative of larger sample volumes, nor are assay results obtained from only a few drill core intersections through a mineable volume (i.e., a stope).

2.4.8 Major controls on arsenic distribution and abundance

It is evident that the *abundance* of As-bearing minerals is the ultimate control of the amount of arsenic found in each sample (Supplementary Table 2.1; Table 2.7, Appendix A). The major minerals controlling As abundance in Garson ores are CGSS and nickeline

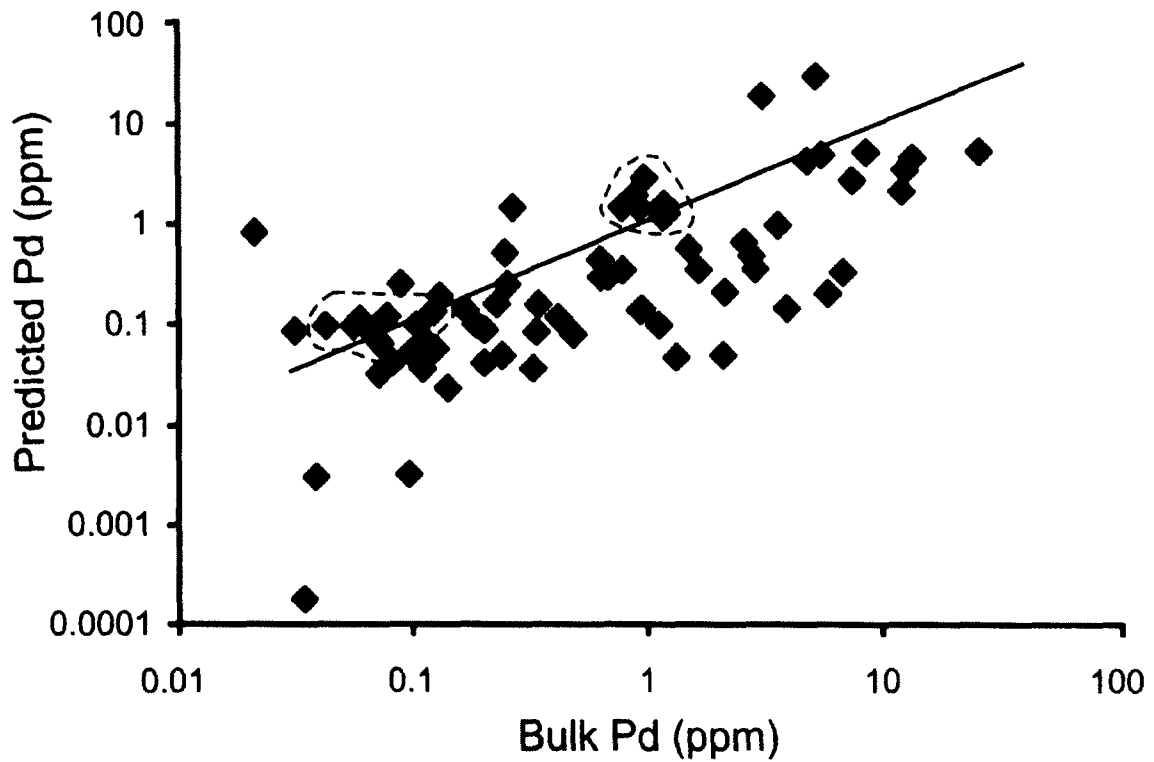


Figure 2.13: Logarithmic plot of bulk rock assay Pd concentrations versus predicted Pd concentrations. Figure shows that predicted values for Pd samples frequently underestimate bulk rock Pd values. Line indicates a one-to-one relationship (perfect correlation). Circled data points are for several assays from a single chip sample.

(Figure 2.6; Figure 2.11). Areas with “spotty” As grades are routinely found in the Garson ore bodies and this heterogeneous distribution can greatly influence the bulk As values in mined material. When low and high As samples from the inclusion-rich massive sulphide ores are compared they show considerable variation in the As host phases (Figure 2.14).

In As-rich samples found in DISS and INMS As abundance is controlled almost entirely by the abundance of CGSS, nickeline, and nickeline-CGSS intergrowths (Figure 2.14). In samples with low As in MASU and WR, CGSS and/or GGSS is the major contributor to As in the bulk rock, with pyrrhotite, pentlandite and sperrylite accounting for only minor quantities of As (Figure 2.14). Combined modal percentages for sulfarsenides and arsenides can range from <0.01 to 5 vol % and reach up to ~42 vol % in one case (Sample A62, stope 1321, 1 west shear 5100L; Table 2.7, Appendix A). The presence of CGSS and/or nickeline in relatively low abundance can result in bulk As concentrations above the acceptable smelter limits (Table 2.7, Appendix A). When sulfarsenides and arsenides are present in quantities even as low as ~0.05 vol %, bulk As concentration will be ~400-500 ppm. Pyrrhotite, chalcopyrite and pentlandite will only contribute to bulk As when arsenides and sulfarsenides are absent or present in very small (trace) quantities (Table 2.7, Appendix A). Arsenic-poor samples tend to contain GGSS grains which are smaller (avg. ~10-20 μm) than most CGSS grains. GGSS will account for bulk As concentrations in very As-poor samples [i.e., below detection limits for As (2.5 ppm)] when present in modal abundances above $\sim 10^{-4}$ vol%. Sperrylite may also account for significant As concentrations in several As-poor samples from the 4800 and

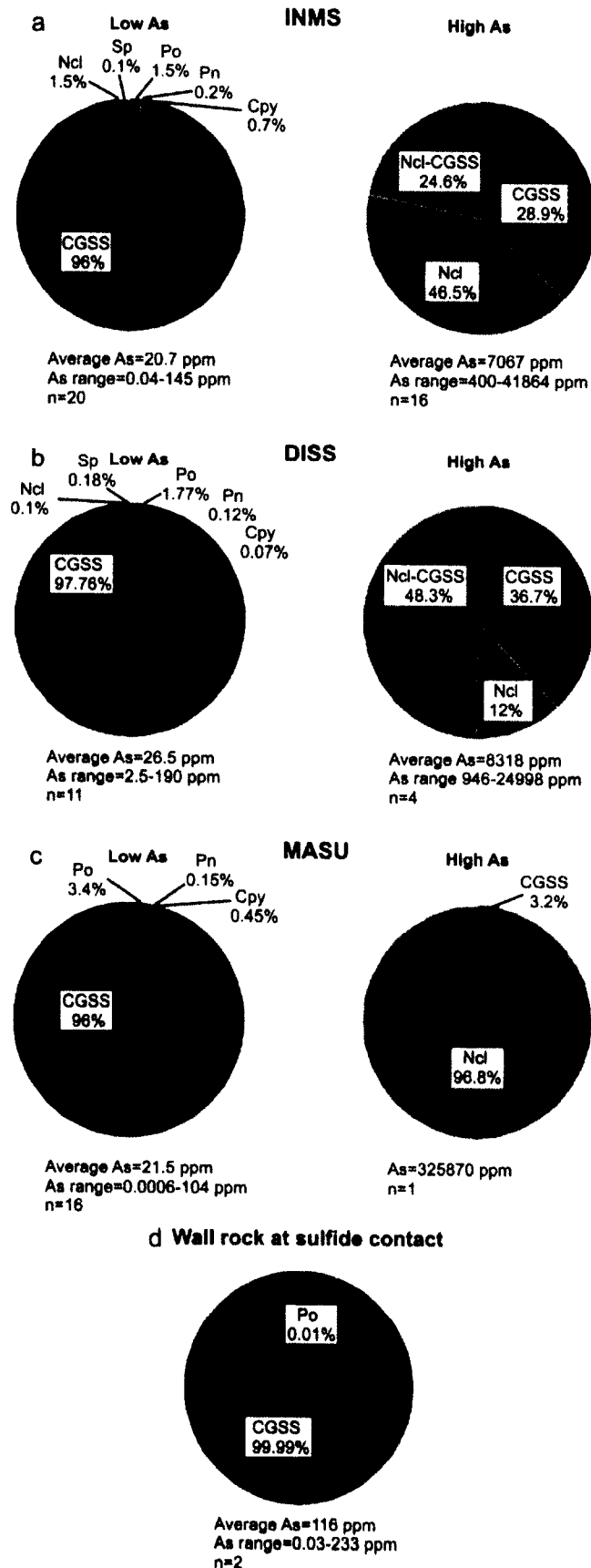


Figure 2.14 (previous page): Pie graphs showing mineralogical controls on As in observed minerals within low and high bulk rock As samples in different ore types at Garson. a) Variation within inclusion-rich massive sulphide ores (INMS); b) Variation within disseminated ores (DISS); c) Variation within massive sulphide ores. Note that most MASU samples are low in As with the exception of one high As sample; d) Variation within wall rock samples at the sulphide contact. Glaucodot-gersdorffite solid solution is incorporated into CGSS, because contribution to bulk As were minor. Mineral abbreviations: CGSS= cobaltite-gersdorffite solid solution; Cpy= chalcopyrite; Ir-Hw= Ir-Rh-bearing minerals; Ncl= nickeline; Ncl-CGSS= nickeline-CGSS intergrowths; Pn= pentlandite; Spy= sperrylite.

and sulfarsenides. Where no As minerals are present, the bulk As concentrations will be low and will be accounted for by the BMS in which very low abundances of dissolved As occur (Table 2.7, Appendix A).

2.4.9 Major controls on PGE distribution and abundance

The main controls on PGE abundance in the ores at the Garson Mine are PGM (telluropalladinite, michenerite, sperrylite, and rarely an unnamed Sn-Ni-Pd-selenide) and PGE-bearing sulfarsenides/arsenides (Figure 2.15; Figure 2.16). The PGM commonly occur as inclusions/infillings in arsenides and sulfarsenides, and therefore, these As-carriers ultimately control a large percentage of PGE in the ores.

Pt/Pd ratios in bulk rock samples range greatly from 0.06 to 30. Pt/Pd ratios for As-rich samples have values ≤ 1 . The highest bulk Pd (>1 ppm) correlates with high As values ($r=0.65$), and in some cases of low As, low Pd are also observed (Figure 2.15; Table 2.11, Appendix A). LA-ICPMS results show that CGSS phenocrysts contain more dissolved Pd, than nickeline, averaging ~ 138 ppm and ~ 44 ppm, respectively (Table 2.4, 2.5, Appendix A). Although nickeline contains some Pd it does not contribute to the overall bulk Pd of most samples, with the exception of those that are unusually rich in nickeline (Figure 2.15; Table 2.5, Appendix A). Concentrations of Pd and Pt are lower in nickeline compared to CGSS, with Pd values less than 130 ppm (avg. 44 ppm) and many analyses of Pt measuring below detection limits (Table 2.4, 2.5, Appendix A). This suggests that increasing amounts of CGSS and nickeline may raise the Pd/Pt ratio of the ores. Samples rich in PGE-rich, As-bearing minerals and Pd-tellurides will yield the

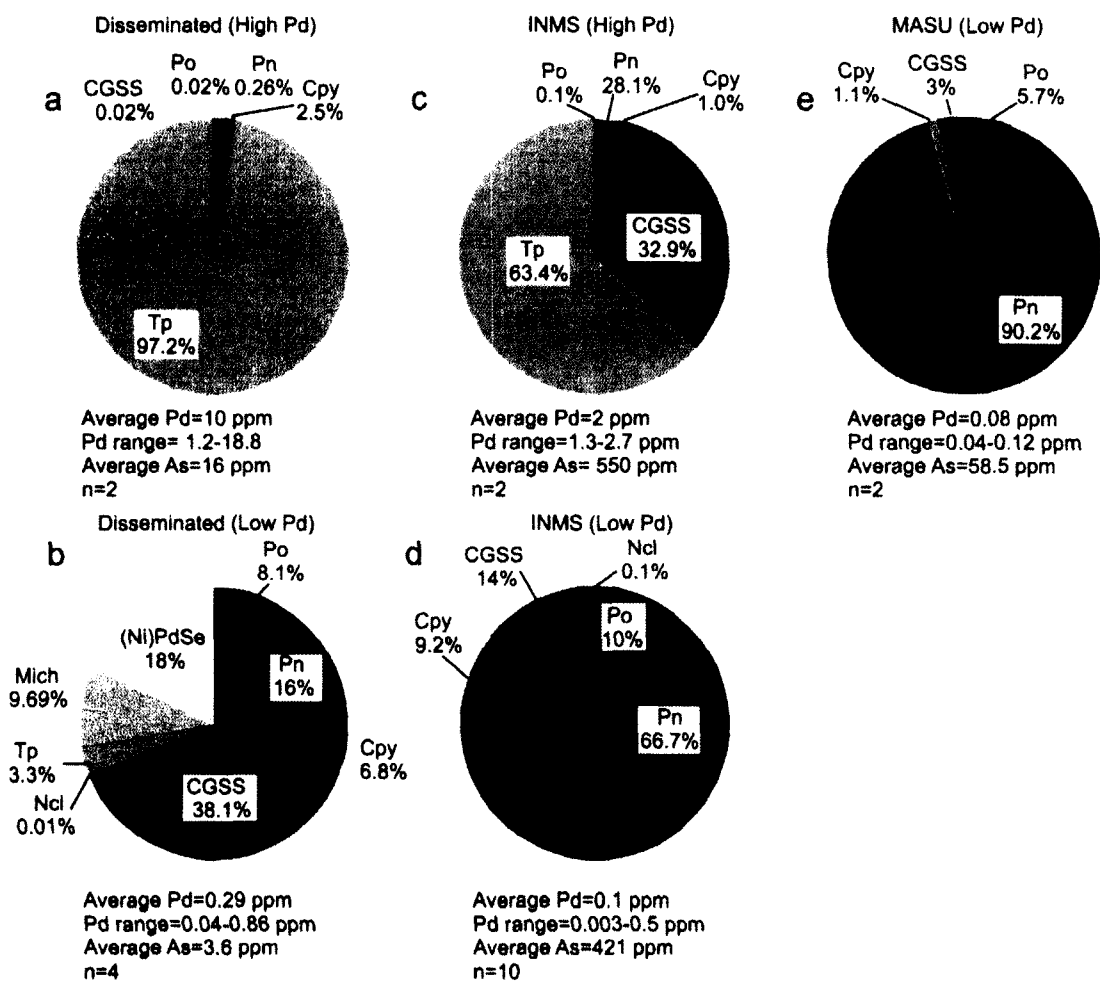


Figure 2.15: Pie graphs showing mineralogical controls on Pd in observed minerals within low and high bulk rock Pd samples in different ore types at Garson. a) distribution among samples from disseminated ore types with high bulk rock Pd; b) distribution among samples from disseminated ore types with low bulk rock Pd; c) distribution among samples from inclusion-rich massive sulphide (INMS) ore types with high bulk rock Pd; d) distribution among samples from inclusion-rich massive sulphide ore types with low bulk rock Pd; e) distribution among samples from massive sulphide (MASU) ore types with low bulk rock Pd. Glaucodot-gersdorffite solid solution is incorporated into CGSS, because contribution to bulk As were minor. Mineral abbreviations: Cpy= chalcopyrite; CGSS= cobaltite-gersdorffite solid solution; Mich= michenerite; (Sn, Ni)PdSe= tin-nickel-bearing palladium selenide; Ncl= nickeline; Pn= pentlandite; Tp= telluropalladinite; Spyl= sperrylite.

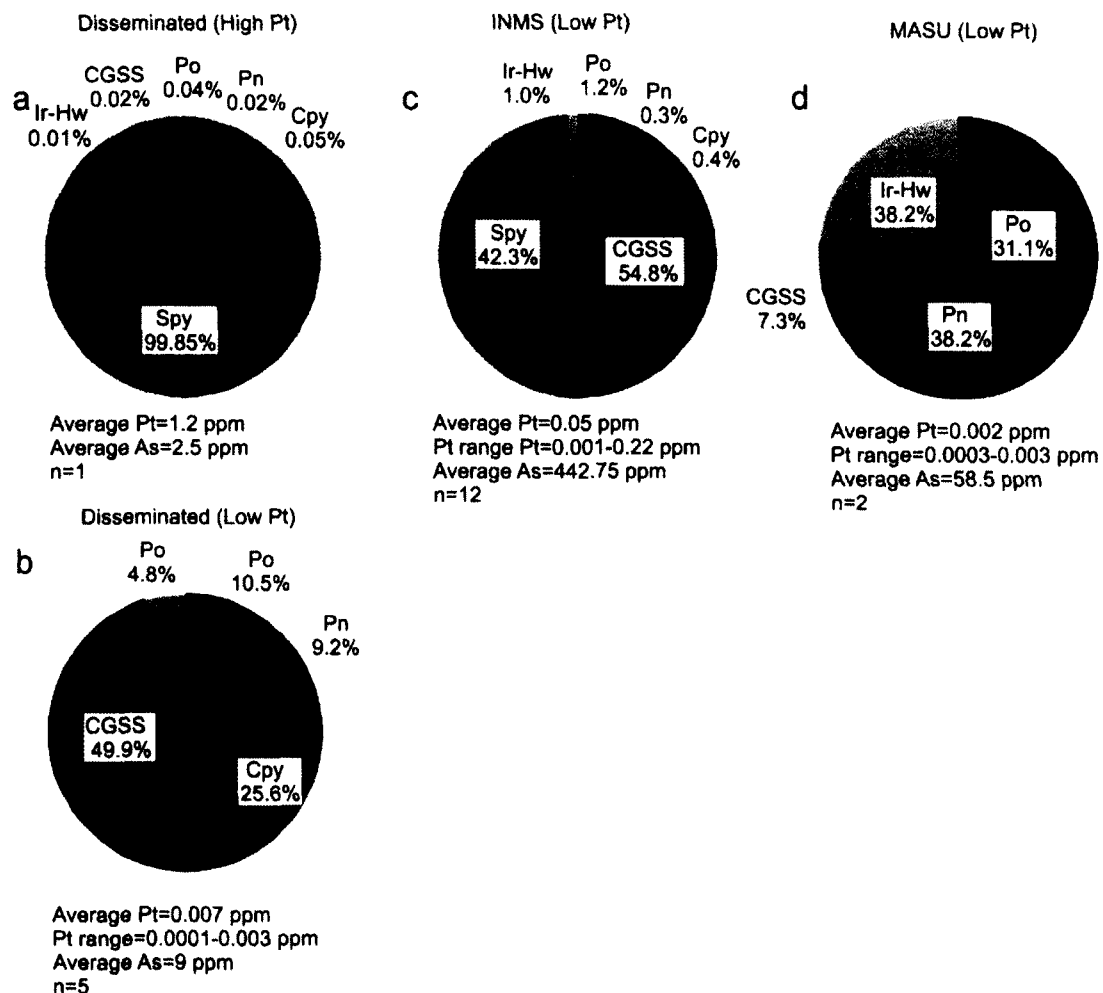


Figure 2.16: Pie graphs showing mineralogical controls on Pt in observed minerals within low and high bulk rock Pt samples in different ore types at Garson. a) distribution among samples from disseminated ore types with high bulk rock Pt; b) distribution among samples from disseminated ore types with low bulk rock Pt; c) distribution among samples from inclusion-rich massive sulphide (INMS) ore types with low bulk rock Pt; d) distribution among samples from massive sulphide (MASU) ore types with low bulk rock Pt. Mineral abbreviations: Cpy= chalcopyrite; CGSS= cobaltite-gersdorffite solid solution; Ir-Rh= Ir-Rh-bearing minerals; Mich= michenerite; (Ni)PdSe= Ni-bearing Pd selenide; Ncl= nickeline; Pn= pentlandite; Tp= telluropalladinite; Spy= sperrylite.

5100 levels (Figure 2.17). Sperrylite is never present as the only As-bearing phase; it always occurs in samples with the main arsenides highest bulk rock concentrations for Pd. The dominant control on Pt is sperrylite which is the most common Pt-bearing mineral in the South Range (Cabri and Laflamme, 1976; Figure 2.16a, c). Platinum is found in sulfarsenides at concentrations lower than Pd (Table 2.4, Appendix A). With CGSS the highest Pt concentrations correlate with the highest Ag, Bi, Te concentrations and shows weak correlation to high As. Where sperrylite is not observed, sulfarsenides, Ir-Rh bearing minerals and major phases play a larger role in Pt distribution in low Pt samples (Figure 2.16b-d). Generally, high concentrations of Pd tend to be associated with high As concentrations (Figure 2.18), which reflects the overall importance of CGSS and nickeline (PGE in solid solution and PGE in inclusions) to Pd distribution. Removal of CGSS and nickeline will negatively impact palladium recovery when desired As concentrations in mill feeds are to be less than 700 ppm (Christopher Davis, personal communication; Figure 2.18). High Pt concentrations can be found in low As samples (Figure 2.18). Only the presence of sperrylite can account for this observation. If sperrylite is the main Pt-bearing phase and is not associated with other major As phases, then corresponding bulk As concentration would not be problematic during mineral processing (i.e., even though sperrylite contains As, As levels would be relatively low) and Pt recovery will not be affected by the removal of CGSS and nickeline. Samples containing abundant CGSS-GGSS and/or nickeline and associated Pd-bearing telluride inclusions will have the highest overall concentrations of Pd, whereas, in Pd-rich, As-poor samples, Pd may be accounted for by just Pd-bearing tellurides (telluropalladinite,

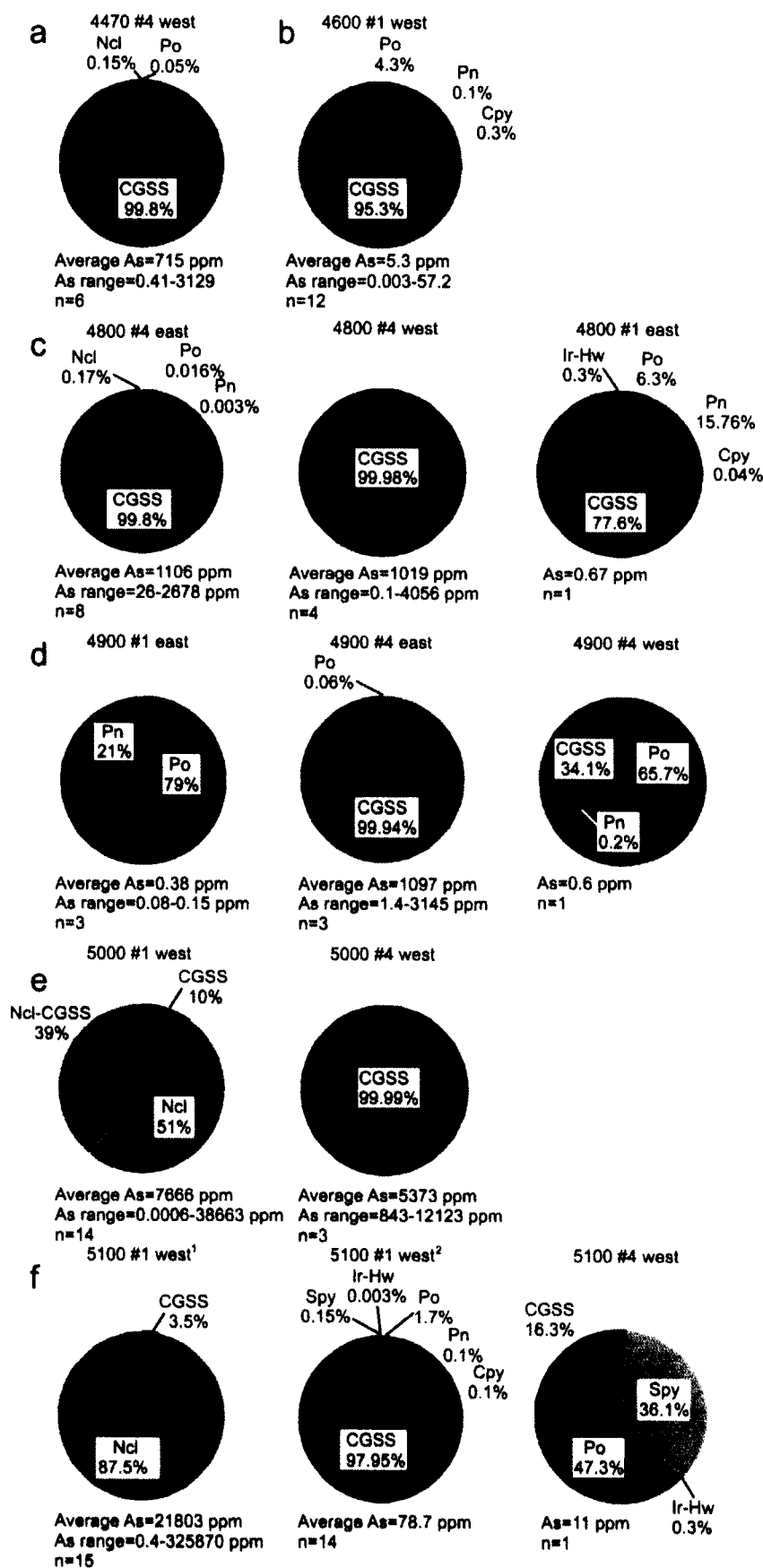


Figure 2.17 (previous page): Pie graphs showing mineralogical controls on As on different levels and shears at Garson. a) As distribution in #4 west shear on 4470 level; b) As distribution in #1 west shear on 4600 level; c) As distribution in #4 east shear, #4 west shear and #1 east shear on 4800 level d) As distribution in #1 east shear, #4 east shear and #4 west shear on 4900 level; e) As distribution in #1 west shear and #4 west shear on 5000 level; f) As distribution in #1 west shear and #4 west shear on 5100 level; two pie graphs are shown for the #1 west shear, the first including an extremely nickeline-rich outlier which increases average bulk As and nickeline control on As and the second excluding this outlier to show a more representative result for both bulk As distribution and As abundance control. In all distribution graphs, GGSS is included with CGSS because its contribution to bulk As is negligible. Mineral abbreviations: Cpy= chalcopyrite; CGSS= Cobaltite-gersdorffite solid solution; Ir-Hw= Ir-Rh-bearing; Ncl= nickeline; Ncl-CGSS= nickeline-CGSS intergrowths; Pn= pentlandite; Po= pyrrhotite; Spy= sperrylite.

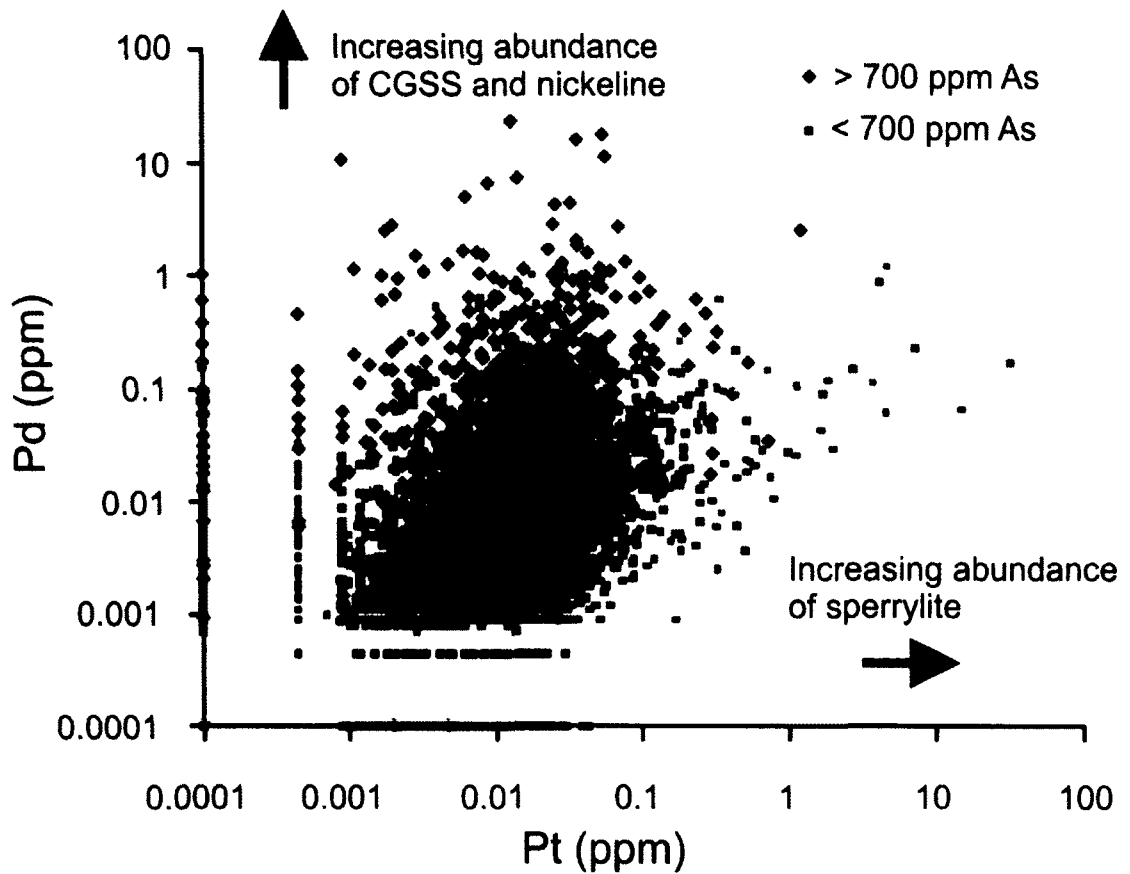


Figure 2.18: Graph showing the distribution of Pt and Pd with respect to As concentration. Data plotted from Vale's Garson database, representing ~ 13,500 assays from all ore types. High Pd values tend to correspond to high concentrations of As. Highest Pt values do not correspond to high concentrations of As. Pt and Pd do not show significant correlation. Note threshold value of 700 ppm corresponds desired limit in mill feed (Christopher Davis, personal communication). Values occurring along axes or in linear arrays represent values that were below detection limit of Pd or Pt.

michenerite). In cases where both As and Pd are low, the presence of rare Pd-bearing PGM as well as the BMS control bulk rock Pd distribution.

In samples with high nickeline abundance (i.e., high As-samples in which bulk As is controlled by nickeline abundance), the excess Pd which would otherwise be scavenged by CGSS was incorporated into MSS. Pentlandite contains significant amount of Pd (up to 20 ppm) in one area (stope 1291, #1 shear west 5000L), and is a main control on Pd abundance in samples with low bulk Pd where Pd-bearing minerals are scarce or not present (Figure 2.15b, d, e). Abundant chalcopyrite and nickeline are observed in samples where high Pd contents were noted in pentlandite, suggesting that either the presence of these minerals (rather than CGSS) or the process controlling nickeline formation (reactions with H₂O from wall rocks, unusually low fO_2) caused MSS and eventually pentlandite to host higher than typical Pd. The abundance of chalcopyrite in sulphide ores has been proposed as being associated with the incorporation of Pd into pentlandite in very similar environments at Sudbury (Dare et al., 2010b). High concentrations of Pd are found in pentlandite spatially associated with chalcopyrite at the Creighton mine (Dare et al., 2010b).

Palladium tends to partition into Cu-rich (ISS) liquid, rather than the related MSS, and the Pd that partitioned into this nearby Cu-rich liquid is thought to have diffused into the pentlandite during cooling because it is incompatible in chalcopyrite, leading to concentrations of up to ~2 ppm Pd in adjacent pentlandite (Dare et al., 2010b). This process may have affected the Garson ores, although samples which contain pentlandite with high Pd do not always contain high abundance of chalcopyrite from which Pd could

have been sourced, indicating that nickeline formation must have also played a role in Pd partitioning into pentlandite (Table 2.2, 2.7, Appendix A).

2.4.10 The effects of PGE and accessory mineral micrograins

The presence of microscopic PGM inclusions in Garson ores was observed through SEM and LA-ICPMS. These grains can bias LA-ICPMS results by contaminating signals and producing anomalously high concentrations of elements in the quantified results that are not truly dissolved trace phases. Micron-sized grains of sphalerite, CGSS-GGSS, nickeline, PGM, and Ag, Pd, Bi, and Ni-bearing tellurides can be observed in BSE images at high magnification. The presence of micrograins is suspected when LA-ICPMS signals show high intensity, short-lived peaks or “spikes” for As, Sb, Pb, Bi, Cu, Te, Pd, and Pt within a background of lower intensity counts suggests contamination of homogeneous mineral hosts by micrograins. For example, in pentlandite that is barren of dissolved Pd but contains Pd-bearing micrograins, LA-ICPMS analyses integrated over a large signal duration will show high concentrations of Pd that are not representative of dissolved Pd. In these cases Pd is accounted for by the Pd-bearing micrograins, not by Pd hosted by pentlandite. In CGSS, for example, high concentrations of Pd are dissolved within the mineral itself (Figure 2.9), as well as occurring in Pd-telluride micrograin inclusions (Table 2.4, Appendix A). On the other hand, it is not clear whether micrograins in fact represent (in all cases) exsolved phases. If so, then integration of signals over micrograin-rich intervals will yield more representative estimates of (originally) dissolved metals. We show that both exsolved and non-exsolved phases (secondary re-precipitation) of these metals are present (Figure 2.8a-f; Figure 2.10).

The presence of micrograins tends to be more prevalent in samples with abundant arsenide/sulfarsenides. This is especially true with the samples A86-91, (stope 1291, #1 west shear 5000L; Figure 2) and A62 (stope 1321, #1 west shear 5100L; Figure 2) that come from high As, nickeline-rich areas. The most problematic deleterious micrograins for mining/processing of ore would be As-bearing minerals (i.e., nickeline, CGSS-GGSS) as well as Pb and Bi-bearing tellurides. These grains are too small to remove economically because milling to such very small grain sizes is rarely cost efficient. PGE and accessory mineral micrograins are present in major base metal sulphides but they are volumetrically insignificant and do not impact overall bulk composition.

2.5 Conclusions

The Garson deposit, a modified contact-footwall style deposit which lies along the South Range of the Sudbury Igneous Complex, is characterized predominantly by pyrrhotite with subordinate pentlandite, chalcopyrite and abundant quartz and variable abundances of host rock inclusions of norite, metabasalt, metasediment and brecciated quartz veins. LA-ICPMS studies show that all major BMS are depleted in PPGE and IPGE, with the exception of Pd in pentlandite in samples with high abundances of chalcopyrite and nickeline. The deposit is locally enriched in As where grains of sulfarsenides (CGSS) and arsenides (nickeline) are the main control on As abundance. The sulfarsenides contain significant amounts of Pd (~198 ppm) and Pt (~88 ppm), and lesser IPGE. Two types of PGE mineralization are observed; (1) high As, high Pd ore dominated by telluropalladinite (main control on Pd) and PGE-bearing sulfarsenides (minor control on Pd, major control on As), and (2) low As, high Pd dominated by Pd-

tellurides dominated by telluropalladinite. In samples with low bulk As and Pd, michenerite, (Sn, Ni)PdSe and the major phases (especially pentlandite) account for Pd, while trace amounts of sulfarsenides account for the As. Platinum mineralization is dominated by sperrylite, which appears to occur heterogeneously. Minor amounts of irarsite-hollingworthite control a very small portion of Pt in some samples.

Regional assimilation of As into the original SIC magma rather than local assimilation of As from metasedimentary host rocks was the probable source of As seen in the Garson ores. Metasedimentary rocks along the South Range show anomalously high concentration of As. Sperrylite, sulfarsenide and arsenide grains began to form early in the deposit history, beginning to form at 1000-1200°C, after the crystallization of the norite and before MSS crystallization based on textural evidence. Earliest sulfarsenide grains would have scavenged PGE, which exsolve down temperature into discrete PGE sulfarsenide grains (irarsite-hollingworthite). Nickeline formation resulted from the local introduction of H₂O from reactions with hydrous silicates in the footwall host rocks. Nickeline commonly occurs as complex intergrowths with CGSS grains. The sulfarsenides and arsenides accumulated along the footwall contact (metabasalt-metasedimentary rocks) due to gravitational settling, while the sulphides were still liquid.

Some PGE mineralization dominated by telluropalladinite and other various Pd-bearing minerals [michenerite, paolovite, (Sn, Ni)PdSe] formed possibly due to the formation of a late-stage semimetal melt or hydrothermal phase. These minerals commonly exhibit open space filling texture, occur as inclusions in arsenides and sulfarsenides and occur along grain boundaries of sulphides and amphibole crystals. A

late-stage semimetal-rich melt (As, Bi, Te) would explain these textures and mineral associations.

Overturning of the deposit occurred in later stages of the deposit history and led to the reversal of footwall and hanging wall rocks. The ores would have been completely solid by the time of overturning since sulfarsenides and arsenides are concentrated along the current hanging wall contact to the south.

There are major limitations with a magmatic model for the As-rich mineralization at Garson, and given that the deposit experienced several periods of deformation, leading to the segregation of sulphide into individual shears, a metamorphic model for the mineralization must also be considered. In this scenario, partial melting of pre-existing As-rich sulfides or mineral assemblages may have resulted in the formation of As-rich liquids that sequestered Pd, Pt, Te, Bi and other metals. These As-rich melts may have accumulated along lithotectonic contacts and recrystallized. Limitations with a metamorphic origin for the As-rich mineralization also exist.

2.6 References

- Ames, D.E., Kjarsgaard, I.M., and Douma, S.L., 2003, Sudbury Ni-Cu-PGE ore mineralogy compilation: Sudbury Targeted Geoscience Initiative (TGI): Geological Survey of Canada Open File 1787, CD-ROM.
- Ames, D.E., and Farrow, C.E.G., 2007, Metallogeny of the Sudbury mining camp, Ontario: Mineral Deposits Division, Geological Association of Canada Special Publication 5, p. 329-350.
- Aniol, G.Z. and Brown, D.L., 1979, Garson Mine Ore Body Characteristics. Inco internal report.
- Arehart, G.B., Chrysosoulis and Kesler, S.E., 1993, Gold and arsenic in iron sulfides from sediment-hosted disseminated gold deposits: implications for depositional processes. *Economic Geology*; v. 88, p. 171-185.
- Ballhaus, C., and Sylvester, P., 2000, Noble metal enrichment processes in the Merensky Reef, Bushveld Complex: *Journal of Petrology*, v. 41, p. 545-561.
- Barlow, A.E., 1904, Origin, geological relations and composition of the nickel and copper deposits of the Sudbury Mining District, Ontario. Geological Survey of Canada, Annual report, p. 1-244.
- Barnes, S.-J., Cox, R.A., and Zientek, M.L., 2006, Platinum-group element, gold, silver and base metal distribution in compositionally zoned sulphide droplets from the Medvezky Creek mine, Norilsk, Russia: *Contributions to Mineralogy and Petrology*, v. 152, p.187-200.
- Barnes, S.-J., Prichard, H.M., Cox, R.A., Fisher, P.C., and Godel, B., 2008, The location of the chalcophile and siderophile elements in platinum-group element ore deposits (a textural, microbeam and whole rock geochemical study): Implications for the formation of the deposits: *Chemical Geology*, v. 248, p. 295-317.
- Barton P.B., 1969, Thermochemical study of the system Fe-As-S: *Geochimica et Cosmochimica Acta*, v. 33, p. 841-857.
- Boerner, D.E. and Milkereit, B., 1999. Structural evolution of the Sudbury impact structure in the light of seismic reflection data *in* B.O. Dressler and V.L. Sharpton, eds., *Large Meteorite Impact and Planetary Evolution*. Boulder, Colorado, Geological Society of America Special Paper 339, v. 419-429.
- Cabri, L.J., 1981, Mineralogy and distribution of the platinum-group in mill samples from the Cu-Ni deposits of the Sudbury, Ontario, area, *in* R.O McGachie and A.G. Bradley, eds., *Precious Metals*, Pergamon Press, p. 23-34.

Cabri, J.L., 1988, Overview on application of platinum mineralogy to mineral exploration and processing, *in* Carson, D.J.T., and Vassiliou, A.H., eds., *Process mineralogy VIII: Applications of Mineralogy to Mineral Beneficiation Technology, Metallurgy and Mineral Exploration and Evaluation, with Emphasis on Precious Metal Ores Symposium*, Minerals, Metals and Materials Society, Phoenix, Arizona, January 25–28, Proceedings, p. 23-31.

Cabri, L.J., and Laflamme, J.H.G., 1976, The mineralogy of the platinum group elements from some copper-nickel deposits of the Sudbury area, Ontario: *Economic Geology*, v. 71, p. 1159-1195.

Cabri, L.J., and Laflamme, J.H.G., 1984, Mineralogy and distribution of platinum-group elements in mill products from Sudbury *in* *Applied Mineralogy* W.C. Park, D.M. Hausen, and R.D. Hagni, eds., *Proc. 2nd International Conference on Applied Mineralogy in the Minerals Industry*, Los Angeles, Metallurgical Society of AIME, p. 911-922.

Carter, W.M., Watkinson, D.H., and Jones, P.C., 2001, Post-magmatic remobilization of platinum-group elements in the Kelly Lake Ni-Cu sulphide deposit, Copper cliff offset, Sudbury: *Exploration and Mining Geology*, v. 10, p. 95-110.

Carter, W.M., Watkinson, D.H., Ames, D.E., and Jones, P.C., 2009, Emplacement of quartz dioritic magmas and Cu-(Ni)-PGE mineralization of the Whistle offset, Sudbury, Canada: *Geological Survey of Canada Open File 6134*, 54 p.

Chen, Y., Fleet, M. E., and Pan, Y., 1993, Platinum-Group Minerals and Gold in Arsenic-Rich ore at the Thompson Mine, Thompson Nickel Belt, Manitoba, Canada: *Mineralogy and Petrology*, v. 49, p. 127-146.

Cheney, E. S., and Lange, I. M., 1967, Evidence for sulfurization and the origin of some Sudbury-type ores: *Mineralium Deposita*; v. 2, p. 80-94.

Cochrane, L.B., 1991, Analysis of the structural and tectonic environments associated with rock-mass failures in the mines of the Sudbury district: Ph. D. thesis, Department of Geological Sciences, Queen's University, 264 p.

Cook, N.J., Halls, C., and Boyle, A.P., 1993, Deformation and metamorphism of massive sulphides at Sulitjelma, Norway: *Mineralogical Magazine*, v. 57, p. 67-81.

Cowan, E.J. and Schwerdtner, W.M., 1994, Fold origin of the Sudbury basin. *In* Lightfoot, P.C., and Naldrett, A. (Eds.), *Proceedings of the Sudbury-Noril'sk Symposium*. Ontario Geological Survey Special, v. 5, p. 45-55.

Cowan, E.J., Riller, U. and Schwerdtner, W.M., 1999, Emplacement geometry of the Sudbury Igneous Complex: Structural examination of a proposed impact melt-sheet *in* B.O. Dressler, and V.L. Sharpton, eds., *Large Meteorite 773 Impacts and Planetary*

Evolution II. Boulder, Colorado, Geological Society of America Special Paper 339, p. 399-418.

Craig, R.J., and Kullerud, G., 1969, The Cu-Zn-S system: Carnegie Institution of Washington Year Book, v. 67, p.177-179.

Dare, S.A., Barnes, S.J., Prichard, H.M., Fisher, P.C., 2010a, The timing and formation of platinum-group minerals from the Creighton Ni-Cu-platinum group element sulphide deposit, Sudbury, Canada: early crystallization of PGE-rich sulfarsenides: *Economic Geology*, v. 105, p.1071-1096.

Dare, S.A., Barnes, S.J., Prichard, H.M., Fisher, P.C., 2010b, The distribution of platinum group elements (PGE) and other chalcophile elements among sulfides from the Creighton Ni-Cu-PGE sulfide deposit, Sudbury, Canada, and the origin of palladium in pentlandite: *Mineralium Deposita*, v. 45, p. 765-793.

Davidson, S. C., 1946, Structural aspect of the geology of Falconbridge nickel nine, Sudbury District, Ontario: *Transactions of the Canadian Institute of Mining and Metallurgy*, v. 46, p. 496-504.

Dietz, R.S., 1964, Sudbury structure as an astrobleme: *Journal of Geology*, v.72, p. 412-434.

Dressler, B.O., 1984,. General Geology of the Sudbury Area, *in* E.G. Pye, A.J. Naldrett, and P.E. Giblin, eds., *The Geology and Ore Deposits of the Sudbury Structure* Ontario Geological Survey, Special Volume 1, p. 57-82.

Dubé, B., and Gosselin, P., 2007, Greenstone-hosted quartz-carbonate vein deposits, *in* Goodfellow, W.D., ed., *Mineral Deposits of Canada: A synthesis of major deposit types, district metallogeny, the evolution of geological provinces and exploration methods*: St. John's, Geological Association of Canada – Mineral Deposits Division, p. 49-73.

Ebel, D.S., and Naldrett, A.J., 1996, Fractional crystallization of sulfide ore liquids at high temperature: *Economic Geology*; v. 91, p. 607-621.

Fanlo, I., Subias, I., Gervilla, F., Manuel, J., 2006, Textural and compositional variability in gersdorffite from the Crescencia Ni-(Co-U) Showing, central Pyrenees, Spain: Primary deposition or re-equilibrium? *The Canadian Mineralogist*; v. 44, p. 1513-1528.

Farrow, C.E.G., 1994, Geology, alteration, and the role of fluids in Cu-Ni-PGE mineralization of the footwall rocks to the Sudbury Igneous Complex, Levack and Morgan townships, Sudbury district, Ontario: Unpublished Ph.D. thesis, Ottawa, Ontario, Carleton University, 373 p.

Farrow, C.E.G., and Lightfoot, P.C., 2002, Sudbury PGE revisited: Toward an integrated model: Canadian Institute of Mining, Metallurgy and Petroleum Special Volume 54, p. 13-130.

Farrow, C.E.G., and Watkinson, D.H., 1997, Diversity of precious-metal mineralization in footwall Cu-Ni-PGE deposits, Sudbury, Ontario: Implications for hydrothermal models of formation: Canadian Mineralogist, v. 35, p. 817-839.

Farrow, C. E. G, Watkinson, D. H., and Jones, P. C., 1994, Fluid inclusions in sulfides from North and South Range Cu-Ni-PGE deposits, Sudbury structure, Ontario. Economic Geology; v. 89, p. 647-655.

Farrow, C.E.G., Everest, J.O., King, D.M. and Jolette, C., 2005, Sudbury Cu (-Ni)-PGE systems: refining the classification using McCreedy West Mine and Podolsky Project case studies: Mineralogical Association of Canada, Short Course 35, p. 163-180.

Fleet, M.E., Chrysoulis, S.L., Stone, W.E., and Weisener, C.G., 1993, Partitioning of platinum-group elements and Au in the Fe-Ni-Cu-S system: Experiments on the fractional crystallization of sulphide melt: Contributions to Mineralogy and Petrology, v. 115, p. 36-44.

Gervilla, F., Leblanc, M., Torres-Ruiz, J., and Hach-Ali, F.F., 1996, Immiscibility between arsenide and sulfide melts: a mechanism for the concentration of noble metals: Canadian Mineralogist, v. 34, p. 485-502.

Gervilla, F., Papunen, H., Kojonen, K., and Johanson, B., 1998, Platinum-, palladium- and gold-rich arsenide ores from the Kylmäkoski Ni -Cu deposit (Vammala Nickel Belt, SW Finland): Mineralogy and Petrology, v. 64, p. 163-185.

Gervilla, F., Cabri, L. J., Kojonen, K., Oberthür, T., Weiser, T. W., Johanson, B., Sie, S. H., Campbell, J. L., Teesdale, W. J., Laflamme, J. H. G., 2004, Platinum-group element distribution in some ore deposits: results of EPMA and micro-PIXE analyses: Microchimica Acta, v. 147, p. 167-173.

Godel, B., and Barnes, S.-J., 2008, Platinum-group elements in sulfide minerals and the whole rocks of the J-M Reef (Stillwater Complex): Implication for the formation of the reef: Chemical Geology, v. 248, p. 272-294.

Godel, B., Barnes, S.-J., and Maier, W. D., 2007, Platinum-group elements in sulphide minerals, platinum-group minerals, and the whole rocks of the Merensky Reef (Bushveld Complex, South Africa): Implication for the formation of the Reef: Journal of Petrology, v. 48, p. 1569-1604.

Golightly, P.J., 1994, The Sudbury igneous complex as an impact melt: Evolution and ore genesis, in Lightfoot, P.C., and Naldrett, A.J. eds., Proceedings of the Sudbury-Noril'sk

Symposium: Sudbury, Ontario Ministry of Northern Development and Mines, Ontario Geological Survey, p. 105-118.

González-Jiménez, J.M., Gervilla, F., Proenza, J.A., Augé, T., Griffin, W.L., and O'Reilly, S.Y., 2010, Contemporaneous segregation of PGE- and BM-rich sulfide melts and chromite crystallization: the Caridad chromite deposit, Mayarí-Baracoa Ophiolitic Belt (Eastern Cuba) [abs]: International Platinum Symposium, 11th, Sudbury, Ontario, Program Abstracts.

Hanley, J.J., Mungall, Pettke, T., Spooner, E.T.C., and Bray, C.J., 2005, Ore metal redistribution by hydrocarbon-brine and hydrocarbon-halide melt phases, North Range footwall of the Sudbury Igneous Complex, Ontario, Canada: *Mineralium Deposita*, v. 40, p. 237-256.

Hanley, J.J., 2007, The role of arsenic-rich melts and mineral phases in the development of high-grade Pt-Pd mineralization within Komatiite-associated magmatic Ni-Cu sulfide horizons at Dundonald Beach South, Abitibi subprovince, Ontario, Canada: *Economic Geology*, v. 102, p. 305-317.

Hawley, J.E., and Hewitt, D.F., 1948, Pseudo-eutectic and pseudo exsolution intergrowths of nickel-arsenides due to heat effects: *Economic Geology*, v. 46, p. 273-279.

Hawley, J. E. and Stanton, R. L., 1962, The facts: the ores, their minerals, metals and distribution (Part II). In *The Sudbury Ores; their mineralogy and origin*: *Canadian Mineralogist*, v. 7, p. 30-145.

Hawley, J.E., 1965, Upside-down zoning at Frood, Sudbury, Ontario: *Economic Geology*, v. 60, 529-575.

Hawley, J.E., Stanton, E.L., and Smith, A.Y. 1968. Psuedo-eutectic intergrowths in arsenical ores from Sudbury: *Canadian Mineralogist*, v. 6, p. 555-575.

Heinrich, C.A., and Eadington, P.J., 1986, Thermodynamic predictions of the hydrothermal chemistry of arsenic, and their significance for the paragenetic sequence of some cassiterite-arsenopyrite-base metal sulfide deposits: *Economic Geology*, v. 81, p. 511-529.

Hem, S.R., and Makovicky, E., 2004a, The System Fe-Co-Ni-As-S. I. Phase Relations in the (Fe,Co,Ni)As_{0.5}S_{1.5} Section at 650°C and 500°C: *Canadian Mineralogist*, v. 42, p. 43-62.

Hem, S.R., and Makovicky, E., 2004b, The System Fe-Co-Ni-As-S. II. Phase Relations in the (Fe,Co,Ni)As_{1.5}S_{0.5} Section at 650°C and 500°C: *Canadian Mineralogist*, v. 42, p. 63-86.

Holwell, D.A., and McDonald, I., 2007, Distribution of platinum-group elements in the Platreef at Overysel, northern Bushveld Complex: A combined PGM and LA-ICP-MS study: *Contributions to Mineralogy and Petrology*, v. 154, p. 171-190.

Holwell, M.A.E., and McDonald, 2010, A review of the behavior of platinum group elements within natural magmatic sulfide ore systems: *Platinum Metals Review*, v. 54, p. 26-36.

Huminicki, M.A.E., Sylvester, P.J., Cabri, L.J., Leshner, C.M., and Tubrett, M., 2005, Quantitative mass balance of platinum-group elements in the Kelly Lake Ni-Cu-PGE deposit, Copper Cliff offset, Sudbury: *Economic Geology*, v. 100, p. 1631-1646.

Hutchinson, D., and McDonald, I., 2008, Laser ablation ICP-MS study of platinum-group elements in sulphides from the Platreef at Turfspruit, northern limb of the Bushveld Complex, South Africa: *Mineralium Deposita*, v. 43, p. 695-711.

Klemm, D.D., 1965, Synthesen und Analysen in den Dreieckdiagrammen FeAsS-CoAsS-NiAsS und FeS₂-COS₂-NiS₂: *Neues Jahrbuche fuer Mineralogie, Abhandlungen*, v. 103, p. 205-255.

Klimczak, C., Wittek, A., Doman, D., and Riller, U., 2007, Fold origin of the NE-lobe of the Sudbury Basin, Canada: Evidence from heterogenous fabric development in the Onaping Formation and the Sudbury Igneous Complex; *Journal of Structural Geology*, v. 29, p. 1744-1756.

Lang, J., Rhys, D. and Naas, C., 2003. Structure and alteration related to gold-silver veins at the Skukum Creek deposit, southern Yukon, in Emond, D.S. and Lewis, L.L. eds., *Yukon Exploration and Geology 2002: Exploration and Geological Services Division, Yukon Region, Indian and Northern Affairs Canada*, p. 267-280

Lausen, C., 1930, Graphic intergrowth of niccolite and chalcopyrite, Worthington Mine, Sudbury, *Economic Geology*, v. 25, p. 356-364.

Lefort, D. T., Hanley, J. J., and Guillong, M., 2011, Subepithermal Au-Pd mineralization associated with an Alkalic porphyry Cu-Au deposit, Mount Milligan, Quesnel Terrane, British Columbia, Canada: *Economic Geology*, v. 106, p. 781-808.

Li, C., and Naldrett, A.J., 1993, Platinum-group minerals from the Deep copper zone of the Strathcona deposits, Sudbury, Ontario: *Canadian Mineralogist*, v. 31, p. 31-44.

Li, C., Naldrett, A.J., Coats, C.J.A., and Johannessen, P., 1992, Platinum, palladium, gold, and copper-rich stringers at the Strathcona mine, Sudbury: Their enrichment by fractionation of a sulfide liquid: *Economic Geology*, v. 87, p. 1584-1598.

- Li, C., Naldrett, A.J., Rucklidge, J.C., and Kilius, L.R., 1993, Concentration of platinum-group elements and gold in sulfides from the Strathcona deposit, Sudbury, Ontario: *Canadian Mineralogist*, v. 31, p. 523-531.
- Lightfoot, P. C., and Zotov, I. A., 2005, Geology and Geochemistry of the Sudbury Igneous Complex, Ontario, Canada: Origin of Nickel Sulfide Mineralization Associated with an Impact-Generated Melt Sheet. *Geology of Ore Deposits*; v. 47, p. 349-381.
- Magyarosi, Z., Watkinson, D.H., and Jones, P.C., 2002, Mineralogy of Ni-Cu-platinum-group element sulfide ore in the 800 and 810 ore bodies, Copper Cliff South mine, and P-T-X conditions during the formation of platinum-group minerals: *Economic Geology*, v. 97, p. 1471-1486.
- Makovicky, E., Karup-Møller, S., Makovicky, M., and Rose-Hansen, J., 1990, Experimental studies on the phase systems Fe-Ni-Pd-S and the Fe-Pt-Pd-As-S applied to PGE deposits: *Mineralogy and Petrology*, v. 42, p. 307-319.
- Makovicky, M., Makovicky, E., and Rose-Hansen, J., 1992, The phase system Pt-Fe-As-S at 850°C and 470°C: *Neues Jahrbuch für Mineralogie Monatshefte*, no. 10, p. 441-453.
- Maurel, C. and Picot, P., 1974, Stabilité de l'allosclérite et de la cobaltite dans les systèmes Co-As-S et Co-Ni-As-S: *Bulletin de la Société Française de Minéralogie et de Cristallographie*, v. 97, p. 251-256.
- McDonald, B.W.R., 1987, Geology and genesis of the Mount Skukum Tertiary epithermal gold-silver vein deposits, southwestern Yukon Territory. Unpublished M. Sc. thesis, University of British Columbia, Vancouver, B.C., 177 p.
- Merkle, R.K.W., 1992, Platinum-group minerals in the middle group of chromitite layers at Marikana, western Bushveld Complex: Indications for collection mechanisms and postmagmatic modification. *Canadian Journal of Earth Sciences*, v. 29, p. 209-221.
- Milkereit, B., Green, A., Berré, E., Boerner, D., Broome, J., Cosec, M., Cowan, J., Davidson, A., Dressler, B., Fueten, F., Grieve, R., James, R., Krause, B., McGrath, P., Meyer, W., Moon, W., Morris, W., Morrison G., Naldrett, A., Peredery, W., Rousell, D., Salisbury, M., Schwerdtner, W., Snajdr, P., Thomas, M. and Watts, A., 1992, Deep geometry of the Sudbury Structure from seismic reflection profiling: *Geology* 20, v. 807-811.
- Molnár, F., Watkinson, D.H., and Jones, P.C., 2001, Multiple hydrothermal processes in footwall units of the North Range, Sudbury Igneous Complex, Canada, and implications for the genesis of vein-type Cu-Ni-PGE deposits: *Economic Geology*, v. 96, p. 1645-1670.

Mukwakwami, J., Lafrance, B., and Leshner, C.M., 2011a, Deformation and remobilization of Ni-Cu-PGE ores at Garson Mine, Sudbury, Ontario; GAC-MAC-SEG-SGA Joint Annual meeting, Ottawa, Ontario, Program Abstracts, p.147.

Mukwakwami, J., Lafrance, B., and Leshner, C.M., 2011b, Back-Thrusting and Overturning of the Southern Margin of the 1.85 Ga Sudbury Igneous Complex at the Garson Mine, Sudbury, Ontario: Precambrian Research; in press.

Mungall, J.E., 2002, Late-Stage Sulfide Liquid Mobility in the Main Mass of the Sudbury Igneous Complex: Examples from the Victor Deep, McCreedy East, and Trillabelle Deposits: *Economic Geology*, v. 97, p. 1563-1576.

Mungall, J.E., and Naldrett, A.J., 2008, Ore deposits of the platinum-group elements: *Elements*, v. 4, p. 253-258.

Mungall, J.E., Ames, D.E., Hanley, J.J., 2004, Geochemical evidence from the Sudbury structure for crustal redistribution by large bolide impacts: *Nature*, v. 429, p. 546-548.

Mungall, J.E., Andrews, D.R.A., Cabri, L.J., Sylvester, P.J., and Tubrett, M., 2005, Partitioning of Cu, Ni,Au, and platinum-group elements between monosulfide solid solution and sulfide melt under controlled oxygen and sulfur fugacities: *Geochimica et Cosmochimica Acta*, v. 69, p. 4349-4360.

Mungall, J. E., 2007, Crystallization of magmatic sulfides: An empirical model and application to Sudbury ores: *Geochimica et Cosmochimica Acta*, v. 71, p. 2809-2819.

Naldrett, A.J., 1969, A portion of the Fe-S-O and its application to sulphide ore magmas: *Journal of petrology*, v. 10, p. 171-201.

Naldrett, A. J., 1984a, Mineralogy and composition of the Sudbury ores, *in* Pye, E.G., Naldrett, A.J., and Giblin, P.E., eds., *The geology and ore deposits of the Sudbury structure*: Toronto, Canada, Ministry of Natural Resources, v. 1, p. 309-325.

Naldrett , A.J., 1984b, Summary, discussion, and synthesis, *in* Pye, E.G., Naldrett, A.J., and Giblin, P.E., eds., *The geology and ore deposits of the Sudbury structure*: Toronto, Canada, Ministry of Natural Resources, v. 1, p. 533-569.

Naldrett, A. J., and Hewins, R.H., 1984, The main mass of the Sudbury igneous complex *in* E.G. Pye, A.J. Naldrett, P. Giblin, eds., *The Geology and Ore Deposits of the Sudbury Structure*: Ontario Geological Survey, Spec. Pub. v. 1, p. 233-251.

Naldrett, A. J., Hewins, R.H, Dressler, B. O., and Rao, B.V., 1984, The Contact Sublayer of the Sudbury igneous complex *in* E.G. Pye, A.J. Naldrett, P. Giblin, eds., *The Geology and Ore Deposits of the Sudbury Structure*: Ontario Geological Survey, Spec. Pub. v. 1, p. 254-273.

- Naldrett, A.J., Asif, M., Gorbachev, N.S., Kunilov, V.I., Stekhin, A.I., Fedorenko, V.A. and Lightfoot, P.C., 1994a, The composition of the Ni-Cu ores of the Noril'sk region: Ontario Geological Survey Special Publication 5, p. 357-372.
- Naldrett, A.J., Pesseran, A., Asif, M., and Li, C., 1994b, Compositional variation in the Sudbury ores and prediction of the proximity of footwall copper-PGE ore bodies: Ontario Geological Survey Special Publication 5, p. 133-146.
- Naldrett, A.J., Asif, M., Schandl, E., Searcy, T., Morrison, G.G., Binney, W.P., and Moore, C., 1999, Platinum group elements in the Sudbury ores: Significance with respect to the origin of different ore zones and to the exploration for footwall ores: *Economic Geology*, v. 94, p. 185- 210.
- Pan, Y., and Fleet, M.E., 1990, Metamorphic petrology and gold mineralization of the White River gold prospect, Hemlo area, in Geoscience Grant Research Program, Summary of Research 1989-1990, Ontario Geological Survey, Miscellaneous paper 150, p. 13-26.
- Panteleyev, A., 1986, A Canadian Cordilleran model for epithermal gold-silver deposits: *Geoscience Canada*, v. 13, p. 101-111.
- Péntek, A., Molnár, F., Watkinson, D.H., and Jones, P.C., 2008, Footwall type Cu-Ni-PGE mineralization in the Broken Hammer Area, Wisner township, North Range, Sudbury structure: *Economic Geology*, v. 103, p.1005–1028.
- Prevec, S.A. and Cawthorn, R.G., 2002, Thermal evolution and interaction between impact melt sheet and footwall: A genetic model for the contact sublayer of the Sudbury Igneous Complex, Canada; *Journal of Geophysical Research*, v. 107, p. 2176-2189.
- Riller, U., Boutelier, D., Schrank, C. and Cruden, A.R., 2010, Role of kilometer-scale weak circular heterogeneities on upper crustal deformation patterns: Evidence from scaled analogue modeling and the Sudbury Basin, Canada. *Earth and Planetary Earth Science Letters*, v. 297, p. 587-597.
- Rousell, D. H., 1984, Structural geology of the Sudbury basin *in* E.G. Pye, A.J. Naldrett, P. Giblin, eds., *The Geology and Ore Deposits of the Sudbury Structure*: Ontario Geological Survey, Spec. Pub. v. 1, p. 83-95.
- Shanks, W.S. and Schwerdtner, W.M., 1991a, Structural analysis of the central and southwestern Sudbury Structure, Southern Province, Canadian Shield: *Canadian Journal of earth Sciences*, v. 28, p. 411-430.
- Shanks, W.S., and Schwerdtner, W.M., 1991b, Crude quantitative estimates of the original northwest-southeast dimension of the Sudbury Structure, south-central Canadian Shield: *Canadian Journal of earth Sciences*, v. 28, p. 1677-1686.

Sillitoe, R. H., 1983, Enargite-bearing massive sulfide deposits high in porphyry copper systems: *Economic Geology*, v. 78, p. 348-352.

Skinner, B.J., Luce, F.D., Dill, J.A., Ellis, D.E., Hagan, H.A., Lewis, D.M., Odell, D.A., Sverjensky, D.A., and Williams, N., 1976, Phase relations in ternary portions of the system Pt-Pd-Fe-As-S: *Economic Geology*, v. 71, p. 1469-1475.

Szabó, E., and Halls, H.C., 2006, Deformation of the Sudbury Structure: Paleomagnetic evidence from the Sudbury breccia: *Precambrian Research*, v. 150, p. 27-48.

Szentpéteri, K., Watkinson, D.H., Molnár, F., and Jones, P.C., 2002, Platinum-group elements-Co-Ni-Fe sulfarsenides and mineral paragenesis in Cu-Ni-platinum-group element deposits, Copper Cliff north area, Sudbury, Canada: *Economic Geology*, v. 97, p. 1459-1470.

Taylor, B.E., 2007, Epithermal Gold Deposits, *in* Goodfellow, W.D., ed., *Mineral Deposits of Canada: A synthesis of major deposit types, district metallogeny, the evolution of geological provinces and exploration methods*: St. John's, Geological Association of Canada – Mineral Deposits Division, p. 113-139.

Therriault, A.M., Fowler, A.D., and Grieve, R.A.F., 2002, The Sudbury Igneous Complex: A differentiated impact melt sheet: *Economic Geology*, v. 97, p. 1521-1540.

Toguri, J.M., Babaie, H., and, Sridhar, R., 1995, The effect of arsenic on the Cu-Ni matte separation process: *Proceedings of the Second International Symposium on Quality in Non-Ferrous Pyrometallurgy*, Vancouver, Canada: Canadian Institute of Mining, Metallurgy and petroleum, p. 311-318.

Tomkins, A.G., 2010, Wetting facilitates late-stage segregation of precious metal-enriched sulfosalt melt in magmatic sulfide systems: *Geology*, v. 38, p. 951-954.

Tomkins, A.G., Pattinson, D.R.M. and Zaleski, E., 2004, The Hemlo gold deposit, Ontario: an example of melting and mobilization of a precious metal – sulfosalt assemblage during amphibolites facies metamorphism and deformation: *Economic Geology*, v. 99, p.1063-1084.

Tomkins, A.G., Frost, B.R., and Pattison, D.R.M., 2006, Arsenopyrite melting during metamorphism of sulphide ore deposits; *The Canadian Mineralogist*, v. 44, p. 1045-1062.

Tomkins, A.G., Pattison, D.R.M., and Frost, B.R., 2006, On the initiation of Metamorphic Sulfide anatexis: *Journal of Petrology*, v. 48, p. 511-535.

Wood, M., 2003, Arsenic in igneous systems: An experimental investigation: Unpublished B.A.Sc. thesis, University of Toronto, 32 p.

Yund, R.A., 1962, The system Ni-As-S; phase relations and mineralogical significance. American Journal of Science, v. 260, p. 761-782.

Yardley, B.W.D., 1989, An introduction to metamorphic petrology: Prentice Hall, London, 264 p.

Zientek, M.L., Likhachev, A.P., Kunilov, V.E., Barnes, S.J., Meier, A.L., Carlson, R.R., Briggs, P.H., Fries, T.L., and Adrian, B.M., 1994, Cumulus processes and the composition of magmatic ore deposits: Examples from the Talnakh district, Russia: Ontario Geological Survey Special Publication 5, p. 373-392

Table 2.1. Averages and ranges for elemental concentrations (ppm) in peridotite of A.M. FNN (n=60)

| Sample | Clap sample | Stage | Shale level | analyses | σ | Fe | Ni | Co | Zn | As | Se | Ko | Br | Pd | Ag | Cd |
|--------|-------------|-------|-------------|----------|-------------------|--------------------|--------------------|-------------------|------------------|--------------------|---------------------|--------------------|----------------------|-------------------|--------------------|------------------|
| A30 | D11 19 (1) | 2424 | #4 W 4470 | 3 | 121.62 (11.1-122) | 8251 (7090-8753) | 0.71 (0.61-0.8) | 6.6 (0.42-0.69) | 1.07 (0.61-2.7) | 87.58 (68-809) | 0.09 (0.07-0.11) | bd | bd | bd | 0.95 (0.7-1.1) | 0.026 (bd-0.08) |
| A31 | D11 19 (2) | 2424 | #4 W 4470 | 3 | 107.14 (90-122) | 9707 (9019-9221) | 1.46 (0.53-3.7) | 1.24 (0.03-3.3) | 0.22 (bd-0.65) | 91.59 (60-97) | 0.27 (0.25-0.29) | 0.0009 (bd-0.003) | bd | bd | 0.86 (0.8-0.9) | bd |
| M106 | D11 20 (1) | 2274 | #4 W 4470 | 3 | 55.35 (0.6-23) | 18984 (1431-24424) | 14.27 (2.1-193) | 0.14 (bd-0.42) | bd | 11.18 (25-17.5) | 0.005 (bd-0.017) | bd | bd | bd | 1.31 (0.75-2.06) | 0.06 (bd-0.103) |
| M107 | D11 20 (2) | 2274 | #4 W 4470 | 3 | 88.93 (0.1-151) | 4302 (4360-7024) | 1.1 (bd-2.8) | 0.12 (0.07-0.5) | 0.04 (bd-0.12) | 36.11 (1.1-5.40) | 0.02 (0.018-0.03) | bd | 0.0005 (bd-0.002) | 0.552 (0.36-0.72) | 0.04 (0.025-0.054) | |
| A37 | D11 20 (3) | 2704 | #4 W 4400 | 3 | 150.41 (124-151) | 9715 (8681-9625) | 0.18 (0.113-0.26) | 19.07 (0.06-55.8) | 0.72 (bd-0.97) | 22.26 (70-42.7) | 0.47 (0.06-0.48) | 0.0055 (bd-0.016) | 0.006 (bd-0.017) | 0.68 (0.59-0.76) | 0.04 (bd-0.11) | |
| A38 | D11 21 | 2274 | #4 W 4400 | 3 | 46.67 (6-146) | 6624 (678-678) | 0.86 (0.1-1) | 0.78 (0.1-1) | bd | 81.51 (7.8-131) | 0.03 (bd-0.04) | bd | 0.011 (bd-0.025) | 0.29 (0.17-0.5) | bd | |
| A40 | D11 26 | 2474 | #4 W 4800 | 3 | 144.37 (140-149) | 6706 (5992-7515) | 4.56 (0.17-11.8) | 0.43 (bd-0.75) | bd | 110.42 (10-120) | 0.08 (0.09-0.086) | bd | bd | bd | 0.5 (0.34-0.63) | bd |
| A41 | D11 27 | 2474 | #4 W 4800 | 3 | 117.21 (106-132) | 6732 (5895-5824) | 0.61 (0.14-0.17) | 0.61 (0.5-0.73) | 0.07 (bd-0.22) | 102.75 (102-140) | 0.21 (0.19-0.22) | 0.0011 (bd-0.002) | bd | 0.0011 (bd-0.009) | 0.07 (0.03-0.11) | bd |
| A42 | D11 28 (1) | 3174 | #4 W 4800 | 3 | 74.21 (63-90) | 6764 (6163-6632) | 0.83 (0.2-1.34) | 0.47 (0.39-0.54) | bd | 98.83 (98-100) | 0.007 (bd-0.02) | 0.0011 (bd-0.002) | bd | bd | 0.26 (0.15-0.46) | bd |
| A43 | D11 28 (2) | 3174 | #4 W 4800 | 3 | 47.61 (75-51) | 6748 (6170-6549) | 1.13 (0.4-8.3) | 0.69 (0.6-0.8) | bd | 111.41 (107-116) | 0.008 (bd) | bd | bd | bd | 1.37 (0.46-2.6) | 0.02 (bd) |
| A44 | D11 28 (3) | 3174 | #4 W 4800 | 3 | 64.46 (52-75) | 6048 (6093-9768) | 1.02 (0.7-1.4) | 0.71 (bd-0.6) | 0.3 (bd-0.55) | 89.93 (88-92) | 0.012 (bd-0.02) | 0.0004 (bd-0.0013) | bd | bd | 0.15 (0.12-0.17) | 0.02 (bd-0.055) |
| A47 | D1 3 (1) | 2524 | #4 W 4800 | 3 | 57.64 (44-73) | 9271 (10721-11023) | 0.56 (0.1-0.76) | 0.54 (0.15-0.7) | bd | 125.64 (12-132) | bd | bd | bd | bd | 1.17 (0.8-1) | bd |
| A65 | D11 15 (1) | 2781 | #1 E 4900 | 3 | 103.41 (80-117) | 3868 (3270-4400) | 0.47 (0.19-0.7) | 0.99 (0.47-1.98) | 0.16 (bd-0.17) | 109.04 (105-113.5) | 0.038 (0.03-0.043) | bd | bd | bd | 0.7 (0.34-1.35) | bd |
| A66 | D11 15 (2) | 2781 | #1 E 4900 | 3 | 78.92 (63-90) | 5348 (4271-6287) | 0.29 (bd-0.6) | 1.02 (bd-2.6) | 0.98 (0.72-1.41) | 107.92 (104-112) | 0.053 (0.025-0.075) | 0.0006 (bd-0.0019) | bd | bd | 0.32 (0.25-0.4) | bd |
| A67 | D11 16 | 2781 | #1 E 4900 | 3 | 80.13 (68-80) | 5430 (3584-7455) | 1.89 (0.1-5.35) | 2.3 (1.1-3.8) | 0.06 (bd-0.18) | 89.55 (86-91) | 0.23 (0.2-0.26) | bd | bd | bd | 0.27 (0.19-0.42) | 2.92 (1.08-5.52) |
| A68 | D11 17 | 2821 | #1 E 4900 | 3 | 89.97 (73-103) | 4707 (4140-5407) | 0.17 (0.09-0.23) | 0.56 (0.35-0.8) | bd | 76.05 (74-77) | 0.4 (0.36-0.46) | 0.0007 (bd-0.002) | bd | bd | 0.37 (0.26-0.49) | 0.02 (bd-0.03) |
| M19 | D1 12 (1) | 2274 | #4 E 4900 | 3 | 40.29 (25-50) | 4502 (4233-6075) | 27.65 (bd-81.30) | 2.34 (0.6-21.6) | bd | 25.24 (bd-39) | bd | bd | bd | bd | 1.83 (0.83-3.62) | 0.04 (bd-0.13) |
| A66 | D11 29 (1B) | 1291 | #1 W 5000 | 3 | 6.29 (4-6) | 121 (12970-3484) | 0.56 (bd-1.57) | 0.57 (0.46-0.72) | 0.35 (0.2-0.62) | 173.42 (16-178) | bd | bd | bd | 0.011 (bd-0.015) | 17.0 (70-35.38) | 0.04 (bd-0.13) |
| A67 | D11 29 (2) | 1291 | #1 W 5000 | 3 | 6.92 (6-70) | 4731 (12475-4768) | 0.12 (bd-0.27) | 0.45 (0.21-0.76) | 0.36 (bd-0.58) | 168.25 (165-175) | bd | bd | bd | bd | 11.23 (2.67-25.87) | bd |
| A68 | D11 29 (3A) | 1291 | #1 W 5000 | 3 | 14.94 (12.3-15.8) | 4720 (4402-5039) | 0.09 (bd-0.3) | 0.66 (0.3-0.97) | 0.31 (bd-0.47) | 141.13 (130-144) | 0.005 (bd-0.008) | bd | bd | 0.012 (bd-0.015) | 6.5 (0.63-18) | 0.02 (bd-0.05) |
| A69 | D11 29 (4B) | 1291 | #1 W 5000 | 3 | 10.54 (7.8-15.1) | 1978 (1807-2255) | 1.54 (0.5-2.8) | 0.77 (0.41-1.25) | 42.04 (0.38-108) | 128.57 (123-134) | 0.004 (bd-0.011) | bd | bd | 0.127 (bd-0.38) | 1.04 (0.58-1.36) | 0.09 (bd-0.15) |
| A80 | D11 29 (4A) | 1291 | #1 W 5000 | 3 | 7.416 (8-8.6) | 3401 (2613-3849) | 0.32 (0.2-0.6) | 0.53 (0.3-0.8) | 31.7 (0.25-93) | 149.21 (140-151) | bd | bd | bd | 0.0116 (bd-0.013) | 1.12 (0.13-2.8) | 0.02 (bd-0.065) |
| A91 | D11 29 (4B) | 1291 | #1 W 5000 | 3 | 5.11 (4.4-5.9) | 3754 (3273-4319) | 0.95 (bd-2.7) | 0.68 (0.52-0.83) | 4.2 (bd-12.6) | 159.9 (157-165) | bd | bd | 0.0016 (bd-0.003) | bd | 3.88 (0.38-10.7) | 0.1 (bd-0.26) |
| A92 | D11 30 | 1291 | #1 W 5000 | 3 | 195.47 (155-240) | 5329 (4805-6638) | 1.22 (0.6-2.2) | 1.17 (0.43-2.5) | bd | 156.4 (150-181) | 0.04 (0.03-0.023) | 0.001 (bd-0.002) | 0.0009 (bd-0.002) | 2.2 (0.14-0.19) | 0.06 (bd-0.15) | |
| M46 | D1 30 (1) | 1291 | #1 W 5000 | 3 | 4.79 (3.4-5.8) | 4822 (3273-5980) | 2.87 (0.2-2.2) | 0.25 (bd-0.44) | 0.16 (bd-0.13) | 61.98 (56-68) | bd | bd | 0.0066 (0.004-0.012) | 1.45 (0.35-2.38) | 0.08 (0.064-0.085) | |
| A49 | D11 1 | 2421 | #1 W 5100 | 2 | 71.7 (59-83) | 7147 (5804-8242) | 2759.75 (bd-4510)* | 5.61 (4.2-7.0) | 0.12 (bd-0.23) | 171.71 (170-174) | 0.048 (0.029-0.07) | 0.03 (bd-0.06) | 0.059 (bd-0.12) | 1.42 (0.35-2.57) | 0.57 (0.22-0.92) | |
| A50 | D11 2 | 2421 | #1 W 5100 | 2 | 13.7 (12.9-14) | 7977 (7271-8223) | 31.86 (0.5-0.8) | 1.71 (0.65-2.8) | 0.65 (bd-1.29) | 144.43 (137-152) | 0.007 (bd-0.015) | bd | bd | bd | 0.22 (0.19-0.24) | 0.09 (0.09-0.1) |
| A51 | D11 3 | 2421 | #1 W 5100 | 2 | 8.68 (8-8.7) | 5285 (4541-6028) | 0.59 (0.4-0.7) | 0.36 (0.15-0.37) | 0.14 (bd-0.27) | 181.21 (172-184) | 0.013 (bd-0.03) | bd | bd | bd | 0.36 (0.22-0.5) | bd |
| A52 | D11 4 | 2421 | #1 W 5100 | 2 | 12.24 (10.3-14.2) | 6182 (5152-7230) | 3.98 (0.6-8.9) | 4.78 (0.77-12.3) | 0.05 (bd-0.14) | 150.17 (147-154) | 0.008 (bd-0.015) | bd | bd | 0.009 (bd-0.018) | 1.03 (0.19-2.7) | 0.14 (0.06-0.28) |
| A53 | D11 5 | 2521 | #1 W 5100 | 3 | 28.95 (18.2-45.8) | 4691 (4016-5697) | 0.88 (0.8-0.9) | 0.42 (0.36-0.46) | bd | 134.51 (130-139) | 0.013 (bd-0.038) | bd | 0.022 (bd-0.044) | 0.58 (0.27-1.05) | 0.03 (bd-0.04) | |
| A54 | D11 6 | 2521 | #1 W 5100 | 3 | 30.45 (26-31) | 5861 (5678-6176) | 0.73 (0.5-1.0) | 0.47 (0.4-0.45) | 0.7 (0.58-0.9) | 135.18 (131-139) | bd | bd | 0.0007 (bd-0.002) | 0.06 (0.04-0.074) | 0.39 (0.13-0.9) | 0.02 (bd-0.06) |
| A59 | D11 11A (1) | 1322 | #1 W 5100 | 3 | 2.27 (1.9-2.7) | 8300 (7709-9003) | 0.19 (bd-0.35) | 0.77 (0.47-1.3) | 0.82 (0.57-1.1) | 176.17 (166-187) | bd | bd | bd | bd | 1.42 (0.17-2.7) | 0.16 (bd-0.32) |
| A60 | D11 11A (2) | 1322 | #1 W 5100 | 3 | 8.76 (7.2-16.4) | 1919 (1734-2069) | 0.33 (0.14-0.5) | 0.41 (0.28-0.5) | 181.29 (bd-178) | 162.11 (147-177) | 0.13 (0.08-0.15) | 0.0007 (bd-0.003) | 0.05 (bd-0.17) | 4.61 (0.89-9.6) | 0.03 (bd-0.053) | |
| A61 | D11 11B (1) | 1321 | #1 W 5100 | 4 | 21.09 (20.1-21.6) | 5048 (4531-6503) | 1.17 (0.54-1.85) | 0.47 (0.3-0.63) | 0.03 (bd-0.13) | 44.47 (41-46) | 0.002 (bd-0.002) | bd | 0.006 (bd-0.005) | 0.48 (0.28-0.85) | 0.01 (bd-0.033) | |
| M81 | D1 51 (1) | 1135 | #1 W 5100 | 3 | 51.16 (37-68.5) | 6216 (4534-6400) | 0.61 (0.33-0.78) | 0.38 (0.3-0.4) | 8.3 (1.1-12.1) | 76.31 (70-80) | 0.002 (bd-0.002) | bd | 0.009 (bd-0.004) | 0.22 (0.09-0.39) | 0.003 (bd-0.011) | |
| M84 | D1 52 (2) | 1135 | #1 W 5100 | 3 | 155.07 (107-183) | 8660 (7653-8553) | 1.56 (1.16-2.1) | 0.18 (bd-0.09) | 0.14 (bd-0.28) | 48.2 (46-54) | 0.015 (bd-0.042) | 0.0004 (bd-0.0004) | 0.007 (bd-0.017) | 0.15 (0.14-0.24) | 0.007 (bd-0.021) | |
| M86 | D1 54 (1) | 1173 | #1 W 5100 | 3 | 65.25 (60-80) | 6290 (5365-6987) | 0.39 (0.3-0.5) | 0.29 (bd-0.51) | 0.25 (0.15-0.72) | 42.76 (45-47) | 0.31 (0.28-0.33) | 0.017 (bd-0.005) | bd | bd | 0.24 (0.13-0.37) | bd |
| M88 | D1 55 (1) | 1214 | #1 W 5100 | 4 | 28.9 (25.5-36.1) | 4180 (3809-4843) | 0.23 (bd-0.37) | 0.29 (bd-0.51) | 0.25 (0.15-0.72) | 42.76 (45-47) | 0.31 (0.28-0.33) | 0.017 (bd-0.005) | bd | bd | 0.24 (0.13-0.37) | bd |
| M91 | D1 58 (1) | 2624 | #4 W 5100 | 1 | 68.65 (41.5-86.5) | 4256 (3078-4652) | 0.23 (bd-0.37) | 0.29 (bd-0.51) | 0.25 (0.15-0.72) | 42.76 (45-47) | 0.31 (0.28-0.33) | 0.017 (bd-0.005) | bd | bd | 0.24 (0.13-0.37) | bd |

1 = numbers not in parentheses indicate averages

2 = numbers in parentheses indicate ranges

* indicates values contaminated by microporosity or trace phase inclusions

bd indicates values below detection limit

NA indicates no recorded value

Table 2.1 Cont'd. Averages and ranges for elemental concentrations (ppm) in pyrochlore (I, A-J; PMs data)

| Sample | Chip sample | Stoichiometry | Shear level | # of analyses | Sn | Sb | Te | Re | Os | Ir | Pt | Au | Pb | Bi |
|--------|-------------|----------------|-------------|--------------------|--------------------|-------------------|--------------------|-------------------|-------------------|---------------------|--------------------|---------------------|--------------------|-------------------|
| A70 | DTL 19 (1) | 2424 #4 W 4470 | 3 | 0.01 (bdl-0.03) | 0.016 (0.01-0.018) | 1.41 (0.95-1.6) | N/A | N/A | bdl | 0.014 (bdl-0.04) | bdl | bdl | 5.16 (1.4-6.2) | 3.04 (2.7-3.6) |
| A71 | DTL 19 (2) | 2424 #4 W 4470 | 3 | 0.05 (0.03-0.07) | 0.005 (bdl-0.016) | 1.77 (1.2-2.2) | N/A | N/A | bdl | bdl | bdl | bdl | 3.47 (1.3-5) | 2.48 (1.5-3.4) |
| M106 | DL 70 (1) | 2274 #4 W 4470 | 3 | 0.89 (0.62-1.25) | bdl (bdl-0.1) | N/A | 0.09 (0.01-0.21) | N/A | bdl | bdl | bdl | bdl | 1.58 (1.3-2.1) | 2.59 (1.4-4.3) |
| M107 | DL 70 (2) | 2274 #4 W 4470 | 3 | 0.15 (0.14-0.18) | 0.006 (bdl-0.018) | N/A | 0.02 (bdl-0.026) | 0.003 (bdl-0.009) | 0.003 (bdl-0.001) | 0.004 (bdl-0.001) | 0.004 (bdl-0.001) | bdl | 0.83 (0.373-1.163) | 1.19 (0.8-2.0) |
| A77 | DTL 23B | 2374 #4 W 4600 | 3 | 0.04 (bdl-0.07) | 0.01 (0.01-0.018) | 1.87 (1.55-2.18) | N/A | N/A | 0.03 (bdl-0.08) | 0.04 (bdl-0.12) | bdl | bdl | 1.54 (0.85-2.03) | 1.11 (0.1-1.7) |
| A78 | DTL 24 | 2221 #4 W 4600 | 3 | 0.02 (bdl-0.03) | 0.005 (bdl-0.015) | 0.66 (0.52-0.8) | N/A | N/A | bdl | bdl | bdl | bdl | 6.62 (0.55-17.3) | 2.18 (0.63-3.8) |
| A80 | DTL 26 | 2474 #4 W 4800 | 3 | 0.03 (bdl-0.054) | bdl | 0.76 (0.65-1.05) | N/A | N/A | bdl | 0.003 (bdl-0.01) | bdl | 0.004 (bdl-0.013) | 0.58 (0.3-0.78) | 1.85 (1.8-1.9) |
| A81 | DTL 27 | 2474 #4 W 4800 | 3 | 0.02 (bdl-0.031) | 0.004 (bdl-0.013) | 0.86 (0.7-0.98) | N/A | N/A | 0.034 (bdl-0.07) | bdl | bdl | bdl | 0.62 (0.45-0.76) | 0.73 (0.6-0.9) |
| A82 | DTL 28 (1) | 3174 #4 W 4800 | 3 | bdl | bdl | 0.99 (0.8-1.13) | N/A | N/A | bdl | bdl | bdl | bdl | 0.56 (0.12-1.3) | 0.18 (0.10-0.33) |
| A83 | DTL 28 (2) | 3174 #4 W 4800 | 3 | 0.01 (bdl-0.029) | 0.01 (bdl-0.025) | 1.15 (0.92-1.38) | N/A | N/A | bdl | bdl | 0.01 (0.03-0.01) | bdl | 2.32 (0.32-5.3) | 0.99 (0.3-1.6) |
| A84 | DTL 28 (3) | 3174 #4 W 4800 | 3 | 0.01 (bdl-0.03) | 0.004 (bdl-0.011) | 3 (0.75-7.35) | N/A | N/A | bdl | bdl | bdl | bdl | 0.52 (0.38-0.6) | 0.45 (0.2-0.8) |
| A07 | DL 7 (1) | 2524 #4 W 4800 | 3 | bdl | bdl | 0.05 (bdl-0.15) | N/A | N/A | bdl | bdl | bdl | bdl | 4.95 (4.7-5.5) | 1.67 (0.99-2.4) |
| A65 | DTL 15 (1) | 2781 #1 E 4900 | 3 | 0.02 (0.013-0.031) | bdl | 1.03 (0.7-1.44) | N/A | N/A | bdl | bdl | bdl | bdl | 0.87 (0.42-1.8) | 1.75 (0.9-2.9) |
| A66 | DTL 15 (2) | 2781 #1 E 4900 | 3 | 0.03 (bdl-0.07) | 0.006 bdl | 1.28 (1.0-1.6) | N/A | N/A | 0.01 (bdl-0.03) | bdl | 0.003 (bdl-0.009) | bdl | 0.38 (0.28-0.48) | 1.16 (0.80-1.6) |
| A67 | DTL 16 | 2781 #1 E 4900 | 3 | 0.02 (bdl-0.036) | 0.015 (0.01-0.02) | 1.19 (0.9-1.7) | N/A | N/A | 0.02 (bdl-0.06) | 0.0026 (bdl-0.008) | bdl | bdl | 0.43 (0.12-0.83) | 1.11 (0.25-1.9) |
| A68 | DTL 17 | 2521 #1 E 4900 | 3 | 0.01 (bdl-0.03) | 0.007 (bdl-0.02) | 0.86 (0.72-1.06) | N/A | N/A | 0.05 (bdl-0.08) | bdl | bdl | bdl | 0.42 (0.16-0.71) | 0.95 (0.47-1.4) |
| M119 | DL 12 (1) | 2774 #4 E 4900 | 3 | 0.71 (0.08-1.72) | 0.008 (bdl-0.023) | bdl | 0.005 (bdl-0.009) | N/A | bdl | 0.006 (bdl-0.0017) | 0.004 (bdl-0.011) | 0.003 (bdl-0.01) | 1.39 (bdl-2.34) | 4.21 (2.6-6.2) |
| A86 | DTL 29 (1B) | 1291 #1 W 5000 | 3 | 0.03 (bdl-0.062) | 0.01 (bdl-0.04) | 1.67 (1.0-2.72) | N/A | N/A | bdl | bdl | bdl | bdl | 1.32 (0.6-2.3) | 1.76 (1.1-2.56) |
| A87 | DTL 29 (2) | 1291 #1 W 5000 | 3 | 0.05 (0.04-0.06) | bdl | 12.93 (1.7-32.5)* | N/A | N/A | bdl | bdl | bdl | bdl | 0.8 (0.04-1.11) | 1.28 (0.47-1.9) |
| A88 | DTL 29 (3A) | 1291 #1 W 5000 | 3 | 0.08 (0.0256-2.9) | 0.01 (bdl-0.02) | 6.66 (bdl-19)* | N/A | N/A | bdl | 0.001 (bdl-0.004) | 0.007 (bdl-0.021) | bdl | 4.13 (3.2-5.9) | 0.62 (0.19-0.5) |
| A89 | DTL 29 (3B) | 1291 #1 W 5000 | 3 | 0.09 (0.03-0.164) | 0.02 (bdl-0.07) | 1.6 (0.6-3.3) | N/A | N/A | bdl | bdl | bdl | bdl | 5.29 (3.5-8.7) | 0.63 (0.4-0.83) |
| A90 | DTL 29 (4A) | 1291 #1 W 5000 | 3 | 0.016 (0.02-0.027) | 0.03 (bdl-0.011) | 1.6 (bdl-3.9) | N/A | N/A | bdl | bdl | bdl | bdl | 1.41 (0.17-3.9) | 1.12 (0.24-2.8) |
| A91 | DTL 29 (4B) | 1291 #1 W 5000 | 3 | 0.07 (0.029-0.13) | 0.008 (bdl-0.023) | 1.89 (0.8-3.8) | N/A | N/A | bdl | bdl | bdl | bdl | 0.71 (0.2-1.6) | 0.67 (0.12-1.2) |
| A92 | DTL 30 | 1291 #1 W 5000 | 3 | 0.046 (0.06-0.05) | 0.006 (bdl-0.019) | 5.4 (bdl-16.1) | N/A | N/A | bdl | bdl | bdl | 0.004 (bdl-0.013) | 0.67 (1.1-4.34) | 3.51 (1.85-6) |
| M146 | DL 30 (1) | 1291 #1 W 5000 | 3 | 0.24 (0.1-0.42) | 0.005 (bdl-0.016) | N/A | N/A | N/A | bdl | bdl | bdl | 0.005 (bdl-0.003) | 2.89 (0.84-6.1) | 1.07 (0.44-2) |
| A49 | DTL 1 | 2421 #1 W 5100 | 2 | 0.38 (0.03-0.73) | bdl | 2.26 (0.52-4) | N/A | N/A | bdl | bdl | bdl | bdl | 35.19 (32-38) | 2.32 (0.8-3.8) |
| A50 | DTL 2 | 2421 #1 W 5100 | 2 | 0.03 (bdl-0.055) | bdl | 0.58 (0.46-0.7) | N/A | N/A | 0.004 (bdl-0.008) | bdl | bdl | 0.006 (bdl-0.012) | 0.52 (0.47-0.56) | 0.51 (0.48-0.55) |
| A51 | DTL 3 | 2421 #1 W 5100 | 2 | 0.04 (0.04-0.059) | 0.009 (bdl-0.018) | 1.45 (0.8-2.1) | N/A | N/A | bdl | bdl | bdl | bdl | 5.34 (1.3-9.4) | 0.99 (0.57-1.4) |
| A52 | DTL 4 | 2421 #1 W 5100 | 2 | 0.03 (bdl-0.06) | bdl | 0.85 (0.8-0.9) | N/A | N/A | bdl | 0.002 (bdl-0.004) | bdl | bdl | 0.45 (0.42-0.49) | 0.35 (0.3-0.4) |
| A53 | DTL 5 | 2421 #1 W 5100 | 3 | 0.06 (0.026-0.12) | 0.005 (bdl-0.014) | 1.13 (0.4-1.6) | N/A | N/A | bdl | bdl | bdl | 0.007 (bdl-0.012) | 1.135 (1.2-30.8) | 3 (1.1-6.5) |
| A54 | DTL 6 | 2271 #1 W 5100 | 3 | 0.05 (0.03-0.07) | bdl | 1.2 (0.6-2.2) | N/A | N/A | bdl | 0.002 (bdl-0.005) | 0.007 (bdl-0.02) | bdl | 3.15 (1.6-5.3) | 2.96 (1.7-5.5) |
| A59 | DTL 11A (1) | 1322 #1 W 5100 | 3 | 0.009 (bdl-0.026) | bdl | 2.31 (1.9-3.0) | N/A | N/A | bdl | bdl | bdl | 0.04 (0.008-0.084) | 0.27 (0.057-0.65) | 0.11 (0.029-0.26) |
| A60 | DTL 11A (2) | 1322 #1 W 5100 | 3 | 0.02 (bdl-0.33) | 0.01 (bdl-0.02) | 2.93 (0.9-5) | N/A | N/A | bdl | 0.002 (bdl-0.006) | bdl | bdl | 2.08 (0.74-3.8) | 4.77 (0.8-12.2) |
| A61 | DTL 11B (1) | 1321 #1 W 5100 | 4 | 0.03 (bdl-0.06) | 0.41 (bdl-1.52) | 4.52 (0.7-9.6) | N/A | N/A | bdl bdl | bdl bdl | bdl bdl | 0.003 (bdl-0.011) | 8.55 (4.5-13.3) | 1.03 (0.55-1.8) |
| M81 | DL 51 (1) | 1135 #1 W 5100 | 5 | 0.15 (0.11-0.2) | 0.002 (bdl-0.007) | N/A | 0.11 (0.006-0.31) | 0.01 (bdl-0.02) | bdl | bdl | bdl | bdl | 4.77 (0.35-13.5) | 1.18 (0.44-3.4) |
| M84 | DL 52 (2) | 1135 #1 W 5100 | 3 | 0.08 (0.04-0.14) | 0.02 (bdl-0.05) | N/A | 0.007 (bdl-0.015) | bdl | bdl | 0.0006 (bdl-0.002) | bdl | bdl | 3.68 (1.6-7.3) | 2.78 (0.69-6) |
| M86 | DL 54 (1) | 1173 #1 W 5100 | 3 | 0.08 (0.026-0.19) | 0.008 (bdl-0.008) | N/A | 0.014 (bdl-0.032) | 0.006 (bdl-0.01) | bdl | bdl | 0.001 (bdl-0.003) | 0.0005 (bdl-0.0014) | 2.42 (0.47-4.8) | 1.03 (0.37-1.9) |
| M88 | DL 55 (1) | 1214 #1 W 5100 | 4 | bdl (bdl-0.04) | bdl | N/A | 0.003 (bdl-0.006) | 0.003 (bdl-0.007) | 0.003 (bdl-0.003) | 0.0002 (bdl-0.0005) | bdl | bdl | 1.23 (0.48-1.9) | 1.45 (0.82-2.2) |
| M91 | DL 58 (1) | 2624 #4 W 5100 | 3 | 0.03 (bdl-0.051) | 0.004 (bdl-0.013) | N/A | 0.02 (0.004-0.042) | 0.04 (0.032-0.06) | 0.001 (bdl-0.003) | 0.001 (bdl-0.004) | 0.0003 (bdl-0.001) | 0.0003 (bdl-0.001) | 0.62 (0.49-0.74) | 0.48 (0.4-0.6) |

* indicates values contaminated by micrograms or trace phase inclusions

bdl indicate values below detection limit

N/A indicates no recorded value

Sample 1 has sample size of analyses

| | | | | | | | | | | | | |
|-----|------------|------|----------|---------------------|--------------------|---------------------|--------------------|--------------------|----------------------|----------------------|--------------------|-----------------------|
| M19 | DL 58 (1) | 2624 | # W 5100 | 7732 (7210.8098) | 0.19 (0.010.58) | 0.19 (0.010.58) | 34.8 (31.9.36) | 0.77 (0.716.0.857) | 0.0013 (0.010.0032) | 0.057 (0.050.061) | 0.25 (0.170.33) | 0.01 |
| M18 | DL 55 (1) | 1214 | # W 5100 | 9487 (6695.10070) | 0.39 (0.010.9) | 0.14 (0.010.41) | 42.7 (40.41) | 0.8 (0.754.0.87) | 0.0008 (0.010.0026) | 0.49 (0.177.0.798) | 0.34 (0.391.07) | 0.01 |
| M6 | DL 54 (1) | 1173 | # W 5100 | 10886 (10769.11104) | 0.4 (0.18.0.8) | 0.34 (0.319.0.35) | 0.17 (0.152.0.194) | 0.79 (0.795.0.802) | 0.0005 (0.010.0014) | 1.17 (1.181.61) | 0.34 (0.320.37) | 0.01 |
| M4 | DL 52 (2) | 1135 | # W 5100 | 10113 (10302.10926) | 13.8 (10.129.7) | 0.36 (0.010.67) | 1.29 (0.015.25) | 55 (44.86) | 0.71 (0.497.0.9) | 0.95 (0.655.1.28) | 1.47 (0.36.6.6) | 0.004 (0.010.07) |
| A9 | DL 11A (1) | 1322 | # W 5100 | 333 (241.139) | 0.34 (0.26.0.43) | 0.39 (0.340.46) | 16.01 (0.45.61.85) | 114 (111.120) | 0.046 (0.031.0.0682) | 14.98 (12.1715.58) | 0.38 (0.26.0.7) | 0.025 (0.010.057) |
| A4 | DL 11.6 | 1322 | # W 5100 | 5288 (5156.5398) | 0.54 (0.01.2) | 0.56 (0.360.866) | 0.22 (0.010.66) | 115 (112.116) | 0.725 (0.7010.762) | 1.87 (1.82.1.91) | 1.61 (1.091.94) | 0.04 (0.010.065) |
| A3 | DL 11.5 | 2271 | # W 5100 | 4817 (4772.4884) | 3.15 (2.01.4.9) | 0.81 (0.598.1.24) | 2.12 (0.584.62) | 138 (129.145) | 0.6 (0.547.0.66) | 1.52 (1.441.63) | 1.19 (1.281.49) | 0.66 (0.038.0.97) |
| A2 | DL 11.4 | 2231 | # W 5100 | 1932 (1884.1962) | 91.5 (51.29.123.3) | 2.54 (0.378.6.18) | 154 (143.162) | 0.32 (0.258.0.379) | 0.0014 (0.010.0041) | 1.49 (1.184.1.85) | 22.5 (0.94.63.6) | 0.24 (0.010.61) |
| A1 | DL 11.3 | 2421 | # W 5100 | 717 (706.727) | 1.09 (1.05.1.14) | 152 (0.52.303) | 144 (134.154) | 0.11 (0.10.114) | 0.002 (0.010.0038) | 1.51 (1.491.53) | 1.68 (0.01.327) | |
| A0 | DL 11.2 | 2421 | # W 5100 | 1725 (1634.1817) | 2.94 (1.31.4.57) | 47 (45.84.8.7) | 189 (186.193) | 0.25 (0.234.0.264) | 0.43 (0.225.0.639) | 3.7 (1.44.5.98) | 0.99 (0.92.1.07) | |
| M6 | DL 10 (1) | 1291 | # W 5000 | 513 (497.528) | 18.5 (4.12.32.87) | 6.59 (0.891.12.99) | 36.17 (0.0172.33) | 46 (39.54) | 0.03 (0.010.059) | 18.88 (17.05.20.21) | 0.57 (0.540.61) | 0.23 (0.010.45) |
| A2 | DL 10 | 1291 | # W 5000 | 28913 (27541.29877) | 76 (10.58.197.3) | 2818 (77.6.7659) | 0.087 (0.010.26) | 147 (142.154) | 4.49 (4.33.4.74) | 0.0009 (0.010.0028) | 1.27 (1.104.1.55) | 7.98 (2.78.15.28) |
| A1 | DL 10 (4A) | 1291 | # W 5000 | 593 (561.619) | 1227 (0.185.681) | 1.66 (0.010.2) | 543 (0.010.3) | 130 (125.137) | 0.079 (0.063.0.104) | 11.19 (7.78.14) | 1.9 (1.39.2.87) | 0.15 (0.010.412) |
| A9 | DL 10 (3B) | 1291 | # W 5000 | 2905 (535.15275) | 1130 (10.77.1154) | 2794 (117.569) | 106 (103.109) | 0.19 (0.181.0.199) | 0.14 (0.1012.0.26) | 76.19 (65.88.85.7) | 16.65 (6.29.27.37) | |
| A7 | DL 10 (2) | 1291 | # W 5000 | 556 (536.574) | 25.46 (0.67.22) | 203 (0.51.607.9) | 24.24 (0.0169.87) | 141 (138.143) | 0.062 (0.0540.076) | 21.31 (19.24.22.5) | 9.22 (4.12.105) | 13.1 (0.016.39.27) |
| A6 | DL 10 (1B) | 1291 | # W 5000 | 476 (454.500) | 165 (11.95.495.1) | 0.55 (0.22.95.43) | 3.69 (5.34.119.17) | 138 (130.152) | 0.050 (0.0460.059) | 15.34 (14.3.17.06) | 15.1 (12.5.42.2) | 2.03 (0.015.65) |
| M19 | DL 12 (1) | 2774 | # F 4900 | 9036 (8595.9356) | 7.3 (0.919.53) | 1.65 (0.010.46) | 33.4 (29.440.9) | 0.55 (0.429.69) | 0.53 (0.440.69) | 0.02 (0.010.056) | | |
| A8 | DL 17 | 2821 | # F 4900 | 10897 (10312.11203) | 0.28 (0.210.393) | 0.39 (0.369.0.446) | 1.65 (0.010.448) | 65.6 (62.67) | 1.88 (1.841.95) | 0.003 (0.010.0041) | 0.83 (0.365.1.52) | 0.02 (0.010.059) |
| A6 | DL 16 | 2781 | # F 4900 | 12715 (12584.12812) | 1.34 (0.151.63) | 0.42 (0.369.0.446) | 0.065 (0.010.43) | 77 (76.77.2) | 2.09 (2.042.12) | 0.0037 (0.010.0066) | 0.21 (0.192.2.3) | 0.011 (0.010.034) |
| A5 | DL 15 (2) | 2781 | # F 4900 | 9805 (8904.10927) | 3.08 (0.295.843) | 40.76 (0.391.121) | 0.065 (0.010.43) | 97 (88.93) | 1.48 (1.41.15.42) | 0.004 (0.010.0117) | 0.29 (0.190.399) | 0.013 (0.010.03) |
| A7 | DL 15 (1) | 2781 | # F 4900 | 12695 (12084.1124) | 1.34 (0.151.83) | 0.12 (0.184.0.253) | 0.88 (84.83) | 1.94 (1.852.04) | 0.004 (0.010.0117) | 1.15 (1.103.1.4) | 0.49 (0.230.66) | 0.013 (0.010.03) |
| A6 | DL 7 (1) | 2574 | # W 4800 | 4757 (727.5213) | 40.8 (32.26.45.79) | 6816 (0.213.40.294) | 4.43 (1.225.79) | 98 (88.104) | 0.58 (0.506.0.677) | 0.01 (0.0119.0.0142) | 0.11 (0.101.0.184) | 1.36 (5.0.081.409.23) |
| A4 | DL 28 (3) | 3174 | # W 4800 | 8865 (8808.8977) | 0.16 (0.010.26) | 0.43 (0.310.52) | 0.07 (0.010.202) | 73.7 (70.6.75.8) | 1.03 (0.946.1.148) | 0.002 (0.010.0044) | 0.21 (0.164.0.295) | 0.41 (0.240.54) |
| A3 | DL 28 (2) | 3174 | # W 4800 | 7641 (7351.8030) | 0.45 (0.330.55) | 0.48 (0.385.0.533) | 0.29 (0.010.6) | 95.1 (94.8.95.4) | 1.006 (0.985.1.024) | 0.0005 (0.010.0163) | 0.38 (0.342.0.414) | 1.14 (1.11.1.22) |
| A2 | DL 28 (1) | 3174 | # W 4800 | 7509 (7469.7530) | 0.27 (0.010.47) | 0.53 (0.455.67) | 0.064 (0.010.194) | 81 (80.88) | 1.01 (0.965.1.035) | 0.0006 (0.010.0196) | 0.1 (0.074.0.12) | 0.69 (0.491.019) |
| A0 | DL 26 | 2474 | # W 4800 | 10954 (10200.11909) | 10798 (73.8810861) | 2250 (3388.67) | 0.66 (0.011.39) | 87.8 (82.93) | 1.31 (1.269.1.375) | 0.13 (0.0033.23) | 2.23 (1.752.2.65) | 11.78 (4.9612.56) |
| A7 | DL 24 | 2271 | # W 4600 | 6154 (6473.6863) | 1.89 (0.194.49) | 0.74 (0.548.0.889) | 0.15 (0.010.25) | 72.3 (68.75) | 0.8 (0.692.944) | 0.0011 (0.00044) | 1.10 (0.941.1067) | 1.18 (0.988.1.395) |
| M17 | DL 70 (2) | 2274 | # W 4470 | 8227 (7300.8828) | 8.05 (0.800.8828) | 0.4 (0.011.21) | 0.084 (0.010.193) | 38.8 (37.340.1) | 0.52 (0.425.61) | 0.12 (0.102.0.137) | 0.39 (0.299.0.54) | 0.002 (0.010.0967) |
| M16 | DL 30 (1) | 2274 | # W 4470 | 7333 (6066.7983) | 75 (0.351.214) | 9.23 (0.391.2216) | 0.5 (0.101) | 36.6 (32.741) | 0.53 (0.455.0.587) | 0.01 (0.00455.0.587) | 1.17 (0.336.2.79) | 0.36 (0.010.58) |
| A7 | DL 19 (2) | 2474 | # W 4470 | 8529 (2348.9324) | 22 (0.4146.9) | 2.02 (0.691.83) | 2.83 (2.051.64) | 76.2 (75.477.6) | 1.32 (1.041.49) | 0.004 (0.010.0061) | 0.97 (0.781.12) | 14.92 (12.519.58) |
| A0 | DL 19 (1) | 2474 | # W 4470 | 8471 (190619.9225) | 5904 (10131.1132) | 5 (11.017112.35) | 0.88 (0.631.2) | 75.8 (75.76) | 1.35 (1.281.47) | 0.079 (0.0173.161) | 0.84 (0.72.105) | 6.26 (3.4610.88) |

individuals who are not receiving any type of treatment for their condition. The results of this study suggest that the use of a single, standardized measure of self-esteem may not be sufficient to capture the complexity of self-esteem in this population. Future research should explore the use of multiple measures of self-esteem, as well as the role of self-esteem in the development and maintenance of substance use disorders.

and a paper on the subject by N.

Table 2.2 (cont'd). Averages and ranges of elemental concentrations (ppm) in pentlandite (A-JR; PMS data)

| Sample & trap sample | Slope | Shear level | n of analyses | Sn | Sb | Fe | Rc | Os | Ir | Pr | Au | Pb | Bi |
|----------------------|-------|-------------|---------------|-----------------------|-----------------------|---------------------|-----------------------|-----------------------|------------------------|---------------------|----------------------|-----------------------|----------------------|
| A70 DTL 19 (1) | 2424 | #4 W 4470 | 3 | 0.018 (bdl-0.075) | 0.2 (0.067-0.273) | 1.63 (1.092-2.06) | NA | 0.012 (bdl-0.037) | bdl | bdl | 0.015 (bdl-0.024) | 7.61 (4.43-11.27) | 0.59 (0.073-1.27) |
| A71 DTL 19 (2) | 2424 | #4 W 4470 | 3 | 0.087 (0.074-0.098) | 0.3 (0.198-0.496) | 4.13 (1.118-9.05) | NA | 0.01 (bdl-0.011) | 0.0072 (bdl-0.0215) | bdl | 0.028 (bdl-0.066) | 38.41 (25.64-55.94) | 2.42 (0.151-6.65) |
| M106 DTL 70 (1) | 2274 | #4 W 4470 | 3 | 0.094 (0.064-0.149) | 0.073 (0.063-0.09) | NA | 0.25 (0.178-0.301) | bdl | 0.0016 (bdl-0.0048) | bdl | 0.013 (bdl-0.032) | 5.05 (0.926-13.25) | 1.21 (bdl-3.37) |
| M107 DTL 70 (2) | 2274 | #4 W 4470 | 3 | 0.179 (0.115-0.247) | 0.065 (0.025-0.101) | NA | 0.17 (bdl-0.311) | 0.0005 (bdl-0.0046) | 0.00096 (bdl-0.0018) | bdl | 0.0036 (bdl-0.0108) | 0.67 (0.276-1.38) | 0.28 (0.155-0.51) |
| A77 DTL 23B | 2374 | #4 W 4600 | 3 | 0.07 (0.047-0.091) | 0.28 (0.056-0.618) | 28.62 (8.6-87.94) | NA | 0.019 (bdl-0.084) | bdl | 0.0044 (bdl-0.013) | 0.012 (bdl-0.0247) | 23.95 (22.71-25.01) | 12.86 (1.171-55.39) |
| A78 DTL 24 | 2221 | #4 W 4600 | 3 | 0.098 (0.075-0.133) | 0.056 (bdl-0.12) | 5.53 (2.89-8.57) | NA | 0.0085 (bdl-0.0256) | bdl | bdl | 0.014 (bdl-0.03) | 18.13 (1.18-37.5) | 1.51 (0.388-3.72) |
| A80 DTL 26 | 2474 | #4 W 4800 | 3 | 0.05 (bdl-0.135) | 0.033 (bdl-0.0997) | 5.54 (3.86-7.6) | NA | 0.006 (bdl-0.019) | 0.0017 (bdl-0.0065) | bdl | 0.018 (0.008-0.033) | 11 (0.99-22.57) | 1.79 (0.623-3.84) |
| A81 DTL 27 | 2474 | #4 W 4800 | 3 | 0.02 (bdl-0.036) | 0.3 (0.206-0.468) | 3.88 (bdl-11) | NA | 0.022 (bdl-0.039) | 0.028 (bdl-0.0839) | bdl | bdl | 31.55 (14.84-55.85) | 2.17 (0.40-4) |
| A82 DTL 28 (1) | 3174 | #4 W 4800 | 3 | 0.007 (bdl-0.0208) | 0.035 (0.0242-0.0416) | 1.44 (1.26-1.69) | NA | 0.008 (bdl-0.0234) | bdl | bdl | bdl | 2.02 (1.48-2.89) | 0.43 (0.187-0.579) |
| A83 DTL 28 (2) | 3174 | #4 W 4800 | 3 | 0.02 (bdl-0.0386) | 0.06 (0.0482-0.0772) | 11.81 (8.68-13.87) | NA | bdl | bdl | 0.0047 (bdl-0.0143) | 0.003 (bdl-0.009) | 0.32 (0.0161-0.658) | 0.058 (bdl-0.097) |
| A84 DTL 28 (3) | 3174 | #4 W 4800 | 3 | bdl | 0.012 (bdl-0.0366) | 0.19 (bdl-0.57) | NA | 0.008 (bdl-0.024) | bdl | bdl | 0.0093 (bdl-0.0281) | 1.22 (0.062-3.44) | 0.063 (0.0194-0.135) |
| A07 DTL 7 (1) | 2524 | #4 W 4800 | 3 | 0.25 (0.143-0.469) | 1.03 (0.7-1.21) | 0.56 (bdl-1.73) | NA | bdl | bdl | 0.0052 (bdl-0.0157) | 0.18 (0.172-0.194) | 572.77 (430.79-726.3) | 3.13 (1.87-4.71) |
| A05 DTL 15 (1) | 2781 | #1 E 4900 | 3 | 0.033 (0.0301-0.0377) | 0.007 (bdl-0.014) | 8.63 (0.62-14.15) | NA | 0.011 (bdl-0.035) | bdl | bdl | bdl | 0.66 (0.0284-1.84) | 0.09 (0.0191-0.241) |
| A06 DTL 15 (2) | 2781 | #1 E 4900 | 3 | 0.059 (0.046-0.074) | 0.006 (bdl-0.0182) | 4.54 (2.61-7) | NA | bdl | bdl | bdl | bdl | 2.28 (1.3-3.11) | 1.84 (1.01-3.01) |
| A07 DTL 16 | 2781 | #1 E 4900 | 3 | 0.015 (bdl-0.047) | 0.06 (0.0258-0.089) | 3.35 (1.86-5.77) | NA | 0.008 (bdl-0.0253) | bdl | bdl | bdl | 0.11 (0.0263-0.196) | 0.26 (0.0269-0.72) |
| A08 DTL 17 | 2821 | #1 E 4900 | 3 | 0.006 (bdl-0.101) | 0.036 (0.0116-0.0548) | 25.95 (1.36-45.02) | NA | 0.06 (0.058-0.072) | bdl | bdl | 0.009 (bdl-0.0276) | 1.06 (0.207-2.2) | 0.99 (0.067-2.77) |
| M19 DTL 12 (1) | 2774 | #4 E 4900 | 3 | 0.11 (0.073-0.138) | bdl | NA | 0.03 (bdl-0.092) | 0.004 (bdl-0.0121) | bdl | bdl | bdl | 0.92 (bdl-2.08) | 0.34 (bdl-0.7) |
| A86 DTL 29 (1B) | 1291 | #1 W 5000 | 3 | 0.59 (bdl-1.7) | 0.14 (0.047-0.312) | 15.22 (3.39-27.43) | NA | 0.01 (bdl-0.033) | 0.0015 (bdl-0.0046) | bdl | 0.003 (bdl-0.0082) | 6.04 (0.94-13) | 1.35 (0.102-3.79) |
| A87 DTL 29 (2) | 1291 | #1 W 5000 | 3 | 0.11 (bdl-0.61) | 0.033 (bdl-0.067) | 12.73 (1.93-21.35) | NA | 0.011 (bdl-0.034) | bdl | bdl | 0.013 (bdl-0.035) | 2.23 (0.212-4.55) | 0.55 (0.017-1.18) |
| A89 DTL 29 (3B) | 1291 | #1 W 5000 | 2 | 4.4 (0.581-8.22) | 0.006 (0.0159-0.121) | 6.42 (5.76-7.08) | NA | 0.0094 (bdl-0.0187) | bdl | bdl | bdl | 2.99 (5.98-54.15) | 0.81 (0.152-1.46) |
| A90 DTL 29 (4A) | 1291 | #1 W 5000 | 3 | 0.27 (0.0245-0.761) | 0.13 (0.0408-0.316) | 3.4 (1.49-5.14) | NA | bdl | bdl | 0.004 (bdl-0.0122) | 0.009 (0.007-0.011) | 4.01 (0.465-10.64) | 1.03 (0.162-6.8) |
| A91 DTL 29 (4B) | 1291 | #1 W 5000 | 3 | 0.35 (0.102-0.76) | 0.11 (0.059-0.194) | 5.33 (3.99-7.57) | NA | bdl | bdl | bdl | 0.018 (bdl-0.055) | 2.67 (2.1-3.54) | 0.96 (0.29-1.44) |
| A92 DTL 30 | 1291 | #1 W 5000 | 3 | 0.24 (0.082-0.534) | 0.05 (bdl-0.091) | 12.77 (7.16-15.73) | NA | bdl | bdl | bdl | 2.54 (bdl-7.59) | 3.94 (1.65-6.37) | 8.88 (1.29-22.4) |
| M46 DTL 30 (1) | 1291 | #1 W 5000 | 2 | 1.04 (0.249-1.84) | 0.069 (0.027-0.11) | NA | bdl | bdl | 0.0078 (0.0065-0.0091) | 0.0095 (bdl-0.019) | bdl | 1.19 (0.378-2.01) | 0.085 (bdl-0.171) |
| A80 DTL 2 | 2421 | #1 W 5100 | 2 | 0.045 (0.035-0.056) | 0.033 (0.0261-0.04) | 5.68 (5.46-5.9) | NA | bdl | bdl | bdl | bdl | 9.56 (4.39-14.73) | 1.68 (1.168-2.19) |
| A81 DTL 3 | 2421 | #1 W 5100 | 2 | 0.047 (0.023-0.072) | 0.009 (bdl-0.0197) | 0.16 (bdl-0.32) | NA | bdl | bdl | 0.013 (bdl-0.026) | 0.019 (0.0087-0.029) | 8.9 (5.76-12.03) | 4.25 (1.2-7.29) |
| A82 DTL 4 | 2321 | #1 W 5100 | 3 | 0.08 (0.047-0.14) | 0.014 (bdl-0.0317) | 5.01 (2.99-7.24) | NA | 0.017 (bdl-0.052) | bdl | 0.003 (bdl-0.026) | 0.04 (bdl-0.121) | 40.72 (11.32-90.69) | 2.8 (0.776-6.11) |
| A83 DTL 5 | 2271 | #1 W 5100 | 3 | 0.043 (0.026-0.055) | 0.22 (0.127-0.323) | 28.63 (15.32-42.06) | NA | 0.006 (bdl-0.019) | bdl | bdl | 0.008 (0.0061-0.011) | 5.21 (4.59-5.55) | 0.4 (0.355-0.464) |
| A84 DTL 6 | 1322 | #1 W 5100 | 3 | 0.11 (0.0344-0.188) | 0.015 (0.0097-0.019) | 2.53 (1.23-4.25) | NA | 0.01 (bdl-0.02) | bdl | 0.005 (bdl-0.016) | 0.0057 (bdl-0.0171) | 7.26 (2.24-13.88) | 0.97 (0.455-1.69) |
| A89 DTL 11A (1) | 1322 | #1 W 5100 | 4 | 0.09 (bdl-0.344) | 0.025 (bdl-0.0581) | 3.34 (0.9-7.97) | NA | bdl | bdl | 0.0027 (bdl-0.0107) | bdl | 1.29 (0.527-2.26) | 0.023 (bdl-0.091) |
| A84 DTL 52 (2) | 1135 | #1 W 5100 | 7 | 0.12 (bdl-0.466) | 0.046 (bdl-0.089) | NA | 0.013 (bdl-0.026) | 0.0076 (bdl-0.0151) | 0.0003 (bdl-0.002) | 0.0041 (bdl-0.015) | 0.0067 (bdl-0.0247) | 5.07 (0.109-17.95) | 2.17 (0.366-8.14) |
| M86 DTL 54 (1) | 1173 | #1 W 5100 | 3 | 0.04 (0.0158-0.0589) | 0.098 (0.034-0.125) | NA | 0.006 (bdl-0.0108) | 0.0028 (bdl-0.0085) | 0.0003 (bdl-0.00057) | bdl | 0.004 (0.003-0.006) | 1.03 (0.409-1.81) | 0.3 (0.167-0.403) |
| M88 DTL 55 (1) | 1214 | #1 W 5100 | 3 | 0.042 (bdl-0.083) | 0.057 (0.032-0.086) | NA | 0.002 (bdl-0.0056) | 0.012 (0.0082-0.0154) | 0.0012 (bdl-0.0037) | bdl | 0.0067 (bdl-0.0162) | 2.24 (0.376-4.49) | 1.4 (0.185-3.69) |
| M91 DTL 58 (1) | 2624 | #4 W 5100 | 3 | 0.037 (0.0257-0.0645) | 0.021 (0.0108-0.0335) | NA | 0.006 (0.0038-0.0083) | 0.051 (0.0451-0.062) | 0.002 (bdl-0.0053) | 0.0017 (bdl-0.0031) | 0.0002 (bdl-0.0006) | 0.32 (0.042-0.811) | bdl |

* indicates values that have been affected by micrograms

bdl indicates values below detection limit

NA indicates no recorded value

Table 2.3. Averages and ranges of elemental concentrations (ppm) in chalcopyrite (d.A. IC-PMIS data)

| Element | Chip sample | Shape | Shear level | Cu | Ni | Zn | As | Se | Ru | Pd | Ag | Cd |
|---------|-------------|-------|-------------|-------------------------------|--------------------|-----------------|--------------------|---------------------|---------------------|---------------------|---------------------|---------------------|
| A70 | DTL 19 (1) | 2424 | #4 W 4470 | 1.52 ¹ (0.18-3.61) | 122.9 (59-231) | 376 (355-400) | 0.85 (bdl-0.254) | 83.7 (80.5-87.8) | 0.18 (0.1-0.293) | 0.197 (0.048-0.48) | 1.36 (1.27-1.5) | 4.93 (4.15-5.44) |
| A71 | DTL 19 (2) | 2424 | #4 W 4470 | 0.25 (0.20-0.27) | 35.12 (29-38) | 428 (374-478) | bdl | 88.6 (85-90.9) | 0.11 (0.103-0.117) | 0.038 (0.024-0.046) | 3.88 (2.72-4.61) | 3.43 (2.5-5.24) |
| M106 | DL 70 (1) | 2274 | #4 W 4470 | 0.15 (0.13-0.16) | 38.79 (36-42) | 423 (384-453) | bdl | 42.7 (41.8-44.4) | 0.07 (0.048-0.101) | - | 0.87 (0.68-1.13) | 34.17 (30.53-36.63) |
| M107 | DL 70 (2) | 2274 | #4 W 4470 | 0.28 (0.03-0.14) | 60.9 (25-123) | 425 (399-439) | 0.06 (bdl-0.192) | 40.15 (6-43) | 0.035 (bdl-0.056) | - | 0.84 (0.58-1.24) | 18.01 (15.94-20.23) |
| A77 | DTL 23B | 2374 | #4 W 4600 | 37.32 (0.09-110) | 1689 (29-4905)* | 530 (381-776) | 0.05 (bdl-0.159) | 62.8 (60.9-64.9) | 0.07 (0.06-0.079) | 0.78 (0.06-0.09) | 9.2 (6.42-12.24) | 6.5 (4.08-8.65) |
| A78 | DTL 24 | 2221 | #4 W 4600 | 0.3 (0.047-0.75) | 40 (34-49) | 414 (406-428) | bdl | 84 (83.3-84.7) | 0.06 (0.041-0.078) | 0.16 (0.15-0.17) | 3.51 (1.376-5) | 14.47 (13.36-15.07) |
| A80 | DTL 26 | 2474 | #4 W 4800 | 0.46 (0.19-0.86) | 63.4 (41-105) | 1163 (389-2710) | bdl | 101.2 (95.1-109) | 0.078 (0.05-0.105) | 0.2 (0.07-0.45) | 4.71 (3.48-5.46) | 18.96 (5.94-43.87) |
| A81 | DTL 27 | 2474 | #4 W 4800 | 2.17 (bdl-3.81) | 309 (263-370) | 339 (324-365) | 0.2 (bdl-0.61) | 99.8 (94.7-103) | 0.12 (0.116-0.125) | 0.03 (0.03-0.038) | 0.49 (0.305-0.814) | 1.96 (1.75-2.22) |
| A82 | DTL 28 (1) | 3174 | #4 W 4800 | 0.15 (0.11-0.21) | 34.1 (31-35) | 416 (376-451) | bdl | 95.6 (88.9-103) | 0.1 (0.089-0.112) | 0.16 (0.13-0.17) | 1.23 (0.794-1.84) | 15.36 (12.8-18.27) |
| A83 | DTL 28 (2) | 3174 | #4 W 4800 | 0.21 (0.09-0.35) | 43.9 (34-56) | 596 (272-1121) | 0.08 (bdl-0.24) | 100.9 (96-104) | 0.13 (0.114-0.143) | 0.16 (0.06-0.3) | 2.58 (2.25-2.86) | 14.26 (6.02-26.63) |
| A84 | DTL 28 (3) | 3174 | #4 W 4800 | 14.87 (0.14-44.27) | 724 (36-2097)* | 1255 (440-3831) | 0.08 (bdl-0.25) | 88.8 (83-91) | 0.086 (0.076-0.105) | 0.28 (0.14-0.5) | 1.38 (0.592-2.26) | 25.37 (13.95-44.51) |
| A65 | DTL 15 (1) | 2781 | #1 E 4900 | 0.31 (0.20-0.37) | 37.5 (33-42) | 360 (345.5-375) | bdl | 103.5 (99.5-110.2) | 0.11 (0.101-0.125) | 0.18 (0.09-0.3) | 1.15 (0.736-1.45) | 13.61 (7.57-22.38) |
| A66 | DTL 15 (2) | 2781 | #1 E 4900 | 0.12 | 36.4 | 330.11 | 0.226 | 98.39 | 0.133 | 0.13 | 0.793 | 8.29 |
| A67 | DTL 16 | 2781 | #1 E 4900 | 0.39 (0.29-0.47) | 42.9 (36.7-49.4) | 363 (339-378) | 0.58 (bdl-1.66) | 89.8 (85.6-94.9) | 0.09 (0.057-0.112) | 0.1 (0.09-0.11) | 1.39 (1.23-1.65) | 7.53 (6.93-8.06) |
| A68 | DTL 17 | 2821 | #1 E 4900 | 0.21 (0.14-0.29) | 31.3 (27.8-36) | 380 (354-417) | 0.036 (bdl-0.107) | 71.5 (66.9-75) | 0.11 (0.074-0.149) | 0.1 (0.09-0.12) | 2.05 (1.63-2.62) | 6.46 (5.88-7.21) |
| M19 | DL 12 (1) | 2774 | #4 E 4900 | 3.73 (1.89-5.56) | 274.4 (248-301) | 442 (364-519) | bdl | 110 (105-115.7) | bdl | 5.9 (2.9-8.91) | 18.25 (11.17-25.34) | |
| A86 | DTL 29 (1B) | 1291 | #1 W 5000 | 0.007 (bdl-0.0215) | 56.4 (40.7-92.7) | 475 (339-643) | 1.82 (bdl-7.12) | 168.4 (158-177.9) | 0.07 (0.055-0.085) | 0.6 (0.5-0.7) | 5.97 (1.8-9.06) | 50.2 (34.64-66.61) |
| A87 | DTL 29 (2) | 1291 | #1 W 5000 | 0.005 (bdl-0.0143) | 57.41 (43.7-73) | 458 (424-511) | 0.7 (bdl-1.81) | 153 (147-162) | 0.06 (0.043-0.071) | 0.66 (0.62-0.8) | 6.52 (3.49-9.48) | 58.59 (52.25-67.12) |
| A88 | DTL 29 (3A) | 1291 | #1 W 5000 | 0.09 (0.029-0.21) | 61.6 (49.74-80.89) | 549 (420-754) | 0.64 (bdl-1.91) | 134.4 (126-139) | 0.12 (0.093-0.147) | 1.32 (0.7-2.4) | 2.73 (2.11-3.8) | 62.39 (53.46-76.44) |
| A89 | DTL 29 (3B) | 1291 | #1 W 5000 | 0.05 (0.02-0.025) | 61.8 (37-123) | 401 (399-458) | 40.46 (bdl-161.25) | 119.4 (117.9-123) | 0.13 (0.114-0.16) | 0.62 (0.54-0.78) | 3.28 (3.06-3.76) | 47.3 (44.44-59.13) |
| A90 | DTL 29 (4A) | 1291 | #1 W 5000 | 0.035 (0.027-0.047) | 47.4 (40-51) | 440 (371-535) | 0.11 (bdl-0.344) | 140.6 (132.2-151) | 0.098 (0.086-0.107) | 0.6 (0.48-0.68) | 5.63 (2.69-10.93) | 42.85 (30.38-51.52) |
| A91 | DTL 29 (4B) | 1291 | #1 W 5000 | 0.008 (bdl-0.016) | 38.8 (22.3-47.8) | 488 (340-754) | 0.8 (0.37-1.83) | 143.4 (138.1-152.7) | 0.11 (0.089-0.142) | 0.5 (0.43-0.74) | 2.65 (2.14-3.07) | 43.16 (33.8-57.25) |
| A92 | DTL 30 | 1291 | #1 W 5000 | 0.32 (0.14-0.6) | 35.1 (29.4-42.1) | 542 (508-606) | bdl | 161.5 (152.9-169.7) | 0.09 (0.083-0.097) | 0.52 (0.44-0.65) | 4.89 (3.55-6.66) | 31.99 (29.47-33.92) |
| M46 | DL 30 (1) | 1291 | #1 W 5000 | 0.018 (bdl-0.056) | 51.2 (39.3-71.6) | 553 (386-815) | 0.87 (bdl-2.6) | 63.1 (56.8-72) | 0.03 (bdl-0.093) | - | 4.96 (1-12.48) | 47.28 (35.22-70.74) |
| A49 | DTL 1 | 2421 | #1 W 5100 | 0.31 (0.16-0.47) | 27.8 (17.3-38.3) | 507 (442-572) | bdl | 164.6 (161.2-168) | 0.1 (0.102-0.104) | 0.39 (0.38-0.41) | 8.15 (7.53-8.78) | 28.57 (25.23-31.9) |
| A50 | DTL 2 | 2421 | #1 W 5100 | 1.09 (0.067-2.12) | 136 (48-224) | 378 (362-394) | 0.11 (bdl-0.227) | 193.1 (186.7-199.5) | 0.085 (0.093-0.077) | 0.25 | 1.53 (0.636-2.43) | 23.49 (21.96-25.01) |
| A51 | DTL 3 | 2421 | #1 W 5100 | 0.15 (0.12-0.175) | 47.5 (34.8-60.2) | 531 (347-714) | 0.21 (bdl-0.42) | 157.3 (156.6-158) | 0.083 (0.059-0.107) | 0.21 (0.2-0.22) | 1.87 (1.4-2.35) | 15.53 (12.51-18.55) |
| A52 | DTL 4 | 2421 | #1 W 5100 | 0.09 (0.03-0.15) | 49.2 (38-60.4) | 401 (396-406) | bdl | 192 (196-194) | 0.09 (0.085-0.096) | 0.34 | 14.91 (4.69-25.13) | 27 (26.77-27.23) |
| A53 | DTL 5 | 2321 | #1 W 5100 | 0.55 (0.21-1.16) | 69.8 (39.8-129) | 400 (359-452) | bdl | 148.7 (12-173) | 0.11 (0.092-0.142) | 0.39 (0.36-0.47) | 4.16 (1.18-9.39) | 28.1 (26.19-29.93) |
| A54 | DTL 6 | 2271 | #1 W 5100 | 0.069 (bdl-0.13) | 35.8 (31.6-41.4) | 324 (280-363) | bdl | 112.2 (100-119) | 0.048 (bdl-0.145) | 0.43 (0.38-0.5) | 7.84 (6.72-8.95) | 22.54 (19.97-25.21) |
| A60 | DTL 11A (2) | 1322 | #1 W 5100 | 0.015 (0.006-0.025) | 54.2 (47.5-61.8) | 484 (473-502) | 0.75 (bdl-1.92) | 162.6 (151.6-182.6) | 0.1 (0.087-0.138) | 0.7 (0.64-0.78) | 7.22 (4.99-8.54) | 62.91 (58.97-68.83) |
| A61 | DTL 11B (1) | 1321 | #1 W 5100 | 0.024 (0.014-0.042) | 96 (47.3-225.1) | 466 (417-528) | 2.1 (0.35-271) | 154 (145.6-160) | 0.1 (0.084-0.124) | 0.4 (0.38-0.44) | 2.715 (2.28-3.26) | 36.37 (32.08-39.57) |
| M81 | DL 51 (1) | 1135 | #1 W 5100 | 0.24 (0.13-0.35) | 36.5 (33.38-3) | 436 (395-458) | bdl | 41.9 (35.4-49.1) | 0.047 (bdl-0.086) | - | 2.19 (1.33-3.73) | 7.07 (5.91-7.69) |
| M84 | DL 52 (2) | 1135 | #1 W 5100 | 0.45 (0.22-0.6) | 44.4 (34.4-61.6) | 522 (416-595) | 0.89 (bdl-2.67) | 72.4 (61.1-85.2) | 0.06 (0.05-0.08) | - | 10.13 (3.42-16.16) | 6.64 (6.1-7.41) |
| M86 | DL 54 (1) | 1173 | #1 W 5100 | 0.16 (0.10-0.26) | 37.4 (37-38) | 379 (368-385) | 0.06 (bdl-0.181) | 48.2 (47-49) | 0.046 (bdl-0.097) | - | 0.7 (0.46-0.924) | 4.05 (2.84-4.98) |
| M88 | DL 55 (1) | 1214 | #1 W 5100 | 0.3 (0.25-0.37) | 39.8 (36.5-41.6) | 362 (338-406) | 0.05 (bdl-0.147) | 41.2 (34.1-48.8) | 0.066 (0.054-0.08) | - | 1.85 (1.01-2.55) | 6.1 (5.77-6.4) |
| M89 | DL 56 (1) | 1213 | #1 W 5100 | 0.58 (0.44-0.7) | 19.4 (13.2-30.7) | 609 (469-845) | bdl | 57.1 (55.9-58.7) | 0.047 (0.04-0.06) | - | 10.43 (8.34-13.06) | 10.93 (9.08-12.77) |

* numbers not in parentheses indicate averages

* numbers in parentheses indicate averages

* indicates values contaminated by micrograins or trace phase inclusions

bdl indicates values below detection limit

NA indicates no recorded value

Pd values are for Pd¹⁰⁵, due to interference of Cu-argide with Pd¹⁰⁵

Table 2.3: Averages and ranges of elemental concentrations (ppm) in chalcopyrite (LA-IC PMS data)

| Element | Chip sample | Stope | Shear level | Co | Ni | Zn | As | Se | Ru | Pd | Ag | Cd |
|---------|-------------|-------|-------------|--|--------------------|-----------------|--------------------|---------------------|---------------------|---------------------|--------------------|---------------------|
| A70 | DTL 19 (1) | 2424 | #4 W 4470 | 1.52 ¹ (0.18-3.61) ² | 122.9 (59-231) | 376 (355-400) | 0.85 (bdl-2.54) | 83.7 (80.5-87.8) | 0.18 (0.1-0.293) | 0.197 (0.048-0.48) | 1.36 (1.27-1.5) | 4.93 (4.15-5.44) |
| A71 | DTL 19 (2) | 2424 | #4 W 4470 | 0.25 (0.20-0.27) | 35.12 (29-38) | 428 (374-478) | bdl | 88.6 (85-90.9) | 0.11 (0.103-0.117) | 0.038 (0.024-0.046) | 3.88 (2.72-4.61) | 3.43 (2.5-5.24) |
| M106 | DL 70 (1) | 2274 | #4 W 4470 | 0.15 (0.13-0.16) | 38.79 (36-42) | 423 (384-453) | bdl | 42.7 (41.8-44.4) | 0.07 (0.048-0.101) | - | 0.87 (0.68-1.13) | 34.17 (30.53-36.63) |
| M107 | DL 70 (2) | 2274 | #4 W 4470 | 0.28 (0.03-0.14) | 60.9 (25-123) | 425 (399-439) | 0.06 (bdl-0.192) | 40 (35.6-43) | 0.035 (bdl-0.056) | - | 0.84 (0.58-1.24) | 18.01 (15.94-20.23) |
| A77 | DTL 23B | 2374 | #4 W 4600 | 37.32 (0.09-110) | 1689 (29-4905)* | 530 (381-776) | 0.05 (bdl-0.159) | 62.8 (60.9-64.9) | 0.07 (0.06-0.079) | 0.78 (0.06-0.09) | 9.2 (6.42-12.24) | 6.5 (4.08-8.65) |
| A78 | DTL 24 | 2221 | #4 W 4600 | 0.3 (0.047-0.75) | 40 (34-49) | 414 (406-428) | bdl | 84 (83.3-84.7) | 0.06 (0.041-0.078) | 0.16 (0.15-0.17) | 3.51 (1.376-5) | 14.47 (13.36-15.07) |
| A80 | DTL 26 | 2474 | #4 W 4800 | 0.46 (0.19-0.86) | 63.4 (41-105) | 1163 (384-2710) | bdl | 101.2 (95.1-109) | 0.078 (0.05-0.105) | 0.2 (0.07-0.45) | 4.71 (3.48-5.46) | 18.96 (5.94-43.87) |
| A81 | DTL 27 | 2474 | #4 W 4800 | 2.17 (bdl-3.81) | 309 (263-370) | 339 (324-365) | 0.2 (bdl-0.61) | 99.8 (94.7-103) | 0.12 (0.116-0.125) | 0.03 (0.03-0.038) | 0.49 (0.305-0.814) | 1.96 (1.75-2.22) |
| A82 | DTL 28 (1) | 3174 | #4 W 4800 | 0.15 (0.11-0.21) | 34.1 (31-35) | 416 (376-451) | bdl | 95.6 (88.9-103) | 0.1 (0.089-0.112) | 0.16 (0.13-0.17) | 1.23 (0.794-1.84) | 15.36 (12.8-18.27) |
| A83 | DTL 28 (2) | 3174 | #4 W 4800 | 0.21 (0.09-0.35) | 43.9 (34-56) | 596 (272-1121) | 0.08 (bdl-0.24) | 100.9 (96-104) | 0.13 (0.114-0.143) | 0.16 (0.06-0.3) | 2.58 (2.25-2.86) | 14.26 (6.02-26.63) |
| A84 | DTL 28 (3) | 3174 | #4 W 4800 | 14.87 (0.14-44.27) | 724 (36-2097)* | 1255 (440-2831) | 0.08 (bdl-0.25) | 88.8 (83-91) | 0.086 (0.076-0.105) | 0.28 (0.14-0.5) | 1.38 (0.592-2.26) | 25.37 (13.95-44.51) |
| A65 | DTL 15 (1) | 2781 | #1 E 4900 | 0.31 (0.20-0.37) | 37.5 (33-42) | 360 (345.5-375) | bdl | 103.5 (99.5-110.2) | 0.11 (0.101-0.125) | 0.18 (0.09-0.3) | 1.15 (0.736-1.45) | 13.61 (7.57-22.38) |
| A66 | DTL 15 (2) | 2781 | #1 E 4900 | 0.12 | 36.4 | 330.11 | 0.226 | 98.39 | 0.133 | 0.13 | 0.793 | 8.29 |
| A67 | DTL 16 | 2781 | #1 E 4900 | 0.39 (0.29-0.47) | 42.9 (36.7-49.4) | 363 (339-378) | 0.58 (bdl-1.66) | 89.8 (85.6-94.9) | 0.09 (0.057-0.112) | 0.1 (0.09-0.11) | 1.39 (1.23-1.65) | 7.53 (6.93-8.06) |
| A68 | DTL 17 | 2821 | #1 E 4900 | 0.21 (0.14-0.29) | 31.3 (27.8-36) | 380 (354-417) | 0.036 (bdl-0.107) | 71.5 (66.9-75) | 0.11 (0.074-0.149) | 0.1 (0.09-0.12) | 2.05 (1.63-2.62) | 6.46 (5.88-7.21) |
| M19 | DL 12 (1) | 2774 | #4 E 4900 | 3.73 (1.89-5.56) | 274.4 (248-301) | 442 (364-519) | bdl | 110 (105-115.7) | bdl | - | 5.9 (2.9-8.91) | 18.25 (11.17-25.34) |
| A86 | DTL 29 (1B) | 1291 | #1 W 5000 | 0.007 (bdl-0.0215) | 56.4 (40.7-92.7) | 475 (339-643) | 1.82 (bdl-7.12) | 168.4 (158-177.9) | 0.07 (0.055-0.085) | 0.6 (0.5-0.7) | 5.97 (1.8-9.06) | 50.2 (34.64-66.61) |
| A87 | DTL 29 (2) | 1291 | #1 W 5000 | 0.005 (bdl-0.0143) | 57.41 (43.7-73) | 458 (424-511) | 0.7 (bdl-1.81) | 153 (147-162) | 0.06 (0.043-0.071) | 0.66 (0.62-0.8) | 6.52 (3.49-9.48) | 58.59 (52.25-67.12) |
| A88 | DTL 29 (3A) | 1291 | #1 W 5000 | 0.09 (0.029-0.21) | 61.6 (49.74-80.89) | 549 (420-754) | 0.64 (bdl-1.91) | 134.4 (126-139) | 0.12 (0.093-0.147) | 1.32 (0.7-2.4) | 2.73 (2.11-3.8) | 62.39 (53.46-76.44) |
| A89 | DTL 29 (3B) | 1291 | #1 W 5000 | 0.05 (0.02-0.025) | 61.8 (37-123) | 401 (399-458) | 40.46 (bdl-161.25) | 119.4 (117.9-123) | 0.13 (0.114-0.16) | 0.62 (0.54-0.78) | 3.28 (3.06-3.76) | 47.3 (44.44-59.13) |
| A90 | DTL 29 (4A) | 1291 | #1 W 5000 | 0.035 (0.027-0.047) | 47.4 (40-51) | 440 (371-535) | 0.11 (bdl-0.344) | 140.6 (132.2-151) | 0.098 (0.086-0.107) | 0.6 (0.48-0.68) | 5.63 (2.69-10.93) | 42.85 (30.38-51.52) |
| A91 | DTL 29 (4B) | 1291 | #1 W 5000 | 0.008 (bdl-0.016) | 38.8 (22.3-47.8) | 488 (340-754) | 0.8 (0.37-1.83) | 143.4 (138.1-152.7) | 0.11 (0.089-0.142) | 0.5 (0.43-0.74) | 2.65 (2.14-3.07) | 43.16 (33.8-57.25) |
| A92 | DTL 30 | 1291 | #1 W 5000 | 0.32 (0.14-0.6) | 35.1 (29.4-42.1) | 542 (508-606) | bdl | 161.5 (152.9-169.7) | 0.09 (0.083-0.097) | 0.52 (0.44-0.65) | 4.89 (3.55-6.66) | 31.99 (29.47-33.92) |
| M46 | DL 30 (1) | 1291 | #1 W 5000 | 0.018 (bdl-0.056) | 51.2 (39.3-71.6) | 553 (386-815) | 0.87 (bdl-2.6) | 63.1 (56.8-72) | 0.03 (bdl-0.093) | - | 4.96 (1-12.48) | 47.28 (35.22-70.74) |
| A49 | DTL 1 | 2421 | #1 W 5100 | 0.31 (0.16-0.47) | 27.8 (17.3-38.3) | 507 (442-572) | bdl | 164.6 (161.2-168) | 0.1 (0.102-0.104) | 0.39 (0.38-0.41) | 8.15 (7.53-8.78) | 28.57 (25.23-31.9) |
| A50 | DTL 2 | 2421 | #1 W 5100 | 1.09 (0.067-2.12) | 136 (48-224) | 378 (362-394) | 0.11 (bdl-0.227) | 193.1 (186.7-199.5) | 0.085 (0.093-0.077) | 0.25 | 1.53 (0.636-2.43) | 23.49 (21.96-25.01) |
| A51 | DTL 3 | 2421 | #1 W 5100 | 0.15 (0.12-0.175) | 47.5 (34.8-60.2) | 531 (347-714) | 0.21 (bdl-0.42) | 157.3 (156.6-158) | 0.083 (0.059-0.107) | 0.21 (0.2-0.22) | 1.87 (1.4-2.35) | 15.53 (12.51-18.55) |
| A52 | DTL 4 | 2421 | #1 W 5100 | 0.09 (0.03-0.15) | 49.2 (38-60.4) | 401 (396-406) | bdl | 192 (190-194) | 0.09 (0.085-0.096) | 0.34 | 14.91 (4.69-25.13) | 27 (26.77-27.23) |
| A53 | DTL 5 | 2321 | #1 W 5100 | 0.55 (0.21-1.16) | 69.8 (39.8-129) | 400 (359-452) | bdl | 148.7 (12-173) | 0.11 (0.092-0.142) | 0.39 (0.36-0.47) | 4.16 (1.18-9.39) | 28.1 (26.19-29.93) |
| A54 | DTL 6 | 2271 | #1 W 5100 | 0.069 (bdl-0.13) | 35.8 (31.6-41.4) | 324 (280-363) | bdl | 112.2 (100-119) | 0.048 (bdl-0.145) | 0.43 (0.38-0.5) | 7.84 (6.72-8.95) | 22.54 (19.97-25.21) |
| A60 | DTL 11A (2) | 1322 | #1 W 5100 | 0.015 (0.006-0.025) | 54.2 (47.5-61.8) | 484 (473-502) | 0.75 (bdl-1.92) | 162.6 (151.6-182.6) | 0.1 (0.087-0.138) | 0.7 (0.64-0.78) | 7.22 (4.99-8.54) | 62.91 (58.97-68.83) |
| A61 | DTL 11B (1) | 1321 | #1 W 5100 | 0.024 (0.014-0.042) | 96 (47.3-225.1) | 466 (417-528) | 2.1 (0.35-271) | 154 (145.6-160) | 0.1 (0.084-0.124) | 0.4 (0.38-0.44) | 2.715 (2.28-3.26) | 36.37 (32.08-39.57) |
| M81 | DL 51 (1) | 1135 | #1 W 5100 | 0.24 (0.13-0.35) | 36.5 (33-38.3) | 436 (395-458) | bdl | 41.9 (35.4-49.1) | 0.047 (bdl-0.086) | - | 2.19 (1.33-3.73) | 7.07 (5.91-7.69) |
| M84 | DL 52 (2) | 1135 | #1 W 5100 | 0.45 (0.22-0.6) | 44.4 (34.4-61.6) | 522 (416-595) | 0.89 (bdl-2.67) | 72.4 (61.1-85.2) | 0.06 (0.05-0.08) | - | 10.13 (3.42-16.16) | 6.64 (6.1-7.41) |
| M86 | DL 54 (1) | 1173 | #1 W 5100 | 0.16 (0.10-0.26) | 37.4 (37-38) | 379 (368-385) | 0.06 (bdl-0.181) | 48.2 (47-49) | 0.046 (bdl-0.097) | - | 0.7 (0.46-0.924) | 4.05 (2.84-4.98) |
| M88 | DL 55 (1) | 1214 | #1 W 5100 | 0.3 (0.25-0.37) | 39.8 (36.5-41.6) | 362 (338-406) | 0.05 (bdl-0.147) | 41.2 (34.1-48.8) | 0.066 (0.054-0.08) | - | 1.85 (1.01-2.55) | 6.1 (5.77-6.4) |
| M89 | DL 56 (1) | 1213 | #1 W 5100 | 0.58 (0.44-0.7) | 19.4 (13.2-30.7) | 609 (469-845) | bdl | 57.1 (55.9-58.7) | 0.047 (0.04-0.06) | - | 10.43 (8.34-13.06) | 10.93 (9.08-12.77) |

¹ numbers not in parentheses indicate averages² numbers in parentheses indicate averages

* indicates values contaminated by micrograins or trace phase inclusions

bdl indicates values below detection limit

NA indicates no recorded value

Pd values are for Pd¹⁰⁸, due to interference of Cu-argide with Pd¹⁰⁵

Table 2.4. Averages and ranges of elemental concentrations (ppm) in gersdierite (HA-IT PMN data)

| Sample | Chip sample | Shape | Shear level | Co | Ni | Cu | Zn | Se | Ru | Rh | Pd | Ag | Cd | Sr | Te | Re | Os | Ir | Pt | Au | Hg | Tl | Pb | Ba | | |
|--------|-------------|-------|-------------|--------|--------|--------|------|------|-------|------|------|------|------|------|-----|------|-------|-------|-------|------|------|------|----|-------|------|------|
| M106 | DI 20(1) | 2274 | ±4 W 4470 | 117500 | 157000 | 2735 | 20 | 15.2 | 10.7 | 138 | 6.0 | 2.2 | 0.25 | 459 | NA | 1.06 | 1.01 | 0.74 | 8.3 | 0.26 | NA | NA | NA | 4.6 | 830* | |
| M106 | DI 20(1) | 2274 | ±4 W 4470 | 109000 | 70100 | 9.8 | 1.1 | 30 | 15.9 | 12.8 | 72 | 27.1 | 0.11 | 212 | NA | 0.37 | 0.42 | 0.25 | 17.9 | 0.26 | NA | NA | NA | 8.1 | 145 | |
| M106 | DI 20(1) | 2274 | ±4 W 4470 | 40300 | 13300 | 4.3 | 0.1 | 13 | 3.1 | 2.5 | 15 | 19.8 | 0.12 | 57 | NA | 0.07 | 0.066 | 0.004 | 3.3 | 0.05 | NA | NA | NA | 4.5 | 41 | |
| M106 | DI 20(1) | 2274 | ±4 W 4470 | 10900 | 32200 | 196 | 8.2 | 20 | 11.5 | 9.0 | 27 | 21.3 | 1.12 | 68 | NA | 0.16 | 2.68 | 0.53 | 54.5 | 0.11 | NA | NA | NA | 15.2 | 82.3 | |
| M106 | DI 20(1) | 2274 | ±4 W 4470 | 136200 | 43300 | 163 | NA | 22 | 7.9 | 3.2 | 40 | 28.8 | 0.17 | 124 | NA | 0.31 | 0.41 | 0.17 | 7.6 | 0.16 | NA | NA | NA | 8.7 | 82.7 | |
| M106 | DI 20(1) | 2274 | ±4 W 4470 | 136200 | 43300 | 163 | NA | 22 | 7.9 | 3.2 | 40 | 28.8 | 0.17 | 124 | NA | 0.31 | 0.41 | 0.17 | 7.6 | 0.16 | NA | NA | NA | 8.7 | 82.7 | |
| M106 | DI 20(2) | 2274 | ±4 W 4470 | 38300 | 251100 | 2900* | NA | 56 | 51 | 44.5 | 80 | 3.6 | 0.17 | 397 | NA | 0.83 | 14.05 | 18.8 | 22 | 0.65 | NA | NA | NA | 26.5 | 191 | |
| M107 | DI 20(2) | 2274 | ±4 W 4470 | 147000 | 17700 | 996* | NA | 60 | 2.5 | 0.5 | 88 | 0.4 | 0.17 | 152 | NA | 0.09 | 0.017 | 0.01 | 3.5 | 2.24 | NA | NA | NA | 0.6 | 18.1 | |
| M107 | DI 20(2) | 2274 | ±4 W 4470 | 147000 | 17700 | 996* | NA | 60 | 2.5 | 0.5 | 88 | 0.4 | 0.17 | 152 | NA | 0.09 | 0.017 | 0.01 | 3.5 | 2.24 | NA | NA | NA | 0.6 | 18.1 | |
| M107 | DI 20(2) | 2274 | ±4 W 4470 | 190300 | 87000 | 70.9 | NA | 51 | 4.5 | 3.1 | 155 | 15.3 | 0.17 | 282 | NA | 0.22 | 0.026 | 0.01 | 6.7 | 0.54 | NA | NA | NA | 11.9 | 126 | |
| M107 | DI 20(2) | 2274 | ±4 W 4470 | 20500 | 201000 | 433 | NA | 72 | 1.7 | 0.32 | 62 | 0.5 | 0.17 | 282 | NA | 0.22 | 0.026 | 0.01 | 6.7 | 0.54 | NA | NA | NA | 11.9 | 126 | |
| M107 | DI 20(2) | 2274 | ±4 W 4470 | 212000 | 118100 | 1210* | NA | 9.5 | 100 | 9.6 | 68 | 2.1 | 1.6 | 0.52 | 107 | NA | 0.18 | 0.538 | 0.62 | 1.1 | 0.06 | NA | NA | 5.2 | 37.5 | |
| M107 | DI 20(2) | 2274 | ±4 W 4470 | 20900 | 28900 | 17.3 | NA | 33 | 5 | 2 | 35 | 6.9 | 0.11 | 0.2 | 107 | NA | 0.18 | 0.538 | 0.62 | 1.1 | 0.06 | NA | NA | 5.2 | 37.5 | |
| M107 | DI 20(2) | 2274 | ±4 W 4470 | 20900 | 28900 | 17.3 | NA | 33 | 5 | 2 | 35 | 6.9 | 0.11 | 0.2 | 107 | NA | 0.18 | 0.538 | 0.62 | 1.1 | 0.06 | NA | NA | 5.2 | 37.5 | |
| M107 | DI 20(2) | 2274 | ±4 W 4470 | 27100 | 108700 | NA | NA | 88 | NA | NA | 136 | NA | NA | NA | NA | NA | 0.14 | 0.14 | NA | 0.19 | NA | NA | NA | 17.5 | 88.1 | |
| M107 | DI 20(2) | 2274 | ±4 W 4470 | 27100 | 108700 | NA | NA | 88 | NA | NA | 136 | NA | NA | NA | NA | NA | 0.14 | 0.14 | NA | 0.19 | NA | NA | NA | 17.5 | 88.1 | |
| A38 | DI 12.24 | 2221 | ±4 W 4600 | 101500 | 150000 | 0.8 | NA | 170 | 12.9 | 1.3 | 1128 | 0.3 | NA | 0.08 | 211 | NA | NA | NA | 20.01 | 0.11 | 0.56 | NA | NA | NA | 1.6 | 5.8 |
| A38 | DI 12.24 | 2221 | ±4 W 4600 | 82500 | 150000 | 3 | NA | 211 | 12.7 | 6 | 1201 | 58.3 | NA | 0.13 | 298 | NA | NA | 0.14 | 0.76 | 51.3 | 1.77 | 0.37 | NA | NA | 11.6 | 46.8 |
| A38 | DI 12.24 | 2221 | ±4 W 4600 | 61200 | 150000 | 11.5 | NA | 178 | 8.9 | 0.11 | 1552 | 3.5 | NA | 0.16 | 185 | NA | NA | NA | 7.6 | 0.29 | 0.56 | NA | NA | NA | 18.1 | 11.6 |
| A38 | DI 28(2) | 3174 | ±4 W 4800 | 182500 | 152000 | 8.1 | NA | 198 | 28.4 | 0.27 | 202 | 2.0 | NA | 0.52 | 167 | NA | NA | 0.12 | 0.20 | 2.4 | 0.35 | 0.16 | NA | NA | 60.2 | 56.5 |
| A38 | DI 28(2) | 3174 | ±4 W 4800 | 267200 | 141700 | 0.8 | NA | 211 | 140.8 | 17.5 | 147 | 5.5 | NA | 0.11 | 166 | NA | NA | 1.36 | 0.77 | 180 | NA | NA | NA | 2.7 | 10.9 | |
| A38 | DI 28(2) | 3174 | ±4 W 4800 | 109500 | 147000 | 0.8 | NA | 199 | 27.9 | 12.6 | 154 | NA | NA | 0.11 | 144 | NA | NA | 0.4 | 0.85 | 205 | 0.14 | NA | NA | 0.067 | 1.28 | |
| A38 | DI 28(2) | 3174 | ±4 W 4800 | 142500 | 160300 | 1.2 | NA | 273 | 100.2 | 40.3 | 143 | 12.8 | 0.3 | 0.17 | 208 | NA | NA | 2.9 | 0.65 | 273 | 0.28 | NA | NA | NA | 18.6 | 35 |
| M19 | DI 12(1) | 2774 | ±4 F 4000 | 165500 | 101000 | 8.9 | 0.2 | 43 | 8.5 | 0.21 | 149 | 6.7 | NA | 0.15 | 196 | NA | 0.80 | 0.01 | 0.015 | 0.55 | 0.59 | NA | NA | NA | 6.9 | 198 |
| M19 | DI 12(1) | 2774 | ±4 F 4000 | 91200 | 129000 | 12.5 | NA | 41 | 5.3 | 0.48 | 150 | 0.9 | NA | 0.11 | 102 | NA | 0.40 | 0.09 | 0.35 | 4.3 | 0.26 | NA | NA | NA | 2.3 | 24.8 |
| M19 | DI 12(1) | 2774 | ±4 F 4000 | 125000 | 51400 | 6.6 | 0.5 | 31 | 8.7 | 2.5 | 95 | 8.5 | 0.01 | 0.04 | 47 | NA | 2.10 | 0.35 | 0.20 | 20 | 0.21 | NA | NA | NA | 2.7 | 57.3 |
| M19 | DI 12(1) | 2774 | ±4 F 4000 | 108100 | 130900 | NA | 0.2 | 50 | 8.3 | 4 | 257 | 0.05 | NA | 0.03 | 113 | NA | 0.06 | 0.07 | 0.018 | 31.4 | 0.06 | NA | NA | NA | 0.04 | 1.1 |
| M19 | DI 12(1) | 2774 | ±4 F 4000 | 81500 | 201300 | NA | NA | 90 | 13 | 7.5 | 285 | NA | NA | 0.15 | 215 | NA | 0.59 | 2.7 | 5.7 | 63.3 | 0.09 | NA | NA | NA | 0.35 | 2.4 |
| A36 | DI 29(1B) | 1291 | ±1 W 5000 | 56300 | 133000 | NA | NA | 379 | 7.5 | 0.21 | 149 | 6.7 | NA | 0.15 | 196 | NA | 0.80 | 0.01 | 0.015 | 0.55 | 0.59 | NA | NA | NA | 6.9 | 198 |
| A36 | DI 29(1B) | 1291 | ±1 W 5000 | 75700 | 148000 | 0.3 | NA | 348 | 11.5 | 0.6 | 165 | 0.10 | 0.3 | 0.11 | 125 | NA | 0.40 | 0.09 | 0.35 | 4.3 | 0.26 | NA | NA | NA | 2.3 | 24.8 |
| A36 | DI 29(1B) | 1291 | ±1 W 5000 | 68100 | 154100 | 60 | NA | 282 | 9.9 | 5.6 | 150 | 0.1 | NA | 0.12 | 137 | NA | 0.40 | 0.09 | 0.35 | 4.3 | 0.26 | NA | NA | NA | 2.3 | 24.8 |
| A37 | DI 29(2) | 1291 | ±1 W 5000 | 49500 | 140100 | 31 | 34.9 | 306 | 7.3 | 0.05 | 167 | 1.3 | 0.4 | 0.07 | 164 | NA | 0.40 | 0.09 | 0.35 | 4.3 | 0.26 | NA | NA | NA | 2.3 | 24.8 |
| A37 | DI 29(2) | 1291 | ±1 W 5000 | 42300 | 155800 | 4.1 | NA | 374 | 7.4 | 0.17 | 132 | 0.2 | NA | 0.20 | 208 | NA | 0.40 | 0.09 | 0.35 | 4.3 | 0.26 | NA | NA | NA | 2.3 | 24.8 |
| A37 | DI 29(2) | 1291 | ±1 W 5000 | 51400 | 151500 | 126 | NA | 368 | 7 | 0.21 | 160 | 3.5 | NA | 0.23 | 191 | NA | 0.40 | 0.09 | 0.35 | 4.3 | 0.26 | NA | NA | NA | 2.3 | 24.8 |
| A37 | DI 29(2) | 1291 | ±1 W 5000 | 9900 | 166100 | NA | NA | 313 | 1.2 | 0.07 | 34 | 62.7 | NA | 0.11 | 106 | NA | 0.40 | 0.09 | 0.35 | 4.3 | 0.26 | NA | NA | NA | 2.3 | 24.8 |
| A37 | DI 29(2) | 1291 | ±1 W 5000 | 71100 | 150300 | 2.2 | NA | 463 | 10.7 | 4.1 | 152 | 1.0 | NA | 0.28 | 217 | NA | 0.40 | 0.09 | 0.35 | 4.3 | 0.26 | NA | NA | NA | 2.3 | 24.8 |
| A37 | DI 29(2) | 1291 | ±1 W 5000 | 72800 | 150000 | NA | NA | 420 | 9.3 | 2.9 | 161 | NA | NA | 0.11 | 207 | NA | 0.40 | 0.09 | 0.35 | 4.3 | 0.26 | NA | NA | NA | 2.3 | 24.8 |
| A37 | DI 29(2) | 1291 | ±1 W 5000 | 102500 | 150000 | 15200* | NA | 26 | 700 | 15.2 | 132 | 203 | 365 | 2.4 | 126 | NA | 0.40 | 0.09 | 0.35 | 4.3 | 0.26 | NA | NA | NA | 2.3 | 24.8 |
| A37 | DI 22(1) | 2471 | ±1 W 5000 | 161600 | 150000 | 37.2 | 3 | 1644 | 25.1 | 6 | 70 | 120 | NA | 0.11 | 633 | NA | 0.40 | 0.09 | 0.35 | 4.3 | 0.26 | NA | NA | NA | 2.3 | 24.8 |
| A37 | DI 22(1) | 2471 | ±1 W 5000 | 109600 | 150000 | 4.4 | 128 | 941 | 16.1 | 0.09 | 135 | 541 | 0.05 | 0.37 | 602 | NA | 0.40 | 0.09 | 0.35 | 4.3 | 0.26 | NA | NA | NA | 2.3 | 24.8 |
| A37 | DI 22(1) | 2471 | ±1 W 5000 | 82400 | 182000 | 9.3 | 0.27 | 118 | 7.6 | 13.5 | 132 | 0.01 | NA | 0.06 | 129 | NA | 0.40 | 0.09 | 0.35 | 4.3 | 0.26 | NA | NA | NA | 2.3 | 24.8 |
| A37 | DI 30(1) | 1291 | ±1 W 5000 | 66300 | 200100 | 46.5 | 0.5 | 128 | 4.3 | 0.31 | 146 | 0.2 | NA | 0.12 | 159 | NA | 0.40 | 0.09 | 0.35 | 4.3 | 0.26 | NA | NA | NA | 2.3 | 24.8 |
| A37 | DI 30(1) | 1291 | ±1 W 5000 | 30800 | 103000 | 117 | 5.3 | 82 | 2.2 | 0.06 | 80 | 39.3 | 0.09 | 0.24 | 116 | NA | 0.40 | 0.09 | 0.35 | 4.3 | 0.26 | NA | NA | NA | 2.3 | 24.8 |
| A37 | DI 30(1) | 1291 | ±1 W 5000 | 30800 | 103000 | 117 | 5.3 | 82 | 2.2 | 0.06 | 80 | 39.3 | 0.09 | 0.24 | 116 | NA | 0.40 | 0.09 | 0.35 | 4.3 | 0.26 | NA | NA | NA | 2.3 | 24.8 |
| A37 | DI 30(1) | 1291 | ±1 W 5000 | 30800 | 103000 | 117 | 5.3 | 82 | 2.2 | 0.06 | 80 | 39.3 | 0.09 | 0.24 | 116 | NA | 0.40 | 0.09 | 0.35 | 4.3 | 0.26 | NA | NA | NA | 2.3 | 24.8 |
| A37 | DI 30(1) | 1291 | ±1 W 5000 | 30800 | 103000 | 117 | 5.3 | 82 | 2.2 | 0.06 | 80 | 39.3 | 0.09 | 0.24 | 116 | NA | 0.40 | 0.09 | 0.35 | 4.3 | 0.26 | NA | NA | NA | 2.3 | 24.8 |
| A37 | DI 30(1) | 1291 | ±1 W 5000 | 30800 | 103000 | 117 | 5.3 | 82 | 2.2 | 0.06 | 80 | 39.3 | 0.09 | 0.24 | 116 | NA | 0.40 | 0.09 | 0.35 | 4.3 | 0.26 | NA | NA | NA | 2.3 | 24.8 |
| A37 | DI 30(1) | 1291 | ±1 W 5000 | 30800 | 103000 | 117 | 5.3 | 82 | 2.2 | 0.06 | 80 | 39.3 | 0.09 | 0.24 | 116 | NA | 0.40 | 0.09 | 0.35 | 4.3 | 0.26 | NA | NA | NA | 2.3 | 24.8 |
| A37 | DI 30(1) | 1291 | ±1 W 5000 | 30800 | 103000 | 117 | 5.3 | 82 | 2.2 | 0.06 | 80 | 39.3 | 0.09 | 0.24 | 116 | NA | 0.40 | 0.09 | 0.35 | 4.3 | 0.26 | NA | NA | NA | 2.3 | 24.8 |
| A37 | DI 30(1) | 1291 | ±1 W 5000 | 30800 | 103000 | 117 | 5.3 | 82 | 2.2 | 0.06 | 80 | 39.3 | 0.09 | 0.24 | 116 | NA | 0.40 | 0.09 | 0.35 | 4.3 | 0.26 | NA | NA | NA | 2.3 | 24.8 |
| A37 | DI 30(1) | 1291 | ±1 W 5000 | 30800 | 103000 | 117 | 5.3 | 82 | 2.2 | 0.06 | 80 | 39.3 | 0.09 | 0.24 | 116 | NA | 0.40 | 0.09 | 0.35 | 4.3 | 0.26 | NA | NA | NA | 2.3 | 24.8 |
| A37 | DI 30(1) | 1291 | ±1 W 5000 | 30800 | 103000 | 117 | 5.3 | 82 | 2.2 | 0.06 | 80 | 39.3 | 0.09 | 0.24 | 116 | NA | 0.40 | 0.09 | 0.35 | 4.3 | 0.26 | NA | NA | NA | 2.3 | 24.8 |
| A37 | DI 30(1) | 1291 | ±1 W 5000 | 30800 | 103000 | 117 | 5.3 | 82 | 2.2 | 0.06 | 80 | 39.3 | 0.09 | 0.24 | 116 | NA | 0.40 | 0.09 | 0.35 | 4.3 | 0.26 | NA | NA | NA | 2.3 | 24.8 |
| A37 | DI 30(1) | 1291 | ±1 W 50 | | | | | | | | | | | | | | | | | | | | | | | |

Table 2.5: Averages and ranges of elemental concentrations (ppm) in nickeline (LA-ICPMS data)

| Sample | Mineral | Chip sample | Stope | Shear level | S | Fe | Co | Cu | Zn | Se | Ru | Rh | Pd | Ag | Cd | Sn | Sb | Te | Re | Os | Ir | Pt | Au | Hg | Tl | Pb | Bi |
|--------|-----------|-------------|-------|-------------|------|-------|-----|------|--------|-----|-------|-------|-----|------|-------|------|------|------|------|-------|--------|--------|------|-------|--------|------|------|
| A86 | Nickeline | DTL 29 (1B) | 1291 | #1 W/5000 | 1944 | 10460 | 195 | 8.8 | bdl | 73 | bdl | bdl | 25 | 5.43 | 1.14 | 0.27 | 1438 | 764 | NA | bdl | bdl | bdl | 3.3 | bdl | bdl | 4.04 | 18.3 |
| A86 | Nickeline | DTL 29 (1B) | 1291 | #1 W/5000 | 7004 | 9918 | 457 | bdl | bdl | 79 | bdl | bdl | 25 | 4.39 | bdl | bdl | 1404 | 705 | NA | bdl | 0.085 | bdl | 2.8 | bdl | bdl | 0.32 | 15.9 |
| A86 | Nickeline | DTL 29 (1B) | 1291 | #1 W/5000 | 1047 | 144 | 235 | bdl | bdl | 74 | 0.11 | bdl | 27 | 0.10 | bdl | 0.05 | 1566 | 836 | NA | bdl | bdl | bdl | 6.8 | 0.28 | 0.024 | bdl | 1.5 |
| A87 | Nickeline | DTL 29 (2) | 1291 | #1 W/5000 | 1211 | 753 | 231 | bdl | bdl | 62 | 0.07 | bdl | 29 | 0.17 | 0.188 | bdl | 1757 | 853 | NA | bdl | 0.14 | bdl | 5.7 | bdl | bdl | 0.08 | 3.3 |
| A87 | Nickeline | DTL 29 (2) | 1291 | #1 W/5000 | 885 | 60 | 181 | bdl | bdl | 58 | bdl | bdl | 27 | 0.48 | bdl | bdl | 1231 | 649 | NA | bdl | bdl | bdl | 3.8 | bdl | bdl | bdl | 5.8 |
| A87 | Nickeline | DTL 29 (2) | 1291 | #1 W/5000 | 2280 | 124 | 235 | bdl | bdl | 59 | bdl | 0.014 | 31 | 0.22 | bdl | bdl | 1485 | 828 | NA | 0.11 | 0.125 | bdl | 4.9 | bdl | bdl | bdl | 4.2 |
| A88 | Nickeline | DTL 29 (3A) | 1291 | #1 W/5000 | 2003 | 1662 | 182 | 1.4 | bdl | 43 | bdl | bdl | 82 | 4.44 | bdl | 0.20 | 1318 | 765 | NA | bdl | bdl | bdl | 4.3 | bdl | bdl | bdl | 4.2 |
| A88 | Nickeline | DTL 29 (3A) | 1291 | #1 W/5000 | 1651 | 148 | 210 | 41 | bdl | 78 | bdl | 0.03 | 104 | 0.81 | bdl | bdl | 1559 | 855 | NA | bdl | 0.079 | bdl | 5.2 | bdl | bdl | 0.16 | 3.8 |
| A88 | Nickeline | DTL 29 (3A) | 1291 | #1 W/5000 | 1587 | 708 | 540 | bdl | bdl | 60 | 0.18 | 0.16 | 89 | 1.00 | bdl | 0.20 | 1246 | 615 | NA | bdl | 0.088 | bdl | 4.8 | bdl | bdl | 0.38 | 7.0 |
| A88 | Nickeline | DTL 29 (3A) | 1291 | #1 W/5000 | 2296 | 1125 | 191 | 9 | bdl | 94 | bdl | bdl | 96 | 7.19 | bdl | bdl | 1857 | 1331 | NA | 0.74 | bdl | bdl | 5.2 | bdl | bdl | 0.34 | 12.0 |
| A90 | Nickeline | DTL 29 (4A) | 1291 | #1 W/5000 | 3359 | 1426 | 156 | bdl | bdl | 84 | bdl | bdl | 22 | 0.30 | bdl | bdl | 2507 | 1207 | NA | bdl | 0.21 | bdl | 4.8 | bdl | bdl | bdl | 1.7 |
| A90 | Nickeline | DTL 29 (4A) | 1291 | #1 W/5000 | 2911 | 2582 | 257 | bdl | bdl | 67 | bdl | bdl | 24 | 0.42 | bdl | bdl | 2164 | 1016 | NA | bdl | bdl | bdl | 4.7 | 0.91 | bdl | 0.35 | 8.5 |
| A90 | Nickeline | DTL 29 (4A) | 1291 | #1 W/5000 | 1666 | 1231 | 244 | bdl | bdl | 69 | bdl | bdl | 22 | 0.45 | bdl | 0.13 | 2420 | 818 | NA | bdl | 0.086 | bdl | 4.6 | bdl | bdl | 0.17 | 3.5 |
| A90 | Nickeline | DTL 29 (4A) | 1291 | #1 W/5000 | 2635 | 169 | 216 | bdl | bdl | 137 | bdl | bdl | 19 | 0.95 | bdl | bdl | 3365 | 1683 | NA | bdl | bdl | bdl | 3.9 | 1.23 | bdl | 0.28 | 16.8 |
| A59 | Nickeline | DTL 11A (1) | 1322 | #1 W/5100 | 2517 | 2208 | 203 | 0.13 | 0.2112 | 46 | 0.036 | 0.004 | 105 | 0.04 | 0.099 | 0.04 | 1797 | 1204 | NA | 0.037 | 0.0082 | 0.0289 | 9.1 | 0.121 | 0.0074 | 0.09 | 1.2 |
| A59 | Nickeline | DTL 11A (1) | 1322 | #1 W/5100 | 1620 | 601 | 145 | 0.17 | 0.226 | 44 | 0.039 | 0.005 | 91 | 0.04 | 0.093 | 0.06 | 1804 | 1047 | NA | 0.055 | 0.0200 | 0.0313 | 8.4 | 0.182 | 0.0118 | 0.09 | 0.7 |
| A59 | Nickeline | DTL 11A (1) | 1322 | #1 W/5100 | 1932 | 1092 | 181 | 0.13 | 0.204 | 48 | 0.026 | 0.005 | 132 | 0.06 | 0.075 | 0.08 | 1874 | 1227 | NA | 0.033 | 0.0066 | 0.0266 | 9.9 | 0.103 | 0.0074 | 0.10 | 0.9 |
| A60 | Nickeline | DTL 11A (2) | 1322 | #1 W/5100 | 1269 | 89 | 218 | bdl | bdl | 72 | bdl | bdl | 7 | 0.31 | bdl | 0.08 | 2110 | 1064 | NA | bdl | 0.0368 | bdl | 7.3 | bdl | bdl | bdl | 4.3 |
| A60 | Nickeline | DTL 11A (2) | 1322 | #1 W/5100 | 1528 | 112 | 210 | 0.52 | bdl | 67 | 0.066 | bdl | 10 | 0.04 | bdl | 0.11 | 2052 | 1061 | NA | bdl | 0.0368 | bdl | 6.6 | 0.336 | bdl | bdl | 1.2 |
| A60 | Nickeline | DTL 11A (2) | 1322 | #1 W/5100 | 2420 | 603 | 219 | bdl | bdl | 81 | bdl | 0.015 | 4 | 6.45 | 0.399 | bdl | 2279 | 1105 | NA | bdl | bdl | bdl | 7.9 | bdl | bdl | bdl | 7.1 |
| A61 | Nickeline | DTL 11B (1) | 1321 | #1 W/5100 | 1417 | 386 | 283 | 0.18 | 3.16 | 78 | 0.063 | 0.005 | 23 | 0.25 | 0.099 | 0.04 | 2397 | 1056 | NA | 0.031 | 0.151 | 0.020 | 7.9 | 0.121 | 0.0075 | 0.02 | 1.7 |
| A61 | Nickeline | DTL 11B (1) | 1321 | #1 W/5100 | 1324 | 92 | 288 | 0.14 | 3.52 | 90 | 0.056 | 0.005 | 20 | 0.07 | 0.113 | 0.04 | 2535 | 1062 | NA | 0.032 | 0.165 | 0.015 | 6.7 | 0.130 | 0.0084 | 0.02 | 3.1 |
| A61 | Nickeline | DTL 11B (1) | 1321 | #1 W/5100 | 1572 | 426 | 293 | 2.2 | 3.45 | 89 | 0.067 | 0.004 | 24 | 0.60 | 0.104 | 0.03 | 2480 | 1045 | NA | 0.044 | 0.908 | 0.020 | 6.9 | 0.127 | 0.0061 | 0.07 | 2.3 |
| A61 | Nickeline | DTL 11B (1) | 1321 | #1 W/5100 | 2943 | 3187 | 314 | 0.2 | 3.68 | 82 | 0.063 | 0.007 | 28 | 0.23 | 0.080 | 0.04 | 2516 | 1169 | NA | 0.056 | 0.073 | 0.017 | 9.1 | 0.120 | 0.0087 | 0.05 | 2.6 |
| M46 | Nickeline | DL 30 (1) | 1291 | #1 W/5000 | 8666 | 998 | 759 | bdl | bdl | 28 | NA | NA | NA | 2.48 | bdl | 0.10 | 5401 | NA | 0.1 | NA | NA | NA | 16.0 | NA | NA | bdl | 4.6 |
| M46 | Nickeline | DL 30 (1) | 1291 | #1 W/5000 | 7659 | 170 | 775 | 0.1 | 0.23 | 30 | NA | NA | NA | 0.52 | bdl | 0.14 | 6207 | NA | 0.08 | NA | NA | NA | 15.8 | NA | NA | bdl | 5.0 |

bdl indicates values below detection limit

NA indicates no recorded value

Table 2.6: Averages and ranges of elemental concentrations (ppm) in Sphalerite (LA-ICPMS data)

| Sample | Mineral | Chip sample | Stope | Shear/level | Co | Ni | Cu | Se | Ag | Cd | Sn | Sb | Te | Au | Hg | Pb | Bi |
|--------|------------|-------------|-------|-------------|-----|-----|-------|-----|------|-------|------|------|------|------|-----|------|------|
| M32 | Sphalerite | DL 22 (1) | 2471 | #1 W/5000 | 253 | 1.6 | 37 | 161 | 1.6 | 23837 | bdl | bdl | bdl | bdl | 8.8 | 1.2 | 0.08 |
| M32 | Sphalerite | DL 22 (1) | 2471 | #1 W/5000 | 226 | 122 | 62.5 | 177 | 2.1 | 23787 | 0.33 | bdl | bdl | bdl | 6.1 | 14.9 | 2.5 |
| M32 | Sphalerite | DL 22 (1) | 2471 | #1 W/5000 | 251 | 1.9 | 2579 | 168 | 1.7 | 22846 | 0.92 | bdl | bdl | bdl | 5.6 | 4.8 | 0.86 |
| M32 | Sphalerite | DL 22 (1) | 2471 | #1 W/5000 | 233 | 1.1 | 25.5 | 157 | 1.5 | 25265 | 0.29 | bdl | bdl | bdl | 6.9 | 4.2 | 0.48 |
| M32 | Sphalerite | DL 22 (1) | 2471 | #1 W/5000 | 259 | 1.6 | 745 | 170 | 1.3 | 24215 | 1.1 | 0.07 | bdl | bdl | 5.1 | 17.4 | 0.64 |
| M32 | Sphalerite | DL 22 (1) | 2471 | #1 W/5000 | 242 | 9.1 | 25.9 | 170 | 6.4 | 24489 | bdl | bdl | bdl | bdl | 7.7 | 1.9 | 0.19 |
| M32 | Sphalerite | DL 22 (1) | 2471 | #1 W/5000 | 254 | 4.2 | 3920 | 177 | 1.4 | 23475 | 10.4 | bdl | bdl | bdl | 6 | 4.6 | 0.93 |
| A49 | Sphalerite | DTL 1 | 2421 | #1 W/5100 | 267 | 1.1 | 4887 | 151 | 5 | 15316 | 2.2 | bdl | 0.6 | bdl | 6.3 | 13 | 4.3 |
| A49 | Sphalerite | DTL 1 | 2421 | #1 W/5100 | 303 | 279 | 102.3 | 212 | 16.5 | 16044 | 0.75 | bdl | 37.4 | 0.02 | 5.4 | 384 | 5.0 |
| A49 | Sphalerite | DTL 1 | 2421 | #1 W/5100 | 228 | 676 | 84.4 | 189 | 14 | 16134 | 2.9 | bdl | 7.8 | 0.05 | 4.5 | 36.8 | 11.5 |

Note: all arsenic values registered below detection limit

bdl indicates values below detection limit

Table 2.7. Summary distribution of major, minor and As-bearing phases with estimated and actual bulk rock assay As values

| Sample | Chip sample | Stope | Shear Level | Bulk Arsenic (ppm) | Predicted As (ppm) | vol % of Po | vol % of Pn | vol % of Cpy | vol % of Sg | vol % of CGSS | vol % of Ncl | vol % of Ncl-CGSS intergrowths | vol % of GGSS | vol % of Spy | vol % of trace phases |
|--------|-------------|-------|-------------|--------------------|--------------------|-------------|-------------|--------------|-------------|---------------|--------------|--------------------------------|---------------|--------------|-----------------------|
| A70 | DTL 19 (1) | 2424 | 4 W 4470 | 1210 | 400 | 70 | 8 | 2 | 20 | 6.28E-02 | - | - | - | - | - |
| A71 | DTL 19 (2) | 2424 | 4 W 4470 | 190 | 0.5 | 71 | 8 | 1 | 20 | - | - | - | - | - | - |
| M105 | DL 69 (1) | 2174 | 4 W 4470 | 86 | 94 | 83 | 6.5 | 1.01E-01 | 10 | 1.37E-02 | 6.14E-04 | - | 3.76E-05 | - | 5.01E-05 |
| M106 | DL 70 (1) | 2274 | 4 W 4470 | 1760 | 667 | 85 | 2 | 5 | 10 | 1.05E-01 | - | - | 3.13E-06 | - | 9.00E-06 |
| M107 | DL 70 (2) | 2274 | 4 W 4470 | 2430 | 3129 | 74 | 5 | 1 | 20 | 4.89E-01 | - | - | 3.49E-03 | - | - |
| M110 | DL 72 (1) | 2524 | 4 W 4470 | 9 | 0.03 | 82 | 15 | 0 | 3 | - | - | - | 2.60E-04 | - | 4.94E-05 |
| A1 | DL 4 (1) | 2171 | 1 W 4600 | 2.5 ¹ | 0.19 | 83 | 11.57 | 2.12E-02 | 5 | - | - | - | - | - | 1.00E-01 |
| A2 | DL 4 (2) | 2171 | 1 W 4600 | 24 | 0.16 | 85 | 5 | 5.00E-01 | 9 | - | - | - | - | - | 6.67E-02 |
| A3 | DL 4 (3) | 2171 | 1 W 4600 | 2.5 | 0.19 | 73 | 16.8 | 1.00E-01 | 10 | - | - | - | - | - | 1.00E-02 |
| A4 | DL 4 (4) | 2171 | 1 W 4600 | 8 | 0.18 | 86.5 | 8.5 | 2.61E-02 | 4.5 | - | - | - | - | - | 4.30E-01 |
| A5 | DL 4 (5) | 2171 | 1 W 4600 | 27 | 2.03 | 81.5 | 9.75 | 3.00E-02 | 5.1 | 3.86E-04 | - | - | - | - | 2.50E-01 |
| A6 | DL 4 (6) | 2171 | 1 W 4600 | 2.5 | 0.16 | 86.15 | 4.17 | 1 | 8.5 | - | - | - | - | - | 9.26E-02 |
| M1 | DL 1.2 (1) | 1973 | 1 E 4600 | 30 | 0.14 | 70 | 5 | 5 | 20 | - | - | - | - | - | 5.24E-02 |
| M2 | DL 1.2 (2) | 1973 | 1 E 4600 | 2.5 | 0.03 | 5 | 5 | 20 | 70 | - | - | - | - | - | 5.12E-02 |
| M3 | DL 1.2 (3) | 1973 | 1 E 4600 | 2.5 | 2.26 | 6 | 4 | 89 | 1 | 3.47E-04 | - | - | - | - | 1.05E-01 |
| M5 | DL 3 (1) | 1973 | 1 E 4600 | 64 | 57.16 | 70 | 10 | 5 | 15 | 8.93E-03 | - | - | - | - | 1.28E-02 |
| M8 | DL 4 (2) | 2171 | 1 E 4600 | 23 | 1.5 | 82 | 10 | 2.00E-02 | 7.5 | - | - | - | 2.12E-04 | - | 5.66E-02 |
| M10 | DL 5 (2) | 2073 | 1 E 4600 | 52 | 0.003 | 2 | 0 | 0 | 98 | - | - | - | - | - | 7.72E-06 |
| A7 | DL 7 (1) | 2524 | 4 W 4800 | 628 | 4056 | 13 | 2 | 0.11 | 85 | 5.13E-01 | - | - | - | - | - |
| A8 | DL 9 (1) | 3024 | 4 E 4800 | 7110 | 2678 | 55 | 3.5 | 2 | 39.5 | 3.97E-01 | - | - | - | - | - |
| A9 | DL 9 (2) | 3024 | 4 E 4800 | 274 | 1189 | 57 | 5 | 3.35E-02 | 38 | 1.77E-01 | - | - | - | - | - |
| A10 | DL 9 (3) | 3024 | 4 E 4800 | 3840 | 556 | 50 | 4 | 7.86E-01 | 46.75 | 8.08E-02 | 1.70E-05 | - | - | - | - |
| A11 | DL 9 (4) | 3024 | 4 E 4800 | 5940 | 1810 | 68 | 5.25 | 1.78E-01 | 26.3 | 2.78E-01 | 1.50E-03 | - | - | - | - |
| A12 | DL 9 (5) | 3024 | 4 E 4800 | 7610 | 950 | 80 | 6 | 1 | 13 | 1.53E-01 | - | - | - | - | - |
| A13 | DL 9 (6) | 3024 | 4 E 4800 | 305 | 1413 | 31 | 3 | 4.20E-01 | 65 | 1.90E-01 | - | - | - | - | - |
| A80 | DTL 26 | 2474 | 4 W 4800 | 22 | 19 | 52 | 8 | 10 | 20 | 6.28E-02 | - | - | - | - | - |
| A81 | DTL 27 | 2474 | 4 W 4800 | 2.5 | 0.1 | 83 | 8 | 3 | 6.9 | - | - | - | - | - | 1 |
| M12 | DL 6 (2) | 2524 | 4 E 4800 | 14 | 0.1 | 92 | 1 | 1.00E-02 | 7 | - | - | - | 3.97E-06 | - | 1.96E-04 |
| M13 | DL 8 (1) | 2974 | 4 E 4800 | 94 | 0.67 | 80 | 13 | 5.00E-01 | 7 | - | - | - | 1.02E-04 | - | 6.31E-05 |
| M15 | DL 9 (1) | 3024 | 4 E 4800 | 122 | 26 | 80 | 5 | 2.00E-02 | 15 | - | - | - | 4.22E-03 | - | 8.20E-06 |
| M16 | DL 10 (1) | 2874 | 4 E 4800 | 141 | 233 | 1 | 0 | 1 | 98 | 2.78E-02 | - | - | - | - | 9.07E-01 |
| A14 | DL 19 (1) | 2983 | 4 E 4900 | 19 | 0.24 | 84.2 | 7.6 | 0.01 | 8.2 | - | - | - | - | - | - |
| A65 | DTL 15 (1) | 2781 | 1 E 4900 | 10 | 0.15 | 78 | 7.2 | 1 | 28.5 | - | - | - | - | - | - |
| A66 | DTL 15 (2) | 2781 | 1 E 4900 | 17 | 0.83 | 82.1 | 5 | 1.00E-01 | 10 | - | - | - | - | - | - |
| A68 | DTL 17 | 2821 | 1 E 4900 | 7 | 0.08 | 74.3 | 4.9 | 1.00E-01 | 20 | - | - | - | - | - | - |
| M18 | DL 11 (2) | 2474 | 4 E 4900 | 8 | 0.6 | 80 | 5 | 1.50E-01 | 15 | - | - | - | 6.39E-05 | - | 3.76E-06 |
| M19 | DL 12 (2) | 2774 | 4 E 4900 | 1040 | 3145 | 77 | 2 | 1 | 20 | 5.14E-01 | - | - | 3.83E-03 | - | 3.40E-06 |
| M20 | DL 12 (1) | 2774 | 4 E 4900 | 992 | - | 77 | 2 | 1 | 20 | 5.00E-01 | - | - | 4.00E-03 | - | 3.00E-06 |
| M23 | DL 15 (1) | 3074 | 4 E 4900 | 286 | 145 | 77 | 8 | 0 | 15 | 2.31E-02 | - | - | 6.23E-04 | - | 1.27E-05 |
| M26 | DL 17 (2) | 3324 | 4 E 4900 | 26 | 1.37 | 42 | 3 | 0.3 | 55 | - | - | - | 2.10E-04 | - | - |
| A20 | SLAB 22 (1) | 2471 | 1 W 5000 | 57 | 44 | 86 | 6 | 4 | 4.24 | 7.14E-03 | - | - | - | - | - |
| A21 | SLAB 22 (2) | 2471 | 1 W 5000 | 103 | 73 | 45 | 5 | 45 | 5.25 | 1.20E-02 | - | - | - | - | - |
| A22 | SLAB 22 (3) | 2471 | 1 W 5000 | 66 | 8.6 | 55 | 12 | 10 | 21.7 | 1.38E-03 | - | - | - | - | 1.70E-02 |
| A23 | SLAB 22 (4) | 2471 | 1 W 5000 | 52 | 6.8 | 74.5 | 8 | 10 | 7.8 | 1.08E-03 | - | - | - | - | 3.10E-03 |
| A24 | SLAB 22 (5) | 2471 | 1 W 5000 | 66 | 108 | 12 | 4 | 80 | 4 | 1.78E-02 | - | - | - | - | 1.69E-01 |
| A25 | SLAB 22 (6) | 2471 | 1 W 5000 | 42 | 34 | 83 | 6.4 | 9 | 2 | 5.57E-03 | - | - | - | - | 1.33E-02 |
| A27 | DL 44 (2) | 2624 | 4 W 5000 | 10000 ² | 12123 | 73.5 | 2.5 | 5.49E-02 | 22.3 | 2 | - | - | - | - | - |
| A29 | DL 44 (4) | 2624 | 4 W 5000 | 2860 | 843 | 3 | 3.80E-01 | 1 | 95 | 1.39E-01 | - | - | - | - | - |
| A86 | DTL 29 (1B) | 1291 | 1 W 5000 | 10000 | 16040 | 45 | 8.5 | 35 | 9.5 | 4.61E-01 | 5.50E-01 | 1.1 | - | - | 1.97E-04 |
| A87 | DTL 29 (2) | 1291 | 1 W 5000 | 7110 | 6048 | 30 | 6 | 51 | 5 | 1.44E-01 | 1.70E-01 | 4.55E-01 | - | - | 4.61E-04 |
| A88 | DTL 29 (3A) | 1291 | 1 W 5000 | 10000 | 38663 | 60 | 1.47E-01 | 10 | 25 | - | 4 | - | - | - | 4.48E-05 |
| A89 | DTL 29 (3B) | 1291 | 1 W 5000 | - | 41864 | 1 | 1.63E-01 | 75 | 18 | - | 4 | 1.82 | - | - | 1.39E-04 |
| A90 | DTL 29 (4A) | 1291 | 1 W 5000 | 10000 | 19618 | 40 | 2.024 | 40 | 17 | 3.65E-02 | 4.00E-01 | 2 | - | - | 1.74E-03 |
| A91 | DTL 29 (4B) | 1291 | 1 W 5000 | - | 23314 | 45 | 1.5 | 40 | 9 | 7.06E-02 | 1.22 | 1.43 | - | - | 4.15E-03 |
| A92 | DTL 30 | 1291 | 1 W 5000 | 55 | 0.0006 | 35 | 0.645 | 60 | 5 | - | - | - | - | - | 6.36E-05 |
| M32 | DL 22 (1) | 2471 | 1 W 5000 | 2150 | 1031 | 30 | 0 | 30 | 40 | 1.78E-01 | - | - | - | - | 2.36E-02 |
| M46 | DL 30 (1) | 1291 | 1 W 5000 | 10000 | 24998 | 5 | 1 | 84 | 10 | 7.51E-01 | 3.91E-01 | 2.15 | - | - | 1.23E-03 |
| M66 | DL 44 (1) | 2624 | 4 W 5000 | 10000 | 3152 | 55 | 5 | 0.042 | 40 | 5.17E-01 | - | - | - | - | - |
| A49 | DTL 1 | 2421 | 1 W 5100 | 286 | 0.62 | 3 | 5.33E-02 | 87 | 10 | - | - | - | - | - | - |
| A50 | DTL 2 | 2421 | 1 W 5100 | 57 | 55 | 90 | 1 | 7 | 6.00E-01 | 8.77E-03 | - | - | - | - | - |
| A51 | DTL 3 | 2421 | 1 W 5100 | 296 | 63 | 40 | 5.5 | 40 | 0 | 1.00E-02 | - | - | - | - | - |
| A52 | DTL 4 | 2421 | 1 W 5100 | 74 | 55 | 70 | 19 | 2.5 | 8.5 | 9.07E-03 | - | - | - | - | - |
| A53 | DTL 5 | 2321 | 1 W 5100 | 22 | 0.49 | 30 | 8 | 40 | 20 | - | - | - | - | - | - |
| A54 | DTL 6 | 2271 | 1 W 5100 | 283 | 0.04 | 15 | 1 | 4 | 80 | - | - | - | - | - | - |
| A55 | DTL 7 | 2221 | 1 W 5100 | 19 | 9.55 | 83 | 4 | 3 | 10 | 1.51E-03 | - | - | - | - | - |
| A62 | DTL 11B (2) | 1321 | 1 W 5100 | 9600 | 325870 | 5 | 2.92E-03 | 42 | 10.79 | 2.07 | 40 | - | - | - | - |
| M81 | DL 51 (1) | 1135 | 1 W 5100 | 2.5 | 0.29 | 73 | 2 | 15 | 10 | - | - | - | 2.51E-05 | - | 4.77E-04 |
| M82 | DL 51 (2) | 1135 | 1 W 5100 | 2.5 | 1.53 | 85 | 2 | 1 | 11 | - | - | - | 1.53E-04 | - | 1.86E-04 |
| M83 | DL 52 (1) | 1135 | 1 W 5100 | 2.5 | 26 | 78 | 2 | 5 | 15 | - | - | - | 4.41E-05 | - | 6.20E-05 |
| M84 | DL 52 (2) | 1135 | 1 W 5100 | 2.5 | 967 | 5 | 5 | 5 | 85 | 1.24E-01 | 8.39E-05 | - | 5.59E-04 | - | 3.86E-04 |
| M85 | DL 53 (1) | 1174 | 1 W 5100 | 2.5 | 0.14 | 45 | 5 | 45 | 5 | - | - | - | - | - | 5.10E-05 |
| M86 | DL 54 (1) | 1173 | 1 W 5100 | 2.5 | 1.32 | 75 | 10 | 5 | 10 | - | - | - | 4.62E-05 | 9.02E-05 | 2.02E-04 |
| M88 | DL 55 (1) | 1214 | 1 W 5100 | 7 | 0.67 | 15 | 3 | 2 | 80 | - | - | - | 8.52E-05 | - | 5.24E-05 |
| M89 | DL 56 (1) | 1213 | 1 W 5100 | 2.5 | 0.24 | 1 | 0 | 30 | 70 | - | - | - | - | - | 8.14E-04 |
| M90 | DL 57 (1) | 1211 | 1 W 5100 | 6 | 0.55 | 75 | 5 | 1 | 20 | - | - | - | 3.81E-05 | 7.62E-06 | 1.90E-06 |
| M91 | DL 58 (1) | 2624 | 4 W 5100 | 11 | 0.48 | 88 | 5 | 5 | 2 | - | - | - | 1.26E-05 | 1.68E-05 | 1.17E-04 |

¹ indicates the lower detection limit for arsenic in the assayed sample² indicates the upper detection limit for arsenic in the assayed sample, the real value could be higher³ trace phases include PGL-bearing minerals as well as Bi, Ag, Pb, Ni-tellurides, galena, and magnetite

List of abbreviations: CGSS=cobaltite-gersdorffite solid solution, Cpy=chalcopyrite, GGSS=glaucondio-gersdorffite solid solution, Ncl=nickeline, Pn=pentlandite, Po=pyrrhotite, Spy=sperrylite

Table 2.8: Averages and ranges (wt %) for major elements in As-bearing minerals (electron microprobe data)

| Sample | Shear | Mineral | As | Ni | Co | Fe | S |
|--------|----------|---------|---------------------|---------------------|---------------------|-------------------|---------------------|
| M105 | 4 W/4470 | CGSS | 45.83 (44.25-47.85) | 11.69 (5.01-23.46) | 16.98 (2.44-25.29) | 5.93 (4.05-8.83) | 19.35 (18.66-19.89) |
| M106 | 4 W/4470 | CGSS | 46.5 (44.79-52.97) | 14 (8.52-24.89) | 15.15 (4.75-21.42) | 5.95 (4.42-9.29) | 18.39 (14.04-19.45) |
| M107 | 4 W/4470 | CGSS | 46.03 (44.98-54.36) | 11.78 (6.55-26.28) | 17.84 (3.59-24.38) | 5.94 (4.38-7.68) | 18.09 (12.71-18.98) |
| M19 | 4 E/4900 | CGSS | 46.46 (45.42-47.42) | 14.25 (7.33-18.76) | 14.24 (8.82-23.15) | 7.11 (5.02-8.42) | 19.19 (18.63-19.78) |
| M20 | 4 E/4900 | CGSS | 46.05 (44.85-47.51) | 14.35 (6.49-19.27) | 14.05 (8.22-24.14) | 6.92 (4.62-8.15) | 18.92 (18.34-19.52) |
| M32 | 1 W/5000 | CGSS | 45.91 (44.03-49.08) | 16.34 (9.26-22.75) | 12.44 (5.63-20.13) | 5.71 (3.52-7.6) | 19.17 (17.31-19.90) |
| M46 | 1 W/5000 | CGSS | 45.91 (41.56-48.41) | 23.36 (16.61-30.09) | 4.16 (0.30-9.64) | 8.72 (5.85-11.20) | 18.3 (12.74-19.58) |
| M66 | 4 W/5000 | CGSS | 46.19 (45.96-46.60) | 19.71 (19.32-20.27) | 7.29 (6.85-7.61) | 7.86 (7.79-7.92) | 18.04 (17.93-18.10) |
| M84 | 1 W/5100 | CGSS | 45.68 (44.87-47.69) | 15.23 (10.97-21.76) | 13.49 (6.46-18.97) | 6.15 (4.98-7.36) | 18.82 (17.61-19.25) |
| M88 | 1 W/5100 | CGSS | 43.3 (37.06-46.9) | 14.96 (7.11-21.00) | 12.43 (8.29-17.16) | 9.61 (5.87-15.94) | 19.49 (17.16-22.93) |
| M110 | 4 W/4470 | GGSS | 45.96 (44.95-46.99) | 13.02 (5.58-20.13) | 16.4 (8.70-25.07) | 6.22 (3.96-7.93) | 18.34 (17.82-18.88) |
| M81 | 1 W/5100 | GGSS | 46.06 (45.36-46.63) | 15.42 (14.23-17.34) | 12.04 (10.66-13.63) | 6.82 (6.31-7.73) | 19.35 (18.76-19.77) |
| M82 | 1 W/5100 | GGSS | 44.4 (40.14-46.72) | 13.5 (5.80-17.69) | 12.6 (9.53-20.45) | 8.11 (6.83-11.15) | 19.49 (18.04-21.36) |
| M83 | 1 W/5100 | GGSS | 44.68 (43.22-45.67) | 14.2 (7.30-17.93) | 13.41 (9.59-20.93) | 7.9 (6.17-10.42) | 19.59 (19.17-19.95) |
| M105 | 4 W/4470 | Ncl | 55.62 (55.21-55.54) | 44 (43.58-44.14) | 0.15 (0.11-0.16) | 0.89 (0.64-0.76) | 0.24 (0.206-0.213) |
| M106 | 4 W/4470 | Ncl* | 54.27 | 25.47 | 4.07 | 4.34 | 13.1 |
| M46 | 1 W/5000 | Ncl | 55.88 (53.49-56.50) | 44.62 (40.34-46.62) | 0.08 (0-0.34) | 0.36 (0.01-1.94) | 0.41 (0.11-4.17) |
| M84 | 1 W/5100 | Ncl | 47.99 (47.88-48.10) | 51.47 (51.08-51.86) | 0.52 (0.391-0.65) | 0.42 (0.40-0.43) | 0.11 (0.07-0.14) |

Note: Totals were corrected to only account for major components

Ncl* indicates nickeline with Co, Ni and S contamination

List of abbreviations; CGSS = cobaltite-gersdorffite solid solution; GGSS = glaucodot-gersdorffite solid solution; Ncl = nickeline

Table 2.9: Point counting of PGE and trace accessory phases

| Host | Sperrylite (PtAs ₂) | Irarsite- hollingworthite | Michenerite (PdBiTe) | PdTe | Paolovite (Pd ₂ Sb) | (Ni,Sn)PdSe | Re-sulfide | BiTe | NiTe | Hessite (Ag ₂ Te) | Altaitite (PbTe) | Molybdenite | Au- bearing | Electrum (AuAg) |
|---------------------|------------------------------------|------------------------------|-------------------------|-------|-----------------------------------|---------------------|------------|-------------|-----------|---------------------------------|---------------------|-------------|----------------|--------------------|
| Po | | 13 | 1 | 1 | 1 | | 1 | 36, 3 (Ag) | 4 | 12 | 1 | 1 | | |
| Po-Cpy ¹ | | | | | | | | 6 | | 1 | | | | |
| Po-Pn | | | | | | 1 (Ni) ² | | 1 | | 15 | | 1 | 1 | |
| Po-CGSS | | | 1 | | | | | 2 | | 5 | | | | |
| Po-GGSS | | 1 | | | | | | | 1 | 1 | | | | |
| Po-Ncl | | | 10 | 4 | | | | | 3 (Pd) | 10 | | | | |
| Po-Ncl-CGSS | | | 4 | | | | | | | | | | | |
| Po-Cpy-Sg | | | | | | | | | | | | 1 | | |
| Po-Ncl-Sg | | | 2 | | | | | | | | | | | |
| Po-Sg | 1 | | 4 | 5 | | | | 11 | 1, 1 (Pd) | 2 | | | | 1 |
| Pn | | | | 1 | 2, 1 (Sb) | | | 7 | | 7 | | | | |
| Pn-Ncl | | | | | | | | | | | | | | |
| Cpy | | 1 | 1 | 3 | | | | 24, 10 (Ag) | 1 | 14 | | | | |
| Cpy-Pn | | | | | | | | | | 7 | | | | |
| Cpy-CGSS | | | 2 | | | | | | | | | | | |
| Cpy-Ncl | 3 | | | 4 | 1 (Te) | 1 (Sn) | | | | | | | | |
| Cpy-Ncl-CGSS | | | | | 1 | | | | | | | | | 2 |
| Cpy-Pn-CGSS | | | | | | | | | | | | | | 4 |
| Cpy-Sg | 1 | | | | | | | 3 | | 3 | | | | |
| Cpy-Sph | | | | 1 | | | | 5 | | 4 | | | | |
| GGSS | | 18 | | | | | | 9 | | 1 | | | | |
| GGSS-Sg | | | | | | | | 1 | | | | | | |
| CGSS | | | 3 | 9 | | | | 39, 1 (Ag) | | 3 | | | | |
| CGSS-Ncl Inter | | | | 1 | | | | | | | | | | |
| Ncl | | | 10 | 4 | | | | | | 59 | | | | 1 |
| Ncl-CGSS | | | 1 | | | | | | | 1 | | | | |
| Ncl-Sg | | | 2 | 1(Cd) | | | | | | | | | | |
| Sph | | | | | | | | 1 | | | | | | |
| Sph-Sg | | | 1 | | | | | 1 | | 2 | | | | |
| Sg | 1 | | | 6 | | | | | | 2 | | | | |
| BiTe | | | | | | | | | 1 | 1 | | | | |
| Totals | 6 | 33 | 42 | 40 | 6 | 2 | 1 | 160 | 12 | 150 | 1 | 3 | 1 | 8 |

¹ indicates multiple mineral hosts (along mineral boundaries) for PGE and trace phases² Metals in parentheses are major component of trace phases

list of abbreviations: BiTe = bismuth-telluride; CGSS = cobaltite-gersdorffite solid solution; CGSS-Ncl inter = cobaltite-gersdorffite solid solution-nickeline intergrowths; Cpy = chalcopyrite;

GGSS = glaucodot-gersdorffite solid solution; Ncl = nickeline; Po = pyrrhotite; Pn = pentlandite; Sg = silicate gangue; Sph = sphalerite

Table 2.10: Representative SEM-EDS analyses of Pd tellurides and trace phases

| Mineral | S | Fe | Ni | Cu | Co | As | Rh | Pd | Ag | Cd | Sn | Sb | Te | Re | Ir | Pt | Au | Bi | Total |
|----------------------------|-------|-------|-------|------|------|-------|-------|-------|-------|-------|-------|-------|-------|-------|------|-------|-------|-------|--------|
| Tsumoite | | | | | | | | | | | | | 54.53 | | | | | 45.47 | 100 |
| Tsumoite | | | | | | | | | | | | | 48.65 | | | | | 51.35 | 100 |
| Tsumoite | | | | | | | | | | | | | 41.69 | | | | | 58.31 | 100 |
| Tsumoite | | | | | | | | | | | | | 44.61 | | | | | 55.39 | 100 |
| Tsumoite | | | | | | | | | | | | | 38.42 | | | | | 61.58 | 100 |
| Tsumoite | | | | | | | | | | | | | 36.47 | | | | | 63.53 | 100 |
| Tsumoite | | | | | | | | | | | | | 31.82 | | | | | 68.18 | 100 |
| Tsumoite (Ag) | | | | | | | | | 6.61 | | | | 33.49 | | | | | 59.9 | 100 |
| Tsumoite (Ag) | | | | | | | | | 12.63 | | | | 35.83 | | | | | 51.54 | 100 |
| Electrum | | | | | | | | | 32.82 | | | | | | | | 67.18 | | 100 |
| Electrum | | | | | | | | | 34.87 | | | | | | | | 65.13 | | 100 |
| Electrum | | | | | | | | | 34.28 | | | | | | | | 65.72 | | 100 |
| Electrum | | | | | | | | | 34.55 | | | | | | | | 65.45 | | 100 |
| Hessite | | | | | | | | | 64.51 | | | | 35.49 | | | | | | 100 |
| Hessite | | | | | | | | | 57.47 | | | | 42.53 | | | | | | 100 |
| Hessite | | | | | | | | | 60.32 | | | | 39.68 | | | | | | 100 |
| Hessite | | | | | | | | | 65.07 | | | | 34.93 | | | | | | 100 |
| Hessite | | | | | | | | | 60.96 | | | | 39.04 | | | | | | 100 |
| Hessite | | | | | | | | | 62.02 | | | | 37.98 | | | | | | 100 |
| Hessite | | | | | | | | | 58.62 | | | | 41.38 | | | | | | 100 |
| Hessite | | | | | | | | | 60.25 | | | | 39.75 | | | | | | 100 |
| Hessite | | | | | | | | | 61.74 | | | | 38.26 | | | | | | 100 |
| Hessite | | | | | | | | | 60.90 | | | | 39.1 | | | | | | 100 |
| Hessite | | | | | | | | | 61.35 | | | | 38.65 | | | | | | 100 |
| Hessite | | | | | | | | | 61.76 | | | | 38.24 | | | | | | 100 |
| Hessite | | | | | | | | | 62.6 | | | | 37.4 | | | | | | 100 |
| Hessite | | | | | | | | | 61.46 | | | | 38.54 | | | | | | 100 |
| Michenerite | | | | | | | | 29.77 | | | | | 31.12 | | | | | 39.11 | 100 |
| Michenerite | | | | | | | | 25.71 | | | | | 31.45 | | | | | 42.84 | 100 |
| Michenerite | | | | | | | | 25.89 | | | | | 29.3 | | | | | 44.81 | 100 |
| Michenerite | | | | | | | | 26.73 | | | | | 28.45 | | | | | 44.82 | 100 |
| Michenerite | | | | | | | | 26.57 | | | | | 30.34 | | | | | 43.09 | 100 |
| Michenerite | | | | | | | | 30.27 | | | | | 47.07 | | | | | 22.67 | 100.01 |
| Michenerite | | | | | | | | 27.16 | | | | | 30.64 | | | | | 42.2 | 100 |
| Michenerite | | | | | | | | 27.71 | | | | | 30.55 | | | | | 41.73 | 99.99 |
| Michenerite | | | | | | | | 27.44 | | | | | 30.39 | | | | | 42.17 | 100 |
| Michenerite | | | | | | | | 26.14 | | | | | 34.47 | | | | | 39.39 | 100 |
| Michenerite | | | | | | | | 25.85 | | | | | 31.43 | | | | | 42.72 | 100 |
| Michenerite | | | | | | | | 26.33 | | | | | 29.24 | | | | | 44.43 | 100 |
| Michenerite | | | | | | | | 25.76 | | | | | 33.29 | | | | | 40.95 | 100 |
| Michenerite | | | | | | | | 26.87 | | | | | 31.32 | | | | | 41.81 | 100 |
| Michenerite | | | | | | | | 27.27 | | | | | 30.81 | | | | | 41.92 | 100 |
| Michenerite | | | | | | | | 28.09 | | | | | 30.28 | | | | | 41.63 | 100 |
| Michenerite | | | | | | | | 25.68 | | | | | 29.94 | | | | | 44.38 | 100 |
| NiTe | | 12.10 | 33.71 | | | | | | | | | | 50.18 | | | | | 4.01 | 100 |
| NiTe | 8.55 | 6.50 | 13.00 | 5.52 | | | | | | | | | 66.44 | | | | | | 100.01 |
| Paolovite | | | | | | | | 64.62 | | | 35.38 | | | | | | | | 100 |
| Paolovite | | | | | | | | 64.83 | | | 35.17 | | | | | | | | 100 |
| Paolovite | | | | | | | | 64.78 | | | 35.22 | | | | | | | | 100 |
| Paolovite (Sb) | | | | | | | | 62.59 | | | 28.91 | 8.5 | | | | | | | 100 |
| PbTe (Sb) | | | | | | | | 47.92 | | | | 24.72 | 27.37 | | | | | | 100.01 |
| PdTe (Cd) | | | | | | | | 7.99 | | 27.72 | | | 64.29 | | | | | | 100 |
| PdBiTe (Sb) | | | | | | | | 43.01 | | | | 20.97 | 20.47 | | | | 15.54 | | 99.99 |
| PdTe | | | | | | | | 33.59 | | | | | 66.41 | | | | | | 100 |
| PdTe | | | | | | | | 15.05 | | | | | 84.95 | | | | | | 100 |
| PdTe | | | | | | | | 8.36 | | | | | 91.64 | | | | | | 100 |
| PdTe | | | | | | | | 41.76 | | | | | 58.24 | | | | | | 100 |
| PdTe | | | | | | | | 42.63 | | | | | 57.37 | | | | | | 100 |
| PdTe | | | | | | | | 46.18 | | | | | 53.82 | | | | | | 100 |
| PdTe | | | | | | | | 44.76 | | | | | 55.24 | | | | | | 100 |
| PdTe | | | | | | | | 11.02 | | | | | 88.98 | | | | | | 100 |
| Ir-Rh-bearing ¹ | 45.50 | 18.20 | 2.40 | | 8.00 | 22.10 | | | | | | | | | 3.80 | | | | 100 |
| Ir-Rh-bearing | 18.68 | 5.37 | 5.75 | | 6.47 | 41.77 | 12.75 | | | | | | | | 6.75 | 2.46 | | | 100 |
| Re-bearing ² | 31.17 | 3.83 | | 4.29 | | | | | | | | | | 60.72 | | | | | 100.01 |
| Sperrylite | | | | | | 66.80 | | | | | | | | | | 33.20 | | | 100 |

¹ analysis shows possible contamination from host mineral gersdorffite (Co, Ni, As)² analysis shows possible contamination from host mineral chalcocopyrite (Cu, Fe)

Table 2.11: Assay results of chip, grid and slab samples

| Sample | Sample type | Thla section | Stope | Level | Shear | Ore type | Mono:Hex | Cu (wt%) | Ni (wt%) | Co (ppm) | Fe (wt%) | As (ppm) | Pb (ppm) | Zn (ppm) |
|----------|-------------|--------------|-------|-------|---------------|------------------|----------|----------|----------|----------|----------|----------|----------|-----------|
| DL63(1) | Chip | M96 | 1971 | 4470 | #1 west shear | INMS | 65.35 | 1.16 | 4.64 | 1360 | 45 | bdl | 857 | 590 |
| DL63(2) | Chip | M97 | 1971 | 4470 | #1 west shear | INMS | 0.100 | 0.58 | 4.79 | 1390 | 47.7 | bdl | 611 | 461 |
| DL64(1) | Chip | M98 | 1971 | 4470 | #1 west shear | INMS | 0.100 | 0.33 | 2.88 | 792 | 50 | 7 | 22 | 55 |
| DL65(1) | Chip | M100 | 2121 | 4470 | #1 west shear | WR | NA | 0.02 | 0.002 | 20 | 8.24 | 16 | 14 | 97 |
| DL65(2) | Chip | - | 2121 | 4470 | #1 west shear | WR | NA | 0.05 | 0.018 | 36 | 11.55 | bdl | 54 | 211 |
| DL66(1) | Chip | M101 | 2171 | 4470 | #1 west shear | INMS | 20.80 | 1.32 | 2.70 | 701 | 42.6 | 7 | 242 | 257 |
| DL66(2) | Chip | M102 | 2171 | 4470 | #1 west shear | DISS | 30.70 | 3.84 | 3.11 | 831 | 34.5 | 10 | 94 | 354 |
| DL67(1) | Chip | M103 | 2421 | 4470 | #1 west shear | INMS | 80.20 | 0.98 | 5.04 | 992 | 37.4 | 23 | 83 | 183 |
| DL68(1) | Chip | M104 | 2461 | 4470 | #1 west shear | INMS | 80.20 | 1.38 | 4.63 | 947 | 45.3 | 12 | 22 | 377 |
| DL69(1) | Chip | M105 | 2174 | 4470 | #4 west shear | INMS | 30.70 | 0.28 | 4.24 | 1070 | 43.3 | 87 | 11 | 150 |
| DL70(1) | Chip | M106 | 2274 | 4470 | #4 west shear | INMS | 60.40 | 3.68 | 3.53 | 2230 | 41.2 | 1760 | 18 | 125 |
| DL70(2) | Chip | M107 | 2274 | 4470 | #4 west shear | INMS | 70.30 | 1.42 | 2.78 | 2460 | 33.9 | 2430 | 2750 | 603 |
| DL71(1) | Chip | M108 | 2424 | 4470 | #4 west shear | Gal-Sph stringer | NA | 0.07 | 0.027 | 14 | 2.73 | bdl | 30 (7%) | 26.9 (7%) |
| DL71(2) | Chip | M109 | 2424 | 4470 | #4 west shear | Gal-Sph stringer | NA | 0.06 | 0.025 | 17 | 1.86 | 19 | 30 (7%) | 14.7 (7%) |
| DL72(1) | Chip | M110 | 2524 | 4470 | #4 west shear | Qtz-rich DISS | 95.5 | 0.13 | 4.51 | 1300 | 48.5 | 9 | 1 | 32 |
| DL196(1) | Grid | A70 | 2424 | 4470 | #4 west shear | INMS | 90.10 | 0.42 | 3.97 | 1225 | 41.6 | 1210 | 22 | 10 |
| DL196(2) | Grid | A71 | 2424 | 4470 | #4 west shear | DISS | 90.10 | 0.52 | 3.76 | 820 | 40.5 | 190 | 26 | 163 |
| DL196(3) | Grid | A72 | 2424 | 4470 | #4 west shear | DISS | 80.20 | 0.39 | 3.49 | 682 | 40.1 | 44 | 29 | 42 |
| DL196(4) | Grid | A73 | 2424 | 4470 | #4 west shear | DISS | 50.50 | 1.14 | 1.32 | 276 | 24.9 | 37 | 17 | 211 |
| DL196(5) | Grid | A74 | 2424 | 4470 | #4 west shear | DISS | 60.40 | 0.28 | 3.27 | 603 | 40.6 | 57 | 27 | 136 |
| DL120 | Chip | - | 2424 | 4470 | #4 west shear | DISS | NA | 0.13 | 0.02 | 12 | 2.35 | 19 | 30 | 23.2 |
| DL121 | Chip | A75 | 2424 | 4470 | #4 west shear | DISS | 90.10 | 1.86 | 0.82 | 271 | 15.35 | 15 | 14.25 | 1685 |
| DL122 | Chip | A76 | 2474 | 4470 | #4 west shear | INMS | 90.10 | 0.34 | 4.2 | 1200 | 48.7 | 50 | 1 | 35 |
| DL121(1) | Chip | M1 | 1971 | 4600 | #1 west shear | DISS | 10.90 | 1.96 | 1.58 | 427 | 28.9 | 30 | 17 | 253 |
| DL121(2) | Chip | M2 | 1971 | 4600 | #1 west shear | DISS | 0.100 | 25.90 | 1.12 | 331 | 34.5 | bdl | 13 | 1795 |
| DL121(3) | Chip | M3 | 1971 | 4600 | #1 west shear | DISS | 0.100 | 28.30 | 1.51 | 435 | 31.8 | bdl | 7 | 1605 |
| DL121(4) | Chip | M4 | 1971 | 4600 | #1 west shear | DISS | 0.100 | 1.51 | 2.8 | 828 | 34.9 | bdl | 12 | 225 |
| DL3(1) | Chip | M5 | 1971 | 4600 | #1 west shear | INMS | 0.100 | 1.66 | 2.61 | 713 | 37.9 | 64 | 10 | 164 |
| DL3(2) | Chip | M6 | 1971 | 4600 | #1 west shear | INMS | 0.100 | 0.57 | 3.83 | 1010 | 47.3 | 35 | 1 | 61 |
| DL4(1) | Chip | M7 | 2171 | 4600 | #1 west shear | MASU | 0.100 | 0.16 | 3.64 | 868 | 50 | bdl | 1 | 52 |
| DL4(2) | Chip | M8 | 2171 | 4600 | #1 west shear | MASU | 0.100 | 0.29 | 4.55 | 1150 | 50 | 25 | 1 | 33 |
| DL5(1) | Chip | M9 | 2071 | 4600 | #1 west shear | WR | NA | 0.07 | 0.03 | 39 | 9.97 | bdl | 20 | 123 |
| DL5(2) | Chip | M10 | 2071 | 4600 | #1 west shear | WR | NA | 0.06 | 0.16 | 82 | 8.93 | 52 | 14 | 119 |
| DL4(1) | Slab | A1 | 2171 | 4600 | #1 west shear | MASU-INMS | 0.100 | 0.16 | 3.44 | 805 | 50 | bdl | 10 | 71 |
| DL4(2) | Slab | A2 | 2171 | 4600 | #1 west shear | MASU-INMS | 20.80 | 0.27 | 4.82 | 1220 | 49.3 | 24 | 19 | 93 |
| DL4(3) | Slab | A3 | 2171 | 4600 | #1 west shear | MASU-INMS | 5.95 | 0.29 | 4.35 | 1090 | 49.9 | bdl | 18 | 115 |
| DL4(4) | Slab | A4 | 2171 | 4600 | #1 west shear | MASU-INMS | 5.95 | 0.10 | 3.95 | 949 | 50 | 8 | 8 | 77 |
| DL4(5) | Slab | A5 | 2171 | 4600 | #1 west shear | MASU-INMS | 0.100 | 0.10 | 4.8 | 1280 | 50 | 27 | 12 | 84 |
| DL4(6) | Slab | A6 | 2171 | 4600 | #1 west shear | MASU-INMS | 15.85 | 0.28 | 3.86 | 908 | 50 | bdl | 23 | 94 |
| DL123b | Chip | A77 | 2374 | 4600 | #4 west shear | DISS | 50.50 | 0.55 | 3.9 | 973 | 48.3 | 15 | 2 | 8 |
| DL124 | Chip | A78 | 2271 | 4600 | #1 west shear | DISS | 20.80 | 0.73 | 4.09 | 840 | 46 | 388 | 927 | 546 |
| DL125 | Chip | A79 | 2321 | 4600 | #1 west shear | INMS | 0.100 | 1.54 | 2.77 | 674 | 46.9 | 27 | 13 | 201 |
| DL6(1) | Chip | M11 | 2524 | 4800 | #4 west shear | INMS | 90.10 | 0.16 | 5.05 | 1320 | 44.2 | 13 | 5 | 6 |
| DL6(2) | Chip | M12 | 2524 | 4800 | #4 west shear | INMS | 85.15 | 0.14 | 3.92 | 938 | 45.6 | 14 | 4 | 7 |
| DL7 | Chip | A7 | 2524 | 4800 | #4 west shear | Qtz-rich DISS | 100.0 | 0.22 | 0.72 | 260 | 11.4 | 628 | 258 | 107 |
| DL8(1) | Chip | M13 | 2974 | 4800 | #1 east shear | MASU-INMS | 65.35 | 0.38 | 4.86 | 1260 | 45.6 | 94 | 1 | 9 |
| DL8(2) | Chip | M14 | 2974 | 4800 | #1 east shear | MASU | 80.20 | 0.40 | 4.5 | 1150 | 44.2 | 31 | 7 | 19 |
| DL9(1) | Chip | M15 | 3024 | 4800 | #4 east shear | INMS | 10.90 | 0.52 | 3.06 | 818 | 39.9 | 122 | 4 | 59 |
| DL9(1) | Slab | A8 | 3024 | 4800 | #4 east shear | INMS | 15.85 | 0.43 | 3.24 | 3420 | 36.6 | 7110 | 12 | 55 |
| DL9(2) | Slab | A9 | 3024 | 4800 | #4 east shear | INMS | 30.70 | 0.26 | 4.04 | 956 | 39.2 | 274 | 7 | 61 |
| DL9(3) | Slab | A13 | 3024 | 4800 | #4 east shear | INMS | 70.30 | 0.64 | 3.25 | 809 | 38.7 | 305 | 21 | 72 |
| DL9(4) | Slab | A10 | 3024 | 4800 | #4 east shear | INMS | 25.75 | 0.38 | 3.64 | 2450 | 36.2 | 3840 | 24 | 43 |
| DL9(5) | Slab | A11 | 3024 | 4800 | #4 east shear | INMS | 70.30 | 0.76 | 3.24 | 2790 | 29.1 | 5940 | 23 | 62 |
| DL9(6) | Slab | A12 | 3024 | 4800 | #4 east shear | INMS | 80.20 | 0.45 | 1.77 | 2830 | 22.3 | 7610 | 17 | 45 |
| DL10(1) | Chip | M16 | 2874 | 4800 | #4 east shear | WR | 50.50 | 0.24 | 0.06 | 109 | 11.9 | 141 | 8 | 159 |
| DL126 | Chip | A80 | 2474 | 4800 | #4 west shear | INMS | 65.35 | 4.85 | 0.84 | 264 | 22.7 | 22 | 1080 | 419 |
| DL127 | Chip | A81 | 2474 | 4800 | #4 west shear | INMS | 40.60 | 0.25 | 4.28 | 1030 | 48.4 | bdl | 1 | 1 |
| DL128(1) | Chip | A82 | 3174 | 4800 | #4 east shear | Qtz-rich DISS | 95.5 | 0.33 | 3.72 | 874 | 45 | 123 | 1 | 8 |
| DL128(2) | Chip | A83 | 3174 | 4800 | #4 east shear | INMS | 90.10 | 0.90 | 1.79 | 945 | 27.1 | 2100 | 22 | 165 |
| DL128(3) | Chip | A84 | 3174 | 4800 | #4 east shear | INMS | 10.90 | 0.14 | 4.8 | 1100 | 48.3 | 174 | 22 | 1 |
| DL11(1) | Chip | M17 | 2474 | 4900 | #4 west shear | WR-INMS | NA | 0.01 | 0.05 | 32 | 11.1 | bdl | 5 | 128 |
| DL11(2) | Chip | M18 | 2474 | 4900 | #4 west shear | INMS | 50.50 | 0.33 | 4.3 | 1010 | 48.1 | 8 | 5 | 34 |
| DL12(1) | Chip | M19 | 2774 | 4900 | #4 east shear | INMS | 50.50 | 0.36 | 2.61 | 1490 | 38 | 1040 | 4 | 106 |
| DL12(2) | Chip | M20 | 2774 | 4900 | #4 east shear | INMS | 70.30 | 0.48 | 2.87 | 1570 | 37.2 | 992 | 3 | 106 |
| DL13(1) | Chip | M21 | 2824 | 4900 | #4 east shear | INMS | 80.20 | 0.31 | 4.14 | 996 | 38.9 | 16 | 1 | 18 |
| DL14(1) | Chip | M22 | 3024 | 4900 | #4 east shear | INMS | 50.50 | 0.24 | 3.82 | 862 | 41.3 | 12 | 6 | 6 |
| DL15(1) | Chip | M23 | 3074 | 4900 | #4 east shear | Qtz-rich INMS | 70.30 | 0.54 | 2.01 | 677 | 26.9 | 286 | 5 | 267 |
| DL16(1) | Chip | M24 | 3224 | 4900 | #4 east shear | INMS | 0.100 | 0.11 | 4.98 | 1155 | 48.5 | 26 | 2 | 1 |
| DL17(1) | Chip | M25 | 3324 | 4900 | #4 east shear | Qtz-rich INMS | 50.50 | 0.08 | 3.11 | 900 | 41 | 26 | 1 | 21 |
| DL17(2) | Chip | M26 | 3324 | 4900 | #4 east shear | Qtz-rich INMS | 65.35 | 0.97 | 3.58 | 833 | 42.7 | 26 | 7 | 8 |
| DL18(1) | Chip | M27 | 3174 | 4900 | #4 east shear | Qtz-rich DISS | 70.30 | 0.18 | 0.06 | 15 | 1.49 | bdl | 1 | 25 |
| DL19(1) | Slab | A14 | 2981 | 4900 | #1 east shear | INMS | 80.20 | 0.46 | 4.71 | 1385 | 49.4 | 19 | 26 | 37 |
| DL19(2) | Slab | A15 | 2981 | 4900 | #1 east shear | INMS | 0.100 | 1.12 | 5.97 | 1840 | 44.7 | 82 | 24 | 65 |
| DL19(3) | Slab | A16 | 2981 | 4900 | #1 east shear | INMS | 75.25 | 0.64 | 7.25 | 2240 | 42.8 | 11 | 24 | 61 |
| DL19(4) | Slab | A17 | 2981 | 4900 | #1 east shear | INMS | 50.50 | 2.14 | 4.04 | 1200 | 45.3 | 15 | 27 | 168 |
| DL19(5) | Slab | A18 | 2981 | 4900 | #1 east shear | INMS | 40.60 | 1.83 | 3.97 | 1200 | 44.1 | 20 | 17 | 133 |
| DL19(6) | Slab | A19 | 2981 | 4900 | #1 east shear | INMS | 85.15 | 1.07 | 2.06 | 796 | 44.8 | 9 | 25 | 105 |
| DL20(1) | Chip | M28 | 2982 | 4900 | #1 east shear | Qtz-rich DISS | 50.50 | 3.83 | 0.28 | 147 | 6.96 | 6 | 53 | 425 |
| DL20(2) | Chip | M29 | 2982 | 4900 | #1 east shear | Qtz-rich DISS | NA | 0.22 | 0.05 | 21 | 2.31 | bdl | 41 | 47 |

List of abbreviations: CSIS: contorted schist; DISS: disseminated; Gal: galena; MASU: Massive sulphide; INMS: inclusion-rich massive sulphide; Qtz-rich DISS: quartz-rich disseminated; Qtz-rich INMS: quartz-rich inclusion-rich massive sulphide; Sph: sphalerite; WR: wallrock
 bdl indicates values below detection limit (2.5 ppm for As)

Table 2.11 Cont'd. Assay results of chip, grid and slab samples

| Sample | Sample type | Thin section | Stope | Level | Shear | Ore type | Pt/Pd | S (wt%) | Sb (ppm) | Au (ppm) | Pt (ppm) | Pd (ppm) | Ag (ppm) | Bi (ppm) |
|----------|-------------|--------------|-------|-------|---------------|------------------|-------|---------|----------|----------|----------|----------|----------|----------|
| DL63(1) | Chip | M96 | 1971 | 4470 | #1 west shear | INMS | 3.67 | 30.6 | 20 | 0.062 | 1.39 | 0.379 | 5.4 | 48 |
| DL63(2) | Chip | M97 | 1971 | 4470 | #1 west shear | INMS | 0.72 | 33.3 | 21 | 0.019 | 0.289 | 0.403 | 2.4 | 6 |
| DL64(1) | Chip | M98 | 1971 | 4470 | #1 west shear | INMS | 5.63 | 33.7 | 13 | 0.022 | 0.428 | 0.076 | 4.4 | bdl |
| DL65(1) | Chip | M100 | 2121 | 4470 | #1 west shear | WR | 5.00 | 0.26 | bdl | 0.0005 | 0.0025 | 0.0005 | 0.25 | bdl |
| DL65(2) | Chip | - | 2121 | 4470 | #1 west shear | WR | 0.83 | 0.67 | bdl | 0.004 | 0.0025 | 0.003 | 0.25 | 3 |
| DL66(1) | Chip | M101 | 2171 | 4470 | #1 west shear | INMS | 5.38 | 27.6 | 12 | 0.023 | 0.56 | 0.104 | 9 | 27 |
| DL66(2) | Chip | M102 | 2171 | 4470 | #1 west shear | DISS | 1.52 | 23.9 | bdl | 0.075 | 0.311 | 0.204 | 15.2 | bdl |
| DL67(1) | Chip | M103 | 2421 | 4470 | #1 west shear | INMS | 0.90 | 24.8 | 12 | 0.061 | 0.472 | 0.523 | 5.5 | bdl |
| DL68(1) | Chip | M104 | 2461 | 4470 | #1 west shear | INMS | 1.02 | 31.7 | 14 | 0.863 | 0.619 | 0.606 | 16 | 41 |
| DL69(1) | Chip | M105 | 2174 | 4470 | #4 west shear | INMS | 2.61 | 29.3 | 19 | 0.066 | 0.618 | 0.237 | 2.2 | bdl |
| DL70(1) | Chip | M106 | 2274 | 4470 | #4 west shear | INMS | 1.01 | 29.7 | 10 | 0.065 | 1.11 | 1.1 | 13.3 | 89 |
| DL70(2) | Chip | M107 | 2274 | 4470 | #4 west shear | INMS | 0.64 | 22.3 | 12 | 0.122 | 0.953 | 1.48 | 6.5 | 46 |
| DL71(1) | Chip | M108 | 2424 | 4470 | #4 west shear | Gal-Sph stringer | 0.16 | 20.7 | 135 | 0.009 | 0.0025 | 0.016 | 95.6 | 2 |
| DL71(2) | Chip | M109 | 2424 | 4470 | #4 west shear | Gal-Sph stringer | 0.87 | 16.75 | 404 | 0.013 | 0.027 | 0.031 | 76.3 | bdl |
| DL72(1) | Chip | M110 | 2524 | 4470 | #4 west shear | Qtz-rich DISS | 2.12 | 33.4 | bdl | 0.004 | 0.218 | 0.103 | 3.1 | bdl |
| DTL19(1) | Grid | A70 | 2424 | 4470 | #4 west shear | INMS | 0.57 | 27.9 | bdl | 0.034 | 0.523 | 0.915 | 2.9 | bdl |
| DTL19(2) | Grid | A71 | 2424 | 4470 | #4 west shear | DISS | 2.14 | 25.2 | bdl | 0.177 | 0.707 | 0.331 | 4.3 | 13 |
| DTL19(3) | Grid | A72 | 2424 | 4470 | #4 west shear | DISS | 2.36 | 25.8 | bdl | 0.018 | 0.42 | 0.178 | 3.5 | 8 |
| DTL19(4) | Grid | A73 | 2424 | 4470 | #4 west shear | DISS | 1.79 | 11.1 | bdl | 0.017 | 0.497 | 0.278 | 2.4 | 9 |
| DTL19(5) | Grid | A74 | 2424 | 4470 | #4 west shear | DISS | 3.73 | 26.3 | bdl | 0.018 | 0.693 | 0.186 | 2.8 | 8 |
| DTL20 | Chip | - | 2424 | 4470 | #4 west shear | DISS | 0.15 | 19.9 | 218 | 0.021 | 0.0025 | 0.017 | 55.6 | bdl |
| DTL21 | Chip | A75 | 2424 | 4470 | #4 west shear | DISS | 5.39 | 12.45 | 151 | 0.126 | 0.194 | 0.036 | 13.5 | 2 |
| DTL22 | Chip | A76 | 2474 | 4470 | #4 west shear | INMS | 2.09 | 30.6 | bdl | 0.01 | 0.404 | 0.193 | 0.9 | 14 |
| DL12(1) | Chip | M1 | 1971 | 4600 | #1 west shear | DISS | 1.74 | 18.15 | 10 | 2.79 | 5.3 | 3.05 | 14.5 | bdl |
| DL12(2) | Chip | M2 | 1971 | 4600 | #1 west shear | DISS | 0.19 | 34.7 | bdl | 0.092 | 0.722 | 3.87 | 74.1 | bdl |
| DL12(3) | Chip | M3 | 1971 | 4600 | #1 west shear | DISS | 0.18 | 31.9 | 18 | 0.241 | 0.207 | 1.15 | 67.7 | bdl |
| DL12(4) | Chip | M4 | 1971 | 4600 | #1 west shear | DISS | 4.69 | 21.3 | bdl | 0.109 | 1.845 | 0.393 | 12.4 | bdl |
| DL3(1) | Chip | M5 | 1971 | 4600 | #1 west shear | INMS | 0.12 | 24.4 | 6 | 5 | 0.858 | 7.33 | 10.9 | bdl |
| DL3(2) | Chip | M6 | 1971 | 4600 | #1 west shear | INMS | 0.82 | 32.8 | bdl | 0.04 | 0.894 | 1.085 | 2.9 | 9 |
| DL4(1) | Chip | M7 | 2171 | 4600 | #1 west shear | MASU | 6.39 | 35.8 | 14 | 0.122 | 1.175 | 0.184 | 1.3 | 9 |
| DL4(2) | Chip | M8 | 2171 | 4600 | #1 west shear | MASU | 6.27 | 34.9 | 14 | 0.136 | 0.483 | 0.077 | 0.5 | 15 |
| DL5(1) | Chip | M9 | 2071 | 4600 | #1 west shear | WR | 1.11 | 0.48 | bdl | 0.005 | 0.01 | 0.009 | 0.25 | bdl |
| DL5(2) | Chip | M10 | 2071 | 4600 | #1 west shear | WR | 0.65 | 0.92 | bdl | 0.019 | 0.022 | 0.034 | 0.25 | bdl |
| DL4(1) | Slab | A1 | 2171 | 4600 | #1 west shear | MASU-INMS | 10.33 | 34.8 | bdl | 0.059 | 1.25 | 0.121 | 3.7 | bdl |
| DL4(2) | Slab | A2 | 2171 | 4600 | #1 west shear | MASU-INMS | 13.47 | 33 | bdl | 0.039 | 0.97 | 0.072 | 3.2 | 7 |
| DL4(3) | Slab | A3 | 2171 | 4600 | #1 west shear | MASU-INMS | 7.95 | 32.3 | bdl | 0.033 | 1.025 | 0.129 | 3.8 | 6 |
| DL4(4) | Slab | A4 | 2171 | 4600 | #1 west shear | MASU-INMS | 23.36 | 34 | 6 | 0.157 | 0.981 | 0.042 | 2.4 | 3 |
| DL4(5) | Slab | A5 | 2171 | 4600 | #1 west shear | MASU-INMS | 14.59 | 33.8 | bdl | 0.024 | 0.861 | 0.059 | 4.3 | bdl |
| DL4(6) | Slab | A6 | 2171 | 4600 | #1 west shear | MASU-INMS | 8.12 | 34.1 | bdl | 0.031 | 0.999 | 0.123 | 3.6 | 10 |
| DTL23(6) | Chip | A77 | 2374 | 4600 | #4 west shear | DISS | 2.69 | 28.7 | bdl | 0.021 | 0.21 | 0.078 | 2.8 | 8 |
| DTL24 | Chip | A78 | 2271 | 4600 | #1 west shear | INMS | 0.45 | 29.3 | bdl | 0.151 | 1.185 | 2.65 | 8.3 | 14 |
| DTL25 | Chip | A79 | 2321 | 4600 | #1 west shear | INMS | 1.73 | 22.9 | bdl | 0.04 | 0.361 | 0.200 | 7.3 | bdl |
| DL6(1) | Chip | M11 | 2524 | 4800 | #4 west shear | INMS | 3.20 | 31.6 | 20 | 0.009 | 0.400 | 0.128 | 1.8 | 8 |
| DL6(2) | Chip | M12 | 2524 | 4800 | #4 west shear | INMS | 4.33 | 31.6 | 12 | 0.011 | 0.411 | 0.095 | 1.9 | 4 |
| DL7 | Chip | A7 | 2524 | 4800 | #4 west shear | Qtz-rich DISS | 0.10 | 7.68 | bdl | 1.63 | 0.027 | 0.264 | 4.6 | 80 |
| DL8(1) | Chip | M13 | 2974 | 4800 | #1 east shear | MASU-INMS | 3.01 | 33.7 | 15 | 0.006 | 0.328 | 0.109 | 0.25 | 11 |
| DL8(2) | Chip | M14 | 2974 | 4800 | #1 east shear | MASU | 3.54 | 31.1 | 21 | 0.007 | 0.191 | 0.054 | 1.6 | 15 |
| DL9(1) | Chip | M15 | 3024 | 4800 | #4 east shear | INMS | 1.89 | 24.6 | 12 | 0.02 | 0.263 | 0.139 | 1.8 | 9 |
| DL9(1) | Slab | A8 | 3024 | 4800 | #4 east shear | INMS | 0.28 | 25 | 5 | 0.147 | 0.999 | 3.56 | 0.8 | 2 |
| DL9(2) | Slab | A9 | 3024 | 4800 | #4 east shear | INMS | 0.51 | 27.1 | bdl | 0.018 | 0.313 | 0.618 | 4.2 | 5 |
| DL9(3) | Slab | A13 | 3024 | 4800 | #4 east shear | INMS | 1.30 | 25.6 | bdl | 0.017 | 0.318 | 0.244 | 1.6 | bdl |
| DL9(4) | Slab | A10 | 3024 | 4800 | #4 east shear | INMS | 0.18 | 24.7 | bdl | 0.182 | 0.39 | 2.11 | 2.3 | bdl |
| DL9(5) | Slab | A11 | 3024 | 4800 | #4 east shear | INMS | 0.25 | 19.55 | bdl | 0.188 | 0.627 | 2.55 | 3.3 | bdl |
| DL9(6) | Slab | A12 | 3024 | 4800 | #4 east shear | INMS | 0.13 | 15.25 | bdl | 0.059 | 0.37 | 2.84 | 2.9 | 4 |
| DL10(1) | Chip | M16 | 2874 | 4800 | #4 east shear | WR | 1.52 | 0.49 | bdl | 0.086 | 0.047 | 0.031 | 0.8 | bdl |
| DTL26 | Chip | A80 | 2474 | 4800 | #4 west shear | INMS | 5.92 | 11.25 | bdl | 0.221 | 1.455 | 0.25 | 14.8 | 2 |
| DTL27 | Chip | A81 | 2474 | 4800 | #4 west shear | INMS | 12.16 | 32.8 | bdl | 0.003 | 0.985 | 0.081 | 1.6 | 11 |
| DTL28(1) | Chip | A82 | 3174 | 4800 | #4 east shear | Qtz-rich DISS | 0.18 | 28.5 | bdl | 0.005 | 0.012 | 0.067 | 2.3 | 13 |
| DTL28(2) | Chip | A83 | 3174 | 4800 | #4 east shear | INMS | 0.67 | 14.9 | bdl | 0.075 | 0.59 | 0.881 | 4.5 | 10 |
| DTL28(3) | Chip | A84 | 3174 | 4800 | #4 east shear | INMS | 0.08 | 34.7 | bdl | 0.013 | 0.012 | 0.157 | 2.1 | 13 |
| DL11(1) | Chip | M17 | 2474 | 4900 | #4 west shear | WR-INMS | 1.60 | 0.09 | bdl | 0.004 | 0.016 | 0.01 | 0.25 | 3 |
| DL11(2) | Chip | M18 | 2474 | 4900 | #4 west shear | INMS | 7.03 | 33.6 | bdl | 0.006 | 0.682 | 0.097 | 3.1 | 2 |
| DL12(1) | Chip | M19 | 2774 | 4900 | #4 east shear | INMS | 0.73 | 23.1 | 11 | 0.058 | 0.875 | 1.195 | 2 | 5 |
| DL12(2) | Chip | M20 | 2774 | 4900 | #4 east shear | INMS | 0.71 | 23 | 7 | 0.054 | 0.838 | 1.185 | 2.5 | 4 |
| DL13(1) | Chip | M21 | 2824 | 4900 | #4 east shear | INMS | 4.71 | 25.9 | 7 | 0.011 | 0.099 | 0.021 | 0.8 | 4 |
| DL14(1) | Chip | M22 | 3024 | 4900 | #4 east shear | INMS | 6.52 | 28.3 | bdl | 0.014 | 0.189 | 0.029 | 0.25 | 4 |
| DL15(1) | Chip | M23 | 3074 | 4900 | #4 east shear | Qtz-rich INMS | 0.20 | 17.6 | bdl | 0.078 | 0.033 | 0.166 | 2.4 | 6 |
| DL16(1) | Chip | M24 | 3224 | 4900 | #4 east shear | INMS | 7.01 | 33.6 | bdl | 0.010 | 0.498 | 0.071 | 0.25 | 12 |
| DL17(1) | Chip | M25 | 3324 | 4900 | #4 east shear | Qtz-rich INMS | 3.48 | 26.6 | 12 | 0.007 | 0.195 | 0.056 | 0.8 | 9 |
| DL17(2) | Chip | M26 | 3324 | 4900 | #4 east shear | Qtz-rich INMS | 3.20 | 28.5 | bdl | 0.003 | 0.227 | 0.071 | 0.25 | bdl |
| DL18(1) | Chip | M27 | 3124 | 4900 | #4 east shear | Qtz-rich DISS | 0.07 | 0.7 | bdl | 0.028 | 0.0025 | 0.037 | 1.1 | 5 |
| DL19(1) | Slab | A14 | 2981 | 4900 | #1 east shear | INMS | 1.22 | 33.5 | bdl | 0.012 | 0.578 | 0.475 | 2.4 | - |
| DL19(2) | Slab | A15 | 2981 | 4900 | #1 east shear | INMS | 1.09 | 29.7 | bdl | 0.02 | 0.482 | 0.442 | 5.8 | 2 |
| DL19(3) | Slab | A16 | 2981 | 4900 | #1 east shear | INMS | 4.43 | 29.3 | bdl | 0.01 | 1.015 | 0.229 | 2.3 | bdl |
| DL19(4) | Slab | A17 | 2981 | 4900 | #1 east shear | INMS | 1.09 | 28.7 | bdl | 0.062 | 0.44 | 0.404 | 6.9 | 8 |
| DL19(5) | Slab | A18 | 2981 | 4900 | #1 east shear | INMS | 1.37 | 29.3 | bdl | 0.014 | 0.468 | 0.342 | 6 | bdl |
| DL19(6) | Slab | A19 | 2981 | 4900 | #1 east shear | INMS | 4.06 | 29.4 | bdl | 0.013 | 0.589 | 0.145 | 4.7 | 2 |

List of abbreviations: CNIS - contorted schist; DISS - disseminated; Gal - galena; MASU - Massive sulphide; INMS - inclusion-rich massive sulphide; Qtz-rich DISS - quartz-rich disseminated; Qtz-rich INMS - quartz-rich inclusion-rich massive sulphide; Sph - sphalerite; WR - wallrock

Table 2.11 (cont'd) Assay results of chip, grid and slab samples

| Sample | Sample type | Thin section | Stope | Level | Shear | Ore type | Mono/Hex | Cu (wt%) | Ni (wt%) | Co (ppm) | Fe (wt%) | As (ppm) | Pb (ppm) | Zn (ppm) |
|------------|-------------|--------------|-------|-------|---------------|---------------|----------|----------|----------|----------|----------|----------|----------|----------|
| DL21(1) | Chip | M30 | 2982 | 4900 | #1 east shear | DISS | 70.30 | 0.19 | 4.22 | 1360 | 38.3 | bdl | 17 | 46 |
| DL21(2) | Chip | M31 | 2982 | 4900 | #1 east shear | DISS | 30.70 | 0.25 | 2.8 | 887 | 28.2 | 20 | 32 | 57 |
| DTL15(1-2) | Chip | A65-66 | 2781 | 4900 | #1 east shear | DISS | 75.25 | 1.83 | 3.25 | 873 | 36.6 | 10 | 2 | 195 |
| DTL16 | Chip | A67 | 2781 | 4900 | #1 east shear | CSSS | 109.0 | 1.00 | 5.48 | 1780 | 50 | 7 | 1 | 75 |
| DTL17 | Chip | A68 | 2821 | 4900 | #1 east shear | INMS | 65.35 | 0.85 | 5.21 | 1690 | 45.3 | 17 | 1 | 58 |
| DTL18 | Chip | A69 | 2821 | 4900 | #1 east shear | MASU | 99.1 | 0.71 | 4.66 | 1330 | 35.4 | 7 | 390 | 640 |
| DL22(1) | Chip | M32 | 2471 | 5000 | #1 west shear | INMS | 50.50 | 21.90 | 0.83 | 873 | 29.6 | 2180 | 76 | 1550 |
| DL22(2) | Chip | M33 | 2471 | 5000 | #1 west shear | INMS | 10.90 | 10.85 | 3.51 | 609 | 40.6 | 22 | 129 | 894 |
| DL22(3) | Chip | M34 | 2471 | 5000 | #1 west shear | INMS | 50.50 | 2.46 | 0.14 | 300 | 8.65 | 772 | 78 | 187 |
| DL22(4) | Slab | A20 | 2471 | 5000 | #1 west shear | MASU-INMS | 15.85 | 10.80 | 3.33 | 546 | 36.6 | 57 | 187 | 953 |
| DL22(2) | Slab | A21 | 2471 | 5000 | #1 west shear | MASU-INMS | 10.90 | 20.70 | 1.8 | 362 | 36.2 | 103 | 192 | 1800 |
| DL22(3) | Slab | A22 | 2471 | 5000 | #1 west shear | MASU-INMS | 15.85 | 9.32 | 4.15 | 681 | 38.5 | 66 | 109 | 625 |
| DL22(4) | Slab | A23 | 2471 | 5000 | #1 west shear | MASU-INMS | 15.85 | 15.85 | 3.89 | 614 | 37.5 | 52 | 101 | 1100 |
| DL22(5) | Slab | A24 | 2471 | 5000 | #1 west shear | MASU-INMS | 55.45 | 26.00 | 0.967 | 182 | 32.6 | 66 | 117 | 1805 |
| DL22(6) | Slab | A25 | 2471 | 5000 | #1 west shear | MASU-INMS | 10.90 | 16.05 | 2.92 | 476 | 38.1 | 42 | 114 | 1200 |
| DL23(1) | Chip | M35 | 2421 | 5000 | #1 west shear | MASU | 0.100 | 1.81 | 4.77 | 917 | 43.9 | 11 | 21 | 149 |
| DL23(2) | Chip | M36 | 2421 | 5000 | #1 west shear | MASU | 65.35 | 2.21 | 6.64 | 1320 | 46.7 | 12 | 18 | 118 |
| DL24(1) | Chip | M37 | 2371 | 5000 | #1 west shear | MASU | 30.70 | 25.00 | 1.85 | 288 | 34.3 | 19 | 61 | 1760 |
| DL24(3) | Chip | M39 | 2371 | 5000 | #1 west shear | MASU | 70.30 | 14.90 | 0.31 | 149 | 20.5 | 400 | 46 | 789 |
| DL25(1) | Chip | M40 | 2321 | 5000 | #1 west shear | WR | NA | 0.05 | 0.07 | 38 | 6.94 | bdl | 26 | 112 |
| DL26(1) | Chip | M41 | 2121 | 5000 | #1 west shear | INMS | 0.100 | 0.41 | 4.2 | 1030 | 48.7 | 15 | 1 | 24 |
| DL28(1) | Chip | M42 | 1292 | 5000 | #1 west shear | DISS | 30.70 | 4.01 | 3.66 | 769 | 41.8 | 14 | 46 | 863 |
| DL28(2) | Chip | NA | 1292 | 5000 | #1 west shear | DISS | NA | 10.60 | 4.38 | 786 | 45.1 | bdl | 62 | 1260 |
| DL29(1) | Chip | M43 | 1292 | 5000 | #1 west shear | DISS | 20.80 | 1.77 | 4.85 | 923 | 37.6 | bdl | 17 | 171 |
| DL29(2) | Chip | M44 | 1292 | 5000 | #1 west shear | DISS | NA | 3.61 | 0.30 | 86 | 18.9 | 6 | 73 | 344 |
| DL29(3) | Chip | M45 | 1292 | 5000 | #1 west shear | INMS | 50.50 | 0.93 | 3.49 | 615 | 38.7 | 10 | 15 | 107 |
| DL30(1) | Chip | M46 | 1291 | 5000 | #1 west shear | DISS | 80.20 | 18.15 | 3.76 | 1745 | 26.1 | 10000 | 17 | 807 |
| DL30(1) | Chip | - | 1291 | 5000 | #1 west shear | DISS | NA | 15.85 | 3.61 | 1310 | 25.4 | 10000 | 26 | 894 |
| DL31(1) | Chip | M47 | NA | 5000 | #1 west shear | INMS | 85.15 | 5.96 | 1.55 | 48 | 11.9 | 18 | 21 | 680 |
| DL32(1) | Chip | M48 | NA | 5000 | host rocks | WR | NA | 0.02 | 0.03 | 38 | 5.05 | 42 | 43 | 90 |
| DL33(1) | Chip | M49 | 1135 | 5000 | host rocks | WR | NA | 0.03 | 0.02 | 40 | 4.9 | 103 | 8 | 82 |
| DL34(1) | Chip | M50 | 1135 | 5000 | #3 west shear | DISS | 20.80 | 1.14 | 4.16 | 991 | 44.2 | 14 | 9 | 72 |
| DL34(2) | Chip | M51 | 1134 | 5000 | #1 west shear | DISS | 35.75 | 10.05 | 1.36 | 486 | 24 | 31 | 15 | 528 |
| DL35(1) | Chip | M52 | 1175 | 5000 | #1 west shear | DISS | 10.70 | 7.09 | 1.54 | 487 | 27.4 | 7 | 10 | 850 |
| DL36(1) | Chip | M53 | 1175 | 5000 | #1 west shear | DISS | 30.70 | 1.29 | 4.42 | 1025 | 39.8 | 10 | 10 | 74 |
| DL36(2) | Chip | M54 | 1175 | 5000 | #1 west shear | DISS | NA | 0.11 | 0.10 | 33 | 1.71 | 10 | 3 | 10 |
| DL36(3) | Chip | M55 | 1141 | 5000 | #3 west shear | DISS | NA | 6.53 | 0.24 | 104 | 17.85 | 21 | 7 | 326 |
| DL37(1) | Chip | M56 | 1141 | 5000 | #1 east shear | Qtz-rich DISS | NA | 4.58 | 3.17 | 1775 | 24 | 2290 | 119 | 752 |
| DL38(1) | Chip | M57 | 1141 | 5000 | #1 east shear | MASU | 30.70 | 0.76 | 4.76 | 1345 | 44.8 | 13 | 10 | 73 |
| DL38(2) | Chip | M58 | 1141 | 5000 | #1 east shear | MASU | 20.80 | 4.97 | 2.03 | 559 | 29 | 46 | 35 | 207 |
| DL39(1) | Chip | M59 | 3061 | 5000 | #1 east shear | DISS | 80.20 | 0.80 | 3.18 | 880 | 28.9 | bdl | 200 | 119 |
| DL40(1) | Chip | M60 | 3061 | 5000 | #1 east shear | DISS | 10.90 | 5.14 | 4.63 | 1405 | 33.8 | 8 | 13 | 605 |
| DL40(2) | Chip | M61 | 1474 | 5000 | #1 east shear | INMS | 60.40 | 1.40 | 3.52 | 910 | 41 | 6 | 14 | 205 |
| DL41(1) | Chip | M62 | 1474 | 5000 | #4 west shear | Qtz-rich DISS | 50.50 | 2.42 | 1.7 | 382 | 24.7 | 43 | 17 | 128 |
| DL41(2) | Chip | M63 | 1974 | 5000 | #4 west shear | Qtz-rich DISS | 10.90 | 0.84 | 2.81 | 660 | 30.7 | 214 | 4 | 177 |
| DL42(1) | Chip | M64 | 2124 | 5000 | #4 west shear | DISS | 50.50 | 0.21 | 4.86 | 1125 | 43.9 | 6 | 4 | 1 |
| DL43(1) | Chip | M65 | 2624 | 5000 | #4 west shear | DISS | 50.50 | 0.26 | 3.33 | 698 | 34.8 | 16 | 4 | 39 |
| DL44(1) | Chip | M66 | 2624 | 5000 | #4 west shear | Qtz-rich DISS | 85.15 | 0.23 | 3.81 | 8380 | 33.1 | 10000 | 25 | 1 |
| DL44(2) | Chip | M67 | 2624 | 5000 | #4 west shear | INMS | 60.40 | 1.10 | 3.03 | 3080 | 37.5 | 3250 | 19 | 69 |
| DL44(1) | Slab | A26 | 2624 | 5000 | #4 west shear | INMS | 80.20 | 0.47 | 3.25 | 10000 | 19.35 | 10000 | 160 | 173 |
| DL44(2) | Slab | A27 | 2624 | 5000 | #4 west shear | INMS | 50.50 | 0.32 | 1.935 | 4140 | 20.4 | 10000 | 12 | 25 |
| DL44(3) | Slab | A28 | 2624 | 5000 | #4 west shear | INMS | 50.50 | 0.65 | 1.36 | 1940 | 16.15 | 4350 | 29 | 79 |
| DL44(4) | Slab | A29 | 2624 | 5000 | #4 west shear | INMS | NA | 0.35 | 0.744 | 1140 | 13 | 2860 | 22 | 72 |
| DL44(5) | Slab | A30 | 2624 | 5000 | #4 west shear | INMS | 60.40 | 0.75 | 0.758 | 293 | 10.35 | 815 | 8 | 85 |
| DL44(6) | Slab | A31 | 2624 | 5000 | #4 west shear | INMS | 70.30 | 0.57 | 1.07 | 201 | 11.05 | 403 | 10 | 71 |
| DL113 | Chip | - | - | 5000 | host rocks | WR | NA | 0.03 | 0.06 | 36 | 4.79 | 25 | 10 | 93 |
| DL114(1) | Chip | A64 | - | 5000 | host rocks | WR | NA | 0.07 | 0.03 | 43 | 10.25 | 24 | 29 | 261 |
| DL114(2) | Chip | A64 | - | 5000 | host rocks | WR | NA | 0.02 | 0.02 | 26 | 5.01 | 41 | 7 | 102 |
| DTL29(1) | Grid | A86 | 1291 | 5000 | #1 west shear | INMS | 50.50 | 10.35 | 2.7 | 948 | 28.6 | 10000 | 61 | 703 |
| DTL29(2) | Grid | A87 | 1291 | 5000 | #1 west shear | INMS | 85.15 | 13.35 | 1.67 | 564 | 27.4 | 7110 | 38 | 783 |
| DTL29(3) | Grid | A88 | 1291 | 5000 | #1 west shear | INMS | 75.25 | 12.20 | 7.23 | 486 | 26.7 | 10000 | 30 | 509 |
| DTL29(4) | Grid | A90 | 1291 | 5000 | #1 west shear | INMS | 60.40 | 15.70 | 3.23 | 1705 | 38.7 | 10000 | 25 | 905 |
| DTL30 | Chip | A92 | 1291 | 5000 | #1 west shear | MASU | 50.50 | 16.30 | 0.89 | 494 | 32.5 | 55 | 28 | 1070 |
| DL45(1) | Chip | M68 | 1224 | 5100 | #4 west shear | INMS | 50.50 | 2.62 | 2.45 | 600 | 26 | 545 | 9 | 255 |
| DL45(2) | Chip | M69 | 1224 | 5100 | #4 west shear | DISS | 85.15 | 0.41 | 5.47 | 1280 | 34.7 | 944 | 8 | 58 |
| DL46(1) | Chip | M70 | 1674 | 5100 | #4 west shear | INMS | 50.50 | 0.37 | 4.11 | 976 | 45.6 | 12 | 7 | 1 |
| DL46(2) | Chip | M71 | 1674 | 5100 | #4 west shear | MASU | 30.70 | 1.13 | 3.79 | 1010 | 42.2 | bdl | 16 | 74 |
| DL46(3) | Chip | M72 | 1674 | 5100 | #4 west shear | DISS | 85.15 | 0.07 | 0.90 | 289 | 22.2 | 7 | 13 | 109 |
| DL47(1) | Chip | M73 | 1874 | 5100 | #4 west shear | DISS | 70.30 | 12.90 | 0.65 | 285 | 23.6 | 52 | 7 | 766 |
| DL47(2) | Chip | M74 | 1874 | 5100 | #4 west shear | INMS | 30.70 | 2.82 | 3.8 | 1070 | 38.3 | 5 | 8 | 256 |
| DL48(1) | Chip | M75 | 1924 | 5100 | #4 west shear | MASU | 70.30 | 0.03 | 5.2 | 1395 | 50 | 13 | 13 | 19 |
| DL48(2) | Chip | M76 | 1924 | 5100 | #4 west shear | MASU | NA | 0.51 | 0.25 | 71 | 6.32 | bdl | 9 | 59 |
| DL49(1) | Chip | M77 | 2074 | 5100 | #4 west shear | MASU | 0.100 | 0.51 | 4.21 | 1150 | 50 | 7 | 9 | 24 |
| DL49(2) | Chip | M78 | 2074 | 5100 | #4 west shear | MASU | 70.30 | 0.29 | 4.99 | 1130 | 47.9 | 5 | 15 | 44 |
| DL50(1) | Chip | M79 | 2424 | 5100 | #4 west shear | INMS | 30.70 | 1.31 | 4.44 | 963 | 44.1 | 32 | 36 | 150 |
| DL50(2) | Chip | M80 | 2424 | 5100 | #4 west shear | INMS | 10.90 | 0.32 | 4.18 | 1070 | 46.7 | 8 | 14 | 54 |
| DL51(1) | Chip | M81 | 1135 | 5100 | #1 west shear | INMS | 0.100 | 3.71 | 4.15 | 1140 | 35.7 | bdl | 28 | 356 |
| DL51(2) | Chip | M82 | 1135 | 5100 | #1 west shear | INMS | 0.100 | 1.36 | 3.71 | 927 | 46.1 | bdl | 19 | 179 |
| DL52(1) | Chip | M83 | 1135 | 5100 | #1 west shear | DISS | 50.50 | 1.61 | 3.91 | 1160 | 32.1 | bdl | 15 | 231 |

List of abbreviations: CSSS - contorted schist; DISS - disseminated; Gal - galena; MASU - Massive sulphide; INMS - inclusion-rich massive sulphide; Qtz-rich DISS - quartz-rich disseminated; Qtz-rich INMS - quartz-rich inclusion-rich massive sulphide; Sph - sphalerite; WR - wallrock.
 bdl indicates values below detection limit (2.5 ppm for As)

Table 2.11 Cont'd. Assay results of chip, grid and slab samples

| Sample | Sample type | Thin section | Stope | Level | Shear | Ore type | Mono:Hex | Cu (wt%) | Ni (wt%) | Co (ppm) | Fe (wt%) | As (ppm) | Pb (ppm) | Zn (ppm) |
|---------|-------------|--------------|-------|-------|---------------|---------------|----------|----------|----------|----------|----------|----------|----------|----------|
| DL52(2) | Chip | M84 | 1135 | 5100 | #1 west shear | DISS | 0.100 | 0.17 | 0.08 | 38 | 14.05 | bdl | 74 | 166 |
| DL53(1) | Chip | M85 | 1174 | 5100 | #1 west shear | CSIS | 40:60 | 13.50 | 1.435 | 464 | 29.9 | bdl | 21 | 1300 |
| DL54(1) | Chip | M86 | 1173 | 5100 | #1 west shear | DISS | 60:40 | 1.28 | 2.22 | 582 | 35 | bdl | 24 | 134 |
| DL55(1) | Chip | M88 | 1214 | 5100 | #1 west shear | DISS | 30:70 | 1.19 | 1.82 | 469 | 22.7 | 7 | 23 | 120 |
| DL56(1) | Chip | M89 | 1213 | 5100 | #1 west shear | Qtz-rich DISS | NA | 7.36 | 0.12 | 65 | 12.6 | bdl | 8 | 579 |
| DL57(1) | Chip | M90 | 1211 | 5100 | #1 west shear | CSIS | 20:80 | 0.78 | 3.8 | 997 | 44.6 | 6 | 17 | 81 |
| DL58(1) | Chip | M91 | 2624 | 5100 | #4 west shear | INMS | 80:20 | 0.16 | 5.13 | 1280 | 50 | 11 | 24 | 53 |
| DL59(1) | Chip | M92 | 3141 | 5100 | #1 east shear | DISS | 85:15 | 19.50 | 1.54 | 549 | 31.1 | bdl | 24 | 886 |
| DL60(1) | Chip | M93 | 3061 | 5100 | #1 east shear | INMS | 85:15 | 1.97 | 4.76 | 1430 | 45.2 | bdl | 67 | 123 |
| DL61(1) | Chip | M94 | 3021 | 5100 | #1 east shear | DISS | 70:30 | 8.82 | 4.78 | 1560 | 46.9 | bdl | 721 | 959 |
| DL62(1) | Chip | M95 | 2874 | 5100 | #1 east shear | INMS | 50:50 | 0.16 | 4.64 | 1340 | 50 | bdl | 123 | 89 |
| DTL01 | Chip | A49 | 2421 | 5100 | #1 west shear | INMS | NA | 28.80 | 0.30 | 74 | 31.2 | 286 | 32 | 1480 |
| DTL02 | Chip | A50 | 2421 | 5100 | #1 west shear | DISS | 1:99 | 4.12 | 3.18 | 163 | 41.4 | 57 | 101 | 219 |
| DTL03 | Chip | A51 | 2421 | 5100 | #1 west shear | MASU | 95:5 | 10.60 | 2.81 | 86 | 49.4 | 296 | 5 | 235 |
| DTL04 | Chip | A52 | 2421 | 5100 | #1 west shear | INMS | 20:80 | 8.94 | 4.49 | 222 | 38.7 | 74 | 48 | 751 |
| DTL05 | Chip | A53 | 2321 | 5100 | #1 west shear | MASU | 1:99 | 6.67 | 4.05 | 483 | 33 | 22 | 49 | 436 |
| DTL06 | Chip | A54 | 2271 | 5100 | #1 west shear | INMS | 0:100 | 5.45 | 3.39 | 496 | 38.4 | 283 | 88 | 760 |
| DTL07 | Chip | A55 | 2221 | 5100 | #1 west shear | MASU | 0:100 | 3.93 | 4.03 | 764 | 44.8 | 19 | 5 | 404 |
| DTL08 | Chip | A56 | 2221 | 5100 | #1 west shear | MASU | 15:85 | 3.15 | 4.19 | 780 | 47.7 | 25 | 21 | 158 |
| DTL09 | Chip | A57 | 2121 | 5100 | #1 west shear | INMS | 0:100 | 10.30 | 1.71 | 451 | 32.5 | 10 | 233 | 1025 |
| DTL10 | Chip | A58 | 2121 | 5100 | #1 west shear | DISS | 0:100 | 4.41 | 2.41 | 557 | 37.1 | 76 | 15 | 318 |
| DTL11b | Chip | A62 | 2171 | 5100 | #1 west shear | MASU | 95:5 | 19.45 | 2.36 | 787 | 37.4 | 9680 | 2 | 457 |
| DTL11a | Chip | A59 | 2171 | 5100 | #1 west shear | INMS | 70:30 | 5.30 | 5.76 | 2800 | 42.2 | 10000 | 9 | 236 |
| DTL12a | Chip | A61 | 1294 | 5100 | host rocks | WR | 70:30 | 6.48 | 4.37 | 604 | 35 | 27 | 4 | 456 |

List of abbreviations: CSIS=concentric schist, DISS=disseminated, Gal=galena, MASU=Massive sulphide, INMS=inclusion-rich massive sulphide, Qtz-rich DISS=quartz-rich disseminated, Qtz-rich INMS=quartz-rich inclusion-rich massive sulphide, Sph=sphalerite, WR=wallrock.

Table 2.11 Cont'd. Assay results of chip, grind and slab samples

| Sample | Sample type | Thin section | Stope | Level | Shear | Ore type | Pt/Pd | S (wt%) | Sb (ppm) | Au (ppm) | Pt (ppm) | Pd (ppm) | Ag (ppm) | Bi (ppm) |
|---------|-------------|--------------|-------|-------|---------------|---------------|-------|---------|----------|----------|----------|----------|----------|----------|
| DL30(2) | Chip | M80 | 2424 | 5100 | #4 west shear | INMS | 7.20 | 32.3 | 19 | 0.072 | 0.331 | 0.046 | 2.5 | bdl |
| DL51(1) | Chip | M81 | 1135 | 5100 | #1 west shear | INMS | 1.42 | 21.2 | 16 | 0.151 | 0.586 | 0.412 | 19.6 | 44 |
| DL51(2) | Chip | M82 | 1135 | 5100 | #1 west shear | INMS | 3.66 | 29.7 | 11 | 0.021 | 0.406 | 0.111 | 6.9 | 43 |
| DL52(1) | Chip | M83 | 1135 | 5100 | #1 west shear | DISS | 1.69 | 20.5 | 13 | 0.067 | 0.571 | 0.338 | 7.4 | 27 |
| DL52(2) | Chip | M84 | 1135 | 5100 | #1 west shear | DISS | 2.71 | 0.34 | bdl | 0.062 | 0.057 | 0.021 | 0.9 | 6 |
| DL53(1) | Chip | M85 | 1174 | 5100 | #1 west shear | CNIS | 0.81 | 23.1 | 8 | 0.315 | 0.071 | 0.088 | 49.1 | 22 |
| DL54(1) | Chip | M86 | 1173 | 5100 | #1 west shear | DISS | 1.97 | 17.2 | 10 | 0.012 | 0.443 | 0.225 | 4.4 | 22 |
| DL55(1) | Chip | M88 | 1214 | 5100 | #1 west shear | DISS | 0.66 | 14.15 | 8 | 0.048 | 0.042 | 0.064 | 7.8 | 18 |
| DL56(1) | Chip | M89 | 1213 | 5100 | #1 west shear | Qtz-rich DISS | 0.14 | 8.98 | 7 | 0.345 | 0.129 | 0.934 | 25.9 | 9 |
| DL57(1) | Chip | M90 | 1211 | 5100 | #1 west shear | CNIS | 15.58 | 29.8 | 23 | 0.027 | 0.857 | 0.055 | 2 | 3 |
| DL58(1) | Chip | M91 | 2624 | 5100 | #4 west shear | INMS | 29.08 | 32.9 | 22 | 0.034 | 1.105 | 0.038 | 1.2 | bdl |
| DL59(1) | Chip | M92 | 3141 | 5100 | #1 east shear | DISS | 0.07 | 29.4 | bdl | 0.178 | 0.012 | 0.18 | 74.9 | 46 |
| DL60(1) | Chip | M93 | 3061 | 5100 | #1 east shear | INMS | 0.93 | 30.3 | 18 | 0.024 | 0.516 | 0.556 | 7 | 39 |
| DL61(1) | Chip | M94 | 3021 | 5100 | #1 east shear | DISS | 3.44 | 32.2 | 21 | 0.015 | 0.602 | 0.175 | 31.5 | 32 |
| DL62(1) | Chip | M95 | 2874 | 5100 | #1 east shear | INMS | 7.00 | 36.2 | 20 | 0.008 | 0.637 | 0.091 | 0.8 | bdl |
| D1L01 | Chip | A49 | 2421 | 5100 | #1 west shear | INMS | 0.65 | 32.1 | bdl | 0.629 | 0.505 | 0.771 | 142 | 57 |
| D1L02 | Chip | A50 | 2421 | 5100 | #1 west shear | DISS | 0.64 | 27.3 | bdl | 1.065 | 0.834 | 1.305 | 24.9 | 94 |
| D1L03 | Chip | A51 | 2421 | 5100 | #1 west shear | MASU | 0.86 | 36.1 | bdl | 0.451 | 4.96 | 5.79 | 63.5 | 104 |
| D1L04 | Chip | A52 | 2421 | 5100 | #1 west shear | INMS | 0.41 | 27.7 | bdl | 4.72 | 2.75 | 6.7 | 39 | 110 |
| D1L05 | Chip | A53 | 2321 | 5100 | #1 west shear | MASU | 1.38 | 24.9 | bdl | 0.41 | 0.929 | 0.671 | 34.3 | 21 |
| D1L06 | Chip | A54 | 2271 | 5100 | #1 west shear | INMS | 3.58 | 26.2 | bdl | 0.393 | 7.42 | 2.07 | 34.1 | 9 |
| D1L07 | Chip | A55 | 2221 | 5100 | #1 west shear | MASU | 6.30 | 27 | bdl | 0.073 | 1.17 | 0.183 | 23.9 | bdl |
| D1L08 | Chip | A56 | 2221 | 5100 | #1 west shear | MASU | 0.11 | 34.6 | bdl | 0.342 | 0.056 | 0.533 | 30.5 | 41 |
| D1L09 | Chip | A57 | 2121 | 5100 | #1 west shear | INMS | 39.29 | 18.15 | bdl | 0.64 | 11 | 0.28 | 47.9 | 52 |
| D1L10 | Chip | A58 | 2121 | 5100 | #1 west shear | DISS | 0.13 | 25 | bdl | 0.289 | 0.044 | 0.34 | 30.9 | 32 |
| D1L11b | Chip | A62 | 2171 | 5100 | #1 west shear | MASU | 0.49 | 32.4 | bdl | 0.321 | 2.55 | 5.17 | 107 | 44 |
| D1L11a | Chip | A59 | 2171 | 5100 | #1 west shear | INMS | 0.31 | 30.8 | 58 | 0.4 | 10.3 | 43.3 | 32.1 | 57 |
| D1L12a | Chip | A63 | 1294 | 5100 | host rocks | WR | 5.09 | 26.2 | bdl | 0.065 | 0.764 | 0.15 | 28.2 | 16 |

List of abbreviations: CNIS=contorted schist; DISS=disseminated; Gal=galena; MASU=Massive sulphide; INMS=inclusion-rich massive sulphide; Qtz-rich DISS=quartz-rich disseminated; Qtz-rich INMS=quartz-rich inclusion-rich massive sulphide; Spl=sphalerite; WR=wallrock

Table 2.12: Bulk rock assay of Cu-rich Ramp at Garson Mine

| Sample | Sample type | Ore body | Drift | Mine Area | Level | Pt/Pd | Cu (wt%) | Ni (wt%) | Co (ppm) | Fe (wt%) | As (ppm) | Pb (ppm) | Zn (ppm) | S (wt%) | Sb (ppm) | Au (ppm) | Pt (ppm) | Pd (ppm) | Ag (ppm) | Bi (ppm) |
|--------------|-------------|----------|-------|-----------|-------|-------|----------|----------|----------|----------|----------|----------|----------|---------|----------|----------|----------|----------|----------|----------|
| R1A (1) | chip | 600 | 687 | Ramp | 720 | 0.44 | 17.65 | 1.71 | 385 | 32.7 | 222 | 283 | 448 | 38.00 | 2.5 | 0.20 | 5.54 | 12.5 | 98 | 15 |
| R1B (1) | chip | 600 | 687 | Ramp | 720 | 0.02 | 9.06 | 9.32 | 6060 | 13.4 | 10000 | 45 | 556 | 15.40 | 146 | 2.16 | 8.55 | 380 | 98 | 47 |
| R1B (2) | chip | 600 | 687 | Ramp | 720 | 0.03 | 16.35 | 5.06 | 2140 | 24.1 | 10000 | 64 | 1230 | 26.10 | 84 | 9.23 | 5.50 | 207 | 105 | 119 |
| R2A (1) | chip | 600 | 655 | Ramp | 820 | 13.80 | 17 | 0.28 | 28 | 22.0 | 48 | 15 | 1050 | 19.25 | bdl | 0.44 | 16.15 | 1.17 | 46.6 | bdl |
| R2A (2) | chip | 600 | 655 | Ramp | 820 | 0.24 | 16.3 | 0.66 | 114 | 19.0 | 1060 | 26 | 397 | 17.95 | 14 | 1.20 | 4.39 | 18.50 | 70.2 | bdl |
| R2A (3) | chip | 600 | 655 | Ramp | 820 | 0.09 | 3.91 | 0.46 | 98 | 13.2 | 168 | 15 | 282 | 3.40 | 5 | 1 | 0.50 | 5.87 | 18.2 | 16 |
| R2B (1) | chip | 600 | 655 | Ramp | 820 | 0.46 | 6.88 | 0.40 | 56 | 15.4 | 24 | 20 | 494 | 8.08 | bdl | 5.64 | 8.04 | 17.45 | 22.1 | 54 |
| R2B (2) | chip | 600 | 655 | Ramp | 820 | 0.42 | 7.42 | 0.22 | 38 | 14.4 | 267 | 19 | 275 | 7.98 | bdl | 1.69 | 2.33 | 5.49 | 31.1 | 38 |
| R2B (3) | chip | 600 | 655 | Ramp | 820 | 0.01 | 9.77 | 18.35 | 10000 | 13.4 | 10000 | 23 | 505 | 15.95 | 526 | 1.76 | 3.41 | 530 | 50.4 | 30 |
| R3A (1) | chip | 600 | 655 | Ramp | 820 | 0.61 | 10.35 | 8.04 | 1100 | 30.4 | 35 | 29 | 374 | 27.90 | bdl | 0.25 | 3.68 | 6.08 | 114 | bdl |
| R3A (1) | chip | 600 | 655 | Ramp | 820 | 0.35 | 18.55 | 2.06 | 343 | 34.0 | 32 | 24 | 643 | 32.40 | bdl | 0.42 | 3.81 | 11 | 97.3 | bdl |
| R3A (2) SLAB | slab | 600 | 655 | Ramp | 820 | 0.32 | 7.94 | 2.20 | 301 | 22.7 | 45 | 21 | 260 | 15.50 | bdl | 0.13 | 1.33 | 4.20 | 55.5 | 13 |
| R3A (3) SLAB | slab | 600 | 655 | Ramp | 820 | 0.45 | 16.45 | 4.26 | 596 | 34.2 | 122 | 33 | 541 | 31.20 | bdl | 0.09 | 3.77 | 8.34 | 111 | 12 |
| R3A (4) SLAB | slab | 600 | 655 | Ramp | 820 | 0.16 | 19.4 | 1.41 | 384 | 36.2 | 1550 | 44 | 629 | 33.60 | bdl | 0.13 | 3.49 | 21.80 | 96.1 | 41 |
| R3A (5) SLAB | slab | 600 | 655 | Ramp | 820 | 0.42 | 9.77 | 2.60 | 363 | 26.6 | 11 | 25 | 325 | 20.50 | bdl | 1.81 | 2.42 | 5.78 | 59.5 | bdl |
| R3A (6) SLAB | slab | 600 | 655 | Ramp | 820 | 0.36 | 17.65 | 4.27 | 571 | 30.7 | 237 | 48 | 532 | 29.30 | bdl | 1.30 | 3.96 | 11.10 | 82.8 | 15 |
| R3B (1) | chip | 600 | 655 | Ramp | 820 | 0.50 | 20.6 | 2.82 | 442 | 33.3 | 66 | 23 | 599 | 34.00 | bdl | 0.28 | 3.57 | 7.19 | 102 | 17 |

bdl indicates values below detection limit (Sb 2.5 ppm; Bi 1 ppm)

Chapter 3: A fluid inclusion study of quartz-sulphide breccias veins in shear-hosted magmatic sulphide ores, Garson Mine, Sudbury, Canada

Darren LeFort*, Jacob Hanley

Dept. of Geology, Saint Mary's University, Halifax, Nova Scotia, Canada

Jung Hun Seo⁺

Dept. of Earth Sciences, ETH Zurich, Zürich, Switzerland

*corresponding author email address: darrenlefort@gmail.com

Number of pages of text: 30

Number of figures: 14

Number of tables: 3

For submission to Economic Geology

Abstract

The Garson deposit (Sudbury, Ontario, Canada) is a structurally and hydrothermally modified contact-style Ni-Cu-PGE sulphide deposit hosted along the contact of the Sudbury Igneous Complex (SIC) and underlying Huronian-age metasedimentary and metavolcanic rocks. The ores are hosted mainly in shear zones related to syn- to post-sulphide deformation (Mazatzal-Labradorian orogeny) and are mainly composed of pyrrhotite, pentlandite and chalcopyrite with minor pyrite. The ores are locally highly enriched in As (avg. ~1030 ppm, range bdl to 36 wt%; n=13727) and platinum-group elements (PGE), which are ultimately controlled by the abundance of arsenides, sulfarsenides, and platinum-group element minerals (michenerite, telluropalladinite).

Massive sulphide emplacement into the shear zones overprinted early metamorphic quartz veins that were brecciated during shearing, forming sulphide-quartz breccia veins and stockworks. Hot cathodoluminescence imaging indicates that the brecciated quartz veins are metamorphic in origin having crystallized at upper greenschist to lower amphibolite conditions. Fluid inclusions in the quartz were classified by the number of

phases present and their liquid:vapor ratios. Fluid inclusions in the quartz are predominantly 2 phase (type IIA) aqueous liquid-vapor and 3 phase (type IIIA) aqueous liquid-vapor-halite inclusions. Fluid inclusions were classified as secondary for those occurring in healed fractures. Inclusions hosted by featureless quartz grains (i.e., showing no evidence of association with growth zones) were called unclassified. Microthermometric studies performed on the fluid inclusions yield wide ranges in temperature of homogenization by vapor disappearance [$T_h^{V+L \rightarrow L}$; type IIA inclusions (98 to >470°C)], and halite dissolution [T_d ; type IIIA inclusions (148 to >470 °C)] and salinity [type IIA inclusions (1.2 to 22.1 wt% NaCl_{equiv.}), type IIIA inclusions (29.9 to >55.8 wt% NaCl_{equiv.})]. Type IIA inclusions with ice melting temperatures (T_m^{ice}) less than -21.1°C have a range in salinity from 25.1 to 31.2 wt% CaCl_{2equiv.}. These wide ranges are not representative of individual inclusion assemblages that show T_h -salinity ranges that are much more restricted. Variations in salinity with time may represent the mixing of high and low salinity fluids. No significant cooling trend is observed in association with this mixing trend. Petrographic evidence for necking down (tapering and variable liquid:vapor ratios) is seen within some single assemblages, as are variations in T_h and/or salinity. These post-entrapment modifications have significantly compromised some fluid inclusion assemblages.

Also present are aqueous inclusions (type IIC; 15-30 vol% vapor bubble) that contain a CO₂ phase that homogenizes upon heating between -4.9 and 29.0°C. Excluding those inclusions that have suffered post-entrapment modification (anomalously low CO₂ homogenization temperatures), the majority of CO₂-bearing inclusions homogenize above 10°C indicating a relatively low pressure of entrapment. Minimum estimates of pressure

of entrapment for type IIIA inclusions range from ~1.9 to 2.6 kbar. Hydrohalite and clathrates were observed in some of the unclassified inclusions. Hydrohalite destabilization, clathrate melting temperatures and CO₂ homogenization temperatures yielded salinities between 4 to 14.4 wt percent NaCl equivalent. Some inclusions in which hydrohalite crystals were not observed yielded wide range salinities (from ice melting T) between 1 to 21 wt percent NaCl equivalent.

LA-ICPMS analysis of the unclassified (two-phase) type IIA and IIC aqueous inclusions show elevated and similar concentrations of As, Pb, Zn and Sb, but very low concentrations of Fe, Cu and S, suggesting that these fluids did not react with/originate from magmatic sulphides or sulphide liquids, and were trapped prior to sulphide mineralization at Garson. Arsenic and other trace elements (Sr, Sb, Ba, Pb, and Bi) correlate with salinity suggesting Cl complexation at the conditions of fluid entrapment.

The circulation of saline fluids through metasedimentary wall rocks occurred before the sulphide emplacement at Garson but after the impact event. Pressure-temperature data derived from representative fluid inclusions overlap with greenschist to lower amphibolite-grade metamorphic conditions that impacted the South Range footwall rocks synchronous to and after the Sudbury event. However, the fluids at Garson have very similar trace element enrichments (Ca, Sr, Ba, Pb, Zn) to pre-ore fluids on the North Range of the SIC, an area relatively unaffected by syn to post SIC regional metamorphism. This indicates that a regional fluid of common parentage (possibly exotic, and not metamorphic in origin) circulated through the footwall prior to ore formation, and was trapped coincidentally in metamorphic quartz veins in the South Range. Post-entrapment modification at Sudbury significantly impacted some fluid

inclusion assemblages and should be taken into consideration when interpreting the P-T evolution of fluids in this environment.

3.0 Introduction

In magmatic Ni-Cu-platinum group element (PGE) sulphide deposits, associated with the Sudbury Igneous Complex, secondary hydrothermal fluids play a role in the remobilizing base and precious metals (Cabri and Laflamme, 1976; Li and Naldrett, 1993; Li et al., 1993; Farrow et al., 1994; Farrow and Watkinson, 1997; Molnár et al., 1997, 1999, 2001; Hanley et al., 2005; Dare et al., 2010; Hanley et al., 2011). Fluid inclusion studies at Sudbury show significant temporal and regional variations in fluid composition, ranging from carbonic-dominated (H_2O - CO_2 -brine and CH_4 -brine) to salt-dominated (CaCl_2 - NaCl - H_2O), and bulk salinity (low salinity, two phase, L+V to high salinity, three phase, L+H+V; Farrow and Watkinson, 1992; Farrow et al., 1994; Molnár et al., 1997, 1999; Hanley et al., 2005). The significant variations are a result of a variety of processes, including mixing of Ca-rich formational waters (from the Archean metamorphic rocks) along the North Range with magmatic, SIC-derived fluids, and the formation of CO_2 -bearing fluids along the South Range. These CO_2 -bearing fluids formed during uplift associated with regional metamorphism related to the Penokean and Mazatzal-Labradorian Orogenic events. Some fluid types are not observed in the North Range which has experienced much less deformation (e.g., metamorphic fluids; Frape and Fritz, 1982; Fueten and Redmond, 1997; Marshall et al., 1999). Some fluid types (i.e., CH_4 and other hydrocarbon-bearing fluids and associated immiscible brines) found in footwall-

style Cu-PGE deposits at Sudbury evolved directly in association with the ores and are shown to have been important volatile components for deposition (Hanley et al., 2005).

In this study, early (pre-sulphide), quartz veins spatially associated with a Ni-Cu-PGE deposit in Sudbury, Ontario, Canada, were studied by fluid inclusion, petrographic and geochemical techniques in order to characterize their physical and chemical evolution, and to elucidate their relationship to the magmatic-hydrothermal deposit, and to provide an assessment of the usefulness of inclusion studies on the South Range of the SIC. The study provides the first quantitative analyses of trace elements in South Range fluids.

3.1 Regional Geology

3.1.1 The Sudbury Structure and its ores

The Sudbury Structure is the second largest known impact structure on Earth that resulted from a bolide impact that occurred at 1850 Ma (Dietz, 1964; Naldrett and Hewins, 1984; Figure 3.1). Massive amounts of brecciation and shock- and heat-induced melting of the country rocks and lower crust occurred after the impact of bolide (Naldrett and Hewins, 1984; Mungall et al., 2004; Lightfoot and Zotov, 2005). The ~60 x 27 km elliptical Sudbury Structure lies in the Canadian Shield at the intersection of the Superior, Southern and Grenville provinces (Dressler, 1984; Therriault et al., 2002). Subsequent regional-scale deformation that was associated with the Mazatzal-Labradorian and Penokean orogenic events modified the original circular impact crater and melt sheet to become a northeast-southwest trending oval shaped structure (Rousell, 1984; Shanks and Schwerdtner, 1991a, b; Figure 3.1). Localized structural modification of the units of the SIC and its contact with its host rocks, hydrothermal activity and low-intermediate-grade

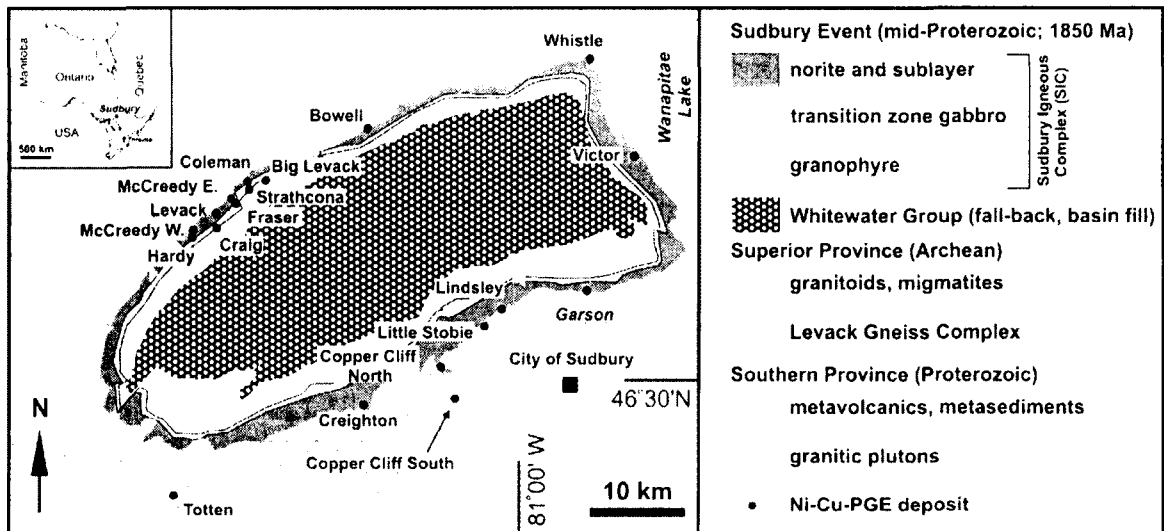


Figure 3.1: Geological map of the Sudbury Igneous Complex. The distribution of the offset dikes, sublayer, norite, transition zone gabbro, and granophyre, the location of Ni-Cu-PGE (including the Garson Mine, the area of study), and associated country rocks are shown. Inset shows the location of Sudbury in central Ontario.

metamorphism (most notably along the South Range) occurred during these periods of deformation (Rousell, 1984; Magyarosi et al., 2002). Sudbury Structure rock lithologies include (i) the Whitewater Group (crater fill), consisting of fallback breccia and sedimentary rocks of the Onaping, Onwatin and Chelmsford Formations, (ii) the Sudbury Igneous Complex ('SIC'), and (iii) brecciated, contact metamorphosed, and partially melted Archean and Paleoproterozoic country rocks situated in the footwall of the SIC (Therriault et al., 2002). The composition of the SIC is much more intermediate (i.e., richer in SiO_2) than conventional layered mafic-ultramafic intrusions due to the crustal component incorporated into the melt sheet (Naldrett and Hewins, 1984; Therriault et al., 2002; Mungall et al., 2004). The distinct layering, great thickness and exceptional degree of preservation the SIC is not typical of melt sheets associated with other terrestrial impacts (Therriault et al., 2002). The SIC has been described as a differentiated impact melt sheet (e.g., Naldrett, 1999; Therriault et al., 2002). Sulphide saturation occurred as the impact melt differentiated into the observable lithological units (Naldrett, 1999). The SIC rock types include noritic and gabbroic mesocumulates occurring beneath granophyric residue (granophyre), and early diorite that emplaced and crystallized into radial and concentric offset dykes in the country rocks (Naldrett, 1999). The South Range country rocks include Huronian-age metavolcanics (basalts and rhyolites), associated granitic plutons, and metasedimentary rocks (e.g., greywackes, wackes and quartzites; Figure 3.1) of the Southern Province. The North Range country rocks include Archean-age granitoids and tonalitic gneisses of the Levack gneiss complex and Cartier granite of the Superior Province (Figure 3.1).

Types of Ni-Cu-PGE mineralization that are observed at Sudbury include (i) Cu-Ni-PGE-rich ores hosted in concentric or radially extensive dioritic offset dykes (e.g., Totten deposits and Kelly Lake), (ii) Ni-rich, PGE-poor contact style ores hosted within the basal units of the SIC (norite, sublayer) or in heterolithic footwall breccia-rich depressions (“embayments”) that are associated with partially melted country rocks at the base of the SIC (e.g., Whistle and Craig deposits, Garson is a structurally modified version of a contact deposit type), and (iii) Cu-PGE-rich footwall-style ores which comprise sharp-walled massive sulphide veins (“high-sulphide”) or blebby-disseminated sulphide ores (“low sulphide”) within psuedotachylite (e.g., McCreedy PM zone, Podolsky; Naldrett et al., 1984a, 1984b; Farrow and Lightfoot, 2002; Farrow et al., 2005; Ames and Farrow, 2007).

Previous studies of the Garson deposit are few and include Hawley et al. (1968) and Aniol and Brown (1979). A current Ph. D. project on the structural aspects of the Garson deposit is in progress (Mukwakwami et al., 2011a, 2011b).

3.1.2 Geology of the Garson deposit

The Garson deposit is hosted along the contact between norite of the SIC sublayer and the metasedimentary-metabasaltic rocks of the Huronian-age Stobie and McKim formations (Southern Province). The Garson desposit is a contact style deposit that was strongly influenced by regional metamorphism. A key compositional characteristic of the Garson ores are that they are locally enriched in As is which are hosted in east-west trending shear zones (named the #1, #2, #3, and #4 shears). Several phases of deformation have fragmented, separated and overturned of the ore zones and led to the current

orientation which dips steeply to the south (Figure 3.2; Mukwakwami et al, 2011a; 2011b). Main Garson Mine lithologies include: (i) metabasalts and metasediments (e.g., greywackes, quartzites) of the Stobie and McKim formations, (ii) the SIC sublayer norite: a noritic, inclusion-rich unit, located at the base of the SIC, (iii) Sudbury breccia, comprised of impact melted and brecciated footwall material; and (iv) an olivine diabase dyke which crosscuts the ore bodies. Above the 4000 ft level, the majority of the #1 shear lies along contact of footwall sublayer norite and the metasedimentary and metabasalts of the hanging wall (Figure 2.2). Below the 4000 level, the #1 shear is hosted entirely within metabasalts and dips steeply to the south (Figure 2.2). The #2 and #3 shear ore bodies are not currently being mined and have not been included in this study. The #4 shear, a volumetrically significant ore body, strikes east-west and dips steeply to the south. It is bound by metavolcanics in its hanging wall and norite along its footwall, a reversal of the #1 shear hanging wall and footwall units.

Several ore types are observed at the Garson deposit and contain varying amounts of major pyrrhotite, chalcopyrite and pentlandite with minor pyrite, and local sphalerite and galena hosted in veins. The main ore types observed in this study are inclusion-rich massive sulphide (INMS), disseminated sulphide ore (DISS) and massive sulphide (MASU).

3.2 Sampling and analytical methods

Samples from quartz-sulphide breccia veins, were selected from various shear-hosted ore zones at different levels in the Garson mine (Figure 3.2b). The samples were prepared into double-polished thin sections. Quartz was visually examined using a petrographic

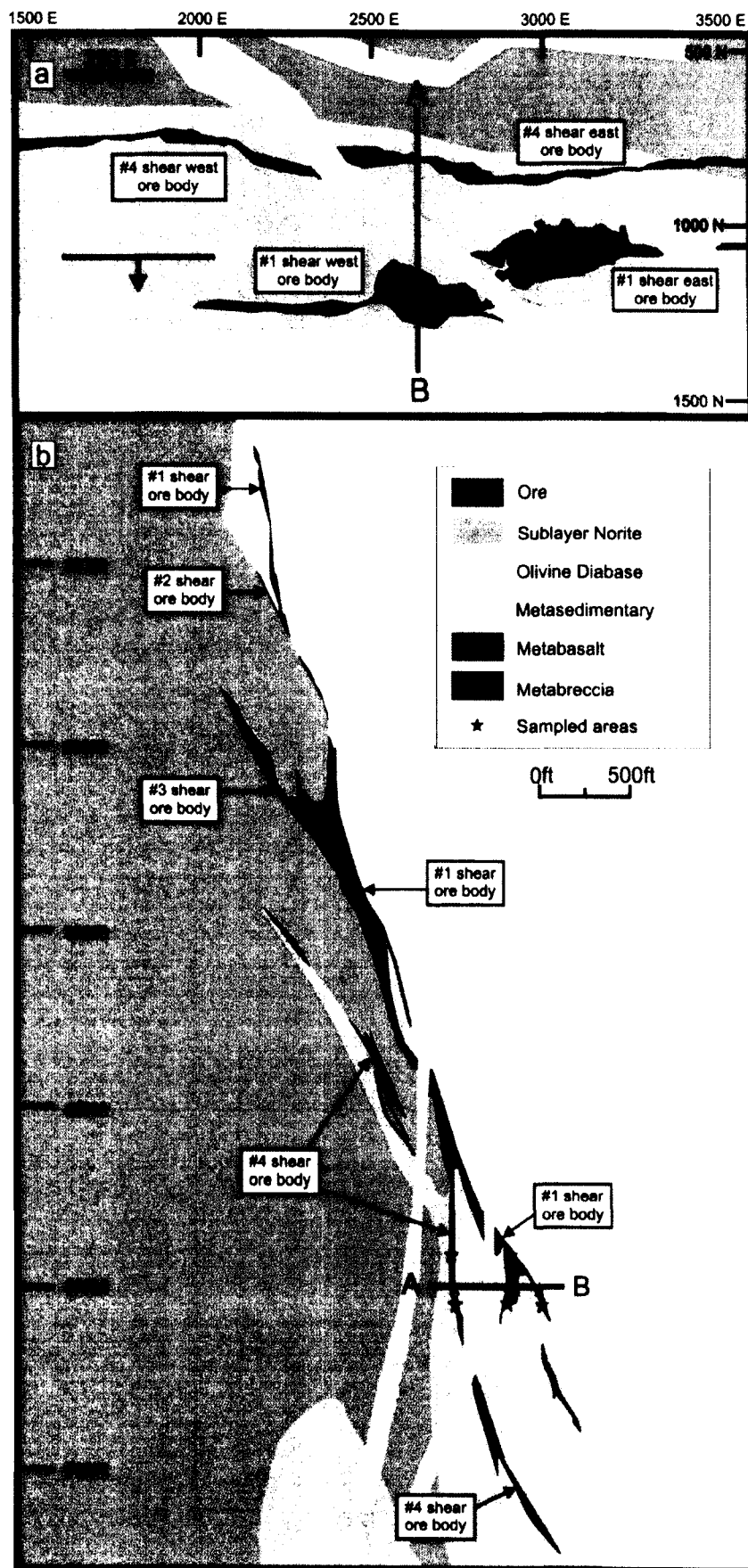


Figure 3.2 (previous page): Plan view and cross section of the Garson deposit. a) Plan view of the #1 and #4 shear-hosted ore bodies on the 5000 level. On this level sulphide ore bodies are exclusively hosted in metabasalt. Line and arrow indicate current dip direction; b) Cross section of the Garson ore bodies facing east, intersecting 2640 easting. Line labeled A-B indicates corresponding sections in each panel. The current orientation is the result of overturning of the ore bodies, which was originally shallowly north-dipping. The #1 and #4 shear zones are hosted at the contact of sublayer norite and metabasalts/metasediments. Below the 4370 level, the #4 shear is hosted entirely in metabasalt. Modified from Aniol and Brown (1979). Stars indicate sampled levels within #1 and #4 shear.

microscope to identify fluid inclusions which could then be studied by LA-ICPMS and microthermometric analysis. Areas of quartz with abundant or ideal (i.e., large, well preserved) fluid inclusions were then cut into very small chips ($\sim 25 \text{ mm}^2$) to facilitate microthermometric analysis.

3.2.1 Microthermometric analyses

A Linkam FTIR 600 heating-freezing stage mounted on an Olympus BX51 microscope (Saint Mary's University, Halifax, Nova Scotia) was used to perform microthermometric measurements. Synthetic fluid inclusion standards containing pure CO_2 (melting at -56.6°C) and pure, critical density H_2O (melting at 0°C and homogenizing at 374.1°C) were used for the stage calibration. The total range of uncertainties associated with the microthermometric measurements vary from $\pm 2\text{--}3^\circ\text{C}$ for temperatures recorded near the limit of working minimum and maximum temperatures for the heating-freezing stage (-190°C and 560°C), to better than $\pm 0.3^\circ\text{C}$ for temperatures recorded near 0°C , based on reproducibility of measurements conducted on the standards and the precision of the instrumentation. Final ice melting temperatures ($T_{\text{m}}^{\text{ice}}$) based on the salinity-freezing point depression relationship of Bodnar (1994) were used to determine the NaCl weight percent equivalency values (i.e., bulk salinity) for the inclusions. For inclusions which registered final $T_{\text{m}}^{\text{ice}}$ lower than -21.2°C (i.e., the eutectic temperature for the NaCl- H_2O system), the salinities were calculated using a salinity-freezing point depression relationship in the $\text{CaCl}_2\text{-H}_2\text{O}$ system (Zhang and Frantz, 1987). Ice melting temperatures lower than -21.2°C indicate that divalent cations

(Ca²⁺, Mg²⁺), in addition to Na⁺, are present as major fluid constituents (Shepherd et al., 1985).

For fluid inclusions containing clathrates that dissolved from 0 to 10°C in the H₂O-NaCl-CaCl₂ system, criteria from Darling (1991) and Diamond (1992) were applied to determine NaCl weight percent equivalency values.

3.2.2 Mineral identification and analysis by SEM-EDS

Scanning electron microscopy (SEM-EDS) was used to image, and to analyze the chemical composition of major and trace mineral phases observed in the Garson ores. Samples were studied using a Leo 1450 VL SEM (Saint Mary's University, Nova Scotia) at an accelerating voltage of 20kV and a beam current ranging from 5-20 nA.

3.2.3 LA-ICPMS analyses

Trace elements in fluid inclusions that are hosted in fragments of quartz veins were quantified by laser ablation ICP-MS at ETH Zurich, Switzerland. Ablation was performed with a fluence of 15 Jcm⁻² using a prototype system similar to the available from GEOLAS (now Coherent Inc.) with a homogenized 193 nm ArF Excimer laser (Günther and Heinrich, 1999). Aerosols were generated using a pulsed beam at 10 Hz and 80-90 mJ output energy generated aerosols. Ablation pit diameters were set slightly larger than the maximum dimension of each inclusion in order to analyze the entire content of the inclusion. An Ar-He gas mixture (He 1.15 L/min; Ar 0.8 L/min) carried sample aerosols into an ELAN 6100 quadrupole ICPMS using similar conditions as Pettke et al. (2004). A representative signal is shown in Figure 3.3 displaying the typical intensities for elements.

Oxide production rates were maintained below 0.3 percent. Mass spectrometer dwell time was set to 10 ms for all masses measured and quantified (Li, B, Na, S, Mg, K, Ca, Mn, Fe, Cu, Zn, As, Rb, Sr, Ag, Sn, Sb, Cs, Ba, Ce, Pb, Bi). Gold and PGE values were consistently below a detection limit of ~1 ppm, while S values were consistently below ~200 ppm. Quantification of trace element concentrations was performed using the software SILLIS (Guillong et al., 2008). This was performed by deconvoluting the mixed fluid inclusion plus the host from the host-only signals after calculation of background-corrected count rates for each isotope, and quantification of inclusion composition. The standard reference glass 610 from NIST (National Institute of Standards and Technology) was used in the calibration of analyte sensitivities. Internal standards used were the weight percent NaCl equiv. content of the fluid inclusions, determined by microthermometric measurement of freezing point depression.

Hot cathodoluminescence (CL) was performed on quartz grains in order to identify the different generations of quartz and therefore, infer fluid inclusion origin. Studies of quartz grains were performed on a Lumic HC4-LM hot-cathode cathodoluminescence microscope used in tandem with a Varian turbomolecular vacuum pump, Olympus BXFM focusing unit and a Kappa DX40C peltier cooled camera equipped with the Kappa camera control: DX40C-285FW software package. Quartz grains mounted on thin sections were placed in a vacuum and photographed in plane-polarized while being exposed to the CL beam. The hot CL was operated at an acceleration voltage between 12.35-13.06 kV, a beam current of 0.34-0.35 mA, a filament current of 2.2-2.3 A, a deflection of 9.5-10 V and a focus of 5.1-5.5 V.

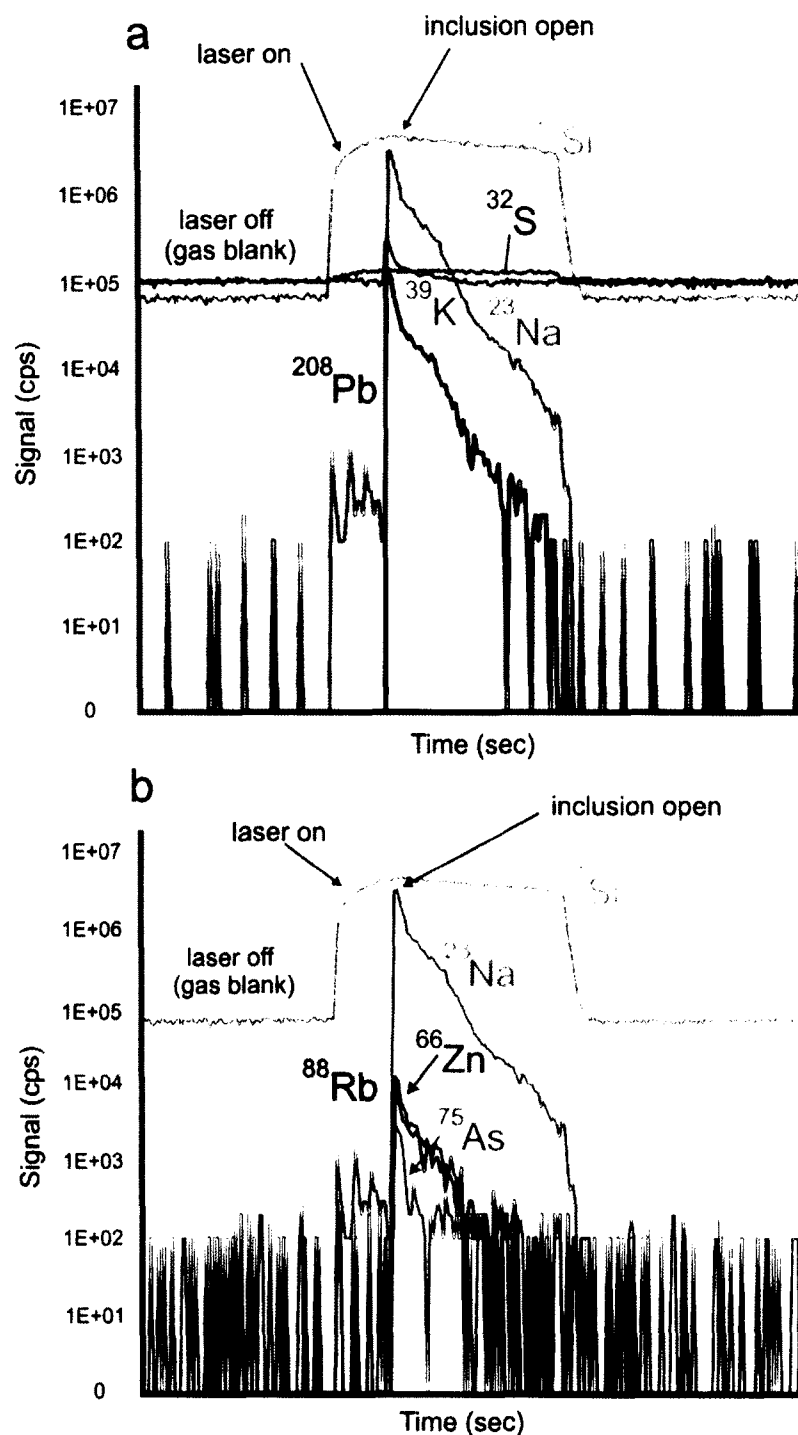


Figure 3.3: Representative signals of elements from an ablated inclusion hosted in quartz by LA-ICPMS. a) Representative signal of an ablated inclusion hosted in quartz by LA-ICPMS. The figure shows overlapping peaks for Pb, K, and Na in the fluid. The host quartz is represented by the orange plateau for ^{29}Si counts; b) Representative signal from the same inclusion as in (a) show overlapping peaks for As, Rb, and Zn in the fluid.

3.3 Results

3.3.1 Vein petrography, classification and timing

The quartz veins found in the Garson ore zones pre-date the sulphide ores. Unambiguous textural relationships show that pre-existing barren quartz veins were brecciated and milled along with host rocks during shearing events and filled in by sulphide melt later on (Figure 3.4). In some cases, the INMS ore type may be considered the equivalent of the quartz-sulphide breccia veins examined here. The breccia veins typically occur along the edges of ore bodies, along ore-host rock contacts and appear to have resulted from the deformation and brecciation of pre-existing quartz veins.

Sulphide crystallization/precipitation in the breccia veins clearly postdates the quartz but may have been synchronous to or postdated the actual quartz fragmentation. Angular to rounded quartz fragments (clasts) are surrounded by sulphides that exhibit open space-filling textures and fracture infilling (Figure 3.4a, b). The infilling sulphides primarily consist of base metal sulphides (pyrrhotite, chalcopyrite and pentlandite; Figure 3.4a-c). In some samples small grains of cobaltite-gersdorffite solid solution (CGSS) and other trace phases such as galena, tellurobismuthite and hessite are observed hosted in or in contact with the quartz fragments (Figure 3.4d, e). Gangue minerals such as amphiboles, biotite and apatite occur within the quartz-sulphide veins and wall rock fragments, milled with the original quartz vein material during shearing also occur, partly imbedded in sulphides (Figure 3.4e). Pre-deformation timing of the veins (i.e., classification of different vein generations) cannot be determined because of destruction of original crosscutting relationships during shearing and brecciation. However, it is evident that the

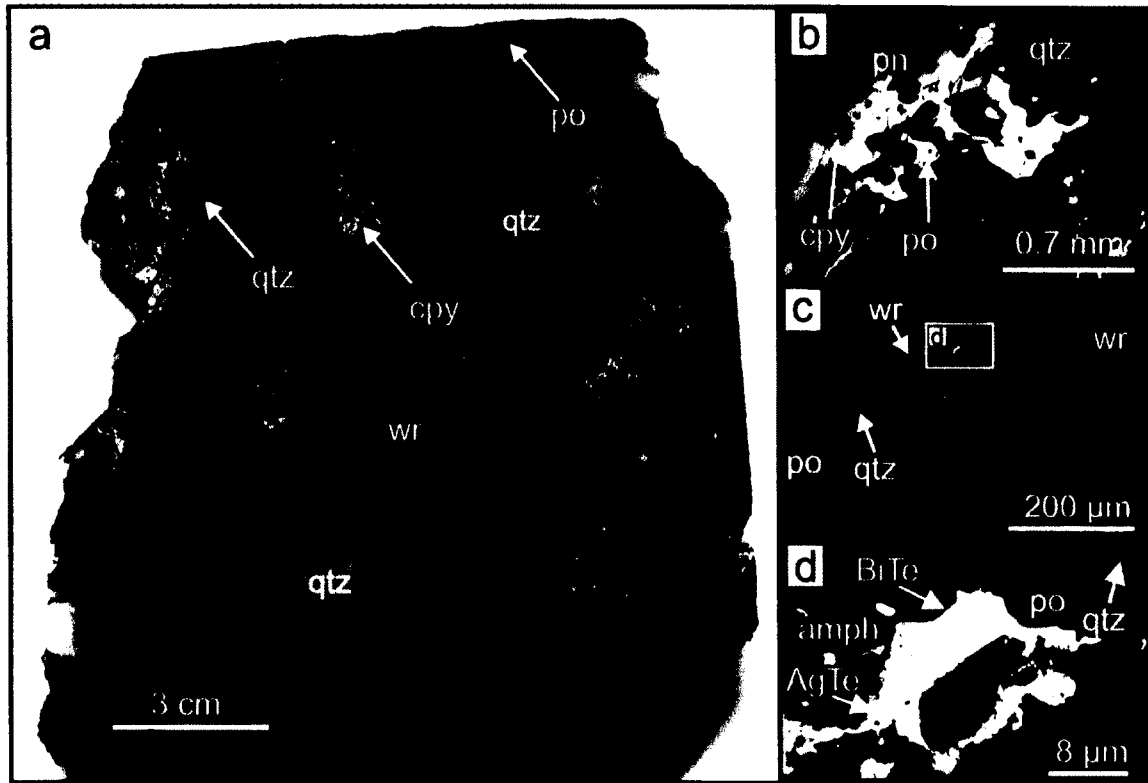


Figure 3.4: Petrographic characteristics of a sulphide-quartz breccias vein hand sample, containing a fragment of wall rock. Petrographic characteristics of a sulphide-quartz breccias vein hand sample, containing a fragment of wall rock. a) Fragmented quartz vein sample displaying infilling sulphides and their relationship to quartz and wall rock fragments; b) Photomicrograph of Po and Cpy displaying infilling texture with quartz grains; c) SEM-BSE image of Po infilling fractures in quartz and wall rocks fragments; d) A composite grain consisting of Ag and Bi- tellurides showing space filling texture.

List of abbreviations: amph= amphibole; AgTe= silver telluride; BiTe= bismuth telluride; cpy= chalcopyrite; pn= pentlandite; po=pyrrhotite; qtz= quartz; wr= wall rock

original quartz veins were filling tension gashes, and larger, bedding subparallel structures in the metasediments. Original vein-wall rock contacts are often also preserved.

The quartz veins appear to have a metamorphic origin. This is indicated by hot cathodoluminescence imaging of the quartz fragments that shows a characteristic reddish-purple emission colour which is unique to metamorphic quartz, and not characteristic of hydrothermal or volcanic/plutonic quartz (Boggs, Jr., et al., 2002; Figure 3.5). Reddish emissions are more typical of quartz crystallized under greenschist-grade conditions, whereas purple emission is more typical of quartz in amphibolite-grade rocks (Figure 3.5; Sprunt et al., 1978; Marshall, 1988; Götze, 2000; Pagel et al., 2000; Boggs, Jr. et al., 2002; Gorobets and Rogojine, 2002).

3.3.2 Fluid inclusion petrography and microthermometry

Classification of fluid inclusion origin and designation of inclusion types was based on petrographic observations at room temperature and utilized formalized criteria from Wilkinson (2001) and Goldstein (2003). Where possible, inclusions were grouped into fluid inclusion assemblages (“FIA”) based on consistency of microthermometric behavior, phase ratios and the occurrence of inclusions in groups along single, temporally and texturally constrained growth features (growth zones, healed fractures). Assemblage designation helps to differentiate inclusions that have experienced necking down or other post-entrapment modifications from unaffected inclusions.

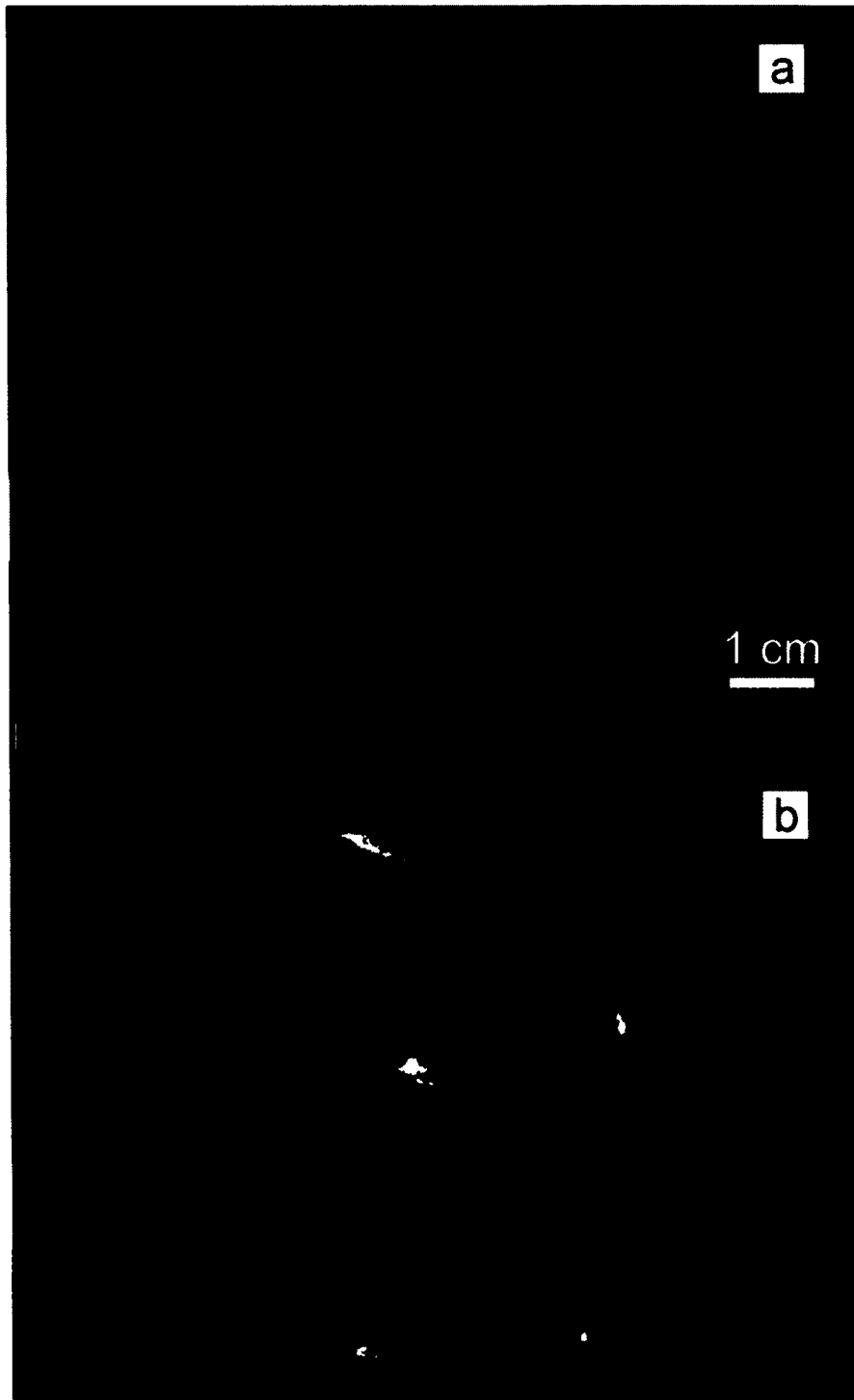


Figure 3.5: Photomicrograph and hot cathodoluminescence (CL) image of a single quartz grain. Photomicrograph and hot CL image of a single quartz grain. a) Photomicrograph of a quartz grain with abundant fractures; b) Hot cathodoluminescence image of the same quartz grain. Note the homogeneous reddish-purple CL emissions and lack of any discernable growth zones. Lighter pink-orange areas healed fractures and bright yellow spots are carbonate inclusions.

Fluid inclusions observed in this study have very similar characteristics to fluid inclusions hosted in Cu-Ni-PGE veins in granitic and metavolcanic rocks at the Little Stobie deposit (South Range; Molnár et al., 1999). A fluid inclusion classification scheme similar to Molnár et al. (1999) was used for this study (Figure 3.6).

Most fluid inclusions were small, with > 90 per cent ranging from 3 to 20 μm . Many inclusions were found in assemblages (small groups of genetically related inclusions; Figure 3.7g). Type I inclusions are characterized by the absence of a vapor phase (Figure 3.6). Type IA are single phase liquid, while type IB are two phase liquid-halite and type IC are three (or four) phase liquid-halite \pm sylvite \pm unknown (Figure 3.6; Figure 3.7f). Type IA and IB inclusions are very rare, are poorly preserved, and contribute little to the data set (Table 3.1, Appendix B). Type IIA and B are two phase liquid-vapor inclusions with varying L-V ratios (approximately 80:20 and 50:50, respectively; Figure 3.7b, c). Type IIA inclusions are well preserved and are much more abundant than type IIB inclusions. Both commonly show a negative crystal shapes (Figure 3.7b, c). Type IIC inclusions are three phase (aqueous liquid-CO₂ liquid-CO₂ vapor).

The CO₂ vapor phase appears only upon cooling to room temperature, surrounded by the CO₂ liquid bubble and homogenizes upon heating at low temperatures (Table 3.1, Appendix B).

Type III inclusions are characterized by the presence of various solid phases as well as a vapor phase (Figure 3.6). Type IIIA inclusions are three phase halite-liquid-vapor (Figure 3.7d, e).

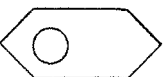
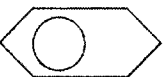

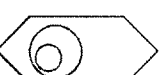
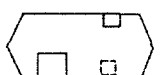


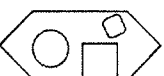


| Dominant (most abundant) | | Minor | | | |
|--------------------------|---|------------------------------------|-----------|--|-----------------------------------|
| Type IIA |  | Liquid+Vapour | Type IIB |  | Liquid+Vapour |
| Type IIIA |  | Liquid+Vapour+Halite | Type IIIC |  | Liquid+Vapour+Vapour |
| Minor | | | | | |
| Type IC |  | Liquid+Halite± Sylvite?±Unknown | Type IIIB |  | Liquid+Vapour+ Halite+Sylvite? |
| Type IA |  | Liquid | Type IIIC |  | Liquid+Vapour+ Halite+Unknown |
| Type IB |  | Liquid+Halite | Type IV |  | CO ₂ |

Figure 3.6: Types of fluid inclusions observed in sulphide, quartz breccias veins in the Garson deposit. Types of fluid inclusions observed in sulphide, quartz breccias veins in the Garson deposit. Type IIA and Type IIIA are the most abundant fluid inclusions observed. Modified after classification scheme of Molnár et al. (2001) at the Stobie Mine, a contact-style Ni-Cu-PGE deposit.

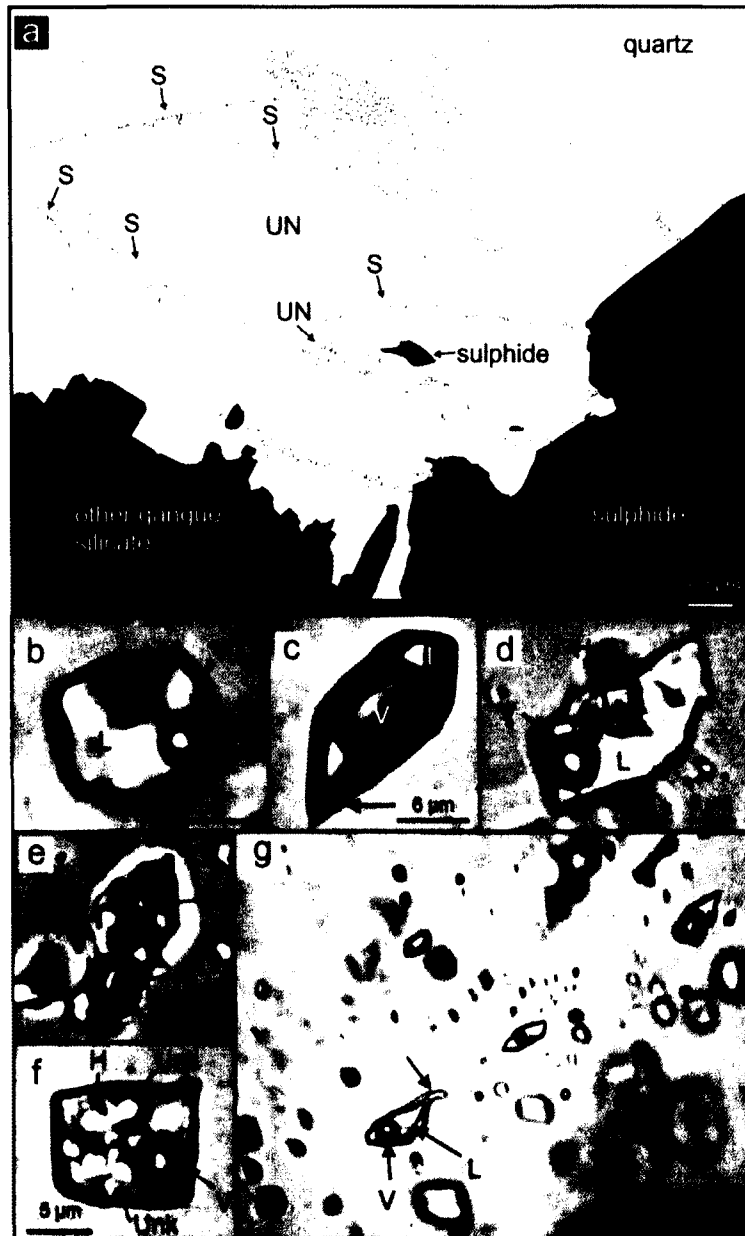


Figure 3.7: Fluid inclusion map and photomicrographs of fluid inclusion assemblages of the dominant type IIA. Fluid inclusion map and photomicrographs of fluid inclusion assemblages of the dominant type IIA. a) A representative quartz chip, mapped from thin section, showing unclassified (UN) and secondary (S) fluid inclusions. Secondary inclusions occur in healed fractures while unclassified inclusions occur in regions of the quartz grains free from fractures. Black areas are sulphide or silicate gangue. Dark grey areas are fractures that contain no fluid inclusions; b-c) Type IIA and IIB inclusions containing liquid (S) and vapor (V) with corresponding vapor:liquid ratios. Arrow pointing to tapered end of inclusion suggestive of necking down; d-e) Typical type IIIA inclusions with vapor bubble and halite crystal (H); f) A type IIIB inclusion with abundant solid phases of halite, sylvite? and unknown phases (Unk); g) An assemblage of fluid inclusions hosted along annealed fractures in quartz.

Type IIIB and C contain sylvite (usually an anhedral, low refractive index, clear solid) and/or an unknown daughter phase (Figure 3.7f). Type IV inclusions are CO₂-bearing with no visible vapor phase and only occur in a few samples, as secondary assemblages hosted in healed fractures in quartz (Figure 3.7a, f). Of the ten types of inclusions observed, type IIA, IIC and type IIIA are by far the most abundant and comprise the bulk of the microthermometric data (Table 3.1, Appendix B).

The fluid inclusions are all hosted in quartz. No growth zones were observed in the quartz, based on petrographic and hot cathodoluminescence observations. Therefore, no inclusions could be designated primary in origin (Figure 3.5). Unclassified inclusions are not secondary as they do not occur in any secondary features of the quartz (i.e., along healed fractures in areas of bright orange cathodoluminescence emission; Figure 3.5). However, the unclassified inclusions are crosscut by and, therefore, pre-date secondary inclusions (Figure 3.7a).

All type IIA-C inclusions homogenized to a liquid phase by contraction and disappearance of the vapor bubble ($L+V \rightarrow L$). The CO₂ liquid phase in type IIC, which appears during cooling, homogenizes with the CO₂ vapor bubble from -5 to 29°C ($L_{aq}+L_{CO2}+V_{CO2} \rightarrow L_{aq}+V_{CO2}$).

The range in overall T_m^{ice} is quite significant when all data is observed (Table 3.1, Appendix B), ranging from -0.5 to -19.6°C and -22.1 to -28.2°C which corresponds to salinities varying from 0.88 to 22.1 weight percent NaCl₂ equivalent, and 25.1 to 31.2 weight percent CaCl₂ equivalent, respectively (Figure 3.8a). Inclusions with T_m^{ice} lower than -21.2°C (the NaCl-H₂O eutectic), which were observed primarily in type IIA inclusions, must contain additional major cations, and, therefore, their bulk salinities

cannot be calculated using NaCl weight percent equivalency and use weight percent CaCl_2 equivalency calculated from Darling (1991) and Diamond (1992). Some fluid inclusions exhibited metastable behavior. The choice of NaCl or CaCl_2 equivalency is arbitrary at this point, being required only to accommodate those inclusions with low eutectic melting points and T_m^{ice} less than -21.2°C and inclusions without these characteristics on single data summary diagrams. A single type IA (single phase liquid) was measured and found to have a T_m^{ice} of -38.9°C , corresponding to 42 weight percent CaCl_2 equivalent. The T_m^{ice} for this inclusion is, however, difficult to obtain due to the lack of a vapor bubble and therefore unreliable. Salinities for inclusions that contain a halite crystal were determined using the temperature of halite dissolution (T_d). Like T_m^{ice} , T_d show a wide range involves varying from 139 to $> 470^\circ\text{C}$, corresponding to salinities 29.2 to >55.8 weight percent NaCl equivalent.

Unclassified fluid inclusions (i.e., not secondary; not occurring along healed fractures in quartz) tend to have lower $T_h^{\text{V+L} \rightarrow \text{L}}$ and lower salinities (wt% $\text{NaCl}_{\text{equiv.}}$). The dominant inclusions with these characteristics are type IIA inclusions (Figure 3.8b). With increasing $T_h^{\text{V+L} \rightarrow \text{L}}$ or T and salinities, secondary, type IIIA become the dominant inclusions (Figure 3.8b). While $T_h^{\text{V+L} \rightarrow \text{L}}$ or T and salinities range significantly throughout the data set, single FIA show much narrower ranges (Figure 3.9).

A few type IIA-C inclusions develop clathrates upon freezing and subsequent heating. The clathrate melting temperatures ranged from 1 to 7.8°C yielding corresponding bulk salinities ranging from 4.3 to 14.5 weight percent NaCl equivalent (Table 3.1). Also observed in one sample was the presence of relatively large ($20\text{-}30\ \mu\text{m}$) inclusions that did not freeze upon cooling to -190°C (lowest temperature limit of the stage) suggesting

significant major cation abundance (Molnár et al, 1999). The inability to freeze the inclusions at the temperature limit of the stage is typical of fluids with abundant divalent cation content. The inclusions are type IIA (L+V), are secondary and have very low T_h , ranging from 98.3 to 101.3°C. Bulk salinities reported in wt% NaCl or CaCl₂ equivalent do not account for concentrations of other major cations (e.g., Ca, Mg if using wt% NaCl_{equiv.}) and, therefore, do not represent the true fluid compositions. Direct measurement of inclusion compositions by LA-ICPMS can be compared to inclusions with measured wt% NaCl equivalencies obtained by ice melting temperatures to determine more accurate major cation compositions (see below).

3.3.3 Metastable phases

In many cases, fluid inclusions containing hydrohalite crystals or clathrates were observed. Hydrohalite crystals melted at temperatures above -10°C, while clathrates melted at temperatures between ~0 and 10°C (Table 3.1, Appendix B). The melting temperatures for hydrohalite (T_m^{hh}) range from 12.3 to 19.7°C (Table 3.1, Appendix B). Ideally, the highest temperature that hydrohalite can represent at equilibrium is ~0.1°C, which corresponds to a peritectic point. However, hydrohalite crystals often show slow melting kinetics and can persist to higher temperatures than expected (Matthew Steele-MacInnis personal communication). Although most fluid inclusions which contain hydrohalite inclusions do not contain a halite crystal, they are of high bulk salinity and also contain significant amounts of CaCl₂ (15.7 to 16.1 wt% NaCl_{equiv.}; 11.1 to 11.4 wt% CaCl_{2equiv.}).

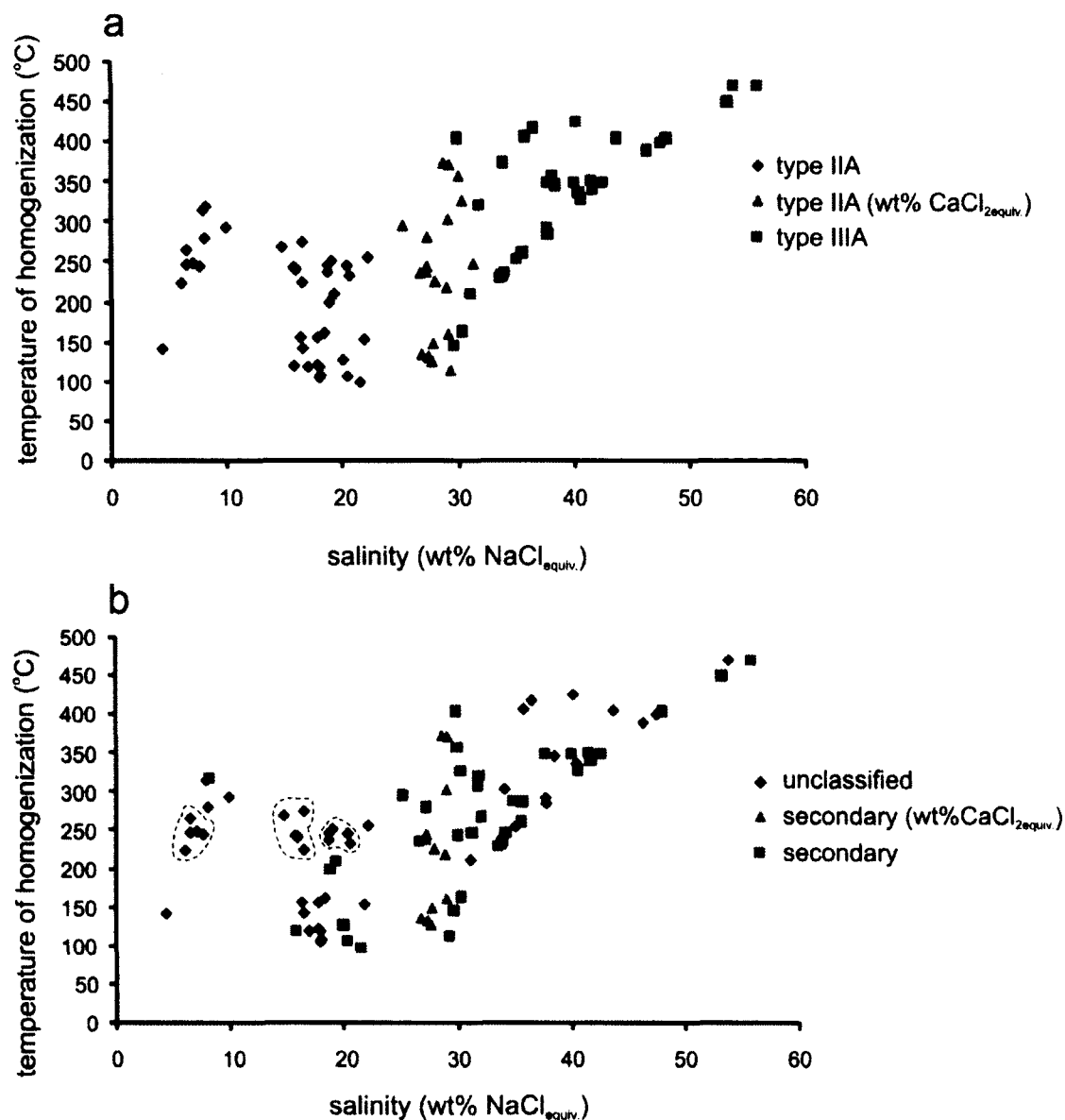


Figure 3.8: Salinity versus temperature of vapor homogenization relationships for microthermometric data. Salinity versus temperature of vapor homogenization relationships for microthermometric data sorted by a) fluid inclusion type (appearance at room temperature) and b) fluid inclusion origin. Data points circled in dotted lines represent single inclusion assemblages shown in Figure 3.9.

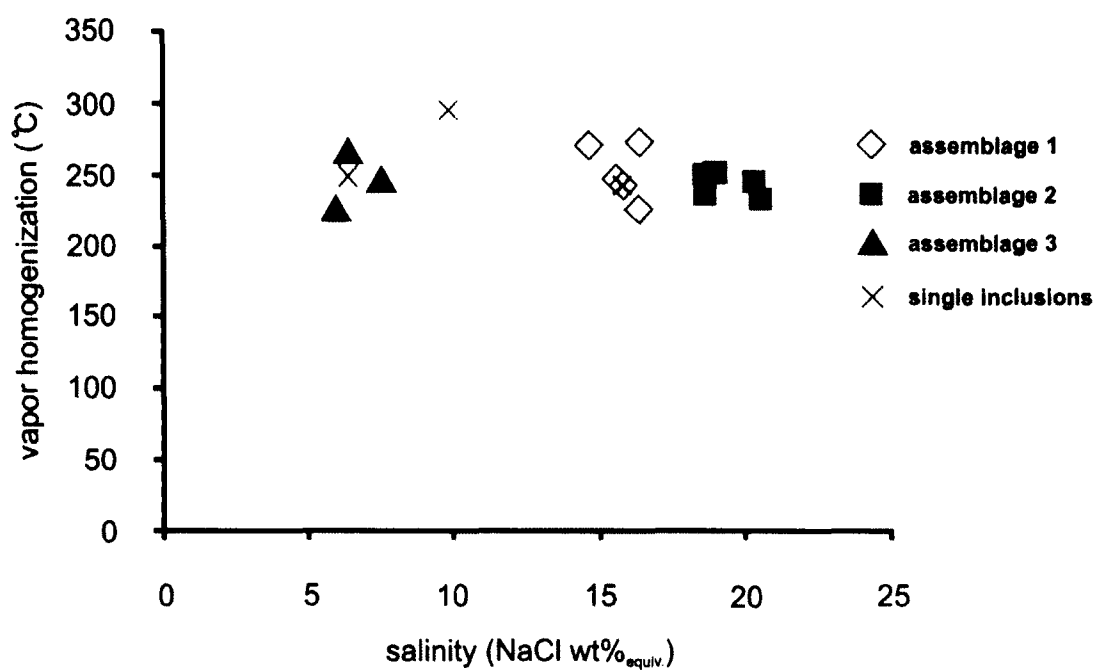


Figure 3.9: Plot showing typical ranges in salinity and vapor homogenization temperature in individual assemblages. Assemblages are compared to data from single inclusions, illustrating the importance of assemblage designation.

In three rare cases involving two phase inclusions (type IIA), inclusions were cooled until observation of freezing was made. Upon heating, T_m^{ice} values were recorded where the disappearance of the ice crystal was observed. Upon further heating, a crystal (hydrohalite) persisted to high temperatures (26.8 to 27.9°C) until it rapidly underwent a phase change from hydrohalite to halite ($T_{\text{hh-hal}}$). For these inclusions, T_m^{ice} , $T_h^{\text{V+L} \rightarrow \text{L}}$, and T_d were recorded and ranged from -25.6 to -28.2°C, 304.5 to 374.6°C and, 138.8 to 299.1°C, respectively. The composition of these metastable inclusions can be determined from T_m^{ice} and T_d using the method of Steele-MacInnis et al. (2011), but depending on which parameter is used (i.e., T_m^{ice} , T_d , T_m^{hh}), calculated results will vary significantly.

3.4 Laser ablation ICP-MS analyses of fluid inclusions

3.4.1 Aqueous inclusions

Analyses of trace element concentration in fluid inclusions from type IIA (n=17), IIC (n=7) and type IV (n=7) in four samples were performed by LA-ICPMS (Table 3.2, Appendix B).

Significant variations in major and trace element concentrations were observed in type IIA and IIC inclusions (Table 3.2, Appendix B). A representative signal (split into two views for clarity) from an ablated unclassified type IIA inclusion is shown in Figure 3.3. The fluids are highly enriched in As (up to 616 ppm; avg. 105 ppm), Zn (up to 1343 ppm; avg. 570 ppm), Sb (up to 110 ppm; avg. 17 ppm), Ba (up to 2795 ppm; avg. 728 ppm) and Pb (up to 4260 ppm; 1228 ppm), but are poor in Cu (range bdl-28 ppm; one analysis 141 ppm; Table 3.2, Appendix B), Fe (range bdl-1200 ppm not including outliers related to Fe and Mn contamination; Table 3.2, Appendix B) and S (<200 ppm; Jung Hun Seo

personal communication; Figure 3.3). A strong correlation between bulk salinity and As, Sb, Ba, Bi, and Pb concentrations is seen (Figure 3.10; Table 3.2, Appendix B).

3.4.2 Type IV CO₂ inclusions

The densities of type IV CO₂ inclusions are considerably less than aqueous inclusions and, therefore, signals show much lower intensity for as many trace elements as possible (i.e., lower count rates; Table 3.3, Appendix B). The largest CO₂ inclusions were studied in order to obtain reliable analyses. The intensities are listed in Table 3.3 (Appendix B). All analyses show peaks of Na, while many inclusions show peaks of Mn, Zn, Rb, Sr, Ba and Pb (Table 3.3, Appendix B), similar to type type IIA and IIC inclusions. Also present in some analyses are peaks of Li, Mg, Al, Fe, Cu, Cs, Sb, and Pt (Table 3.3, Appendix B). The presence of salts (e.g., Na, Mn, Ba) in these inclusions infers the presence of H₂O, which can occur as a thin film along the edges of an inclusion and is optically invisible. The salts would not be dissolved in CO₂ as it is a non-polar solvent.

3.5 Discussion

3.5.1 Comparison to other studies

While the majority of ore deposits found at Sudbury are primary magmatic in origin, footwall-style deposits are thought have a significant hydrothermal component, having their metal contents modified by fluids (Cabri and Laflamme, 1976; Ballhaus and Stumpfl, 1986; Li and Naldrett, 1993; Li et al., 1993; Farrow et al., 1994; Farrow and Watkinson, 1997; Molnár et al., 1997, 1999, 2001; Hanley et al., 2005; Péntek et al., 2008; Dare et al., 2010; Hanley et al., 2011). Many authors have performed detailed

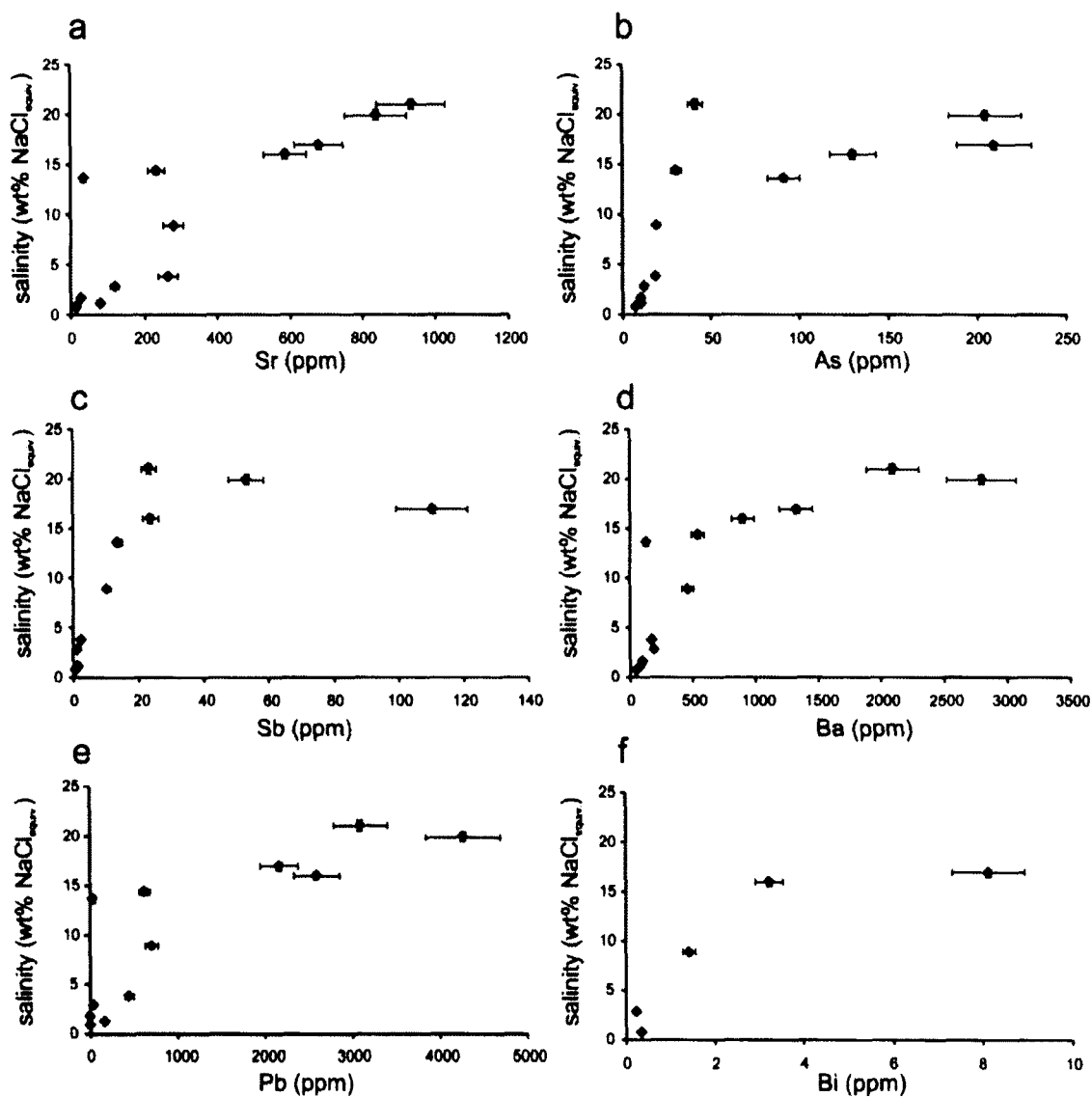


Figure 3.10: Plot of relationship between salinity and trace element concentrations, determined by LA-ICPMS. Note the correlations between salinity and concentrations of a) Sr; b) Ba; c) As; d) Sb; e) Pb; and f) Bi.

studies on ore-related fluid inclusions in the Sudbury area (Farrow and Watkinson, 1992; Farrow et al., 1994; Molnár et al., 1997, 2001; Marshall et al., 1999; Hanley et al., 2005; Péntek et al., 2008).

Authors have suggested that at least three types of fluid circulated through or interacted with the host rocks of the Sudbury Igneous Complex (Farrow and Watkinson, 1992; Molnár et al., 1997; Marshall et al., 1999; Molnár et al., 2001; Hanley et al., 2005; Péntek et al., 2008; Hanley et al., 2011). The unusually high divalent cation content of some fluid inclusions may indicate the involvement of a Ca-rich groundwater that is found deep within the Archean rocks along the North Range (Frape and Fritz, 1982). During cooling and crystallization of the Sudbury Igneous Complex, it has also been recognized that an early-stage high-temperature, Cl-rich fluid was exsolved. Some combination of these two fluids went on to interact with magmatic sulphides, possibly leading to remobilization and precipitation of some quantity of metals in veins and disseminations in the footwall; it is still unclear the extent and importance of this process (Molnár et al., 1997, 2001; Marshall et al., 1999; Hanley et al., 2005; Péntek et al., 2008), although recent work suggests that remobilization occurred only locally in the footwall and did not involve metal transport from the contact to the footwall (Hanley et al., 2011). A third generation of fluid is thought to have been associated with regional tectonic events and not with Ni-Cu-PGE mineralization. These fluids may have formed during the Penokean or Mazatzal-Labradorian Orogenic events (Molnár et al., 1997, 2001; Marshall et al., 1999; Mukwakwami et al., 2011b). During migration of these metamorphic fluids along pre-existing north-south and northwest-southeast trending fractures, the fluids boiled through the transition from lithostatic to hydrostatic pressure

caused by regional uplift. Boiling is thought to have produced two immiscible fluids with variable salinity and a carbonic component (Molnár et al., 2001).

Elemental concentrations in type II fluids obtained in this study were compared to other fluids from Sudbury and in other magmatic-hydrothermal settings (Figure 3.11). In general, the major and trace element composition of the South Range fluids from the Garson deposit show similarities in bulk element concentrations to those in other felsic- and mafic-associated ore deposits including porphyry-epithermal systems [Figure 3.11b, c, d, f; Pudack et al. (2009) at Nevados de Famatima, Argentina; Kouzmanov et al., 2010 at Rosia-Poieni, Romania] and PGE-bearing, mafic-ultramafic layered intrusions [Figure 3.11g; Hanley (2006) at the Stillwater Complex, Montana, USA]. With the exception of ore metals, magmatic-hydrothermal fluids have similar major and trace element composition regardless of which type of deposit or parental rock they are associated with (Figure 3.11).

Fluids at Garson also predate ore formation. There are two pieces of evidence for this: First, the quartz in which the inclusions are hosted texturally pre-dates sulphides at Garson. Second, inclusions contain very low Cu, Fe and S concentrations (Figure 3.3a; Table 3.2, Appendix B), inconsistent with what would be expected for a moderately oxidizing, saline fluid phase that equilibrated with or precipitated chalcopyrite-rich sulphides (Figure 3.11; Pudack et al., 2009; Kouzmanov et al., 2010). A few inclusions have anomalously high Cu and Fe contents but these are not representative and may indicate the presence of some contaminating (accidentally trapped) phases in the inclusions unrelated to true fluid composition. Comparison of this pre-ore fluid at Garson can be made to two other fluids at Sudbury. First, the Garson fluids show similar metal enrichments to pre-ore fluids found

along the North Range of the Sudbury Igneous Complex (Figure 3.11a; Hanley et al., 2005). Both South Range and North Range pre-ore fluids are distinctly enriched in Pb, Zn, Ba, and Sr, and depleted in Cu and S, with comparable Pb/Zn (~1-3) and Sr/Rb (~20-40) ratios (Hanley et al., 2005; Figure 3.11a; Table 3.2, Appendix B). Concentrations of Ca in both fluids are also very similar (Figure 3.11; Table 3.2). Frape and Fritz (1982) describe this Ca-enrichment (and associated Sr-enrichment; Hanley et al., 2005) as typical of most of the North Range groundwaters (Figure 3.11e) and is the result of equilibration of those fluids with plagioclase-rich Archean-age gneisses. However, it appears that South Range fluids also show these characteristics. With the exception of As and Sb that may have been leached from surrounding metasedimentary rocks on the South Range, the similar patterns of major and trace element abundance, notably a marked enrichment in Ca, Pb, Zn, Ba and Sr, in North and South Range pre-ore fluids shows that (i) these fluids are genetically-related, despite the large (regional) spatial extent over which these fluids were sampled, and (ii) that groundwater alone does not explain their composition, since the groundwaters at Garson are rich in Sr but poor in metals like Pb and Zn (Figure 3.11e).

3.5.2 Post-entrapment modifications

The fluids in the sulphide-quartz breccia veins display a wide range of salinities and temperatures of homogenization that may be related in part to real variations in fluid temperature and salinity with time (see below) but may also be related to necking down and other post-entrapment changes. Necking down, which occurs synchronous to inclusion maturation, was commonly observed and indicated in thin section by the characteristic tapered ends of adjacent inclusions (Figure 3.7c, g) and by varying

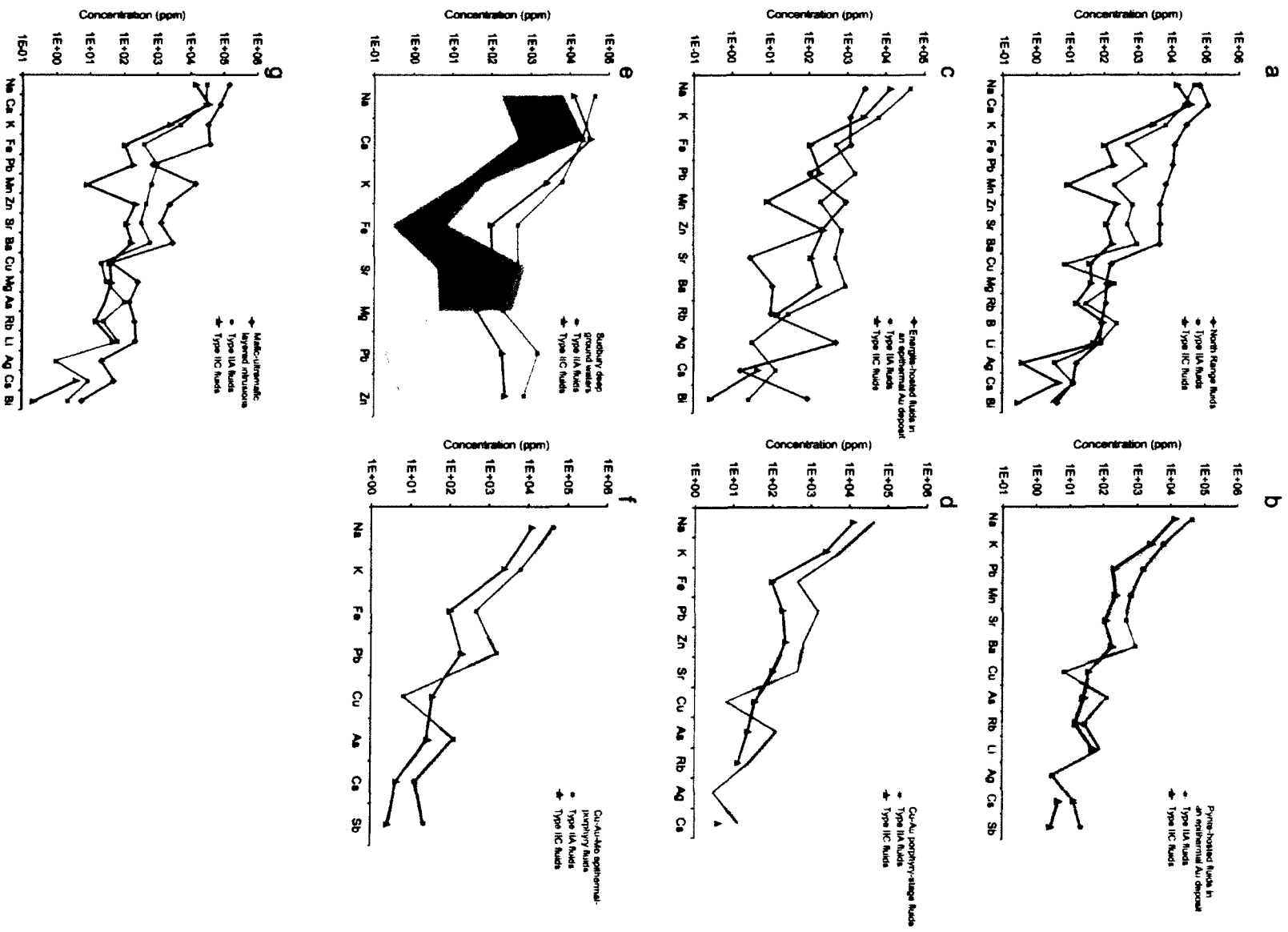


Figure 3.11: Comparison of element concentrations in quartz hosted fluids from type IIA and IIC, occurring along the South Range (this study) to fluid inclusion compositions in other magmatic-hydrothermal systems and formational waters. a) North Range footwall pre-ore fluids, Sudbury (Hanley et al., 2005); **b)** Pyrite-hosted fluids in an epithermal Au system; **c)** enargite-hosted fluids in an epithermal Au system; **d)** silicate-hosted brines in a Cu-Au porphyry deposit (Rosia Poieni, Romania; Kouzmanov et al., 2010); **e)** Modern saline groundwaters at five different mines, Sudbury (Frape and Fritz, 1982); **f)** Fluids in a Cu-Mo-Au epithermal-porphyry deposit (Nevados de Fatima; Pudack et al., 2009); **g)** Fluids from pegmatites in the Stillwater layered mafic-ultramafic intrusion (Hanley, 2006). A few inclusions are excluded from the diagrams that had anomalously high Cu, Fe and Mn contents (due to entrapment of accidental phases unrelated to fluid composition; Table 3.2, Appendix B).

liquid:vapor ratios observed in inclusions within a single fluid inclusion assemblage (Figure 3.7b, c, g).

Other types of post-entrapment modification include (i) water loss by leakage or diffusion, a process that can influence both bulk salinity (for inclusions that saturate a halite daughter crystal) and vapor:liquid ratio (i.e., vapor-out temperature), (ii) stretching, which modifies the inclusion volume and its associated homogenization behavior and, (iii) oxidation, which artificially increases bulk salinity due to the breakdown of water inside the inclusions and outward diffusion of H_2 (Mavrogenes and Bodnar, 1994; Hanley et al., 2008).

While ranges in data for individual assemblages may show little variation, temperature-salinity data from single inclusions (not classified by assemblage) and even some single assemblages are not appropriate for interpretation (Figure 3.8; Figure 3.9; Table 3.1, Appendix B). Figure 3.12 summarizes the quality of the fluid inclusion data from single assemblages. All of the changes described above may have occurred at Garson. For example, two phase inclusions (type IIA) that experienced necking down or stretching show a wide range of vapor disappearance temperatures within a single inclusion assemblage (Figure 3.12a, assemblage a, d). Even though the approximate range of measurements for these modified inclusions overlaps with assemblages that have experienced little modification (e.g., Figure 3.12a, assemblages h and i), it is impossible for inclusions trapped simultaneously to show such a range in temperature, salinity and density.

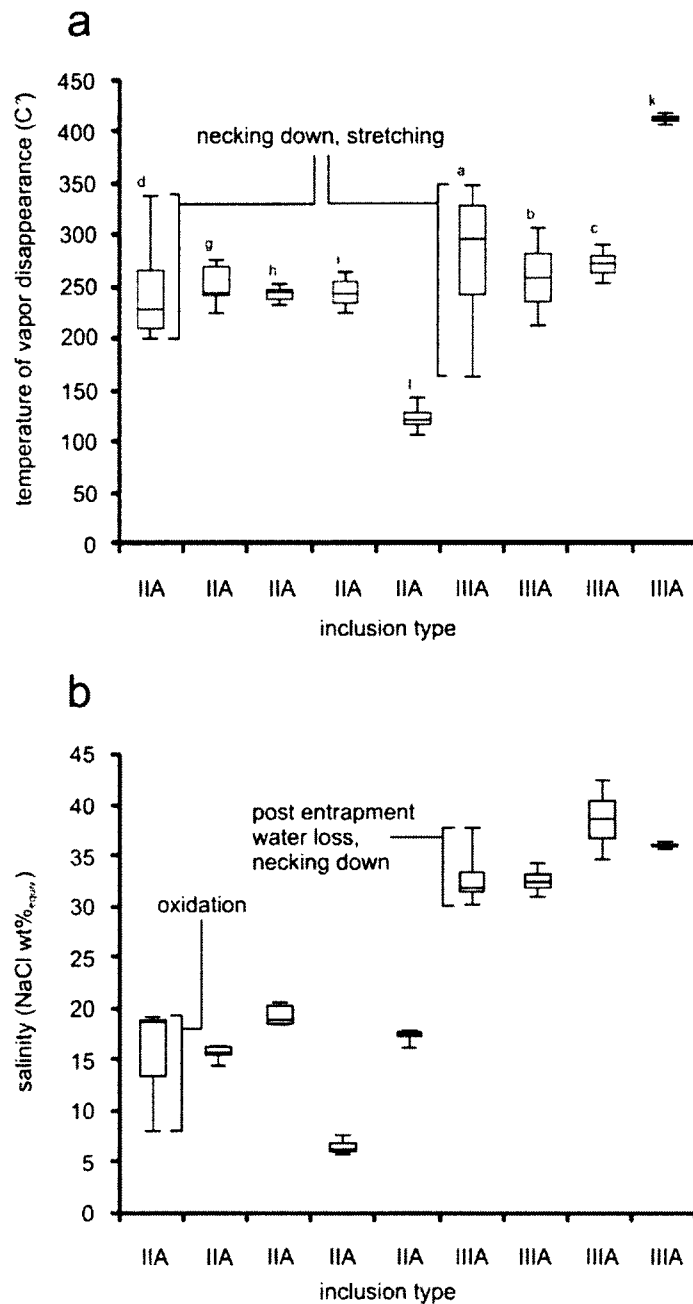


Figure 3.12: Box and whisker plots of microthermometric characteristics of individual inclusion assemblages. Plots show range in a) temperature of vapor bubble disappearance, and b) bulk salinity. Letters in frame a) correspond to assemblages listed in Table 3.1 (Appendix B) and are the same for both diagrams a) and b). Assemblages displaying largest ranges in temperature of vapor bubble disappearance temperature and bulk salinity (a and d) suggest that necking down and other post-entrapment changes have taken place, when compared to other assemblages of the same inclusion type.

Assemblages containing three phase inclusions (type IIIA) that necked down or experienced post-entrapment water loss after a halite crystal began to crystallize are also observed and show a wider than acceptable range in inclusion salinity (Figure 3.12b, assemblage a). Two phase inclusion assemblages that show both a wide range in inclusion salinity and homogenization temperature (Figure 3.12a and b, assemblage a, d) must have also experienced oxidation in addition to necking down or stretching.

This treatment of data shows that fluid inclusions at Sudbury have experienced changes in composition and volume that will negatively impact interpretation if inclusions are not grouped into assemblages. Similar evidence for post-entrapment modification has been shown for inclusions on the North Range of Sudbury, even in areas that are free of regional metamorphic overprinting (e.g., Hanley et al., 2011). The majority of fluid inclusion studies at Sudbury, however, have not recognized this problem and obtained inclusion data for single inclusions of a given type from different areas within a sample or deposit (e.g., Molnár et al., 1997, 2001; Hanley et al., 2005; Péntek et al., 2008). The consequence of this treatment of data is that subtle but real variations in fluid salinity and temperature are not adequately recognized.

Despite the effect of necking down and other post-entrapment changes we can still observe general trends in the data set, and several assemblages appear to be largely unmodified. These assemblages show very limited range in temperature of vapor disappearance and salinity, and comparison of these assemblages to one another is worthwhile (e.g., Figure 3.12a and b, assemblages c,g,h,i,k,l). For example, the general transition from type IIA to type IIIA inclusions is marked by a significant increase in fluid salinity but with relatively little change in temperature of vapor disappearance.

Some assemblages that show anomalously high or low salinity or temperature of vapor disappearance cannot be explained by post-entrapment changes (e.g., Figure 3.12a, assemblages l and k; Figure 3.12b, assemblage i). These real variations in T and salinity are discussed below.

3.5.3 Evolution of the fluids along the South Range of the SIC

Some authors have suggested that the association of lower density CO₂-bearing inclusions and high temperature, more saline inclusions indicates the mixing of magmatic and metamorphic fluids components (Marshall et al., 1999). Metamorphic fluids are ubiquitous in any system where rocks are experiencing deformation and where they are augmented by the migration of fluids through available pore spaces involving the infiltration of a fluid released from devolatilization reactions (e.g., Hewitt, 1973; Greenwood, 1975; Crawford et al., 1979; Thompson, 1983; Lamb and Valley, 1984; Sisson and Hollister, 1990). Influxes of H₂O-rich and/or CO₂-rich fluids may be related to emplacement of a pluton or retrograde reactions that occur after peak metamorphic conditions (Sisson and Hollister, 1990), suggesting that the initial source of any regional fluid would be obscured by many subsequent processes.

In addition to potential magmatic fluid (SIC-related) and groundwater components, a regional and/or contact metamorphic origin for the fluids trapped within the quartz-sulphide breccia veins at the Garson mine is possible since the wall rocks of the SIC in this region were not only undergoing at least some deformation related to the onset of the Penokean Orogeny (1.89 to 1.83 Ga; pre- to syn-ore formation; Shanks and Schwerdtner,

1991a, b; Klimczak et al., 2007), but were also being heated and dehydrated by the adjacent SIC (Coats and Snajdr, 1984).

The origin of the quartz fragments which are contained within the quartz-sulphide breccia veins is difficult to constrain due to the destruction of primary features and original spatial relationships. The original quartz veins must have formed after Sudbury event (1.85 Ga) since any fluid inclusions related to quartz vein formation that are observed today would not have survived the shock metamorphic conditions associated with the impact. The quartz and wallrock fragments occur as inclusions in the sulphide within the breccia veins. Therefore, the quartz veins must have already been present before ore formation at Garson, and were deformed prior or synchronous to sulphide emplacement. The veins may have formed as the result of thermal metamorphism which often involves dehydration reactions associated with consumption and reprecipitation of quartz in host metapelites. This metamorphism could have been related to contact metamorphism or regional metamorphism associated with the Penokean or late orogenic events. The problem with this interpretation is that Hanley et al. (2005) suggested that fluids along the North Range of the SIC, with compositions and thermometric characteristics similar to fluids at Garson, had exsolved from crystallizing magmatic sulphides. They could not have been metamorphic fluids owing to the lack of regional metamorphism associated with the Penokean or later orogenic events. Additionally we have shown that the interpretation of Hanley et al. (2005) does not seem plausible due to the lack of Cu and S in the inclusions in that study and at Garson (Table 3.2).

Using fluid inclusion microthermometric and compositional data, the hypothesis that the fluids at the Garson deposit are metamorphic in origin was tested. Minimum

conditions of entrapment for three-phase fluid inclusions (type IIIA) which homogenize by halite dissolution were constrained by the temperature of halite dissolution (providing a minimum T) and a barometer developed by Becker et al. (2008). Trapping P could only be estimated using this barometer for a few type IIIA inclusion. In part, this is due to the problem of post-entrapment stretching, whereby inclusions that experienced stretching will yield anomalously low (and incorrect) entrapment pressures. These inclusions show anomalously high and variable vapor bubble disappearance temperatures relative to halite dissolution. Inclusions with the lowest vapor-out temperatures relative to halite dissolution temperatures (i.e., the least modified) were used to determine pressure of entrapment. Only three inclusions met the criteria set by Becker et al. (2008) for use of the barometer ($T_h^{L+V+H \rightarrow L+H} < T_d$; $T_h^{L+V+H \rightarrow L+H} > 200^\circ\text{C}$; $T_d > 300^\circ\text{C}$). Figure 3.13 shows the graphical P determination. The three inclusions plotted on this diagram fall between ~1870 and ~2600 bars, corresponding to minimum entrapment depth at a minimum entrapment temperature between ~350 and 450°C (Table 3.1, Appendix B). These entrapment pressures were used to calculate the corresponding depths of entrapment using an average density for overlying rocks of 2800 kg/m³ (i.e., metamorphosed basalts and sedimentary rocks). A range in minimum entrapment depth between 6.5 and 9.1 km is estimated.

The results of this determination are plotted, along with fluid inclusion isochores and other relevant P-T fields, in Figure 3.14. The minimum pressure and temperature of entrapment of type IIIA inclusions that homogenize by halite dissolution (plotted as black boxes in Figure 3.14) fall entirely within the isochore field for type IIA and IIIA (green field in Figure 3.14). Fluid inclusion isochores for type IIA, IIC and IIIA were calculated

using standard equations of state from Zhang and Frantz (1992) and Bowers and Helgeson (1983) and are plotted as a series of coloured fields in Figure 3.14 (fields defined by minimum and maximum isochores in each fluid inclusion assemblage). Only isochore fields for inclusion assemblages that showed narrow ranges in temperature of vapor bubble disappearance and salinity (i.e., unmodified) were modeled. Isochores for type IIA and IIIA inclusions lie within the estimated P-T field for peak metamorphic conditions associated with the Penokean Orogeny for the South Range of the SIC (based on mineral thermobarometry and phase equilibria; Magyarosi, 1998), suggesting that they may represent regional metamorphic fluids trapped at upper greenschist to lower amphibolite conditions, consistent with the reddish-purple CL emission colours observed in their host quartz (Figure 3.5), and the temperature range for final equilibration of sulfarsenides in the ores at Garson that ranges from 300-600°C, with the majority (90%) of sulfarsenide compositions falling between the 500 and 600°C isotherms (see Chapter 2; Lefort et al., 2012, submitted). Alternately, given that fluids of similar fluids are observed on the North Range (i.e., lacking syn-post SIC regional metamorphism) they may represent contact metamorphic fluids or fluids of an exotic origin that were trapped at conditions *coincident* to those of regional metamorphism.

Type IIC and IIA inclusions have similar P-T characteristics; type IIC inclusion isochores pass just to the left of the field determined by Magyarosi (1998) for South Range peak metamorphic conditions. Aside from the presence of a CO₂ liquid phase at room temperature in type IIC fluids, type IIA and IIC fluids are compositionally very similar in terms of trace and major element patterns (Figure 3.11a) and for these reasons, are interpreted here to be genetically related. Anomalously high temperature fluids (e.g.,

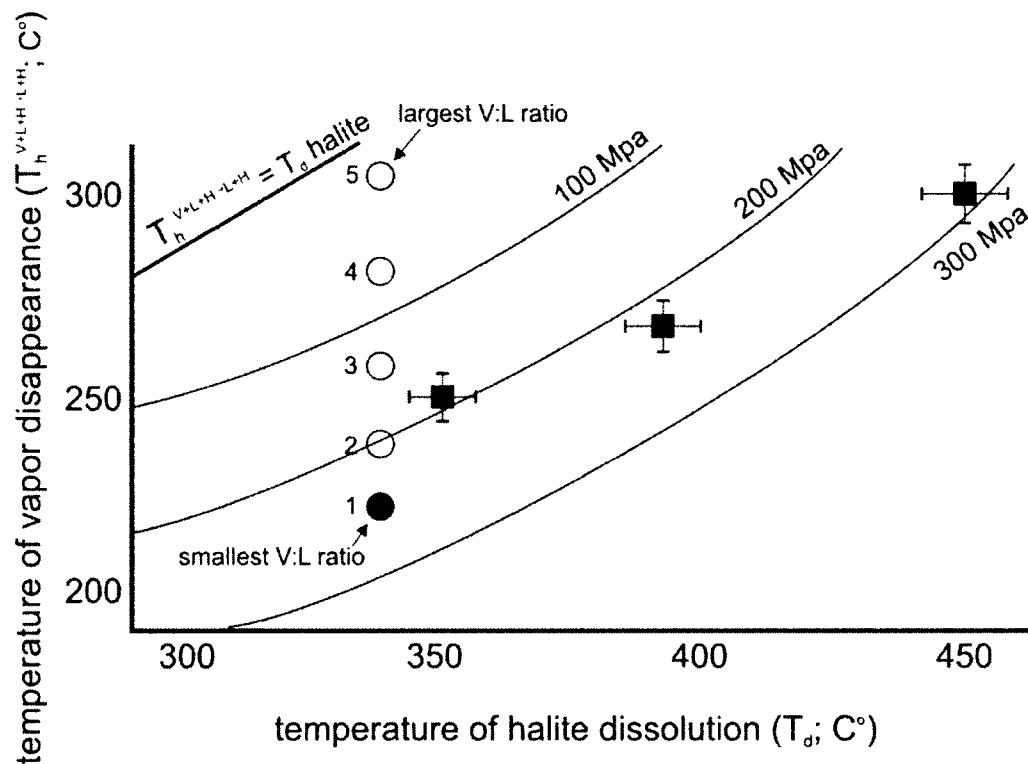


Figure 3.13: Schematic representation showing the relationship between temperature of vapor disappearance and temperature of halite dissolution (after Becker et al., 2008). In the case of post-entrapment stretching, inclusion 1 represents the original inclusion before stretching, and inclusions 2–5 show increasing amounts of stretching. All of these inclusions will show similar temperatures of halite dissolution, but will display a wide range in temperature of vapor bubble disappearance. The inclusion with the lowest temperature of vapor disappearance (inclusion 1; solid black dot) preserves density properties closest the original trapping fluid. Black squares represent inclusions (in this study) that show the least amount of post entrapment modification (highest T_d relative to temperature of vapor disappearance) and provide estimate of minimum trapping pressure. Inclusions that experience over-pressuring after entrapment cannot be used in this figure and would show decrepitation halos. This diagram only applies to inclusions with $T_h^{L+V+H} \rightarrow L < T_d$ (i.e., inclusions that homogenize by halite dissolution).

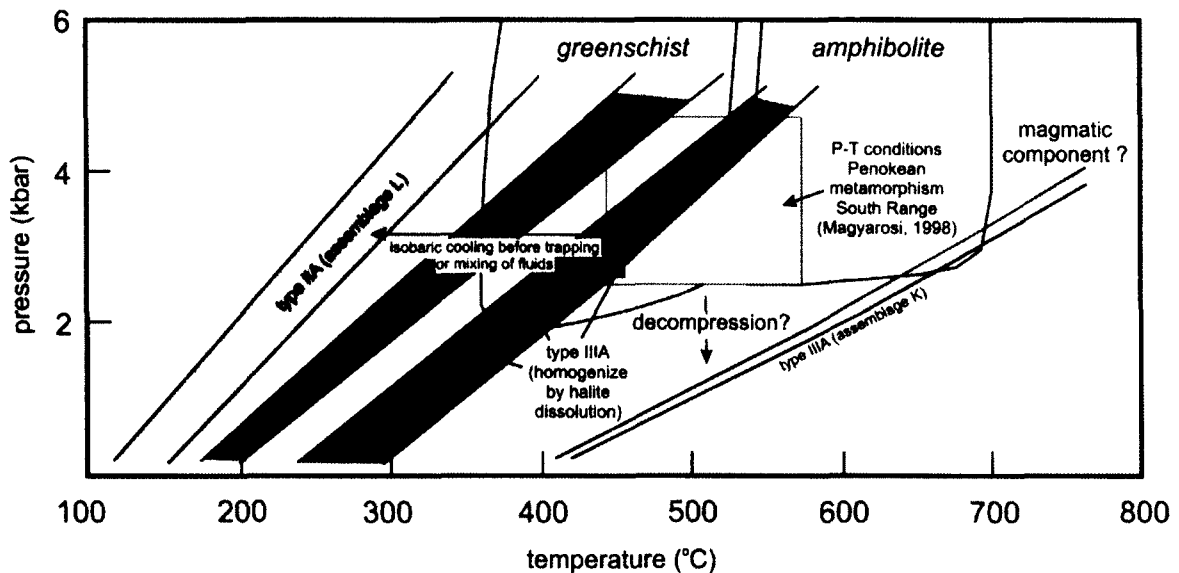


Figure 3.14: Constraints on pressure-temperature (P-T) evolution of dominant fluid types observed at the Garson Mine. P-T diagram shows the position of fluid inclusion isochores for assemblages in which homogenization occurred by vapor bubble disappearance and that showed narrow ranges in homogenization behavior and bulk salinity (little post-entrapment modification). Most isochoric fields pass through the field of conditions estimated from metamorphic mineral assemblages along the South Range (upper greenschist-lower amphibolite; Magyarosi, 1998). Minimum trapping P-T for three type IIIA inclusions that homogenized by halite dissolution are also shown. Assuming constant confining pressure, variations in trapping temperature may be related to isobaric cooling of a single fluid (type IIA) or fluid mixing, whereas variations in bulk salinity (from type IIIA to type IIA inclusions) must be related to mixing. The exception is a single assemblage of type IIIA inclusions that shows anomalously high temperature that may be representative of a magmatic fluid component. Fields for P-T conditions of greenschist and amphibolite facies are adapted from Yardley (1989).

trapped in type IIIA assemblage K; Figure 3.12) may represent a magmatic end-member fluid. Anomalously cooler fluids (e.g., trapped in type IIA assemblage I; Figure 3.12) may be the result of mixing of the metamorphic or exotic fluid with cooler groundwaters, but may also be the result of isobaric cooling of type IIA fluids prior to inclusion entrapment.

With decreasing salinity (transition from type IIA to type IIC fluids), the concentrations of As, Sb, Bi, Pb, and other lithophile trace elements decrease (Figure 3.10), indicating that the solubility of these elements in the Garson environment was a function of fluid salinity, and that they were transported as chloride complexes at the conditions of predicted entrapment. Given that type IIA texturally pre-date type IIIA inclusions (Figure 3.7a), the general trend of increasing salinity from unclassified type IIA to secondary IIIA without a corresponding significant change in temperature may have resulted from mixing of a lower salinity metamorphic fluid with a higher salinity fluid phase (e.g., groundwater or magmatic-derived fluid; Figure 3.8, Figure 3.9, Figure 3.12). Mixing of high and low salinity fluids is observed in many ore deposits and can act as a mechanism for precipitation of ore metals that are remobilized during metamorphism, provided that the metals are introduced by the high salinity end-member (e.g., Force et al., 1986; Sun and Eadington, 1987; Hayashi and Ohmoto, 1991; Haynes et al., 1995; Matthäi et al., 1995; Hayba, 1997; Lefort et al., 2011). However, whereas higher concentrations are observed in higher salinity fluids inclusions at Garson, lower salinity inclusions are not devoid of these elements. Therefore, the transition from type IIA to type IIIA fluids, or type IIA to type IIC, although representative of real compositional changes in bulk salinity did not involve introduction of fluid end-members

uniquely enriched in As, Sb, Bi, Pb, Sr, and Ba. In this case, these elements were present in all fluid variants and must have been commonly sourced via fluid rock interaction or some reservoir that also influenced the composition of North Range fluids simultaneously, in agreement with the previous suggestion of an exotic origin for these fluids despite them being trapped at regional or contact metamorphic conditions.

3.6 Conclusions

Microthermometric studies of pre-mineralization fluid inclusions found in sulphide-quartz breccia veins in the shear-hosted ore zones at the Garson Ni-Cu-PGE deposit indicate the mixing of an early low salinity fluid with a high salinity, slightly higher temperature fluid. Although homogenization temperatures and salinities vary significantly within the whole data set, many single inclusion assemblages show very restricted temperatures of homogenization and salinities. The dominant fluid types at Garson show similar trapping conditions and trace element compositions suggesting that the fluids are genetically related. The range of possible pressures and temperatures for fluid entrapment ($T = \sim 350\text{--}550^\circ\text{C}$; $P = \sim 2\text{--}4.5$ kbar) coincide to upper greenschist-lower amphibolite conditions, and consistent with final equilibration conditions for sulfarsenides in the Garson ores.

This study presents the first LA-ICP-MS data of fluid inclusions from the South Range of the SIC. The quartz-hosted, pre-ore fluids are characterized by high Ca, Ba, As, Sb, Pb, Zn, and Sr, and low Cu, Fe, and S, and are very similar in composition to early (pre-ore) hydrothermal fluids found in the North Range footwall deposits (with the exception to As and Sb; Figure 3.11). This suggests that the fluids at Garson circulated at

a regional scale and were not strongly modified by local host rocks. Trapping of the fluids occurred at the conditions of contact or regional metamorphism but they were not necessarily of metamorphic origin. Low concentrations of Cu and S rule out the possible reaction of the fluids with sulphides, confirming the pre-ore timing of the fluids. The high concentrations of As within the fluids may have been sourced from the surrounding metasedimentary rocks of the Stobie and the McKim formations.

3.7 References

- Ballhaus, C. G. and Stumpfl, E. F., 1986, Sulphide and platinum mineralization in the Merensky Reef: evidence from hydrous silicates and fluid inclusions. *Contributions of Mineralogy and Petrology*, v. 94, p. 193-204.
- Becker, S. P., Fall, A., and Bodnar, R. J., 2008, Synthetic fluid inclusions. XVII. PVTX properties of high salinity H₂O-NaCl solutions (>30 wt% NaCl): Application to fluid inclusions that homogenize by halite disappearance from porphyry copper and other hydrothermal ore deposits: *Economic Geology*, v. 103, p. 539-554.
- Bodnar, R.J., 1994, Synthetic fluid inclusions: XII. The system H₂O–NaCl. Experimental determination of the halite liquidus and isochores for a 40 weight percent NaCl solution: *Geochimica et Cosmochimica Acta*, v. 58, p. 1053–1063.
- Boggs, Jr., S., Kwon, Y-I., Goles, G.G., Rusk, B.G., Krinsley, D., and Seyedolali, A., 2002, Is quartz cathodoluminescence color a reliable provenance tool? A quantitative examination: *Journal of Sedimentary Research*, v. 73, p. 408-415.
- Bowers, T.S., and Helgeson, H.C., 1983, Calculation of the thermodynamic and geochemical consequences of nonideal mixing in the system H₂O-CO₂-NaCl on phase relations in geologic systems: metamorphic equilibria at high pressures and temperature: *American Mineralogist*, v. 68, p. 1059-1075.
- Cabri, L.J., and Laflamme, J.H.G., 1976, The mineralogy of the platinum group elements from some copper-nickel deposits of the Sudbury area, Ontario: *Economic Geology*, v. 71, p. 1159–1195.
- Coats, C.J.A., and Snajdr, P., 1984, Ore deposits in the North Range, Onaping Levack area, Sudbury, in E.G. Pye, A.J. Naldrett, P. Giblin, eds., *The Geology and Ore Deposits of the Sudbury Structure*: Ontario Geological Survey, Spec. Pub. v. 1, p. 327-346.
- Crawford, M.L., Kraus, D.W., and Hollister, L.S., 1979, Petrologic and fluid inclusion study of calc-silicate rocks: Prince Rupert, British Columbia. *American Journal of Science*, v. 279, p. 1135-1159.
- Dare, S.A., Barnes, S.J., Prichard, H.M., Fisher, P.C., 2010, The timing and formation of platinum-group minerals from the Creighton Ni-Cu-platinum group element sulphide deposit, Sudbury, Canada: early crystallization of PGE-rich sulfarsenides: *Economic Geology*, v. 105, p.1071-1096.
- Darling, R.S., 1991, An extended equation to calculate NaCl contents from final clathrate melting temperatures in H₂O-CO₂-NaCl fluid inclusions: Implications for P-T isochore location: *Geochimica Cosmochimica Acta*, v. 55, p. 3869 –3871.

- Diamond, L.W., 1992, Stability of CO₂ clathrate hydrate + CO₂ liquid + CO₂ + aqueous KCl-NaCl solutions: Experimental determination and application to salinity estimates of fluid inclusions: *Geochimica Cosmochimica Acta*, v. 56, p. 273-280.
- Farrow, C.E.G., and Watkinson, D.H., 1992, Alteration and the role of fluids in Ni, Cu and platinum-group element deposition, Sudbury Igneous Complex contact, Onaping-Levack area, Ontario: *Mineralogy and Petrology*, v. 46, p. 67-83.
- Farrow, C. E. G., and Watkinson, D. H., 1997, Diversity of precious-metal mineralization in footwall Cu-Ni-PGE deposits, Sudbury, Ontario: Implications for hydrothermal models of formation: *Canadian Mineralogist*, v. 35, p. 817-839.
- Farrow, C.E.G., and Lightfoot, P.C., 2002, Sudbury PGE revisited: Toward an integrated model: *Canadian Institute of Mining, Metallurgy and Petroleum Special Volume 54*, p. 13-130.
- Farrow, C. E. G, Watkinson, D. H., and Jones, P. C., 1994, Fluid inclusions in sulphides from North and South Range Cu-Ni-PGE deposits, Sudbury structure, Ontario. *Economic Geology*; v. 89, p. 647-655.
- Force, E. R., Back, W., Spiker, E. C., and Knauth, L. P., 1986, A ground-water mixing model for the origin of the Imini Manganese deposit (Cretaceous) of Morocco: *Economic Geology*, v. 81, p. 65-79.
- Frape, S.K., and Fritz, P., 1982, The chemical and isotopic composition of saline groundwaters from the Sudbury basin: *Canadian Journal of Earth Sciences*, v. 19, p. 645-661.
- Fueten, F., Redmond, D.J., 1997, Documentation of a 1450 Ma contractional orogeny preserved between the 1850 Ma Sudbury impact structure and the 1 Ga Grenville orogenic front, Ontario. *Geological Society of America Bulletin* 109, 268-279.
- Goldstein, R. H., 2003, Petrographic analysis of fluid inclusions, *in* Samson, I., Marshall, D. and Anderson, A. eds., *Fluid Inclusions: analysis and Interpretation: Mineralogical Association of Canada, Short Course Series*. v. 32, p. 9-54.
- Gorobets, B.S., and Rogojine, A.A., 2002, Luminescent spectra of minerals: All-Russia Institute of Mineral Resources (VIMS), Moscow, 302 p.
- Götze, J., 2000, Cathodoluminescence microscopy and spectroscopy in applied mineralogy: TU Bergakademie Freiberg Akademische Buchhandlung Merbachstrasse, Freiberg, 128 p.
- Greenwood, H.J., 1975, Buffering of pore fluids by metamorphic reactions: *American Journal of Science*, v. 275, p. 573-593.

Guillong, M.M., Maier, D.L., Allan, M.M., Heinrich, C.A., and Yardley, B.W.D., 2008, Appendix A6: SILLS: a MATLAB based program for the reduction of laser ablation ICP-MS data of homogeneous materials and inclusions, *in* Sylvester P., ed., *Laser Ablation ICP-MS in the Earth Sciences: Current Practices and Outstanding Issues*: Mineralogical Association of Canada Short Course Series, v. 40, 6 p.

Günther, D., and Heinrich, C., 1999, Comparison of the ablation behaviour of 266 nm Nd: YAG and 193 nm ArF excimer lasers for LA-ICP-MS analysis. *Journal of Analytical atomic Spectrometry*, v. 14, p. 1369-1374.

Hanley, J.J., 2006, Experimental and fluid inclusion constraints on the ore metal content and origin of volatiles associated with large Ni-Cu-PGE deposits: Ph.D. thesis, Canada, University of Toronto. 285 p.

Hanley, J.J., Mungall, Pettke, T., Spooner, E.T.C., and Bray, C.J., 2005, Ore metal redistribution by hydrocarbon-brine and hydrocarbon-halide melt phases, North Range footwall of the Sudbury Igneous Complex, Ontario, Canada: *Mineralium Deposita*, v. 40, p. 237-256.

Hanley, J.J., Mungall, J.E., Pettke, T., Spooner, E.T.C., and Bray, C., 2008, Fluid and melt inclusions of magmatic origin in the Ultramafic and Lower Banded Series, Stillwater Complex, Montana, U.S.A.: *Journal of Petrology*, v. 49, p. 1133-1160.

Hanley, J.J., Ames, D.E., Barnes, J., Sharp, Z.D., 2011, Interaction of magmatic fluids and silicate residues with saline groundwater in the footwall of the Sudbury Igneous Complex, Ontario, Canada: new evidence from bulk rock geochemistry, fluid inclusions and stable isotopes: *Chemical Geology*, v. 281, p. 1-25.

Hayashi, K.I. and Ohmoto, H., 1991, Solubility of gold in NaCl- and H₂S-bearing aqueous solutions at 250–350°C: *Geochimica et Cosmochimica Acta*, v. 55, p. 2111-2126.

Hayba, D. O., 1997, Environment of ore deposition in the Creede mining district, San Juan Mountains, Colorado; Part V, epithermal mineralization from fluid mixing in the OH vein: *Economic Geology*, v. 92, p. 29-44.

Haynes, D. W., Cross, K. C., Bills, R. T., and Reed, M. H., 1995, Olympic Dam ore genesis: A fluid-mixing model: *Economic Geology*, v. 90, p. 281-307.

Hewitt, D.A., 1973, The metamorphism of micaceous limestones from south-central Connecticut: *American Journal of Science*, v. 273A, p. 444-446.

Kouzmanov, K., Petke, T., Heinrich, C.A., 2010, Direct Analysis of Ore-Precipitating Fluids: Combined IR Microscopy and LA-ICP-MS Study of Fluid Inclusions in Opaque Ore Minerals: *Economic Geology*, v. 105, p. 351-373.

Lamb, W., and Valley, J.W., 1984, Metamorphism of reduced granulites in low CO₂ vapor-free environment: *Nature*, v. 312, p. 56-58.

Lefort, D. T., Hanley, J. J., and Guillon, M., 2011, Subepithermal Au-Pd mineralization associated with an Alkaline porphyry Cu-Au deposit, Mount Milligan, Quesnel Terrane, British Columbia, Canada: *Economic Geology*, v. 106, p. 781-808.

Li, C., and Naldrett, A.J., 1993, Platinum-group minerals from the Deep copper zone of the Strathcona deposits, Sudbury, Ontario: *Canadian Mineralogist*, v. 31, p. 31-44.

Li, C., Naldrett, A.J., Rucklidge, J.C., and Kilian, L.R., 1993, Concentration of platinum-group elements and gold in sulphides from the Strathcona deposit, Sudbury, Ontario: *Canadian Mineralogist*, v. 31, p. 523-531.

Magyarosi, Z., 1998, Metamorphism of the Proterozoic rocks associated with the Sudbury Structure: Unpublished M. Sc. Thesis, Carlton University, Ottawa, Canada, 101 p.

Marshall, D.J., 1988, Cathodoluminescence of geological materials: Unwin-Hyman, Boston, 146 p.

Marshall, D., Watkinson, D., Farrow, C., Molnár, F., and Fouillac, A.M., 1999, Multiple fluid generations in the Sudbury igneous complex: fluid inclusion, Ar, O, H, Rb and Sr evidence: *Chemical Geology*, v. 154, p. 1-19.

Matthäi, S. K., Henly, R. W., and Heinrich, C. A., 1995, Gold precipitation by fluid mixing in bedding parallel fractures near carbonaceous slates at the Cosmopolitan Howley gold deposit, northern Australia: *Economic Geology*, v. 90, p. 2123-2142.

Mavrogenes, J.A. and Bodnar, R.J., 1994, Experimental evidence and geologic implications of hydrogen movement into and out of fluid inclusions in quartz: *Geochimica et Cosmochimica Acta*, v. 58, p. 141-148.

Molnár, F., Watkinson, D.H., Jones, P.C. and Gatter, I., 1997, Fluid inclusion evidence for hydrothermal enrichment of magmatic ore at the contact zone of the Ni-Cu-platinum-group element 4b deposit, Lindsley Mine, Sudbury, Canada: *Economic Geology*, v. 92, p. 674-685.

Molnár, F., Watkinson, D.H. and Everest, J.O., 1999, Fluid-inclusion characteristics of hydrothermal Cu-Ni-PGE veins in granitic and metavolcanic rocks at the contact of the Little Stobie deposit, Sudbury, Canada: *Chemical Geology*, v. 154, p. 279-301.

Molnár, F., Watkinson, D.H. and Jones, P.C., 2001, Multiple hydrothermal processes in footwall units of the North Range, Sudbury Igneous Complex, Canada, and implications for the genesis of vein-type Cu-Ni-PGE deposits: *Economic Geology*, v. 96, p. 1645-1670.

Mukwakwami, J., Lafrance, B., and Leshner, C.M., 2011a, Deformation and remobilization of Ni-Cu-PGE ores at Garson Mine, Sudbury, Ontario; GAC-MAC-SEG-SGA Joint Annual meeting, Ottawa, Ontario, Program Abstracts, p.147.

Mukwakwami, J., Lafrance, B., and Leshner, C.M., 2011b, Back-Thrusting and Overturning of the Southern Margin of the 1.85 Ga Sudbury Igneous Complex at the Garson Mine, Sudbury, Ontario: Precambrian Research; in press.

Mungall, J.E., Ames, D.E., and Hanley, J.J., 2004, Magmatic sulfide deposits: Geology, geochemistry and exploration: Berlin, Springer, 727 p.

Pagel, M., Barbin, V., Blanc, P., Ohnenstetter, D., 2000, Cathodoluminescence: Springer-Verlag, Berlin, Heidelberg, New York, 529.

Péntek, A., Molnár, F., Watkinson, D.H. and Jones, P.C., 2008, Footwall-type Cu-Ni-PGE mineralization in the Broken Hammer area, Wisner Township, North Range, Sudbury Structure: Economic Geology, v. 103, p. 1005-1028.

Pettke, T., Halter, W. E., Webster, J. D., Aigner-Torres, M., and Heinrich, C.A., 2004, Accurate quantification of melt inclusion chemistry by LA-ICP-MS: a comparison with EMP and SIMS and advantages and possible limitations of these methods: Lithos, v. 78, p. 333-361.

Pudack, C., Halter, W. E., Heinrich C. A., and Pettke, T., 2009, Evolution of Magmatic Vapor to Gold-Rich Epithermal Liquid: The Porphyry to Epithermal Transition at Nevados de Famatina, Northwest Argentina: Economic Geology, v. 104, no. 4, p. 449-477.

Shanks, W.S. and Schwerdtner, W.M., 1991a, Structural analysis of the central and southwestern Sudbury Structure, Southern Province, Canadian Shield. Canadian Journal of earth Sciences; v. 28, 411-430.

Shanks, W.S. and Schwerdtner, W.M., 1991b, Crude quantitative estimates of the original northwest-southeast dimension of the Sudbury Structure, south-central Canadian Shield. Canadian Journal of earth Sciences; v. 28, p. 1677-1686.

Shepherd, T. J., Rankin, A. H. and Alderton, D.H.M., 1985, A Practical Guide to Fluid Inclusions: Blackie, Glasgow, 239 p.

Sisson, V. B., and Hollister, L. S., 1990, A fluid-inclusion study of metamorphosed polytic and carbonate rocks, south central Maine: American Mineralogist, v. 75, p. 59-70.

Sprunt, E.S., Dengler, L.A., Sloan, D., 1978, Effects of metamorphism on quartz cathodeluminescence: *Geology*, v. 6, 305-308.

Steele-MacInnis, M., Bodnar, R.J., and Naden, J., 2011, Numerical model to determine the composition of H₂O-NaCl-CaCl₂ fluid inclusions based on microthermometric and microanalytical data: *Geochimica et Cosmochimica Acta*, v. 75, p. 21-40.

Sun, S. S., and Eadington, P. J., 1987, Oxygen isotope evidence for the mixing of magmatic and meteoric waters during Tin mineralization in the Mole Granite, New South Wale, Australia: *Economic Geology*, v. 82, p. 43-52.

Thompson, A.B., 1983, Fluid-absent metamorphism: *Journal of the Geological Society of London*, v. 140, p. 533-54

Wilkinson, J. J., 2001, Fluid inclusions in hydrothermal ore deposits: *Lithos*, v. 55, p. 229-272.

Yardley, B.W.D., 1989, An introduction to metamorphic petrology: Prentice Hall, London, 264 p.

Zhang, Y. and Frantz, J.D., 1987, Determination of the homogenization temperatures and densities of supercritical fluids in the system NaCl-KCl-CaCl₂-H₂O using synthetic fluid inclusions: *Chemical Geology*, v. 64, p. 335-350.

Appendix B

Table 3.1 Microthermometric data for inclusions from the Garson deposit

| Sample | Chip | $T_m^{H_2O}$ | T_m^{L-V} | $T_h^{L-V-H_2O}$ | T_h^{L-V-S} | T_h | Clath _m | T_{ho} | $T_{ho}^{CO_2}$ | wt% NaCl _{eq} | wt% CaCl ₂ _{eq} | Size (µm) | Phase | Type | Origin | Assemblage |
|--------|--------|--------------|-------------|------------------|---------------|-------|--------------------|----------|-----------------|------------------------|-------------------------------------|-----------|---------|------|--------------|------------|
| A11 | Chip 2 | - | 193.7 | - | - | - | - | - | - | - | - | 10 | H-L-V | IIA | Secondary | |
| A11 | Chip 2 | - | 347.7 | - | - | - | - | - | - | - | - | 10 | H-L-V | IIA | Secondary | |
| A11 | Chip 2 | - | 218.9 | - | - | - | - | - | - | - | - | 8 | H-L-V | IIA | Secondary | |
| A11 | Chip 2 | - | 298.6 | - | - | - | - | - | - | - | - | 5 | L-V | IIA | Secondary | |
| A11 | Chip 2 | - | 240.1 | - | - | - | - | - | - | - | - | 3 | L-V | IIA | Secondary | |
| A11 | Chip 2 | - | 298.3 | - | - | - | - | - | - | - | - | 3 | L-V | IIA | Unclassified | |
| A11 | Chip 1 | - | 165.8 | - | - | 165.8 | - | - | - | 30.27 | - | 15 | H-L-V | IIA | Secondary | a |
| A11 | Chip 1 | - | 322.5 | - | - | 198.8 | - | - | - | 31.8 | - | 9 | H-L-V | IIA | Secondary | a |
| A11 | Chip 1 | - | 268.9 | - | - | 202.3 | - | - | - | 31.98 | - | 10 | H-L-V | IIA | Secondary | a |
| A11 | Chip 1 | - | 277 | - | - | - | - | - | - | - | - | 10 | L-V | IIA | Secondary | a |
| A11 | Chip 1 | - | 350 | - | - | 293.3 | - | - | - | 37.63 | - | 12 | H-L-V | IIA | Secondary | a |
| A11 | Chip 1 | -24.6 | 212.5 | - | - | 183.2 | - | - | - | 31.06 | 27.7 | 9 | H-L-V | IIA | Unclassified | b |
| A11 | Chip 1 | - | 304.3 | - | - | 239.6 | - | - | - | 34.64 | - | 12 | H-L-V | IIA | Unclassified | b |
| A11 | Chip 1 | - | 298.1 | - | - | 350 | - | - | - | 39.93 | - | 15 | H-L-V | IIA | Secondary | |
| A11 | Chip 1 | - | 289.4 | - | - | 253.5 | - | - | - | 34.87 | - | 15 | H-L-V | IIA | Secondary | c |
| A11 | Chip 1 | - | 254.3 | - | - | 350 | - | - | - | 42.5 | - | 20 | H-L-V | IIA | Secondary | c |
| A11 | Chip 1 | - | 308.5 | - | - | 196.1 | - | - | - | 31.68 | - | 40 | H-L-V | IIA | Secondary | |
| A11 | Chip 1 | - | 320 | - | - | - | 5.6 | - | - | 8.1 | - | 10 | L-V | IIA | Secondary | d |
| A11 | Chip 1 | -15.7 | 211.5 | - | - | - | - | - | - | 19.21 | - | 3 | L-V | IIA | Secondary | d |
| A11 | Chip 1 | -15.1 | 200.7 | - | - | - | - | - | - | 18.72 | - | 3 | L-V | IIA | Secondary | d |
| A11 | Chip 1 | - | 247.4 | - | - | - | - | - | - | - | - | 3 | L-V | IIA | Secondary | d |
| A11 | Chip 1 | - | 231.8 | - | - | 230.8 | - | - | - | 33.52 | - | 10 | H-L-V | IIA | Secondary | e |
| A11 | Chip 1 | - | 233.7 | - | - | 263 | - | - | - | 35.52 | - | 20 | H-L-V | IIA | Secondary | |
| A11 | Chip 1 | - | 228.3 | - | - | 234.5 | - | - | - | 33.74 | - | 10 | H-L-V | IIA | Secondary | |
| A11 | Chip 1 | -27.2 | 327.7 | - | - | - | - | - | - | - | 30.2 | 10 | L-V | IIA | Secondary | f |
| A11 | Chip 1 | - | 235.3 | - | - | 238 | - | - | - | 33.95 | - | 10 | H-L-V | IIA | Secondary | f |
| A28 | Chip 1 | - | 96.3 | - | - | 147.9 | - | - | - | 29.58 | - | 20 | H-L-V-U | IIIC | Secondary | |
| A28 | Chip 1 | -26.2 | 115.9 | - | - | - | - | - | - | - | 29.2 | 18 | L-V | IIA | Secondary | |
| A28 | Chip 1 | -3.7 | - | -4.6 | 340 | - | - | - | - | 6.01 | - | 15 | L-V-V | IIIC | Unclassified | |
| A28 | Chip 1 | -5 | 315.8 | - | - | - | - | - | - | 7.86 | - | 20 | L-V | IIIB | Unclassified | |
| A28 | Chip 1 | -5.1 | 280.7 | - | - | - | - | - | - | 8 | - | 15 | L-V | IIA | Unclassified | |
| A28 | Chip 1 | -4.4 | 249.8 | - | - | - | - | - | - | 7.02 | - | 15 | L-V | IIA | Unclassified | |
| A28 | Chip 1 | - | 336.5 | - | - | 326.7 | - | - | - | 40.35 | - | 15 | H-L-V | IIA | Unclassified | |
| A28 | Chip 1 | - | 470 | - | - | 454.1 | - | - | - | 53.76 | - | 20 | H-L-V | IIA | Unclassified | |
| A28 | Chip 1 | - | 335.1 | - | - | - | - | - | - | - | - | 10 | H-L-V | IIA | Secondary | |
| A28 | Chip 1 | - | 309.4 | - | - | - | 217.8 | - | - | - | - | 15 | L-V | IIA | Unclassified | |
| A28 | Chip 1 | - | 440.9 | - | - | 470 | - | - | - | 55.79 | - | 20 | H-L-V | IIA | Secondary | |
| A28 | Chip 1 | - | 313.2 | - | - | 470 | - | - | - | 55.79 | - | 15 | H-L-V | IIA | Secondary | |
| A28 | Chip 1 | - | 286.5 | - | - | 470 | - | - | - | 55.79 | - | 15 | H-L-V | IIA | Secondary | |
| A28 | Chip 1 | - | 346.3 | - | - | 403.2 | - | - | - | 38.4 | - | 8 | H-L-V | IIA | Unclassified | |
| A28 | Chip 2 | -10.7 | 269.7 | - | - | - | - | - | - | 14.67 | - | 15 | L-V | IIA | Unclassified | g |
| A28 | Chip 2 | -12.5 | 225.6 | - | - | - | - | - | - | 16.43 | - | 12 | L-V | IIA | Unclassified | g |
| A28 | Chip 2 | -11.9 | 241.4 | - | - | - | - | - | - | 15.86 | - | 10 | L-V | IIA | Unclassified | g |
| A28 | Chip 2 | -12.5 | 275.4 | - | - | - | - | - | - | 16.43 | - | 10 | L-V | IIA | Unclassified | g |
| A28 | Chip 2 | -11.7 | 244.2 | - | - | - | - | - | - | 15.67 | - | 8 | L-V | IIA | Unclassified | g |
| A28 | Chip 2 | -17.4 | 233.9 | - | - | - | - | - | - | 20.52 | - | 10 | L-V | IIA | Unclassified | h |
| A28 | Chip 2 | -17.1 | 246.5 | - | - | - | - | - | - | 20.3 | - | 8 | L-V | IIA | Unclassified | h |
| A28 | Chip 2 | -15.4 | 252.2 | - | - | - | - | - | - | 18.96 | - | 10 | L-V | IIA | Unclassified | h |
| A28 | Chip 2 | -15 | 247.1 | - | - | - | - | - | - | 18.63 | - | 5 | L-V | IIA | Unclassified | h |
| A28 | Chip 2 | -15 | 238.5 | - | - | - | - | - | - | 18.63 | - | 5 | L-V | IIA | Unclassified | h |
| A28 | Chip 2 | - | 200.0 | - | - | - | - | 19.7 | - | - | - | 20 | ? | ? | Secondary | |
| A28 | Chip 2 | - | 210.1 | - | - | - | - | 12.5 | - | - | - | 5 | ? | ? | Secondary | |
| A28 | Chip 2 | - | 211.2 | - | - | - | - | 12.3 | - | - | - | 5 | ? | ? | Secondary | |
| A28 | Chip 2 | -11.9 | 242.9 | - | - | - | - | - | - | 15.86 | - | 12 | L-V | IIA | Unclassified | |
| A28 | Chip 2 | -6.5 | 294.1 | - | - | - | - | - | - | 9.86 | - | 10 | L-V | IIA | Unclassified | |
| A28 | Chip 2 | -4 | 247.9 | - | - | - | - | - | - | 6.45 | - | 10 | L-V | IIA | Unclassified | |
| A28 | Chip 2 | -3.7 | 225 | - | - | - | - | - | - | 6.01 | - | 8 | L-V | IIA | Unclassified | i |
| A28 | Chip 2 | -4.8 | 245.8 | - | - | - | - | - | - | 7.59 | - | 15 | L-V | IIA | Unclassified | i |
| A28 | Chip 2 | -4 | 266.2 | - | - | - | - | - | - | 6.45 | - | 8 | L-V | IIA | Unclassified | i |
| A31 | Chip 1 | - | 405 | - | - | 155.2 | - | - | - | 29.86 | - | 15 | H-L-V | IIA | Secondary | |
| A31 | Chip 1 | - | 405 | - | - | 405 | - | - | - | 47.99 | - | 20 | H-L-V | IIA | Secondary | |
| A31 | Chip 2 | - | 288.6 | - | - | 264.5 | - | - | - | 35.61 | - | 15 | H-L-V | IIA | Secondary | |
| A31 | Chip 2 | - | 405 | - | - | 363 | - | - | - | 43.63 | - | 20 | H-L-V | IIA | Unclassified | |
| A31 | Chip 3 | - | 425 | - | - | 324.1 | - | - | - | 40.1 | - | 15 | H-L-V | IIA | Unclassified | |
| A31 | Chip 3 | -25.6 | 374.6 | - | - | 236.5 | - | - | 27.9 | 33.83 | 28.6 | 15 | H-L-V | IIA | Unclassified | |
| A31 | Chip 3 | - | 302.3 | - | - | 341.5 | - | - | - | 41.62 | - | 15 | H-L-V | IIA | Secondary | |
| A31 | Chip 3 | -26 | 304.8 | - | - | 138.8 | - | - | 26.8 | - | 29 | 8 | H-L-V | IIA | Unclassified | |
| A31 | Chip 3 | - | 247.1 | - | - | 292.8 | - | - | - | 37.63 | - | 8 | H-L-V | IIA | Unclassified | |
| A31 | Chip 3 | - | 271.8 | - | - | 389.3 | - | - | - | 46.26 | - | 10 | H-L-V | IIA | Unclassified | |
| A31 | Chip 3 | -25.7 | - | - | - | - | 13.2 | - | - | - | 28.7 | 20 | L-V | IIA | Secondary | |
| A31 | Chip 3 | - | 302.9 | - | - | 450 | - | - | - | 53.26 | - | 15 | H-L-V | IIA | Secondary | |
| A31 | Chip 3 | -26.9 | 358.4 | - | - | 299.1 | - | - | 27.5 | 38.1 | 29.9 | 15 | H-L-V | IIA | Secondary | |
| A31 | Chip 4 | - | 200 | - | - | 255.3 | - | - | - | 35 | - | 25 | H-L-V | IIA | Unclassified | |
| A31 | Chip 4 | -38.9 | - | - | - | - | - | - | - | - | 42 | 15 | L | IA | Unclassified | j |

$T_m^{H_2O}$: ice melting temperature; $T_h^{L-V-H_2O}$: temperature of homogenization final vapor; T_h^{L-V-S} : temperature of homogenization CO₂ vapor bubble; T_h^{L-V-U} : temperature of homogenization of CO₂; liquid phase; T_h : temperature of halite dissolution; Clath_m: clathrate melting temperature; T_{ho} : hydrohalite dissolution temperature; $T_{ho}^{CO_2}$: temperature of transition from hydrohalite to halite crystal

List of abbreviations: H= halite; L= liquid; S= sylvite; U= unknown; V= vapor; xtal= crystal
Measurements with a * indicate the heating limit for that sample

Table 3.1 (Cont.) Microthermometric data for inclusions from the Garson deposit

| Sample | Chip | $T_m^{(a)}$ | $T_h^{(1,2,3)}$ | $T_h^{(3,4,5,6,7)}$ | $T_h^{(1,2,3,4)}$ | T_d | $Clath_{(m)}$ | $T_{(h)}^{(b)}$ | $T_{(h)}^{(c)}$ | wt% NaCl _{total} | wt% CaCl ₂ _{total} | Size (µm) | Phase | Type | Origin | Assemblage |
|--------|--------|-------------|-----------------|---------------------|-------------------|-------|---------------|-----------------|-----------------|---------------------------|--|-----------|----------|------|-----------------|------------|
| A31 | Chip 4 | - | - | - | - | - | - | - | - | - | - | 10 | L | IA | Unclassified | j |
| A31 | Chip 4 | - | 245.4 | - | - | 157.4 | - | - | - | 29.96 | - | 15 | H-L-V | IIA | Secondary | |
| A31 | Chip 4 | 28.2 | 249.2 | - | - | 181.2 | - | - | - | 30.97 | 31.2 | 10 | H-L-V | IB | Secondary | |
| A31 | Chip 4 | - | 249.3 | - | - | 241.2 | - | - | - | 34.13 | - | 15 | H-L-V-S? | IIIB | Secondary | |
| A31 | Chip 4 | -25.9 | 219.8 | - | - | - | - | 15.6 | - | - | 28.9 | 12 | L-V | IIA | Unclassified | |
| A31 | Chip 5 | - | 352.1 | - | - | 339.6 | - | - | - | 41.45 | - | 15 | H-L-V | IIA | Secondary | |
| A31 | Chip 5 | - | 406.6 | - | - | 266.6 | - | - | - | 35.75 | - | 10 | H-L-V | IIA | Unclassified | k |
| A31 | Chip 5 | - | 417.7 | - | - | 277 | - | - | - | 36.47 | - | 20 | H-L-V-S | IIIB | Unclassified | k |
| A31 | Chip 5 | - | - | - | - | 285.5 | - | - | - | 37.7 | - | 15 | H-L-V | IIA | Unclassified | k |
| A31 | Chip 5 | - | 470 | - | - | 470 | - | - | - | 55.79 | - | 15 | H-L-V | IIA | Secondary | |
| A31 | Chip 5 | - | 283.7 | - | - | 329.6 | - | - | - | 40.58 | - | 12 | H-L-V | IIA | Secondary | |
| A54 | Chip 1 | -14.2 | 109.8 | - | - | - | - | - | - | 17.96 | - | 15 | L-V | IIA | Unclassified | |
| A54 | Chip 1 | -12.3 | 157.5 | - | - | - | - | - | - | 16.24 | - | 15 | L-V | IIA | Unclassified | |
| A54 | Chip 1 | -14.6 | 163.1 | - | - | - | - | - | - | 18.3 | - | 15 | L-V | IIA | Unclassified | |
| A54 | Chip 1 | -13 | 120.3 | - | - | - | - | - | - | 16.89 | - | 15 | L-V | IIA | Unclassified | |
| A54 | Chip 1 | -13.9 | 157.3 | - | - | - | - | - | - | 17.7 | - | 10 | L-V | IIA | Unclassified | |
| A54 | Chip 1 | -23.7 | 136.2 | - | - | - | - | - | - | - | 26.7 | 10 | H-L-V | IIA | Unclassified | |
| A54 | Chip 1 | -19.1 | 155 | - | - | - | - | - | - | 21.75 | - | 8 | L-V | IIA | Unclassified | |
| A54 | Chip 1 | -? | 181.8 | - | - | - | - | - | - | - | - | 12 | L-V | IIA | Unclassified | |
| A54 | Chip 1 | - | 143.1 | - | - | - | - | - | - | - | - | 8 | H-L-V | IIA | Secondary | |
| A54 | Chip 2 | -24.7 | 150 | - | - | - | - | - | - | - | 27.7 | 8 | L-V | IIA | Unclassified | |
| A54 | Chip 2 | -26 | 162.1 | - | - | - | - | - | - | - | 29 | 8 | L-V | IIA | Unclassified | |
| A54 | Chip 2 | - | 135.5 | - | - | - | - | - | - | - | - | - | - | - | Secondary | |
| A54 | Chip 2 | -24.3 | 132.9 | - | - | - | - | - | - | - | 27.3 | 10 | L-V | IIA | Unclassified | |
| A54 | Chip 2 | -24.6 | 127.5 | - | - | - | - | - | - | - | 27.6 | - | L-V | IIA | Unclassified | |
| A54 | Chip 2 | - | 143.1 | - | - | - | 7.8 | - | - | 4.33 | - | - | L-V | IIA | Unclassified | |
| A54 | Chip 2 | - | 166.3 | - | - | 400 | - | - | - | 47.44 | - | 8 | H-L-V | IIA | Unclassified? | |
| A54 | Chip 2 | -23.6 | 237.8 | - | - | - | - | - | - | - | 26.6 | 10 | L-V | IIA | Secondary | |
| A54 | Chip 2 | - | 237.2 | - | - | - | - | - | - | - | - | 8 | L-V | IIA | Secondary | |
| A54 | Chip 2 | -13.9 | 123 | - | - | - | - | - | - | 17.7 | - | 8 | L-V | IIA | Unclassified | l |
| A54 | Chip 2 | -14.1 | 120.2 | - | - | - | - | - | - | 17.87 | - | 8 | L-V | IIA | Unclassified | l |
| A54 | Chip 2 | -14.1 | 106.6 | - | - | - | - | - | - | 17.87 | - | 10 | L-V | IIA | Unclassified | l |
| A54 | Chip 2 | -12.5 | 143.6 | - | - | - | - | - | - | 16.43 | - | 12 | L-V | IIA | Unclassified | l |
| A54 | Chip 2 | -11.7 | 121.7 | - | - | - | - | - | - | 15.67 | - | 10 | L-V | IIA | Pseudosecondary | |
| A54 | Chip 2 | -17.1 | 108.4 | - | - | - | - | - | - | 20.3 | - | 10 | L-V | IIA | Pseudosecondary | |
| A54 | Chip 2 | -18.6 | 100.6 | - | - | - | - | - | - | 21.4 | - | 10 | L-V | IIA | Pseudosecondary | |
| A54 | Chip 2 | -16.6 | 129.1 | - | - | - | - | - | - | 19.92 | - | 10 | L-V | IIA | Pseudosecondary | |
| A82 | Chip 1 | - | 99.6 | - | - | - | - | - | - | - | - | 20 | L-V | IIA | Secondary | |
| A82 | Chip 1 | - | 101.3 | - | - | - | - | - | - | - | - | 20 | L-V | IIA | Secondary | |
| A82 | Chip 1 | - | 98.3 | - | - | - | - | - | - | - | - | 30 | L-V | IIA | Secondary | |
| A82 | Chip 1 | - | 99.7 | - | - | - | - | - | - | - | - | 20 | L-V | IIA | Secondary | |
| A82 | Chip 2 | -24.2 | 245.8 | - | - | - | - | - | - | - | 27.2 | 5 | L-V | IIA | Unclassified | |
| A82 | Chip 2 | -26.1 | 173.1 | - | - | - | - | - | - | - | 29.1 | 8 | L-V | IIA | Unclassified | |
| A82 | Chip 2 | - | 286.9 | - | - | - | - | - | - | - | - | 5 | L-V | IIA | Secondary | |
| A82 | Chip 2 | -24.9 | 227.3 | - | - | - | - | - | - | - | 27.9 | 8 | L-V | IIA | Unclassified | |
| A82 | Chip 2 | -24.1 | 239.6 | - | - | - | - | - | - | - | 27.1 | 10 | L-V | IIA | Unclassified | |
| A82 | Chip 2 | -19.6 | 256.7 | - | - | - | - | - | - | 22.1 | - | 10 | L-V | IIA | Unclassified | |
| A82 | Chip 2 | -22.1 | 296.9 | - | - | - | - | - | - | - | 25.1 | 15 | L-V | IIA | Secondary | |
| A82 | Chip 2 | -24.2 | 282.4 | - | - | - | - | - | - | - | 27.2 | 15 | L-V | IIA | Secondary | |
| M54 | NA | -1.2 | - | - | - | - | - | - | - | 1.22 | - | 15µm | L-V | IIA | Secondary | |
| M54 | NA | -16.9 | - | - | - | - | - | - | - | 19.53 | - | 20µm | L-V | IIA | Secondary | |
| M54 | NA | -16.2 | - | - | - | - | - | - | - | 19.05 | - | 20µm | L-V | IIA | Secondary | |
| M87 | chip 1 | -4.4 | - | -1.5 | - | - | - | - | - | 6.16 | - | 20µm | L-V-V | IIIC | Secondary | |
| M87 | chip 1 | -1.7 | - | 22.9 | - | - | - | - | - | 2.07 | - | 20µm | L-V-V | IIIC | Secondary | m |
| M87 | chip 1 | -1.4 | - | - | - | - | - | - | - | 1.57 | - | 20µm | L-V | IIA | Secondary | m |
| M87 | chip 1 | - | - | - | - | - | 1 | - | - | 14.46 | - | 15µm | L-V-V | IIIC | Secondary | |
| M87 | chip 1 | -6.5 | - | 5.5 | - | - | - | - | - | 9.08 | - | 35µm | L-V-V | IIIC | Secondary | |
| M87 | chip 1 | -2.3 | - | 2.8 | - | - | - | - | - | 3.06 | - | 15µm | L-V-V | IIIC | Secondary | n |
| M87 | chip 1 | -0.7 | - | 8 | - | - | - | - | - | 0.35 | - | 20µm | L-V-V | IIIC | Secondary | n |
| M87 | chip 2 | -24.1 | - | - | - | - | - | - | - | - | 27.1 | 50µm | L-V | IIA | Secondary | |
| M87 | chip 2 | -23.4 | - | - | - | - | - | - | - | - | 26.4 | 40µm | L-V | IIA | Secondary | |
| M87 | Chip 3 | -5.8 | - | - | - | - | - | - | - | 8.14 | - | 15µm | L-V | IIA | Secondary | |
| M87 | Chip 3 | -18.2 | - | - | - | - | - | - | - | 20.52 | - | 15µm | L-V | IIA | Secondary | |
| M87 | Chip 3 | -12.2 | - | - | - | - | - | - | - | - | - | 20µm | L-V | IIA | Secondary | |
| M87 | Chip 3 | -16.7 | - | - | - | - | - | - | - | 19.37 | - | 25µm | L-V | IIA | Secondary | |
| M87 | Chip 3 | -13.1 | - | - | - | - | - | - | - | 16.34 | - | 20µm | L-V | IIA | Secondary | |
| M87 | Chip 3 | -12.1 | - | - | - | - | - | - | - | 15.37 | - | 20µm | L-V | IIA | Secondary | |
| M87 | Chip 3 | -3.3 | - | - | - | - | - | - | - | - | - | 20µm | L-V | IIA | Secondary | |
| M87 | Chip 3 | -9.2 | - | - | - | - | - | - | - | - | - | 15µm | L-V | IIA | Secondary | |
| M15 | chip 2 | - | - | - | - | - | 2.8 | - | - | 12.21 | - | 30µm | L-V | IIIB | Secondary | |
| M76 | chip 1 | - | - | 20.7 | - | - | 1.8 | - | - | 13.48 | - | 15µm | L-V-V | IIIC | Secondary | |
| M76 | chip 1 | - | - | 22.6 | - | - | 1.6 | - | - | 13.74 | - | 15µm | L-V-V | IIIC | Secondary | |
| M76 | chip 1 | -2.4 | - | - | - | - | - | - | - | 3.23 | - | 20µm | L-V | IIIB | Secondary | |
| M76 | chip 1 | - | - | 24 | - | - | 1.4 | - | - | 13.98 | - | 20µm | L-V-V | IIIC | Secondary | |

$T_m^{(a)}$ = ice melting temperature; $T_h^{(1,2,3)}$ = temperature of homogenization final vapor; $T_h^{(3,4,5,6,7)}$ = temperature of homogenization CO₂ vapor bubble; $T_h^{(1,2,3)}$ = temperature of homogenization of CO₂ liquid phase; T_d = temperature of halite dissolution; $Clath_{(m)}$ = clathrate melting temperature; $T_{(h)}^{(b)}$ = hydrohalite dissolution temperature; $T_{(h)}^{(c)}$ = temperature of transition from hydrohalite to halite crystal

List of abbreviations: H = halite; L = liquid; S = sylvite; U = unknown; V = vapor; xtal = crystal

Measurements with a "+" indicate the heating limit for that sample

Table 3.1 (Cont): Microthermometric data for inclusions from the Carson deposit

| Sample | Chip | T_m^{ice} | T_h^{V-L} | T_h^{V-V-L} | T_h^{L-L-V} | T_d | T_{clath} | $T_{ho}^{CO_2}$ | $T_{ho}^{H_2O}$ | wt% NaCl _{liquid} | wt% CaCl _{2 liquid} | Size (μm) | Phase | Type | Origin | Assemblage |
|--------|--------|-------------|-------------|---------------|---------------|-------|-------------|-----------------|-----------------|----------------------------|------------------------------|-----------|-------|------|-----------|------------|
| M76 | chip 1 | - | - | 14.2 | - | - | 2.8 | - | - | 12.21 | - | 15um | L-V-V | HC | Secondary | |
| M76 | chip 1 | - | - | 13.4 | - | - | 1.8 | - | - | 13.48 | - | 15um | L-V-V | HC | Secondary | |
| M76 | chip 1 | -1 | - | - | - | - | - | - | - | 0.88 | - | 15um | L-V-V | HC | Secondary | |
| M76 | chip 1 | -0.7 | - | 25.7 | - | - | - | - | - | 0.35 | - | 15um | L-V-V | HC | Secondary | |
| M76 | chip 1 | 1.9 | - | 19.6 | - | - | - | - | - | 12.67 | - | 30um | L-V-V | HC | Secondary | |
| M76 | chip 1 | -1.2 | - | 22.9 | - | - | - | - | - | 1.22 | - | 15um | L-V-V | HC | Secondary | |
| M76 | chip 1 | -1.2 | - | 18.6 | - | - | - | - | - | 1.22 | - | 15um | L-V-V | HC | Secondary | |
| M76 | chip 1 | -0.5 | - | 20.6 | - | - | - | - | - | 0.88 | - | 15um | L-V-V | HC | Secondary | |
| M76 | chip 1 | -0.5 | - | 17.8 | - | - | - | - | - | 0.88 | - | 15um | L-V-V | HC | Secondary | |
| M78 | chip 2 | -3.3 | - | - | - | - | - | - | - | 4.65 | - | 30um | L-V | HA | Secondary | |
| M78 | chip 2 | -5.4 | - | 29 | - | - | - | - | - | 7.59 | - | 15um | L-V-V | HC | Secondary | |
| M78 | chip 2 | -2.2 | - | 16.1 | - | - | - | - | - | 2.9 | - | 15um | L-V-V | HC | Secondary | |
| M78 | chip 2 | -10.6 | - | - | - | - | - | - | - | 13.85 | - | 20um | L-V | HA | Secondary | |
| M78 | chip 2 | -8.7 | - | - | - | - | - | - | - | 11.81 | - | 50um | L-V | HA | Secondary | |
| M78 | chip 2 | -10.8 | - | - | - | - | - | - | - | 14.04 | - | 20um | L-V | HA | Secondary | |

T_m^{ice} = ice melting temperature; T_h^{V-L} = temperature of homogenization final vapor; T_h^{V-V-L} = temperature of homogenization CO₂ vapor bubble; T_h^{L-L-V} = temperature of homogenization of CO₂ liquid phase; T_d = temperature of halite dissolution; T_{clath} = clathrate melting temperature; $T_{ho}^{CO_2}$ = hydrohalite dissolution temperature; $T_{ho}^{H_2O}$ = temperature of transition from hydrohalite to halite crystal

List of abbreviations: H = halite; L = liquid; S = sylvite; U = unknown; V = vapor; stal = crystal

Measurements with a "-" indicate the heating limit for that sample

Table 3.2: LA-ICP-MS analyses of fluid inclusions from the Garson deposit

| Sample | Chip I | NaCl wt% | Type | Li | B | Na | Mg | K | Ca | Mn | Fe | Cu | Zn | As | Rb | Sr | Ag | Sn | Sb | Cs | Ba | Ce | Pb | Bi |
|--------|--------|----------|------|-----|-----|-------|-----|-------|-------|-------|--------|------|------|-----|----|-----|-----|-----|-----|----|------|-------|------|-----|
| M76 | 1 | 14.83 | IIA | 40 | 240 | 46800 | bdl | 8020 | bdl | 20 | 245 | 12 | 350 | 617 | 56 | 231 | 1.0 | 17 | 12 | 19 | 849 | bdl | 350 | 2.0 |
| M76 | 1 | 15.43 | IIA | 71 | 273 | 49300 | bdl | 8200 | bdl | 12 | bdl | bdl | 30 | 35 | 46 | 173 | bdl | bdl | 2 | 15 | 469 | bdl | 14 | 1.6 |
| M76 | 1 | 14.33 | IIA | 37 | 410 | 44700 | 19 | 7560 | bdl | 102 | bdl | bdl | 621 | 438 | 53 | 237 | bdl | bdl | 28 | 17 | 926 | bdl | 746 | bdl |
| M87 | 3 | 16.05 | IIA | 82 | 291 | 58500 | 19 | 8260 | bdl | 154 | 1190 | 9 | 1140 | 130 | 19 | 584 | 7.8 | 21 | 23 | 16 | 896 | 0.66 | 2590 | 3.2 |
| M87 | 3 | 21.11 | IIA | 126 | 483 | 76900 | 820 | 12800 | bdl | 360 | bdl | bdl | 1340 | 41 | 35 | 933 | 3.7 | bdl | 23 | 30 | 2090 | bdl | 3090 | bdl |
| M87 | 3 | 8.95 | IIA | 25 | 124 | 20100 | bdl | 1551 | 26100 | 30 | bdl | bdl | 320 | 19 | 10 | 278 | bdl | bdl | 10 | 6 | 457 | bdl | 705 | 1.4 |
| M87 | 3 | 19.99 | IIA | 117 | bdl | 59600 | 46 | 18500 | bdl | 755 | bdl | bdl | 1230 | 205 | 42 | 836 | bdl | bdl | 53 | 14 | 2790 | bdl | 4260 | bdl |
| M87 | 3 | 16.99 | IIA | 312 | 298 | 56200 | bdl | 4660 | bdl | 3520* | 14500* | bdl | 1070 | 210 | 36 | 678 | bdl | 103 | 110 | 15 | 1330 | bdl | 2160 | 8.1 |
| M87 | 1 | 8.33 | IIA | 52 | 78 | 19600 | bdl | 1500 | 16000 | 29 | bdl | bdl | 266 | 18 | 34 | 229 | bdl | 7 | 2 | 10 | 509 | bdl | 589 | bdl |
| M87 | 1 | 4.8 | IIA | 5 | 25 | 4800 | bdl | 399 | bdl | 31 | 30 | 1 | 99 | 2 | 3 | 91 | 0.2 | bdl | 1 | 1 | 189 | bdl | 413 | bdl |
| M87 | 3 | 16.0 | IIA | 140 | 244 | 51700 | bdl | 9130 | bdl | 81 | bdl | 11 | 728 | 127 | 30 | 538 | bdl | bdl | 0 | 12 | 954 | bdl | 1440 | 3.9 |
| M87 | 3 | 13.47 | IIA | 52 | 255 | 41100 | bdl | 4750 | 25200 | 452 | 895 | bdl | 762 | 77 | 19 | 563 | 1.9 | bdl | 17 | 10 | 950 | bdl | 1630 | 1.0 |
| M87 | 3 | 12.54 | IIA | 67 | 304 | 37200 | 20 | 5910 | bdl | 250 | 644 | bdl | 946 | 67 | 24 | 732 | bdl | bdl | 19 | 14 | 1220 | bdl | 1850 | bdl |
| M87 | 3 | 16.70 | IIA | 67 | 190 | 54600 | bdl | 6280 | bdl | 67 | 188 | 3 | 826 | 73 | 26 | 498 | 1.4 | 12 | 11 | 16 | 676 | bdl | 2300 | bdl |
| M87 | 3 | 15.53 | IIA | 122 | 359 | 49700 | 20 | 4620 | bdl | 2610* | 9590* | 9 | 817 | 129 | 19 | 771 | 1.7 | bdl | 25 | 9 | 533 | bdl | 2540 | 3.1 |
| M87 | 3 | 14.26 | IIA | 110 | 219 | 44400 | 457 | 2890 | bdl | 632 | bdl | bdl | 936 | 76 | 27 | 546 | 9.7 | bdl | 50 | 29 | 767 | 31.83 | 1560 | bdl |
| M87 | 3 | 16.48 | IIA | 93 | 242 | 53700 | bdl | 5900 | bdl | 127 | 201 | 5 | 583 | 71 | 31 | 545 | 2.2 | bdl | 8 | 13 | 643 | bdl | 1900 | 1.2 |
| M76 | 1 | 13.7 | IIC | 25 | 163 | 23900 | bdl | 11000 | bdl | bdl | bdl | 141* | 798 | 91 | 15 | 34 | bdl | bdl | 13 | 3 | 123 | bdl | 33 | bdl |
| M76 | 1 | 1.74 | IIC | 1 | 15 | 3970 | 12 | 334 | 5040 | 2 | bdl | bdl | 12 | 10 | 4 | 25 | bdl | bdl | 0 | 1 | 93 | bdl | 4 | bdl |
| M76 | 1 | 0.88 | IIC | 9 | 41 | 3200 | 41 | 522 | bdl | 2 | 142 | 28 | 34 | 7 | 3 | 12 | 0.5 | bdl | 1 | 1 | 44 | bdl | 7 | 0.3 |
| M87 | 1 | 2.9 | IIC | 27 | 66 | 9960 | bdl | 896 | bdl | 19 | 55 | 1 | 160 | 12 | 16 | 119 | 0.2 | bdl | 1 | 4 | 187 | bdl | 47 | 0.2 |
| M87 | 1 | 14.44 | IIC | 161 | 262 | 25970 | bdl | 1700 | 54900 | bdl | bdl | 10 | 44 | 30 | 38 | 231 | bdl | bdl | 0 | 12 | 538 | bdl | 618 | bdl |
| M87 | 1 | 3.87 | IIC | 93 | 83 | 15200 | 65 | bdl | 43500 | 3210* | 28500* | 3 | 412 | 18 | 15 | 263 | bdl | bdl | 2 | 7 | 168 | bdl | 446 | bdl |
| M87 | 1 | 1.22 | IIC | 22 | 73 | 4800 | bdl | 321 | bdl | bdl | bdl | bdl | 138 | 10 | 7 | 78 | bdl | bdl | 1 | 4 | 70 | bdl | 172 | bdl |

* indicates analyses with Fe-Mn or Cu contamination

Table 3.3: Count rate intensities for CO₂ inclusions obtained by LA-ICPMS

| Fluid inclusion | Li | Na | Mg | Al | Mn | Fe | Cu | As | Zn | Rb | Sr | Sb | Cs | Ba | Ce | Pb |
|-----------------|---------|---------|---------|---------|---------|---------|---------|---------|---------|---------|---------|---------|---------|---------|---------|---------|
| F04 | - | 1.0E+04 | - | - | - | - | - | - | - | - | 1.0E-03 | - | - | - | - | - |
| F05 | - | 1.0E+03 | - | - | - | - | - | - | - | - | 1.0E+03 | - | - | 2.0E+02 | - | - |
| F06 | 1.0E+04 | 3.0E+04 | 1.0E+03 | 1.0E+04 | 1.0E+04 | - | 1.0E+03 | - | 1.0E+03 | 1.0E+03 | 2.0E+04 | - | 1.0E+03 | 3.0E+03 | 8.0E+02 | 1.0E+05 |
| F07 | - | 1.0E+03 | - | - | - | - | - | - | 5.0E+02 | - | - | - | - | - | - | 8.0E+02 |
| F08 | - | 2.0E+03 | - | - | 2.0E+03 | - | - | - | - | - | 1.0E+03 | - | - | 1.0E+03 | - | 1.0E+03 |
| F09 | - | 1.0E+05 | - | - | 1.0E+04 | - | - | - | - | 1.0E-03 | 5.0E-04 | - | - | 5.0E+03 | - | 1.0E+03 |
| F11 | - | 5.0E+05 | - | - | 7.0E+05 | 5.0E+03 | - | 1.0E+03 | 1.0E+03 | 5.0E+02 | 8.0E+03 | 5.0E+02 | 3.0E+02 | 1.0E+03 | - | 1.0E+04 |

Chapter 4: Application

4.0 Mineral processing

Mineral processing of pentlandite and chalcopyrite of the Garson ores consists of four main stages; comminution (crushing and grinding), beneficiation and flotation (separation and concentration), smelting and refining. Base metals, such as Cu and Ni, are hosted in minerals which cannot be separated by gravitational methods; therefore they are separated through flotation to form “concentrates”. The concentrates commonly contain both small quantities of precious metals (treated as “credits”) and deleterious metals (treated as “penalties”).

Flotation (or depression) of harmful or unwanted ore minerals is a method of mitigating contamination of concentrates. In internal studies conducted by Vale, solutions containing sodium sulphite, triethylenetetramine (TETA) and MAA (a solution of magnesium chloride, ammonium chloride, and ammonium hydroxide) have been used to suppress the flotation of sulfarsenides and arsenides, while allowing pentlandite and chalcopyrite flotation. These studies were performed on pure (end-member) minerals phases present in unrealistically high abundances (i.e., 10 vol%). The effectiveness of these solutions at suppressing sulfarsenides and arsenides have not been tested on ore samples containing more realistic minor to trace abundances of these minerals (i.e., less than 0.1 vol %) nor in ore samples exhibiting the significant compositional variation (i.e., Co:Ni ratio) in these phases that are documented in this study.

Simple gravity separation is a commonly used method for concentrating minerals. For gravity separation differences in specific gravity alone will not be the only factor for separation. The size of the particles will also play an important role, as will the medium in which the particles are suspended (air, water, brine, or heavy media). For this method to be effective the density contrasts between minerals to be separated from one another

should be 1.5:1 and all particles should be milled to the same size and size fraction. At Garson, the contrast in density between the dominant sulfarsenide mineral [i.e., CGSS (SG=6.11) and pentlandite (SG=4.8)] is less than 1.5:1 and therefore, gravity separation may not be effective. However, in some high As regions where As abundance is controlled mainly by nickeline (SG=7.8), gravity separation may be used effectively.

Grinding is a process which can account for up to ~40% of the mineral processing plant's operating costs. The *majority* of CGSS and nickeline grains observed in this study in the Garson ores are large enough that they can be completely liberated from sulphide ores during routine crushing and grinding (i.e., 95% of grains are > 70 µm; routine grinding size). The CGSS, GGSS and nickeline grains that are smaller (5% of grains are < 70 µm) will contribute As to the concentrates, but with effective blending of *milled* As-poor and As-enriched ores containing these residual small sulfarsenide-arsenide grains, the negative impact of these phases in downstream mill and smelting operations can be minimized.

At Sudbury, PGE are produced as byproducts of Ni and Cu mining, milling, smelting, and refining most of the PGE (either as inclusions or in solid solution) are hosted in CGSS-GGSS and nickeline will not be recovered if CGSS-GGSS flotation is suppressed. The PGM will not be liberated from these phases during routine grinding, due to the relatively small sizes (< 20 µm). Small PGM grains that are not hosted in sulfarsenides or arsenides will also be lost because they will not be able to be separated from their host minerals effectively.

4.1 Sampling

Currently, the Sudbury ores are blended with Garson ore comprising 7-10% of the total processed ore mass. However, the amount of Garson ore processed as a % of the total

feed is expected to increase within the next few years. Systematic identification of As-rich regions in the Garson ore zones has proved difficult due to the very heterogeneous distribution of sulfarsenides and arsenides at all scales of characterization (thin section, chip sample or drill core interval, stope). Consequently, volumetrically insignificant amounts of As-rich ore currently contaminate a much larger low As volume of ore. Areas with high As are flagged and As-rich ore is stored separately in on-surface stockpile. However, on surface, the storage of the ore is problematic because of the detrimental effects of sulphide oxidation to Ni recovery. The misrepresentivity of sampling methods also means that low As ores are also sent to high As stockpiles, exacerbating Ni recovery and overall mine productivity.

While visual identification of large grains of sulfarsenides and arsenides in hand sample and drill core is possible, the effectiveness of this tool will only be significant for samples containing large sulfarsenide-arsenide grains that can be spotted in dim lighting conditions underground or by hand lens in the core shack. However, it should be an activity that is encouraged because samples containing large grains (phenocrysts) of CGSS and nickeline are characteristic of high- As regions along sulphide-wall rock contacts. Focus should be placed on avoiding *the hanging wall of overturned ore bodies* since these areas contain the highest endowment of As due to original settling of CGSS-GGSS and nickeline phenocrysts on this surface.

More systematic and representative identification of As-rich and other accessory metal/precious metal rich areas will require a *significant* increase in drill core intersections through ore zones. Possibly, a more rapid method of developing better spatial models for PGE and As distribution would be the application of hand-held X-ray fluorescence spectrometry in the core shack.

4.2 Exploration

There are three main exploration implications from this study. First, the presence of As-rich metasedimentary (or sedimentary) rocks to magmatic-hydrothermal deposits may indicate that ores will be locally contaminated in As and that As-rich phases will be primary hosts for the platinum-group elements. Associated base metal sulphides that are unusually depleted in PGE may indicate that sulfarsenide/arsenide saturation occurred in a magmatic Ni-Cu-PGE sulphide system hosted in metasediments. Second, detection of As-rich fluids through fluid inclusion microanalyses demonstrates that As was mobile during post-cumulus hydrothermal events. Therefore, As contamination of sulphide ores may not be restricted to primary magmatic events and can be the result of infiltration of host-rock associated metamorphic fluids that were circulating coincident to magmatic sulphide ore formation. Similarly, detection of anomalous As contents in otherwise As-poor host rocks may serve as an effective pathfinder for finding magmatic sulphide deposits from which As was leached during post-cumulus processes. Finally, routine sampling and assaying techniques for characterizing the deleterious and precious metal content of modified magmatic sulphide ore deposits must be much better informed through detailed mineralogical studies since the distribution and trace element composition of mineral phases, the relative heterogeneity or homogeneity of metals contained within the ores, and the presence of micrograins play such a key role in metal recovery.